Design and Simulation of MEMS-Based Insulin Micro-Pump with Integrated Micro-Needle Array

by

FARSHID MESHKINFAM

A Thesis Submitted in Partial Fulfillment
of the Requirements for the Degree of

Master of Applied Science
Mechanical Engineering

The Faculty of Engineering and Applied Science

Department of Mechanical Engineering

University of Ontario Institute of Technology

November 2015

Copyright © 2015 by Farshid Meshkinfam

Dedication

To the loves of my life; Mahsa
And my son; Ryan,
Who has been our life inspiration since the night he was born.

Abstract:

One of the most effective treatments for diabetes type 1 and 2 is the administering Insulin. Single needle mechanical insulin pumps are heavy and painful. A generation of micro-needle-based MEMS-based drug delivery devices can be an excellent solution for insulin dosing. The stackable structure provides minimum dimensions and makes the final product to be patchable in any flat area of human skin and in combination with micro-needle array; it provides a safe, painless and robust injection application.

In this study we address various aspects of design and simulation of a MEMS-based piezoelectric insulin micro-pump including PDMS micro-valves and micro-needle array. We investigate the micro-pump performance for different activating frequencies and different voltage at human skin interfacial pressure to match minimum to maximum deliver targets/requirements for total range of diabetic patients.

COMSOL multiphysics is used to simulate and investigate the performance of a MEMS-based insulin micro-pump with a piezoelectric actuator pumping a viscous Newtonian fluid. The nature of this study is nonlinear therefore we use a fully coupled system with two-way boundary couplings. Fully coupling physics provide real time relationship between different parameters and pump's outputs. Three simulation modules; Structural Mechanic, Piezoelectric Device and Fluid-Structure Interaction are used to study the 2-D/3-D models of this MEMS based concept. Post processing and ODE also are used to create different required outputs.

Acknowledgment:

I would like to sincerely appreciate Professor Ghaus Rizvi for his great support and guidance during my research and education studies at UOIT. I would also like to thank my friend Shawn Garmsiri for his help and support.

And I do know without Mahsa, my love and my life, I would have never been able to get this done.

Table of Contents

List of Figures:

List of Tables:

Nomenclature:

D	Diameter (mm, µm)
f	Frequency (Hz)
F	Volume force vector (N/m^3)
n	Normal Vector (unit length)
p	Pressure (Pa)
Pi	Interstitial fluid pressure (Pa)
q	Heat flux vector (W/m^2)
Q	contains the heat sources (W/m^3)
s	Boundary length parameter (mm, µm)
T	Absolute temperature (K)
t	Time (s)
u	Velocity vector (m/s)
u	Displacement Vector (m, mm, µm)
V	Voltage (volt)
$\dot{V}$	Flow rate (µl/min)
W	Mass/Weight (kg)
ρ	Density (kg/m^3)
µ	Viscosity (Pa·s, mPa.s)
τ	Viscose stress tensor (Pa, mbar))
σ (Γ)	Stress Tensor (N/m^2)

CHAPTER 1: Introduction

1.1 Diabetic Facts

The MEMS based positive displacement insulin micro-pump [1-3] has a Piezoelectric Actuator on top of a diaphragm membrane made from Silicone glass. Induced vibrations from piezoelectric actuator create positive/negative volume in the pump's main chamber, which pulls fluid from inlet gate and pushes it toward outlet gate. The gating process is governed by two PDMS flapper check valves that control the fluid direction from inlet toward outlet leading to micro-needle array. A distributer connects outlet gate to the micro-needle substrate, and finally the established discharge pressure pushes the fluid out of Silicone micro-needles to skin epidermis, right above the dermis layer [4].

Diabetes is a chronic, often debilitating and sometimes fatal disease, in which the body either cannot produce insulin or cannot properly use the insulin it produces. Insulin is a hormone that controls the amount of glucose (sugar) in the blood. Diabetes leads to high blood sugar levels, which can damage organs, blood vessels and nerves. The body needs insulin to use sugar as an energy source [5].

1.2 Diabetes type 1

Type 1 diabetes occurs when the immune system mistakenly attacks and kills the beta cells of the pancreas. No, or very little, insulin is released into the body. As a result, sugar builds up in the blood instead of being used as energy. About five to 10 per cent of people with diabetes have type

1 diabetes. Type 1 diabetes generally develops in childhood or adolescence, but can develop in adulthood. Type 1 diabetes is always treated with insulin. Meal planning also helps with keeping blood sugar at the right levels. Type 1 diabetes also includes latent autoimmune diabetes in adults (LADA), the term used to describe the small number of people with apparent type 2 diabetes who appear to have immune-mediated loss of pancreatic beta cells [5].

Type 1 diabetes is usually diagnosed in children and young adults, and was previously known as juvenile diabetes [5].

1.3 Diabetes type 2:

Type 2 diabetes occurs when the body can't properly use the insulin that is released (called insulin insensitivity) or does not make enough insulin. As a result, sugar builds up in the blood instead of being used as energy. About 90 per cent of people with diabetes have type 2 diabetes. Type 2 diabetes more often develops in adults, but children can be affected. Depending on the severity of type 2 diabetes, it may be managed through physical activity and meal planning, or may also require medications and/or insulin to control blood sugar more effectively [5].

1.4 Complications of diabetes

Having high blood sugar can cause diabetes-related complications, like chronic kidney disease, foot problems, non-traumatic lower limb (leg, foot, toe, etc.) amputation, eye disease (retinopathy) that can lead to blindness, heart attack, stroke, anxiety, nerve damage, and erectile dysfunction (men). Diabetes-related complications can be very serious and even life-threatening. Properly managing blood sugar levels reduces the risk of developing these complications. All people with type 1 diabetes and many with type 2 diabetes need insulin to manage blood glucose (sugar)

levels. What is important is to live well with diabetes. Sometimes, people feel scared, nervous, or guilty about having to start insulin therapy, and that's okay. Taking insulin to help manage diabetes may be hard to understand at first. They might be scared of taking injections. What is important to remember is that using insulin can help the patients to manage their glucose (sugar) levels, which can prevent complications related to diabetes [5].

1.5 Cost of Diabetes

1.5.1 Diabetes costs in USA

The cost of diabetes in USA based on updated data from March 6, 2013 are:

- $245 billion: Total costs of diagnosed diabetes in the United States in 2012
- $176 billion for direct medical costs
- $69 billion in reduced productivity

After adjusting for population age and sex differences, average medical expenditures among people with diagnosed diabetes were 2.3 times higher than what expenditures would be in the absence of diabetes [5].

1.5.2 Diabetes costs in Canada

Data from the Public Health Agency of Canada's Economic burden of illness in Canada (EBIC) 2000 [6] provide a conservative estimate of $2.5 billion (CAD) in year 2000 for the total cost of diabetes, excluding cost associated with diabetes complications. Further to this, because individuals with diabetes are at an increased risk of developing other chronic diseases, factoring in a proportion of the costs incurred to treat these related illnesses, conditions, and complications

would result in a larger share of health care costs incurred in a population with diabetes. According to a study conducted in 1998, the total costs of diabetes were 3.6 times higher when the costs associated with long-term complications of diabetes (including neurological disease, peripheral vascular disease, cardiovascular disease, kidney disease, and eye disease) were included. Given the strong association between cardiovascular disease and diabetes, cardiovascular-related care alone was found to account for about a quarter of the total health care costs of individuals with diabetes [6].

1.6 Insulin

Insulin is a hormone produced by the pancreas to control the amount of glucose (sugar) in the blood. Without insulin, glucose builds up in the bloodstream. This can lead to serious health problems, such as blindness, heart disease, kidney problems, amputation, nerve damage, and erectile dysfunction [5].

1.7 Types of insulin

Several different types of insulin are available. Types of insulin differ by how long they work, how quickly they start working, and when they are most effective. By understanding how your prescribed insulin works, you can time your meals, snacks, and activity levels. Patients might start on one or more injections each day. When prescribing insulin, the diabetes health-care team will consider several factors, such as treatment goals, age, lifestyle, meal plan, general health, plus risk and awareness of low blood glucose (hypoglycemia). There is no “one size fits all” plan. When taking insulin, patient needs to check the blood glucose (sugar) levels regularly. Regular checks give important information about how the glucose levels vary during the day, how much insulin is needed, and help to determine if the patient is on track managing diabetes. Understanding and acting on the results of the blood glucose (sugar) checks is the best way to keep the glucose levels

in their target range. The health-care team provide the insulin plan to meet patient's needs. It will take time to fine-tune patient's insulin routine, and it may change over time depending on life events (such as a major illness) or changes in lifestyle (such as a change in physical activity) [5].

1.8 Insulin Pumps

Most of commercial available Insulin pumps are small computerized devices that deliver insulin in two ways:

- In a steady measured and continuous dose (the "basal" insulin)
- As a surge ("bolus") dose, at your direction, around mealtime.

Doses are delivered through a flexible plastic tube called a catheter. With the aid of a small needle, the catheter is inserted through the skin into the fatty tissue and is taped in place. The insulin pump is not an artificial pancreas (because you still have to monitor your blood glucose level), but pumps can help some people achieve better control, and many people prefer this continuous system of insulin delivery over injections. Pumps can be programmed to releases small doses of insulin continuously (basal), or a bolus dose close to mealtime to control the rise in blood glucose after a meal. This delivery system most closely mimics the body's normal release of insulin [5].

1.9 Advantages of Using an Insulin Pump

Some advantages of using an insulin pump instead of insulin injections are:

- Using an insulin pump means eliminating individual insulin injections
- Insulin pumps deliver insulin more accurately than injections

- Insulin pumps often improve A1C. The A1C test is a blood test that provides information about a person's average levels of blood glucose, also called blood sugar, over the past 3 months. The A1C test is sometimes called the hemoglobin A1c, HbA1c, or glycohemoglobin test
- Using an insulin pump usually results in fewer large swings in your blood glucose levels
- Using an insulin pump makes delivery of bolus insulin easier. A bolus dose is insulin that is specifically taken at meal times to keep blood glucose levels under control following a meal. Bolus insulin needs to act quickly and so short acting insulin or rapid acting insulin will be used
- Insulin pumps allow patient to be flexible about when and what patient eats
- Using an insulin pump reduces severe low blood glucose episodes
- Using an insulin pump eliminates unpredictable effects of intermediate- or long-acting insulin
- Insulin pumps allow to exercise without having to eat large amounts of carbohydrate [5].

1.10 Disadvantages of Using an Insulin Pump

Although there are many good reasons as to why using an insulin pump can be an advantage, there are some disadvantages.

The disadvantages of using a pump are that it:

- Can cause weight gain
- Can cause diabetic ketoacidosis (DKA) if your catheter comes out and you don't get insulin for hours

- Can be expensive
- Can be bothersome since you are attached to the pump most of the time
- Can require a hospital stay or maybe a full day in the outpatient center to be trained

There are pluses and minuses to using a pump. Even though using an insulin pump has disadvantages, most pump users agree the advantages outweigh the disadvantages [5].

1.11 Design Objective and Targets

The purpose of this study is to design a micro-pump with acceptable delivery rate/range of flow/pressure for insulin administration. The main design targets for drug delivery pumps similar to this case study, are flow rates and discharge pressure ranges. These are the main basic requirements for designing this pump. Especially flow rate is extremely important in insulin delivery since it directly affects the health condition of diabetic patient. Acceptable pressure range is also important to enable the pump to overcome the existing interstitial fluid pressure in human skin. In next chapter we will review the motivation and objectives in more detail to define the pump specifications but here we only mention the basic requirements of insulin delivery for flow and pressure based on experimental medical facts and evidences to introduce them as our primary design targets

1.11.1 Flow Targets

In general, approximately one-half of the TDD (Total Daily Dose) is administered as basal rate for insulin pump application. For most patients, basal rates are in the range of 0.01 to 0.015 units per kg per hour (ie, for a 60 kg woman approximately 0.6 to 0.9 units per hour). The basal rates are adjusted empirically based on glucose monitoring results [7]. Each standard 100 units is equal to 1 ml insulin.

Based on these medical experimental facts, the insulin pump must be able to deliver a flow range from zero to 0.5 µl/min for full range of human weights (infant to 250 kg weight).

Our focus in this study is on administration of basal or Long-acting insulins. Normally the rest of TDD will be administered as Rapid-acting insulins like Lispro about an hour before main meals 3 time per day. Table 1.6 provides details information about Rapid-acting insulins. With adding a separate reservoir to the unit and with accommodation of a fluid micro-switch, the proposed micro-pump can be used for both Long-acting and Rapid-acting insulin administration.

Insulin type	Onset of action	Peak effect	Duration of action
Lispro, aspart, glulisine	5 to 15 minutes	45 to 75 minutes	Two to four hours
Regular	About 30 minutes	Two to four hours	Five to eight hours
NPH	About two hours	4 to 12 hours	18 to 28 hours
Insulin glargine	About two hours	No peak	20 to >24 hours
Insulin detemir	About two hours	Three to nine hours	6 to 24 hours*
NPL	About two hours	Six hours	15 hours
Insulin degludec	About two hours	No peak	>40 hours
NPH: neutral protamine hagedorn; NPL: neutral protamine lispro.			

Table 1.1 Pharmacokinetics of the most commonly used insulin preparations [7]

1.11.2 Pressure Targets

Interstitial fluid pressure (Pi) has been measured in human skin by micro-pipettes (tip diam. 2–4 μm) and compared to pressures obtained by wick-in-needle technique. The micro-pipettes were connected to a servo-controlled counter-pressure system (Wiederhielm) and were introduced into the skin distally at the dorsum of the fifth finger after immobilization of the upper extremity. The wick-in-needle was introduced at the dorsum of the hand. With the finger at heart level and at a room temperature of 24 ± 1°C, the mean Pi measured by micro-puncture was -3.1 mmHg (range -

5 to -0.5 mmHg), while the corresponding mean Pi measured with wick-in-needle was 0.0 mmHg (range -1.7 to +3 mmHg). During venous stasis, Pi increased as measured by both methods, but the increase recorded by micro-puncture was largest. It is concluded that the wick-in-needle probably overestimates Pj in the normally hydrated human skin of (the hand due to inflammation at the implantation site, and that the overestimation diminishes as tissue hydration increases [8].

As a result, we consider maximum +3 mmHg (about 400 Pa) as output pressure to provide a realistic and feasible pressure for an affective injection.

CHAPTER 2: Literature Review

2.1 Introduction

When other method of drug deliver like pill and traditional injection are not effective, transdermal delivery is an attractive alternative, but due to extremely low permeability of the human skin, this method also has limitations. Micro-Electro-Mechanical-System (MEMS) technology provides novel means in terms of both micro-needles array and piezoelectric pump, with the former one to increase permeability of human skin with efficiency, safety and painless delivery, and the latter one to decrease the size of the pump. This will promote the development of biomedical sciences and technology and makes medical devices more humanized. The micro-needle array can be mounted and stacked up with the main body of the insulin pump. Comparing to existing mechanical pumps, the piezoelectric pump is more precise and smaller and provides a painless and robust insulin administering. The piezoelectric pump and micro-needle array also have potential applications in the chemical and biomedical fields for localized chemical analysis, programmable drug-delivery systems, and very small, precise fluids sampling. The flapper micro-valves have a leakage free performance provide precise delivery of fluid at pump outlet. The existing commercial units are so energy dependent to electrical sources and batteries. With using advanced energy harvesting technology we can provide energy independent system and with a packaging insulin reservoir inside the applying patch, we can mimic human pancreas function to provide totally normal life and day to day activities to diabetic patients.

As anyone diagnosed with Diabetes Mellitus will tell you, pricking yourself and sticking yourself with a needle up to 8 times a day is far from optimal. The traditional method for Diabetes treatment

is to check your blood sugar 4 times a day, and then administer a specified dose of insulin based on the blood sugar level detected. Each insulin shot administered helps to control blood sugar but it also causes a shock to the system and can cause a cumulative, negative effect on the organs of the body. Continues administering of insulin is the best way to prevent the negative effect of multiple injections and brings back a healthy life to the patient.

Transdermal delivery technology has many advantages, including: minimal trauma at penetration site due to needle small size, no condition limit, painless drug delivery for penetration depth with few nerves, and precise control of volume of drug delivery. Micro-Electro-Mechanical-Systems (MEMS) technology is envisioned for improved transdermal delivery as a micro-needle array. After several years of research, many mechanical systems are now feasible on a micro scale. Devices like micro-pumps, micro-needles, miniature mixers, etc. are widely studied for transdermal delivery. At the present, the bio-MEMS applications to the medical field can be divided into two levels. Primary level is to enhance performances of the traditional medical devices. The secondary level is to manufacture new medical devices based on the MEMS technology. However few of them have turned into commercial products by far. Most of bio-MEMS devices are still on the research level. One reason is that any bio-medical device is complicated itself. The other important reason is that the packaging of the bio-MEMS device is the bottleneck to block the applications of micro-devices in clinical practices.

The motivation of this study is to design a real time insulin administering to mimic application of a natural pancreas system in human body.

2.2 Market Review

2.2.1 Mechanical pump with manual glucose measuring

Figure 2.1 below shows one of the traditional insulin pumps as drug delivery system available in market. Most traditional insulin pumps have a fine injection needle that should be inserted below skin to the fat layer. Glucose level is measured separately outside the body with a drop of blood and then dosage instructions are entered into the pump's small processor and the appropriate amount of insulin is then injected into the body in a calculated controlled manner. This method has a very low reliability, high error level with a huge and heavy mechanical pump that is associated with pain when the needle is inserted to skin.

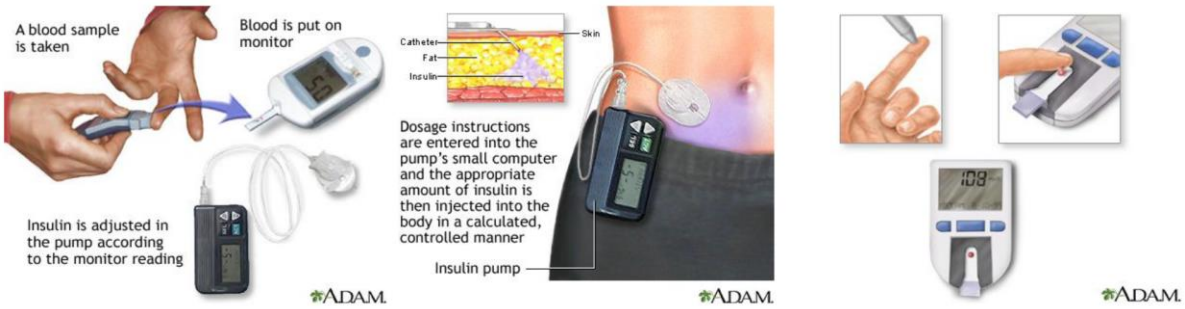

Figure 2.1 Traditional insulin delivery system (http://www.adam.com)

2.2.2 Unified Insulin Pump, Glucose monitoring system

In Figure 2.2, a glucose monitoring system is shown. It shows a unified system for insulin administration which mimics the natural function of the pancreas. Specifically, a sensor implanted in the waist area is used in conjunction with a small insulin reservoir and dispense system worn externally on the waist. A micro-reed sensor is a component of the implant and is used for calibration and mode changes in a manner similar to a pacemaker. The reed switch is an electrical switch operated by an applied magnetic field. It consists of a pair of contacts on ferrous metal

reeds in a hermetically sealed glass envelope. With this system, when very small changes in the blood sugar level occur, a small amount of insulin is administered, which corrects the sugar level. This minimizes the “shock to the system”, allowing people with diabetes to live longer, healthier lives. The pump itself is still using traditional mechanical system with needle. It is heavy and painful.

Figure 2.2 Unified insulin Pump (http://www.meder.com)

2.2.3 Micro-Pump drug delivery system

In figure 2.3 one of the most advanced micro-pump for drug delivery systems, in clinically available in market, is shown. It shows a robust design with minimum size/weight and high accuracy and volumetric efficiency. The concept is based on DEBIOTECH design [3]. The system still needs a robust injection module such as micro-needle array, associated with the pump.

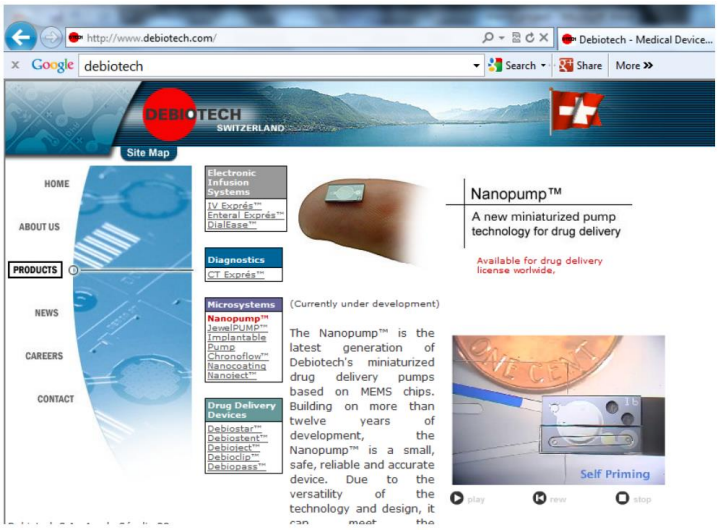

Main performance specification		
Flow rate	0 to 100 µl/h	This is the linear range, stroke volume is constant and the flow rate is proportional to the frequency (Frequency range 0-0.2Hz).
Priming rate	250 µl/h	This is the maximum flow rate in the uncontrolled range. (Frequency 2Hz).
Stroke volume	150 nl	Minimum dosage unit.
Leakage	Non measurable < 0.05 ml/h	Forward and backward leak with 150 mbar overpressure applied on inlet respectively on outlet.
Accuracy	± 5%	Overall accuracy of the stroke volume within nominal conditions.
Inlet pressure Outlet pressure	-350 to +350 mbar -400 to +200 mbar	
Viscosity	0-10 mPa.s	
Actuation voltage	-40V/ +110V	Voltage applied to the piezo disc.
Compression ratio	$e=deltaV/V_0=1.15$	The pump is self priming and tolerant to small air bubbles.
Reliability	$1.8\ 10^8$ stroke 67 days	(equivalent to 25yr of use). Accelerated dry test at 10Hz : no measurable degradation. Real time liquid flow test 0.05Hz (see plot below).
Chip dimensions	16x12x1.86mm	

Figure 2.3 DEBIOTECH micro-pump. One of the most advanced drug delivery system in clinically available in market. (http://www.debiotech.com)

2.2.4 Real time glucose sensors

2.2.4.1 Noviosense glucose sensors

NovioSense [9] is a new type of glucose sensor. It is a non-invasive, wireless sensor to continuously monitor glucose levels in tear fluid to enhance care and treatment of diabetes patients. The sensor enables the introduction of new medical device systems to improve the glucose management of diabetes patients and thus to significantly improve the quality of life of people living with diabetes. Inventors of the patented technology are Hans Hanssen and Rob Tweehuysen, founders and directors of NovioTech BV, an accelerator for such developments. Wearable sensors have garnered considerable recent interest owing to their tremendous promise for a plethora of applications. Yet the absence of reliable non-invasive chemical sensors has greatly hindered progress in the area of on-body sensing. Electrochemical sensors offer considerable promise as wearable chemical sensors that are suitable for diverse applications owing to their high performance, inherent miniaturization, and low cost. A wide range of wearable electrochemical sensors and biosensors has been developed for real-time non-invasive monitoring of electrolytes

and metabolites in sweat, tears, or saliva as indicators of a wearer's health status. With continued innovation and attention to key challenges, such non-invasive electrochemical sensors and biosensors are expected to open up new exciting avenues in the field of wearable wireless sensing devices and body-sensor networks, and thus find considerable use in a wide range of personal health-care monitoring applications, as well as in sport and military applications. The main highlights of this design are:

- Major advances in the development of wearable electrochemical sensors and biosensors.
- Non-invasive monitoring of chemical constituents in sweat, tears, or saliva.
- Monitoring of wearer's health or fitness. [9]

This is still a research concept and needs more clinical tryouts to be accepted as a reliable real time measuring [9].

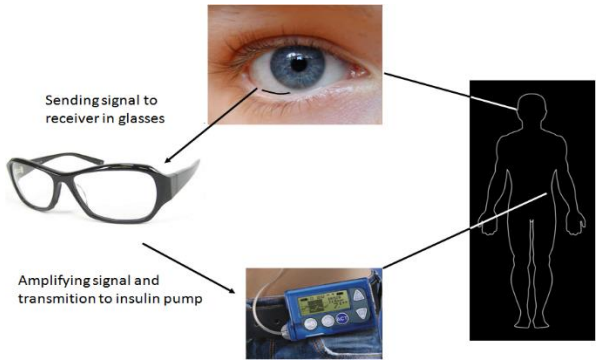

Figure 2.4 NovioSense glucose sensor concept [9]

2.2.4.2 Implantable Glucose Sensor (Working principle)

The Electrochemical Sensors are the most versatile and better developed than any other chemical sensors. Depending on the operating mode, they are divided into: sensors which measure voltage (*potentiometric*), those which measure electric current (*amperometric*), and those which rely on the measurement of conductivity or resistivity (*conductometric*).

In Figure 2.5, the general structure of Biochemical Micro-sensors is shown. In Figure 2.6, a construction and the application properties of a micro-machined silicon sensor for continuous glucose monitoring are presented. The sensor uses the conventional enzymatic conversion of glucose with amperometric detection of H2O2. The innovation is the precise diffusion control of the analyte through a porous silicon membrane into a silicon etched cavity containing the immobilized enzyme [10].

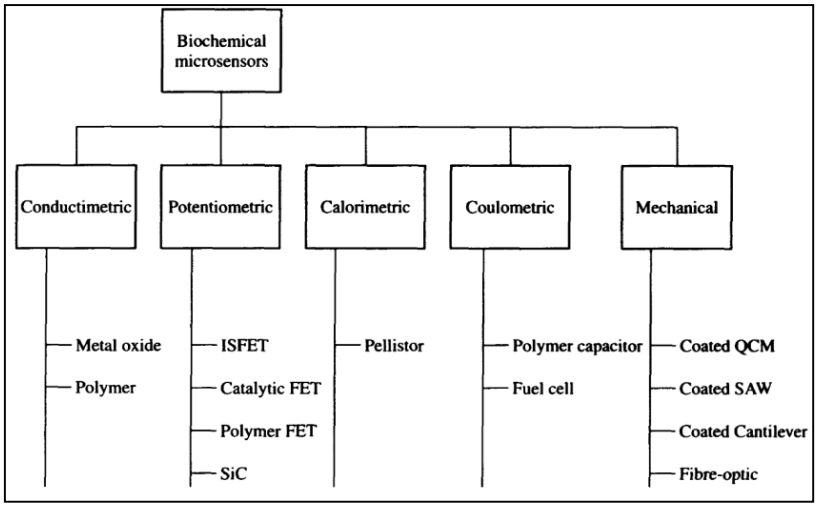

Figure 2.5 Bio-Chemical Micro-Sensors types [10]

The silicon MEMS (Micro Electro Mechanical System) sensor, Figure 2.6 (A), has one cavity which is covered by a pore membrane is etched into the membrane. The platinum working

electrode is deposited on the backside of this pore membrane at the cavity ground. Glucose oxidase (GOD) is immobilised inside of the cavity by a matrix of agarose gel and crosslinking with glutaraldehyde. The complete sensor is inserted into a polymeric flow cell in which the reference electrode as well as the counter electrode are integrated. The measurement principle of the cavity sensor is illustrated in Figure 2.6(B) below [10].

For measurement, analyte solution is pumped through the inlet cannula in the flow through cell. While passing the pore membrane, an amount of glucose, that is proportional to its concentration, diffuses through the pores into the cavity. Glucose molecule are oxidised enzymatically to gluconolactone. In a second reaction step hydrogen peroxide is generated and oxidised electrochemically at the +500mV (versus Ir/IrOx) polarized platinum working electrode [10].

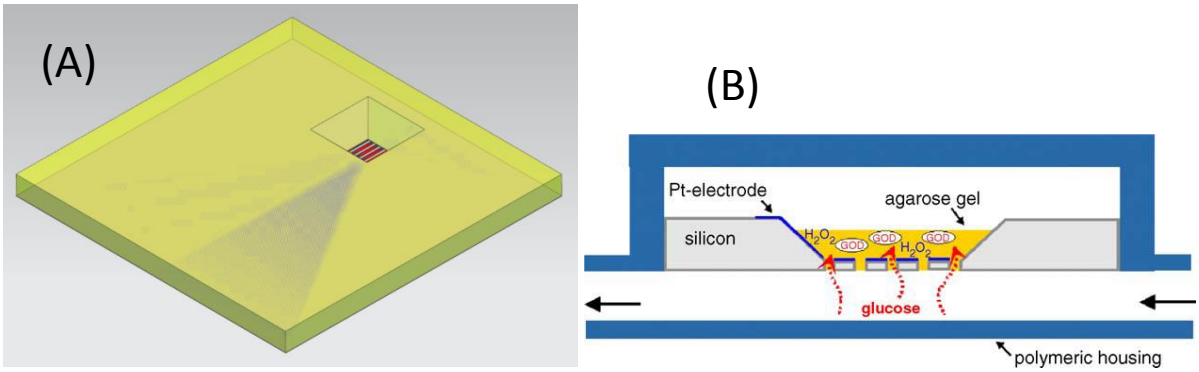

Figure 2.6 Scheme of the MEMS sensor function [10]

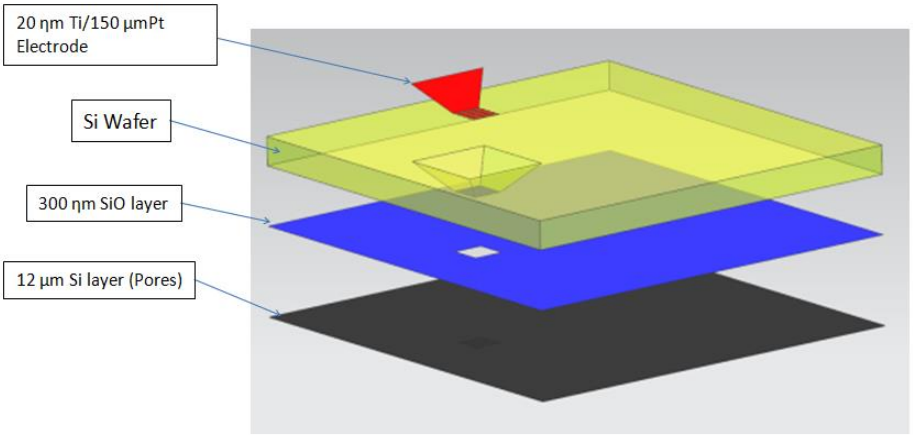

Figure 2.7 Glucose Sensor Construction

The fabrication of the sensor is achievable by MEMS technology (Figure 2.7). The sensor is easily implantable and can be hook up with a RF system to signal out patient's real time glucose level.

2.3 Energy Harvesting Systems

2.3.1 PZT Nanogenerator

Dr. Zhong Lin Wang of the Georgia Institute of Technology has reported that he and his team constructed nanogenerators with enough energy to potentially power LCDs, LEDs and laser diodes by moving your various limbs. These micro-powerhouses strands of piezoelectric zinc oxide, 1/500 the width of a single hair strand, can generate electrical charges when flexed or strained. Wang and his team of researchers shoved a collection of their nanogenerators into a chip 1/4 the size of a stamp, stacked five of them on top of one another and can pinch the stack between their fingers to generate the output of two standard AA batteries around 3 volts.(Figure 2.8) The

nanogenerators have been demonstrated as potential technology for harvesting energy from any source of ultrasonic wave and body movement [11-13].

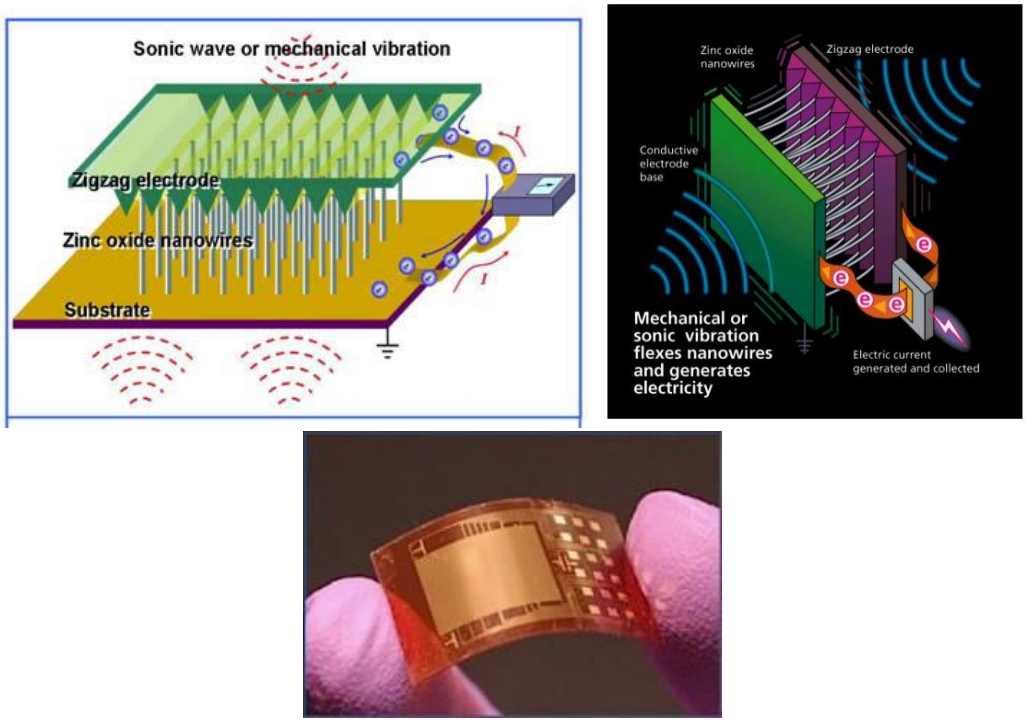

Figure 2.8 Piezoelectric Nanogenerator [11-13]

2.3.2 Thermal Nanogenerator

A team from Wake Forest University's Center for Nanotechnology and Molecular Materials has created a new thermoelectric fabric they call Power Felt. It's constructed of "tiny carbon nanotubes locked up in flexible plastic fibers," though the final product looks and feels like fabric, and creates and electrical charge from changes in temperature in contact with any hot source like sun light or even warmth from human body (hot in this case referring to temperature and thus wholly inoffensive science).

Thermoelectrics are materials capable of the solid-state conversion between thermal and electrical

energy. Carbon nanotube/polymer composite thin films are known to exhibit thermoelectric effects, however, they are expensive and not easy to work with. In the referenced study, it demonstrates individual composite films of multi-walled carbon nanotubes (MWNT)/poly-vinyl-idene fluoride (PVDF) that are layered into multiple element modules that resemble a felt fabric. The thermoelectric voltage generated by these fabrics is the sum of contributions from each layer, resulting in increased power output. Since these fabrics have the potential to be cheaper, lighter, and more easily processed than the commonly used thermoelectric bismuth telluride, the overall performance of the fabric shows promise as a realistic alternative in a number of applications such as portable lightweight electronics [14].

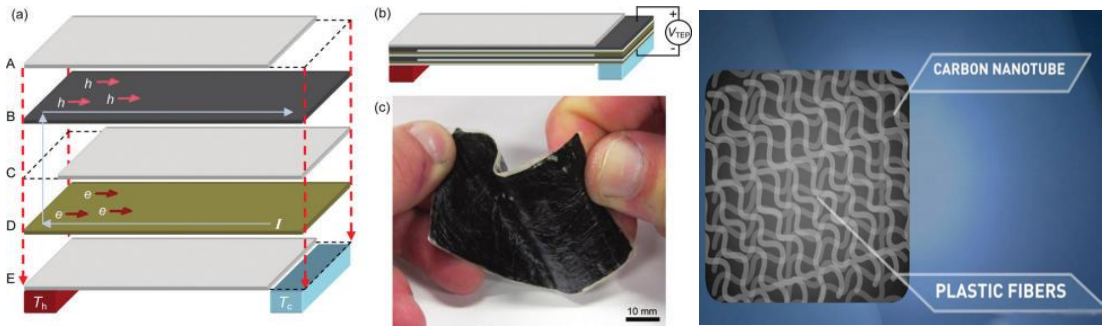

Figure 2.9 Power Felt Nanogenerator [14]

2.4 Literature Review

2.4.1 Van Lintel (DEBIOTECH) implantable pumps

Micro-pump Working principals:

The original Van Lintel design [1] (Figure 2.10), has an open-loop controlling system with ± l0% accuracy in a low flow rate range (0-100 µl/h). It has a constant stroke volume (150 nl) over a wide range of working conditions [1].

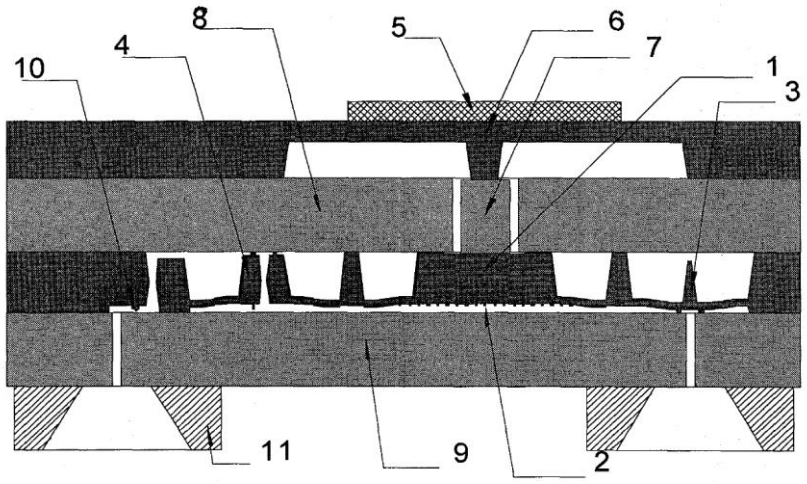

Figure 2.10 Schematic cross section of Van Lintel pump [1]

Pumping membrane (1), chamber (2), outlet (3), inlet (4), piezoelectric ceramic disc (5, crosshatched), actuation membrane (6), glass pin (7), upper (8) and lower (9) glass plates, two titanium fluid connectors (11, hatched).

The new, low cost, high-performance silicon micro-pump developed for a disposable drug delivery system [3] (Figure 2.11) demonstrates a linear (Open Loop) with accuracy of ± 5% for flow rates up to 2 ml/h with intrinsic insensitivity to external conditions. The stroke volume of 160 nl is maintained constant. The manufacturing technology is based on the use of SOI (Silicon on Insulator) wafer, silicon DRIE (Deep Reactive Ion Etching) and the sacrificial etch of the buried oxide layer in order to release the structures. Silicon on insulator (SOI) technology refers to the use of a layered silicon–insulator–silicon substrate in place of conventional silicon substrates in semiconductor manufacturing, especially microelectronics, to reduce parasitic device capacitance, thereby improving performance. Deep reactive-ion etching (DRIE) is a highly isotropic etch process used to create deep penetration, steep-sided holes and trenches in

wafers/substrates, typically with high aspect ratios The result is a small size chip, suitable for cost-effective manufacturing in high volume. [3].

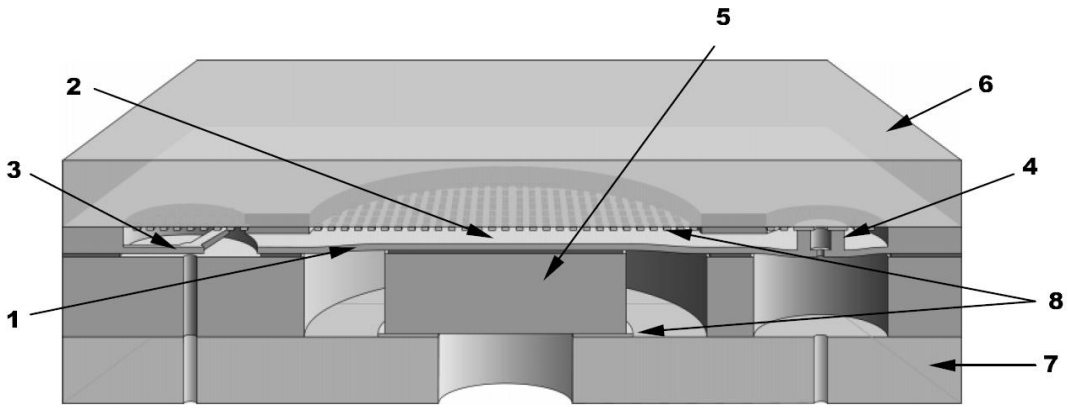

Figure 2.11 Schematic cross section of DEBIOTECH SA new model based on Van Lintel pump [3]

Pumping membrane (1), Pumping chamber (2), Inlet Check Valve (3), Outlet Check Valve (4), Large Mesa (Hill) (5), The Upper Glass Plate (6), Lower Glass Plate (7), The thin layer (8) deposited on the glass surface in contact with the silicon pumping membrane, thus avoiding important squeeze film effect.

The micro-pump is based on the design published by Van Lintel and al. [1-2]. The working principle (shown in figure 2.11) is a volumetric pump with a pumping membrane, which compresses the pumping chamber (2). An inlet (3) and an outlet (4) check valves direct the liquid flow. The chip is a stack of three layers bonded together: one central silicon piece with micro-machined pump structures sandwiched between two glass pieces, one having fluidic access holes.

Figure 2.12 shows the new 3-arm inlet valve, providing almost zero leakage pump gating system.

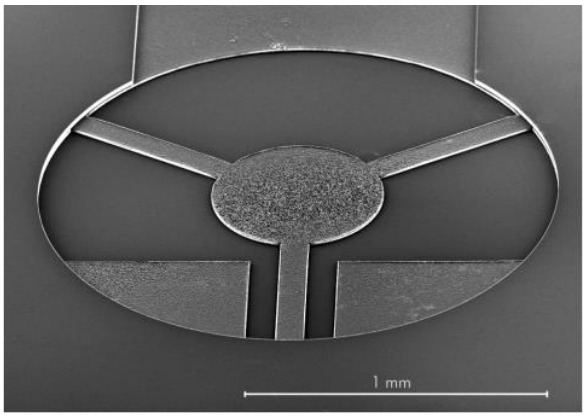

Figure 2.12 A 3D view of the 3-arms inlet valve [3]

Performance review:

Figure 2.13 shows a plot of the volume of liquid pumped vs. time at a frequency of 0.05 Hz. The acquisition frequency is 1 Hz. The pulsatile nature of the flow rate is clearly visible with a very reproducible stroke volume (standard deviation 1.1 nl)

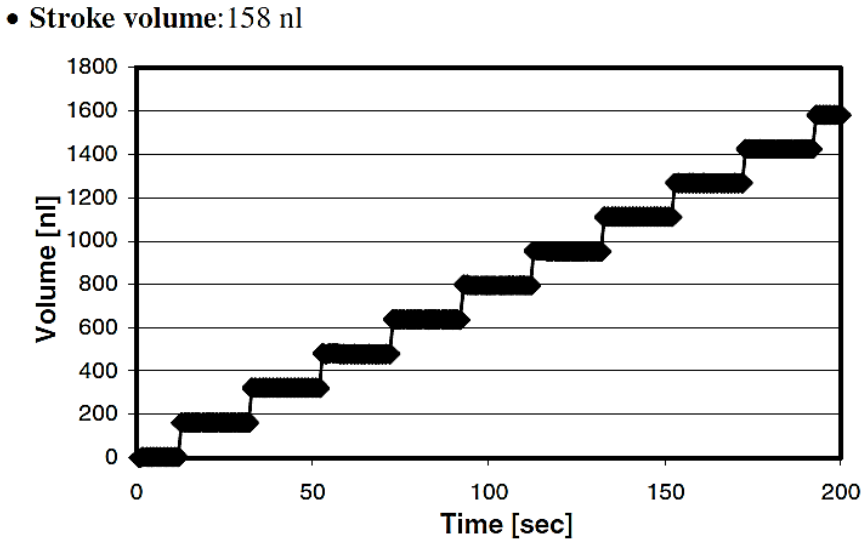

Figure 2.13 Volume - Time [3]

Figure 2.14 shows a plot of the stroke volume as function of the actuation frequency. This characteristic shows that the stroke volume is almost constant, i.e. the flow rate is proportional to the frequency up to approximately 3 Hz, corresponding to a flow rate of 1.7 ml/h or a maximum of 2 ml/h in the non-proportional range.

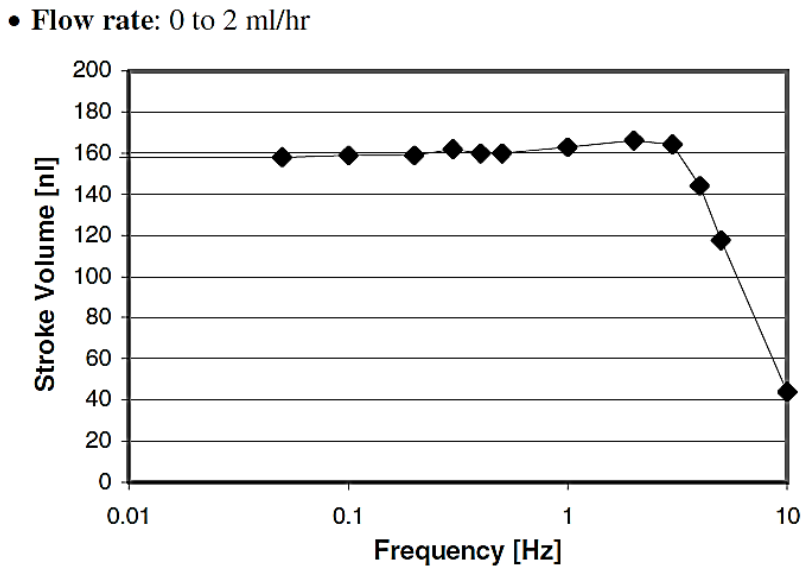

Figure 2.14 Stroke Volume - Frequency [3]

Figure 2.15 shows a plot of the stroke volume as a function of outlet pressure showing the relative insensitivity towards variations of pressure up to 200 mbar. Note that the upper limit of outlet pressure essentially depends on the power of the actuator. This pump chip has demonstrated consistent stroke volume with pressure up to 1 bar.

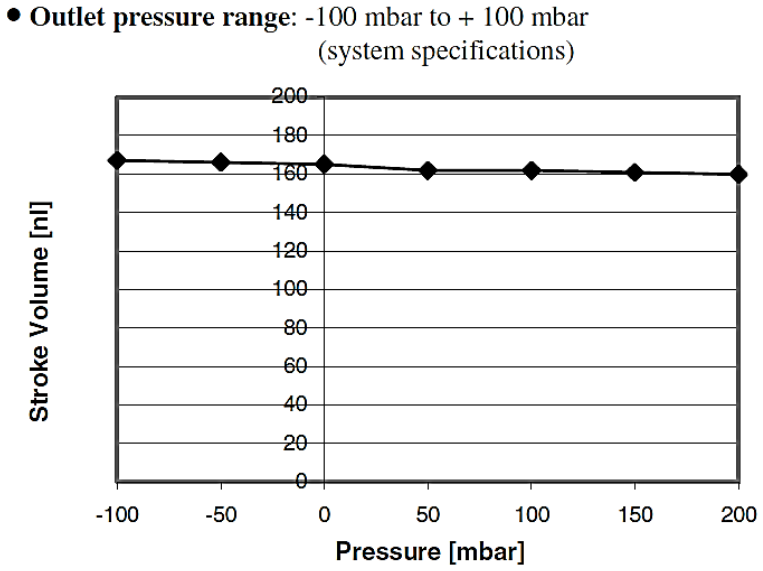

Figure 2.15 Stroke Volume - Pressure [3]

Figure 2.16 shows a plot of the stroke volume as a function of inlet pressure showing the relative insensitivity towards variations of pressure. Note that the upper limit of inlet pressure depends on the pretension of the outlet valve, after which the pump is in free flow mode.

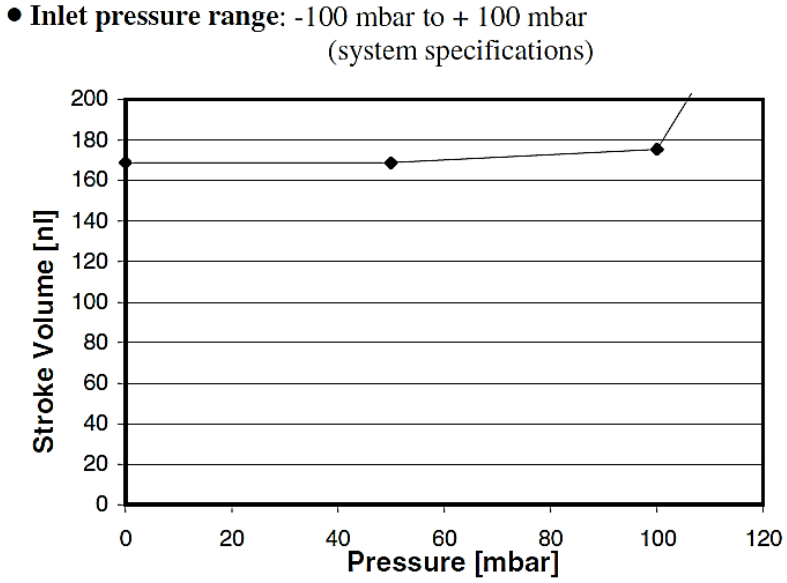

Figure 2.16 Stroke Volume - Pressure [3]

Other characteristics:

• **Leakage**: The leak rate of the pump has not yet been properly characterized. However, tests on functional pumps with pressurized inlet (+50 mbar) and outlet (+100 mbar) have not revealed leak rates higher than 1 µl/h, which is sufficient for the required accuracy.

• **Viscosity**: The application require that the chip pumps liquids of various compositions at temperatures ranging from 5°C to 40°C within the nominal accuracy and without compensation table. This can be achieved because of the double limiter concept. This capability was already demonstrated by the previous generation of pump [1] up to 10 mPa.s .

• **Accuracy**: We expect this pump to meet the required overall accuracy of ±5% within the specified conditions.

• **Longevity**: The expected lifetime of this pump chip used in a disposable drug delivery set is limited to a few weeks. However, for alternative applications, this requirement will likely be extended up to one year. Although this longevity has naturally not yet been demonstrated on this chip, we have acquired reliability data for almost two years with the previous generation of pump (Figure 2.17) [3]

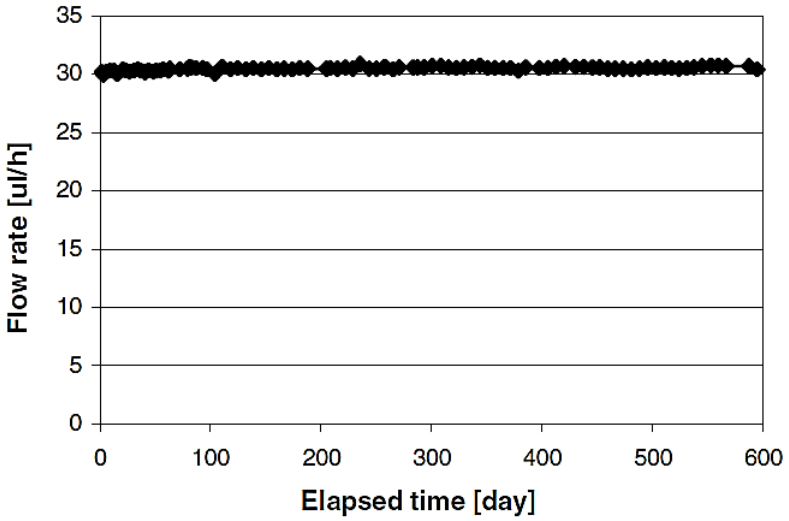

Figure 2.17 Flow rate – Elapsed time [3]

In Figure 2.20 a plot of the flow rate stability of the micro-pump is shown. The actuation frequency is 0.05 Hz and the sampling period is one week.

• **Drug compatibility**: The materials in contact with the drug are exclusively silicon, silicon dioxide, Pyrex glass and titanium, all known to be biocompatible. For a variety of drugs with a pH ranging from neutral to extreme acid, drug compatibility is ensured as follows:

- No damage (corrosion) to the device

- No damage to the PAI (Pharmaceutically Active Ingredient)

- No release of toxic products in the drug.

2.4.2 PZT Drug Delivery Pump

Figure 2.18 shows a Piezoelectric pump based on the design published by Van Lintel [1]. The working principals is very similar the volumetric pumps that was addressed before. The piezoelectric element made from quartz, Li TaO3, PZT or ZnO that is bonded to the membrane with a conductive silver epoxy. It has cantilever valves to prevent leakage. There is a micro-needle set attached to the pump output [4].

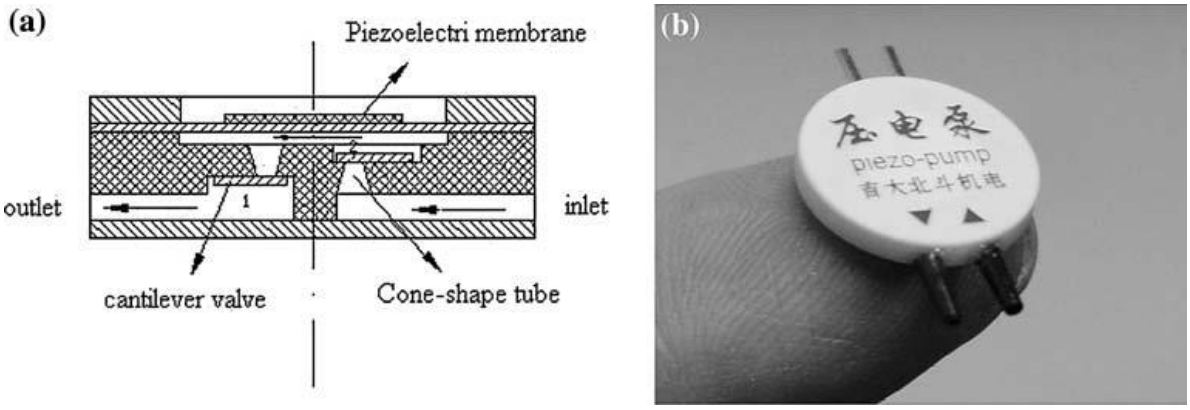

Figure 2.18
(a) Schematic design of the piezoelectric pump
(b) PZT pump compared to a forefinger [4]

Figure 2.19 shows the device set up for the pump included with the reservoir and micro-needle array.

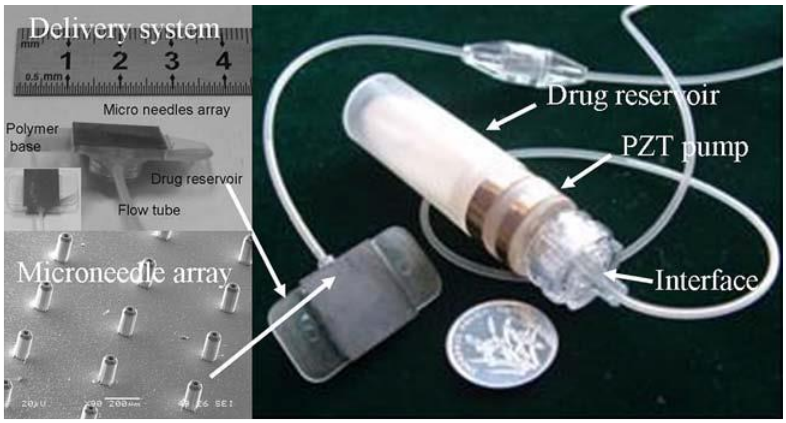

Figure 2.19 PZT Device set up [4]

Performance review:

Figure 2.20 shows the relationship between flow rate and back pressure for this pump. Flow rates are increasing at the beginning with frequency but then the flow will stall when frequency goes beyond 250 Hz for this particular pump design. Seems the cantilever check valves won't work properly in higher frequencies which is predictable due to dynamic nature of high frequency turbulent flows with high Reynold numbers. At the same frequency with increasing the back pressure, flow rate would drop.

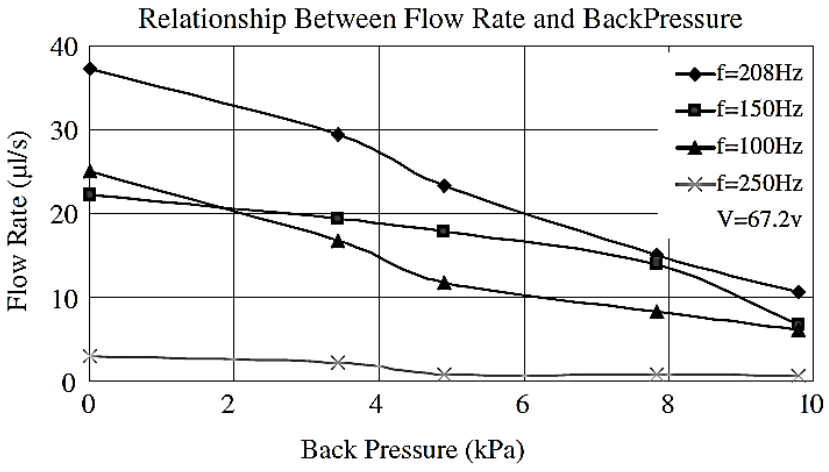

Figure 2.20 Flow rate – Back Pressure [4]

In Figure 2.21, we see flow rate will increase with voltage in any given frequency. Pump performance shows that right after 67.2 Volts, flow rate stays constant. This voltage presents an optimum value for maximum pump flow delivery.

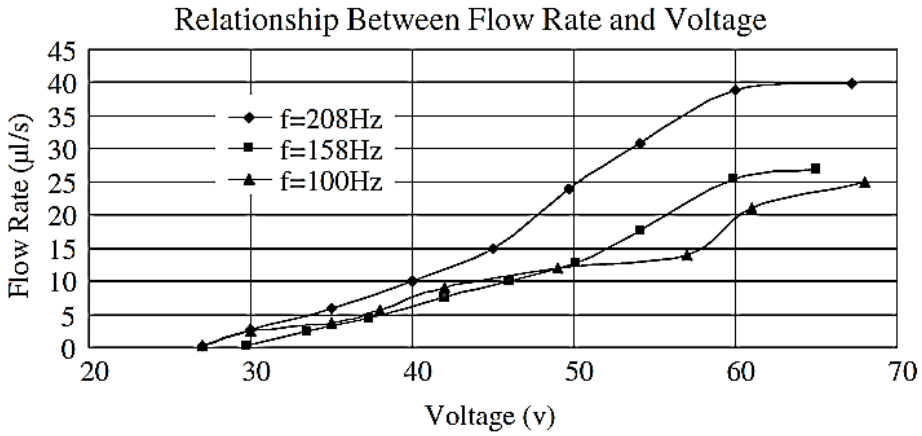

Figure 2.21 Flow rate - Voltage [4]

Figure 2.22 shows the pump flow delivery for 67.2 volts at different frequencies. Again, flow rates drop after 250 Hz. For the same reason the performance of this type of pumps rather than simulation works, should be tested experimentally to find the accurate frequency stall point [4].

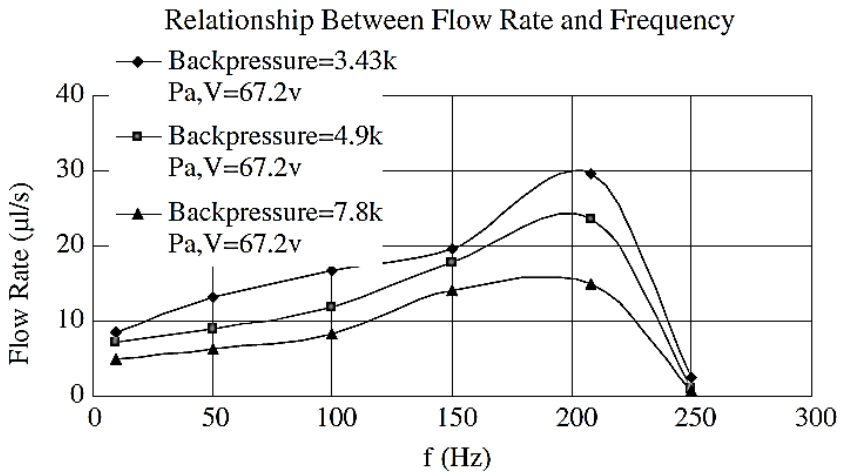

Figure 2.2 Flow rate - Frequency [4]

2.4.3 High Frequency PZT Micro-Pump

Some studies provide the high frequency performance of piezoelectric micro-pumps. Figure 2.23 shows the design and concept of this pump.

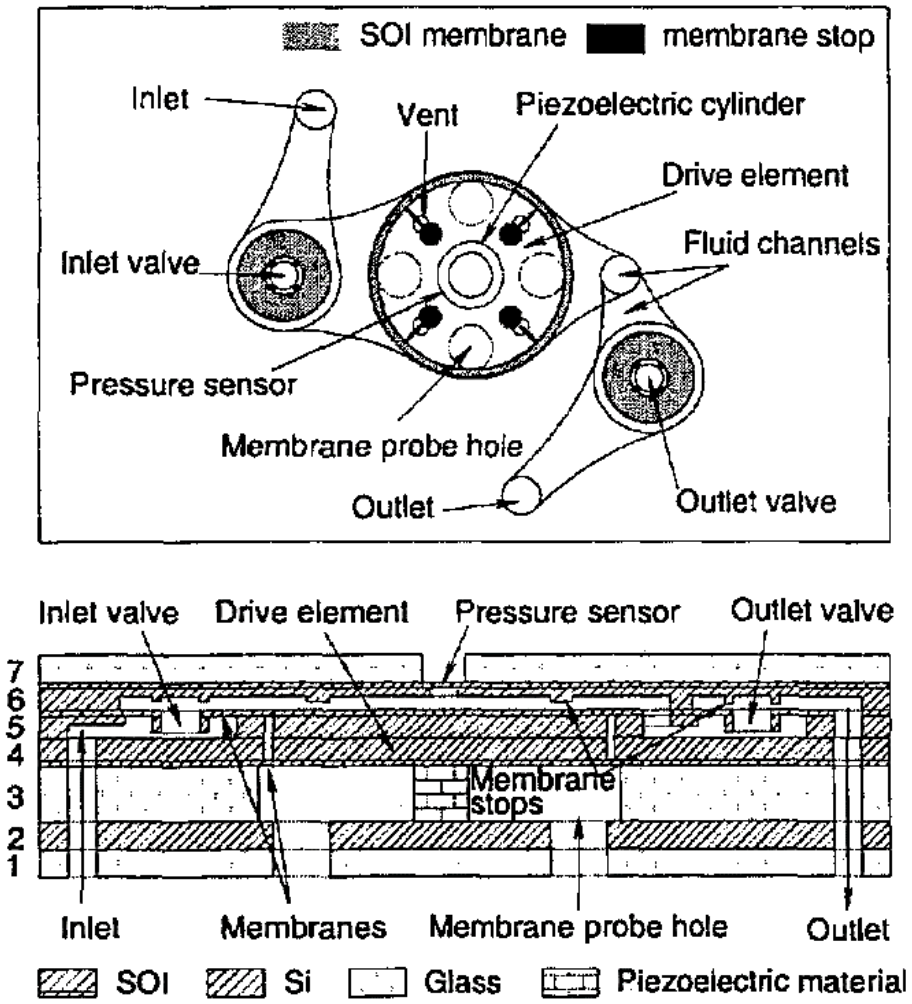

Figure 2.23 High frequency PZT pump [15]

Figure 2.24 shows that the performance behavior of the pump should be carefully investigated for high frequencies although it shows quite linear nature in first levels of frequencies [15].

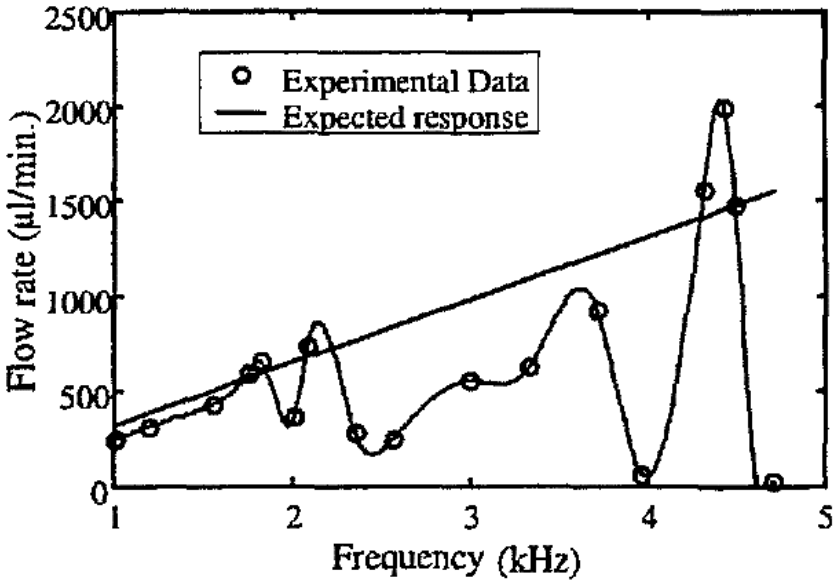

Figure 2.24 Flow rate vs frequency for 1200 V peak-to-peak voltage and zero pressure differential. [15]

Generally with increasing pressure, flow rate drops and simply with increasing voltage, flow rate increases.

2.4.4 Valveless Micro-Pumps

There are several studies out there showing design and application of valveless concepts. One of the greatest reviews is shown in figure 2.25 below.

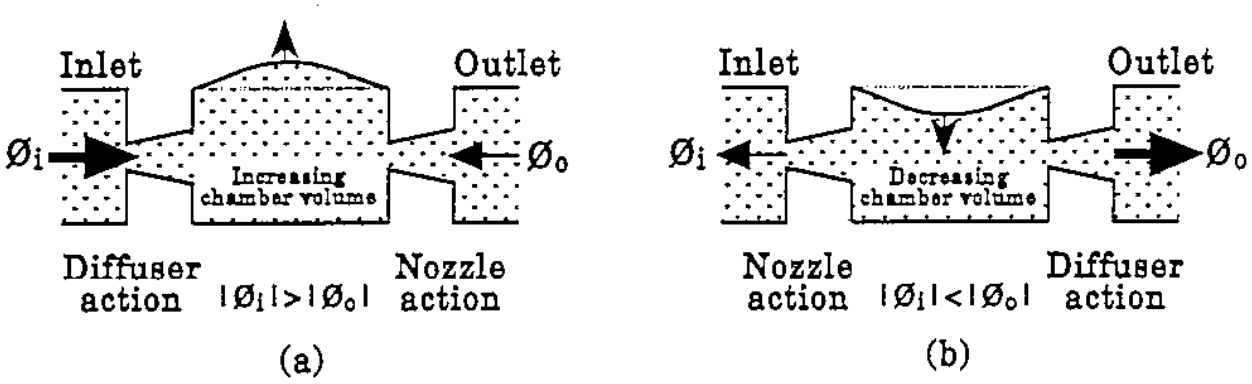

Figure 2.25 - Diffuser-based pump (a) Supply mode, (b) Pump mode [16]

Figure 2.26 shows an anti-phase double-chamber concept.

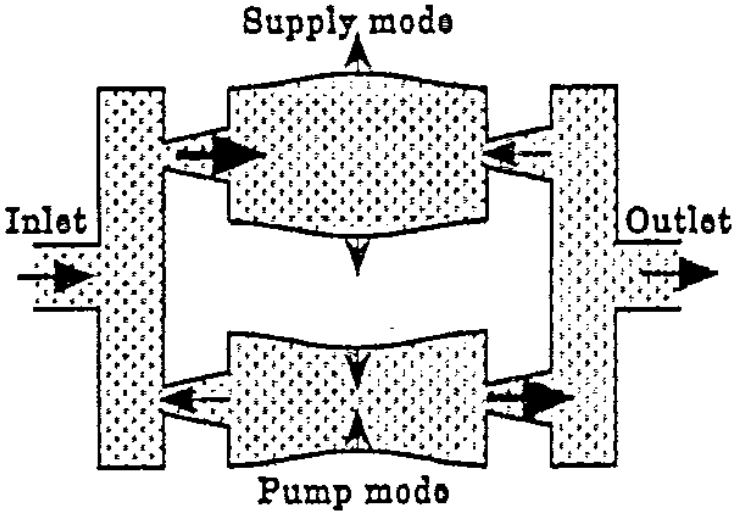

Figure 2.26 Push-pull anti-phase operation of the parallel arrangement of a double-chamber diffuser pump with four diaphragms. [16]

In this concept, micro-dynamic diffusers are used to control fluid flow direction. The concept mostly works for higher frequencies and is very sensitive to increasing backpressure. Leakage and volumetric efficiency are the main problems for these type of pumps for administering insulin and since the needle head of our insulin pump is involved with blood network of skin, the back flow of blood/insulin mix to the main cavity is possible which creates problems for pump during time regarding performance and accuracy. Both flow and pressure increase with increasing diaphragm amplitude.

The maximum flow rate at zero pump pressure is a function of diaphragm amplitude for anti-phase operation. Pressure will increase with diaphragm amplitude at zero volume flow in the similar way.

In any given voltage, with increasing the pressure, the outflow drops quickly to almost zero level. In figure 2.27, the high frequency nature of micro-diffusers is shown. Micro-diffusers are dynamic gates and they do not perform cooperatively in low frequencies.

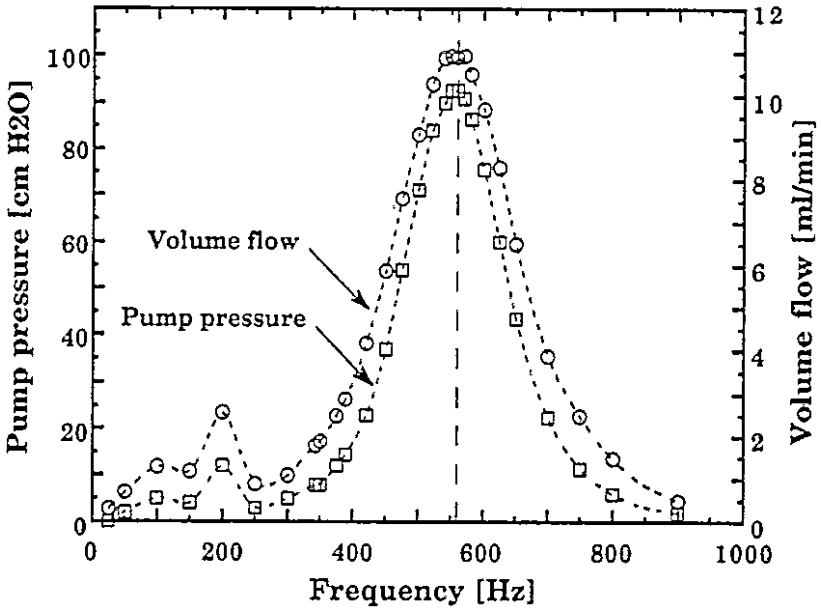

Figure 2.27 Maximum Flow (at zero pump pressure) and maximum pump pressure (at zero volume flow) versus diaphragm exciting frequency for double-chamber pump with anti-phase operation for 80V peak-to-peak exciting voltages. [16]

And eventually in Figure 2.28, stationary pressure-flow characteristics are shown for the diffuser and nozzle directions of the double-chamber pump with anti-phase operation, at no diaphragm activation. The diagram shows that with the same pressure drop, the volume flow is more for a diffuser direction than a nozzle direction. That is why more fluid will supply in during supply modes, more fluid will pump out during pump modes.

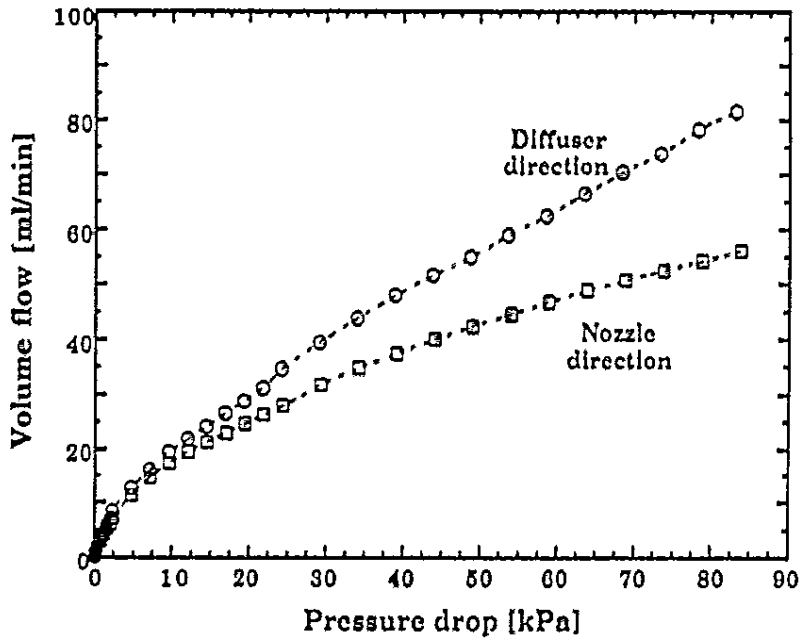

Figure 2.28 Stationary pressure-flow characteristics for the diffuser and nozzle directions at no diaphragm activation. [16]

In Figure 2.29, a simulation study [17] shows variation of inflow/Outflow with time. The simultaneous overlapping the supply and pump modes shows the existing of excessive leakage. This type of the pumps are good for fluid transferring but they are not recommended for insulin administering.

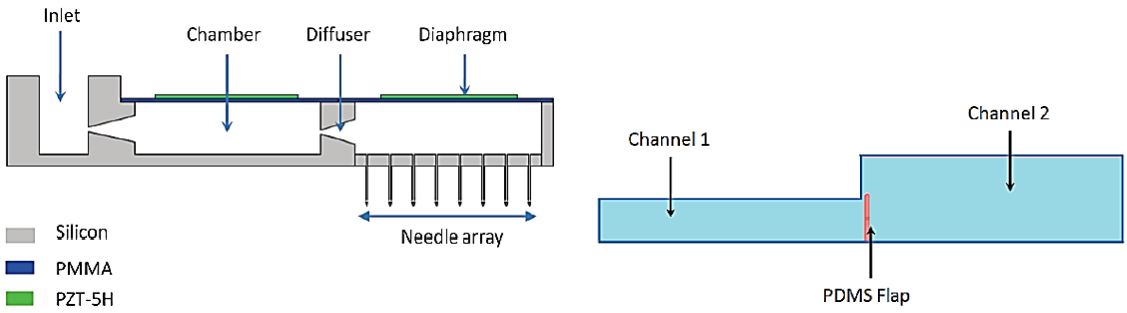

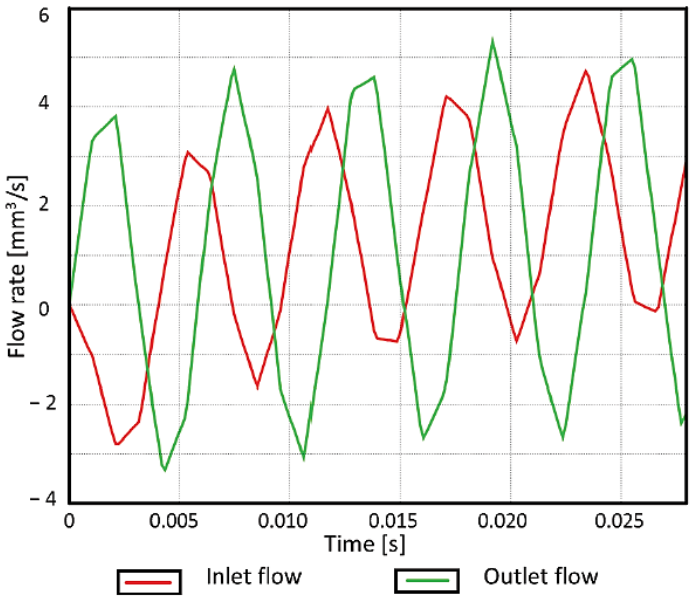

Figure 2.29 Typical inflow/Outflow versus time for Valveless diffuser-based pumps. [17]

One of the best applications for valveless micro-pumps is to use them as a series of connected pumps to create a Peristaltic Micro-pump [18]. Figure shows a schematic diagram of a portable valve-less peristaltic micro-pump (Figure 2.30).

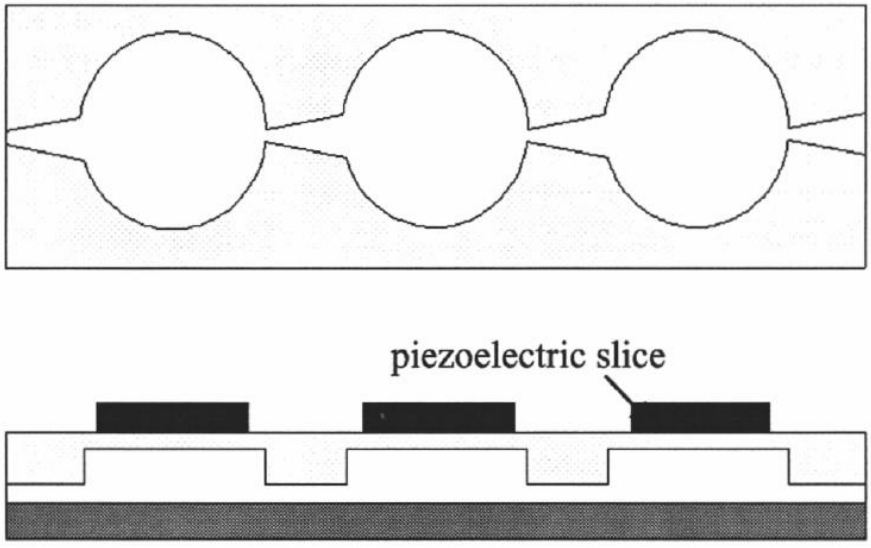

Figure 2.30 A schematic diagram of a portable valve-less peristaltic micro-pump. [18]

2.5 Motivation and Objectives

The traditional methods of insulin administration need multiple shots per day and it is significantly inaccurate. The manual injection is also very painful. Pricking yourself and sticking yourself with a needle up to 8 times a day is far from optimal. Each insulin shot also causes a shock to the system and can cause a cumulative, negative effect on the organs of the body. Most of the insulin pumps available in market are single needle mechanical pumps which are heavy and painful. The other types of PZT insulin pumps, although provide an optimized design size but still not robust enough for day to day activities because the micro-needle array is not integrated to the pump main body. We have proposed a stackable/integrated micro-needle concept that makes the completed pump assembly patchable to any flat area of human skin. Therefore, the objective of this study is investigating the possibility of an insulin administration, as a MEMS-based micro-pump, which mimics the natural function of the pancreas. With a real time controlling the blood sugar and insulin injection, "shock to the system" will be minimized. Providing electrical source of energy (batteries) is always an issue for packaging and system reliability. Using independent advance technology in Energy Harvesting will help the system to be run for ever without any needs to change the batteries. With miniature insulin micro-pump integrated with micro-needle array patch and energy harvesting units, more normal physical activity will be provided for the diabetes patients.

In this feasibility research, we have successfully proposed packaging of a piezoelectric micro-pump integrated with micro-needles array. The size of our designed and packaged pump system is smaller than the other mechanical systems. The size of the pump system has a diameter of 15 mm with the thickness of Max 2.1 mm (almost 2.5 mm with cover patch). The final applying patch

would be in the size of adult hand palm including the integrated pump/needle array/computer system/insulin reservoir/energy harvesting systems and secured RF communication system. Comparing to the old designs, the new proposed design is energy independent, is much lighter, gives the patient more comfort in day to day activities and is easy to relocate to other areas of skin if necessary (Figure 2.31, 2.32 and 2.33).

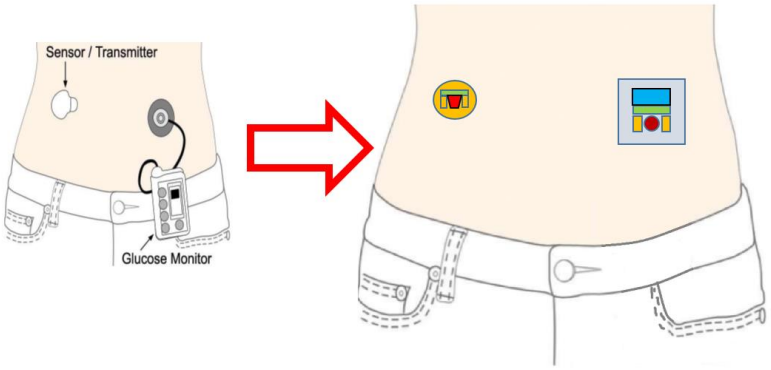

Figure 2.31 Integrated Glucose sensor and insulin Pump and Micro-Needle Patch

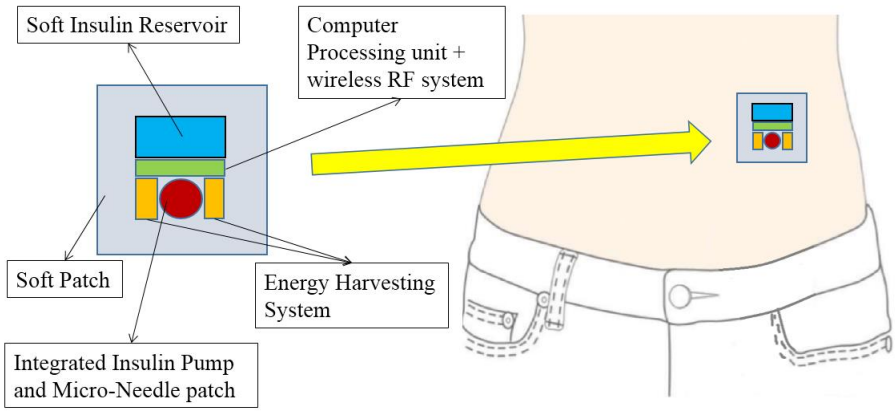

Figure 2.32 Integrated insulin Micro-Pump and Micro-Needle Patch

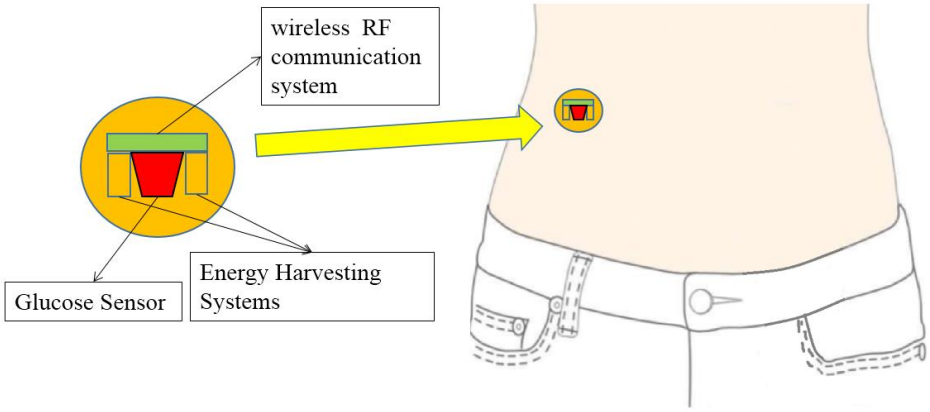

Figure 2.33 Integrated implantable Glucose sensor

Based on the medical experimental facts that were mentioned before, the insulin Pump must be able to deliver a flow range of about above zero to at least 0.5 µl/min for full range of human weights (infant to 250 kg weight).

The pressure targets as previously showed, are any pressure above 3 mmHg (400 Pa) as maximum interstitial fluid pressure in human skin.

Our focus in this study is only on Design and Simulation of the micro-pump in respect to application feasibility and performance. Glucose sensor and Processing/RF unit can be investigated as future studies.

CHAPTER 3: Design and Specification

3.1 Piezoelectric Micro-pump concept design

The main concept of the proposed micro-pump is a positive displacement MEMS-based Piezoelectric-activated micro-pump with two flapper check valves. The concept is based on Vin-Lantel [1] micro-pump original design with some modifications. The micro-pump is designed specifically for diabetic patients who need basal insulin administering on their skin. The micro-pump design is based on the minimum dosage requirement for diabetic patients. It has a main chamber with piezoelectric actuator attached above it on the diaphragm and two flapper check valves and micro-needle array attached to the main body. Compared to other proposed pumps in existing literature, the micro-needle array is attached to the main pump section and the stackable concept leads to reduced dimensions in this design.

3.2 Flow/Pressure targets

In general, approximately one-half of the TDD (Total Daily Dose) is administered as basal rate. For most patients, basal rates are in the range of 0.01 to 0.015 units per kg per hour. For example, a 60 kg woman approximately needs 0.6 to 0.9 units per hour (0.116 µl/min). The basal rates are adjusted empirically based on glucose monitoring results [7]. This means for different range of patients from infant to an adult person with obesity and 250 kg weight, based on the required basal rates for type 1 diabetics patients, the designed insulin pump must be able to deliver a flow range of zero to above 0.5 µl/min and this is our design target for this micro-pump.

According to study that is mentioned earlier [8], any pressure over +3 mmHg (about 400 Pa) is feasible for an affective injection. However, the pump is designed to maintain the pressure far above this target to ensure reliable performance.

3.3 General Dimensions and Materials

The general dimensions (Figure 3.1) of the pump with substrate structure is up to 15 mm in diameter and 2.35 mm in height (thickness) including main chamber and any required structure and covers around it. The designed hollow micro-needles are 200 µm in length and 30 µm in diameter at the pitch of 500 µm.

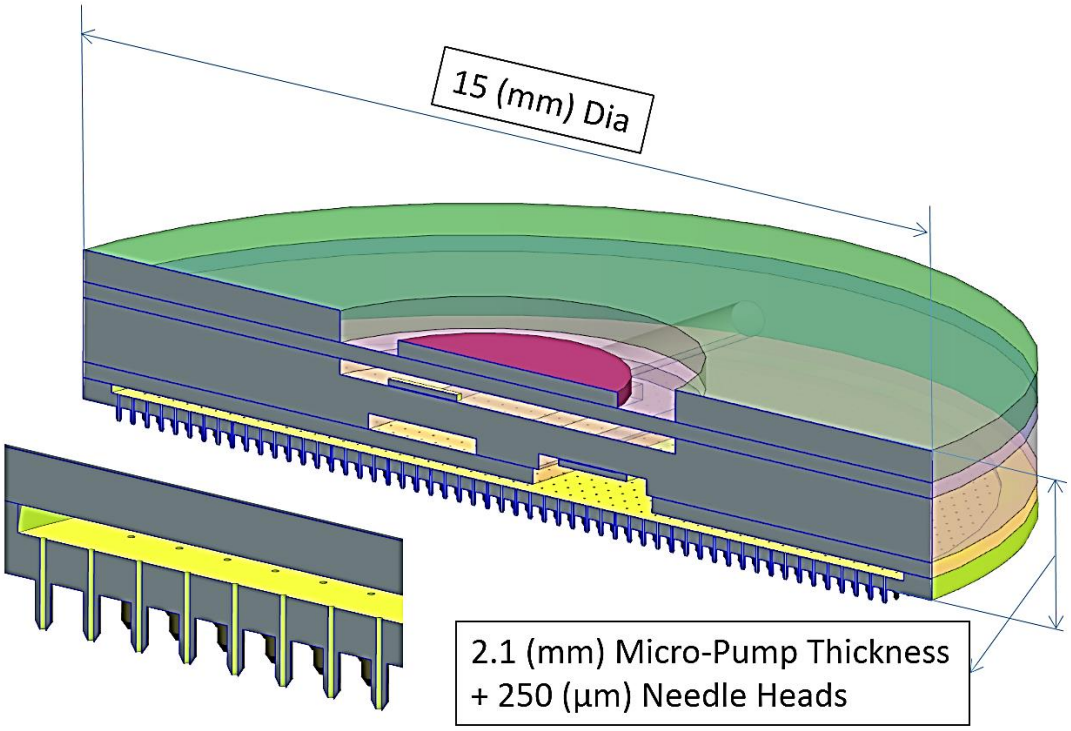

Figure 3.1 General dimensions and a cross section of micro-pump and micro-needles.

Figure 3.2 shows the input/output direction of the micro-pump. The insulin is taken from side input gate and goes out from micro-needle to the dermis layer of the skin.

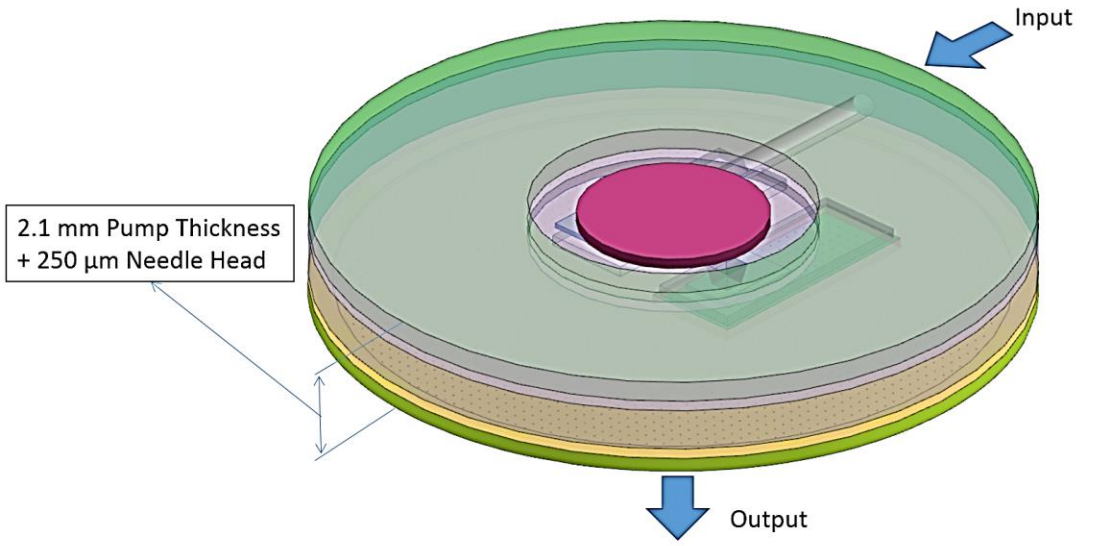
Input
2.1 mm Pump Thickness
+ 250 µm Needle Head
Output

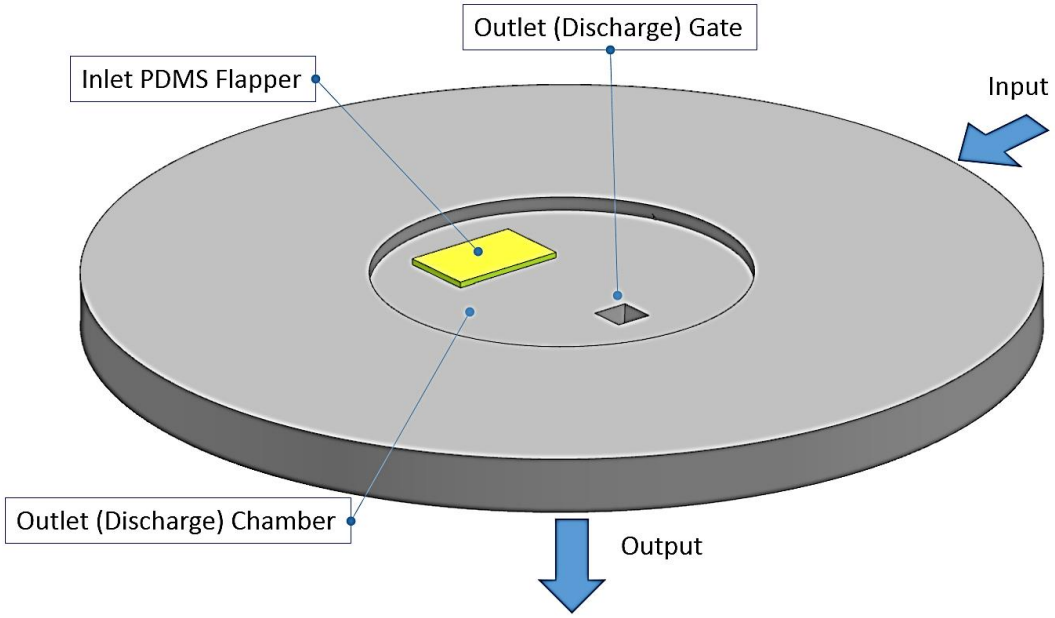
Outlet (Discharge) Gate
Inlet PDMS Flapper
Input
Outlet (Discharge) Chamber
Output

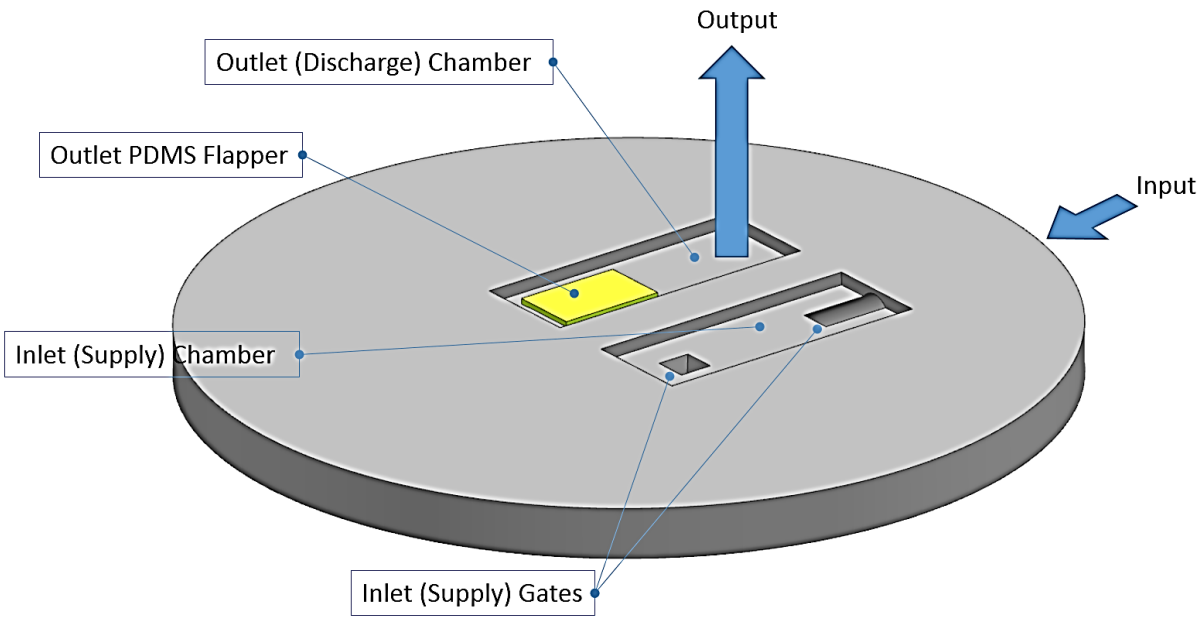

Figure 3.2 General dimensions and layout of Supply/Discharge process of micro-pump

The main frame/structure material is a Silicone based solid. The diaphragm disk is made of Silica glass. The Piezoelectric material is Lead Zirconate Titanate (PZT-5H). PDMS - Polydimethylsiloxane is used for check valve flappers. The thickness of PDMS flappers is 10µm, and the cantilever length is 100 µm. PDMS is a highly elastic polymer material and therefore is very durable [24]. PDMS is the best choice for flapper valve applications. The fabrication method can be as simple as epoxy gluing or MEMS technology methods as "soft lithography" method [25]. The micro-needle array substrate is made of solid Silicone through a deep-reactive ion etching (DRIE) manufacturing method [4]. Figure 3.3 shows the pump stack up layers. The main Si wafer as the pump main body and micro-needle array are fabricated based on MEMS technology and are epoxy glued to the rest of the layers [4] (Figure 3.3).

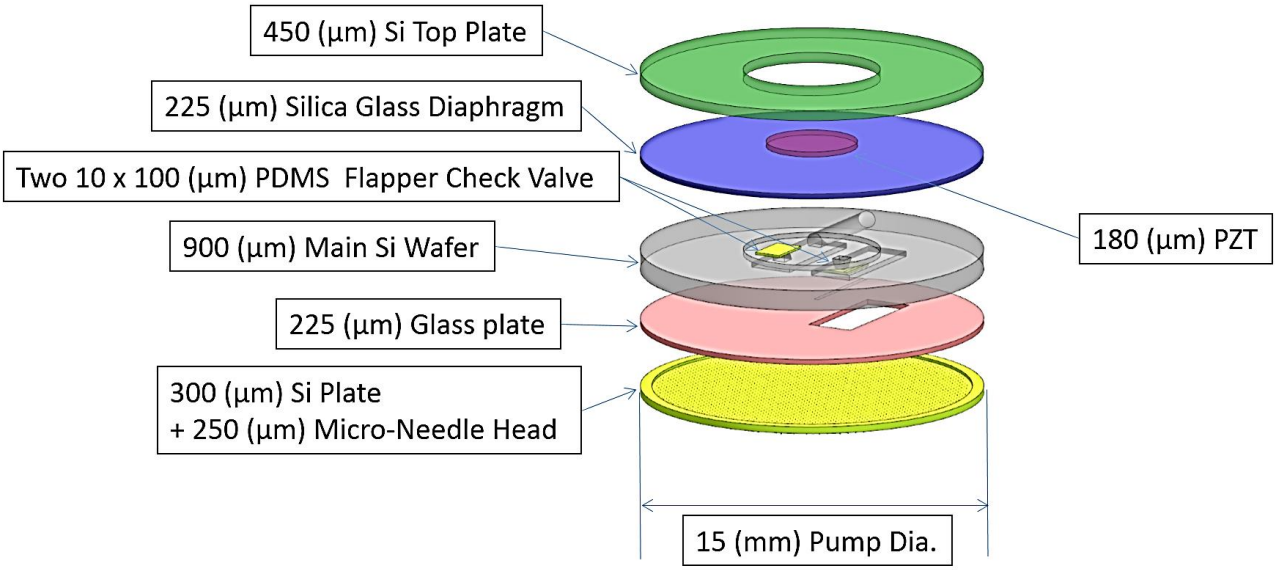

Figure 3.3 Micro-pump materials specification

Silicon and Silica glass are the best practice materials for basic MEMS substrates [21]. Silicone is an easy to etch and micro-machining and is an excellent candidate for MEMS structure. Silica Glass is the best material for vibrating diaphragm concept. It has higher module of elasticity and toughness and resists and endures well through cyclic load. PZT-5H has the maximum deflection to voltage among all materials in COMSOL material library. This is essential to minimize the maximum required voltage for required outflow. Some experimental studies [4] use Silicon or Silicon Glass for the flapper check valves. Silicon glass perform perfectly for higher pressures/frequencies but for lower pressure/outflow application softer materials as PDMS work better. PDMS is the best material for low frequency/force/flows when we try to reach minimum flow delivery in such application as insulin administration.

3.4 Micro-pump's working principals

The MEMS based positive displacement insulin micro-pump has a Piezoelectric Actuator on top of a diaphragm membrane made from Silicone glass. Induced vibrations from PZT actuator create positive/negative volume in the pump's main chamber, which pull fluid from Inlet gate and pushes it toward outlet gate. The gating process is governed by two PDMS Flapper check valves that control the fluid flow direction from inlet toward the outlet which leads to an array of micro-needles. A distributer connects the outlet gate to micro-needles substrate, and finally, the established discharge pressure pushes the fluid out of Silicone micro-needle array to skin epidermis, right above skin dermis layer.

Anisotropic wet etching techniques will be used to create the main pump cavity. The rest of layers will be assembled by stack up gloving technics to the main silicone body. We will also use conductive silver epoxy bonding to attach piezoelectric actuator to the pump diaphragm.

Deep reactive ion etching (DRIE) technique will be used to manufacture micro-needle array out of a silicon wafer.

There are many studies providing different design and manufacturing techniques for needle shapes. Figure 3.4 shows one of the best designs for micro-needle. It is an array of hollow, metal micro-needles next to a 27-gauge hypodermic needle. The micro-needles taper from a 300 µm base to a tip diameter of 75 µm over a 500 µm length and are arranged in a 4x4 array (i.e., 16 needles). Arrays of this geometry were used for insulin delivery experiments. Image is coming from a scanning electron microscopy. This method uses Laser micro-machining and nickel electrodepostion techniques [19].

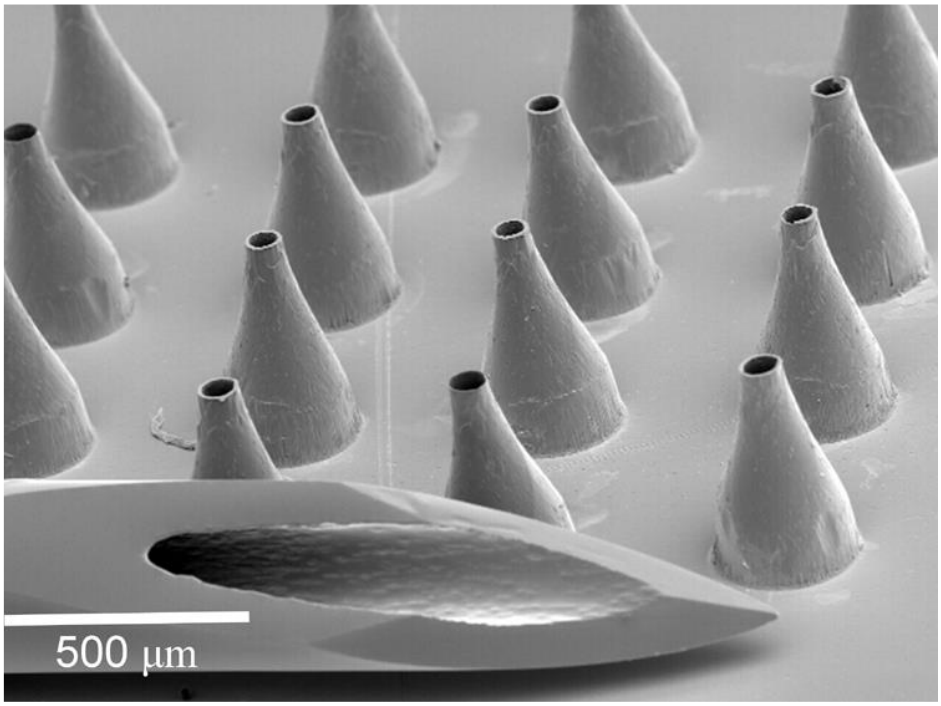

Figure 3.4 Nickle electrodeposition, hollow metal micro-needle array [19]

Another study (Figure 3.5) provides a MEMS-based micro-needle array designed and fabricated by employing a bi-mask technique to facilitate sharp tips, a cylindrical body and side ports. The array has advantages like ease of fabrication and bonding, and high needle density and robustness. In addition, the micro-needle comprises side ports which minimizes the potential for clogging. This micro-needle array can be used for fluid extraction and drug delivery systems; e.g., biological sampling, and insulin delivery into the human body [20].

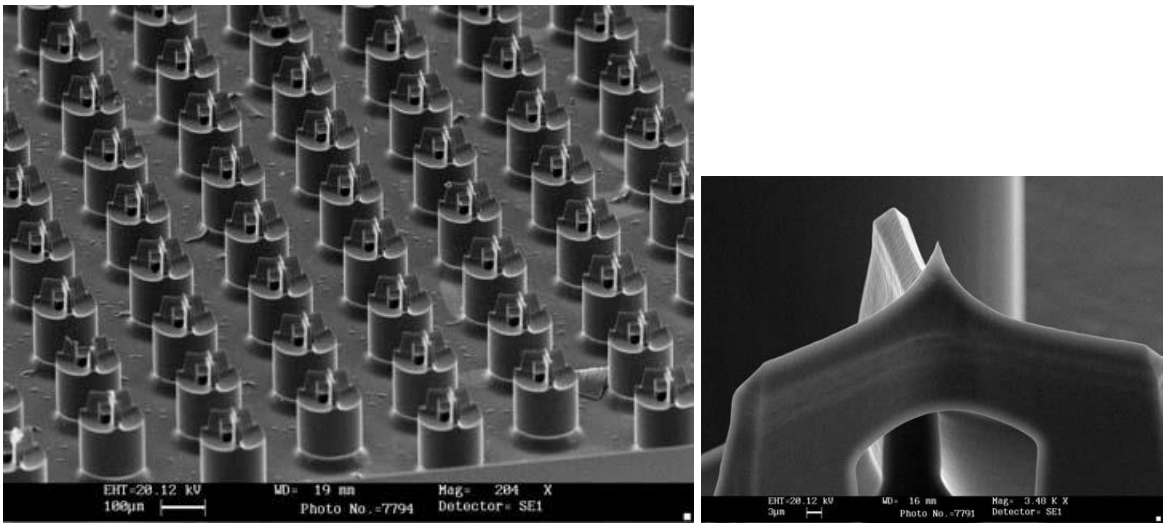

Figure 3.5 MEMS-based micro-needle array [20]

For the purpose of this study we use Figure 3.6 concept based on an experimental study [4] that uses a MEMS-based concept of micro-needle array created on a silicone wafer with DRIE (deep-reactive ion etching) method to create needle main cylinder and Anisotropic wet etching techniques to obtain sharp edges in the needle tips [4].

In figure 3.7 a 3d model that has been designed based on this concept is shown.

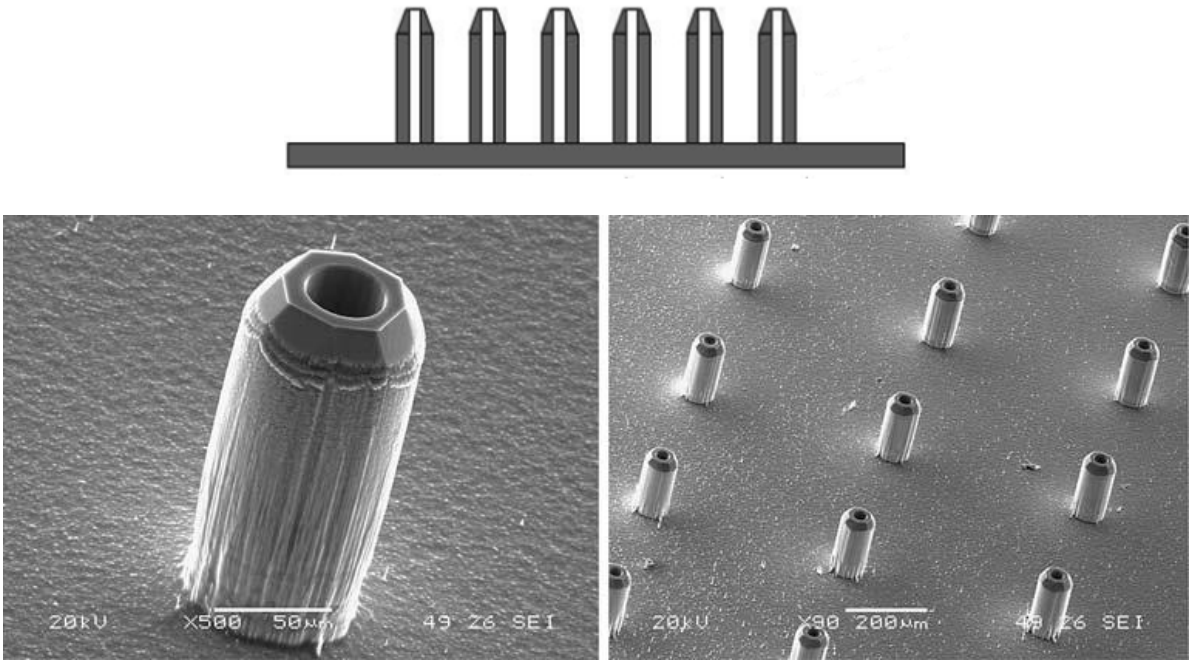

Figure 3.6 MEMS-based micro-needle array [4]

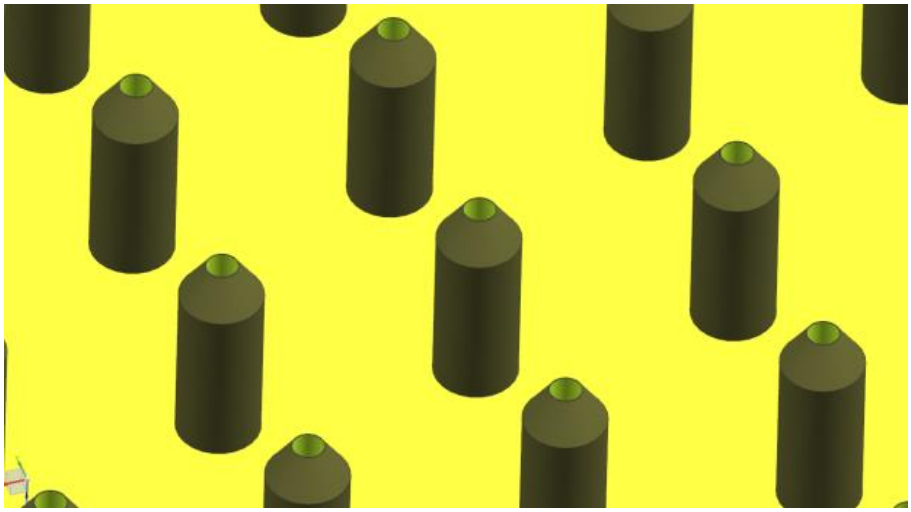

Figure 3.7 Micro-needle 3D created model

We use an array of 30 hollow micro-needles (5 x 6 rows) with 200 µm in length and 30 µm in diameter at the pitch of 500 µm. 30 needles are enough for a flow rate of zero to 0.5 µl/min for an insulin administering device. For simulation purposes, there is no difference between micro-

machined metal-based or MEMS-based silicon micro-needle arrays but in practice metal-based micro-needle are more reliable and durable for these type of applications.

3.5 MEMS-based micro-pump fabrication

Although our focus in this study is not the manufacturing techniques of fabricating this micro-pump, however we bring a brief review of the best-proposed manufacturing techniques to make this device. Besides all regular fabrication methods like depositing, masking, litho and wet etching, we also consider advanced methods of fabrication as anisotropic wet etching techniques, deep-reactive ion etching (DRIE), gloving to stack up the layers and conductive silver epoxy bonding for piezoelectric actuator. Figures 3.8 through 3.15 illustrate all stages of proposed manufacturing process of this micro-pump including the main silicon body and micro-needle array [21].

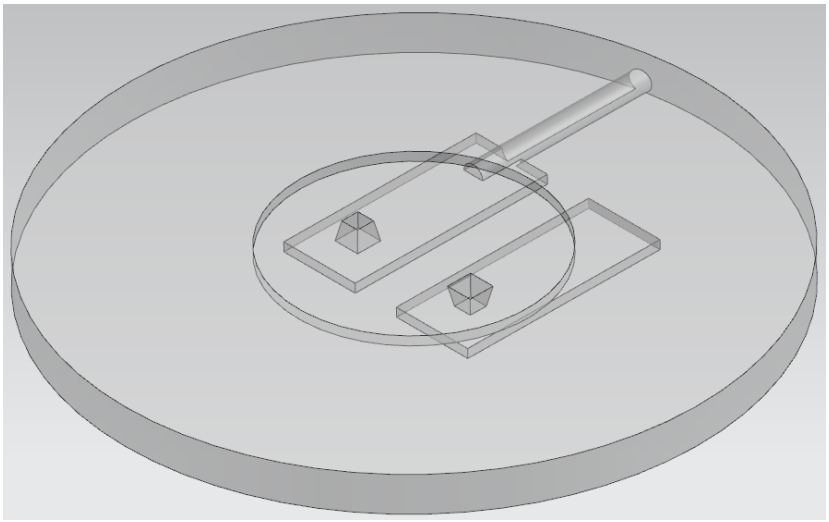

Figure 3.8 Micro-pump fabrication process

Main Si Plate:

1. Masking
2. Litho
3. Wet Etching

4. Micro-Machining

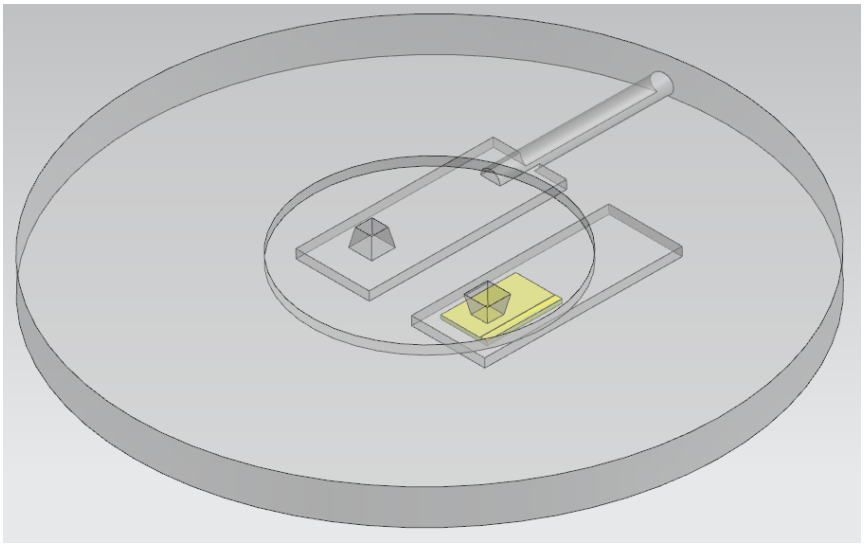

Figure 3.9 Micro-pump fabrication process

Discharge check valve (Si or PDMS Flapper):

1. Depositing
2. Soft Litho (or epoxy glue)
3. Masking
4. Wet Etching

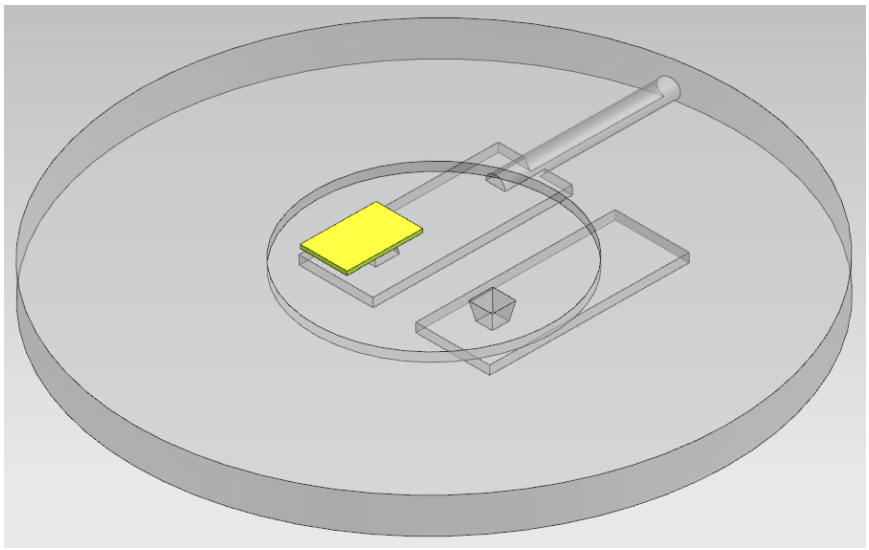

Figure 3.10 Micro-pump fabrication process

Suction check valve (Si or PDMS Flapper) :

1. Depositing
2. Soft Litho (or epoxy glue)
3. Masking
4. Wet Etching

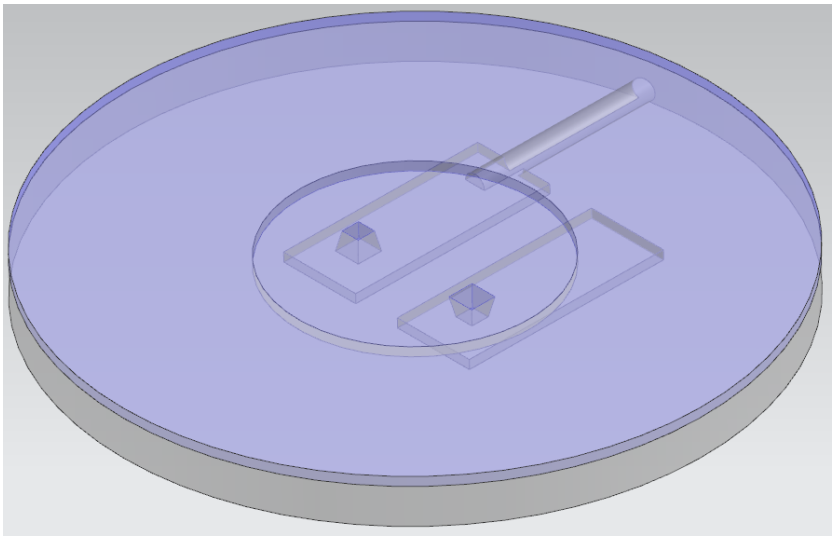

Figure 3.11 Micro-pump fabrication process

Diaphragm glass plate:

1. Micro-machining
2. Bonding

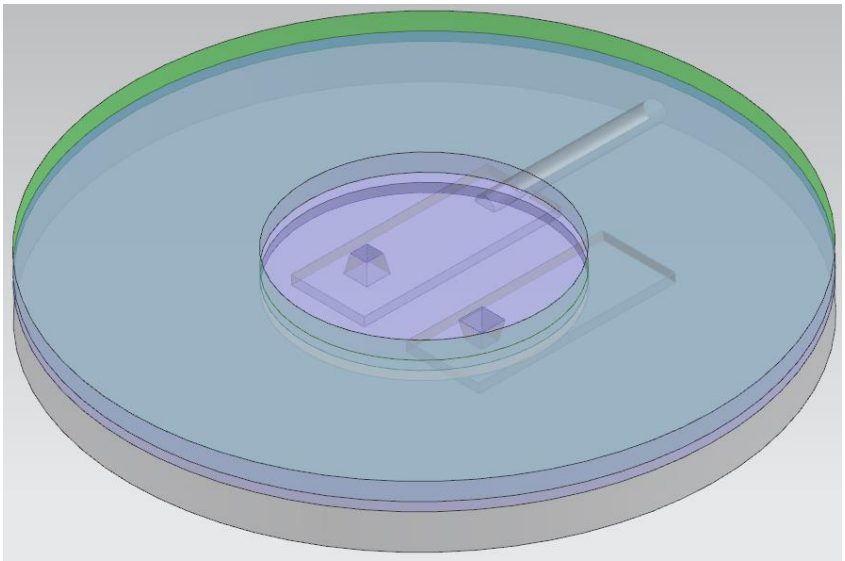

Figure 3.12 Micro-pump fabrication process

Si top plate:

1. Micro-machining
2. Bonding

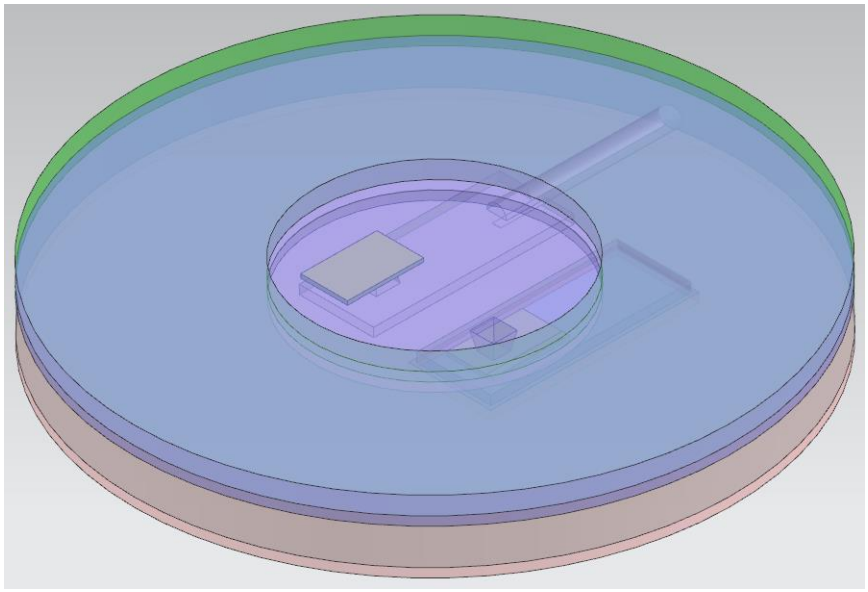

Figure 3.13 Micro-pump fabrication process

Bottom glass plate:

1. Micro-machining
2. Bonding

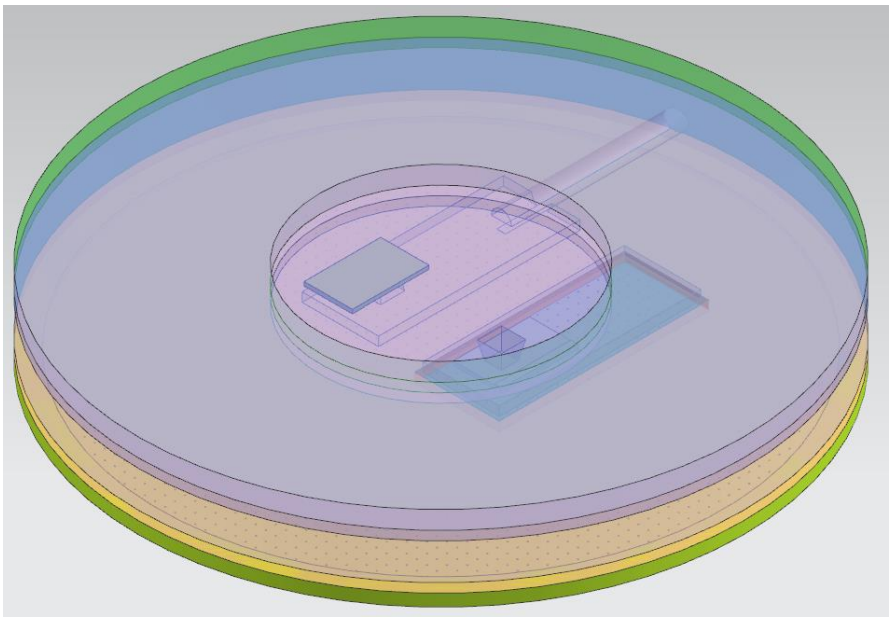

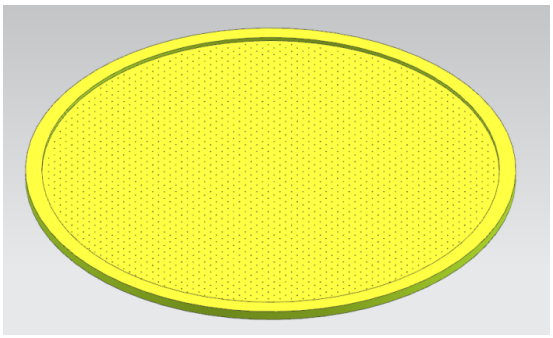

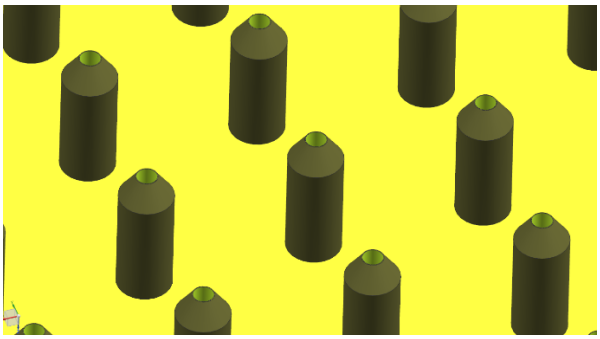

Figure 3.14 Micro-pump fabrication process

Micro-needle array/patch:

1. Masking
2. Litho
3. Wet Etching
4. Anisotropic wet etching
5. Deep-reactive ion etching (DRIE)
6. Bonding

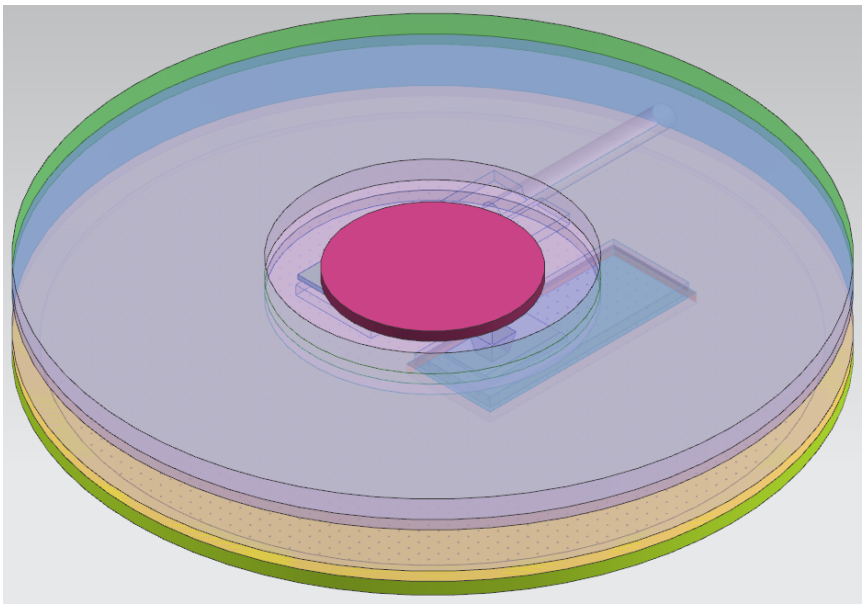

Figure 3.15 Micro-pump fabrication process

Piezoelectric actuator:

1. Conductive silver epoxy bonding

CHAPTER 4: Theory and Data Analysis

4.1 Introduction

The design of positive volumetric insulin pump is significantly a multiphysics problem where the volumetric change of the main pump chamber and the amount of pumped fluid are directly coupled. We used COMSOL Multiphysics to investigate the performance of a MEMS based insulin micro-pump with a piezoelectric actuator pumping a viscous Newtonian fluid. The model captures the accumulated out-flow, the netflow or flow fluctuations based on deflection of piezoelectric actuator which moves with the diaphragm disk in positive/negative directions, to induce discharge pressures at micro-needle array based on different input voltages and different exciting frequencies.

Three modules; Structural Mechanic, Piezoelectric Device and Fluid-Structure Interaction were used to study the 2-D/3-D models of this MEMS based concept. Fully Coupling Physics provide real time relationship between different parameters and pump's outputs. Post processing and ODE also are used to create different required outputs.

In following sections, we will introduce the different physics and approaches to model a multiphysics system based on these theories.

4.2 Simulation Model set up

The positive displacement Micro-Pump model is a combination of 3 physics; Structural Mechanics (solid), Piezoelectric Device (pze) based on Electrostatic (es), fully coupled with a Fluid-Structure Interaction (fsi) module. A Laminar Navier-Stokes equation used to simulate this problem.

Figure 4.1 shows a schematic of 2D model of this micro-pump.

A wave signal at specific frequency excites the piezoelectric disk. Diaphragm disk and piezoelectric actuator move together and FSI moving mesh transfers the stress/strain to fluid domain. Moving fluid-mesh follows solid deformation. FSI interface automatically handled by Nonlinear models. With the action of flapper check valve, fluid flows from inlet to outlet. The fluid flow is described by the Navier-Stokes equations with laminar incompressible Newtonian flow and free boundaries at the inlet and outlet. The flapper material in check valves is PDMS which is suitable for a low stress/strain but high cycle applications. We used a standard Hyperelastic material model for this application. At the end, a Two-Way, fully coupled solver was used to calculate the results. Integration coupling variables are used to track the discharged fluid and the volume of the fluid inside the pump. A non-slip FSI boundary is automatically set up along the inner wall of the pump. COMSOL handles the fluid structure interaction using an Arbitrary Lagrangian-Eulerian (ALE) formulation. This involves a Lagrangian framework for the solid and an Eulerian framework for the fluid. A moving mesh model is used to track the deformation of the fluid mesh. The two-way coupling is captured along the FSI boundary by the fluid applying forces on the solid, and the solid displacement imposing a moving wall boundary condition on the fluid.

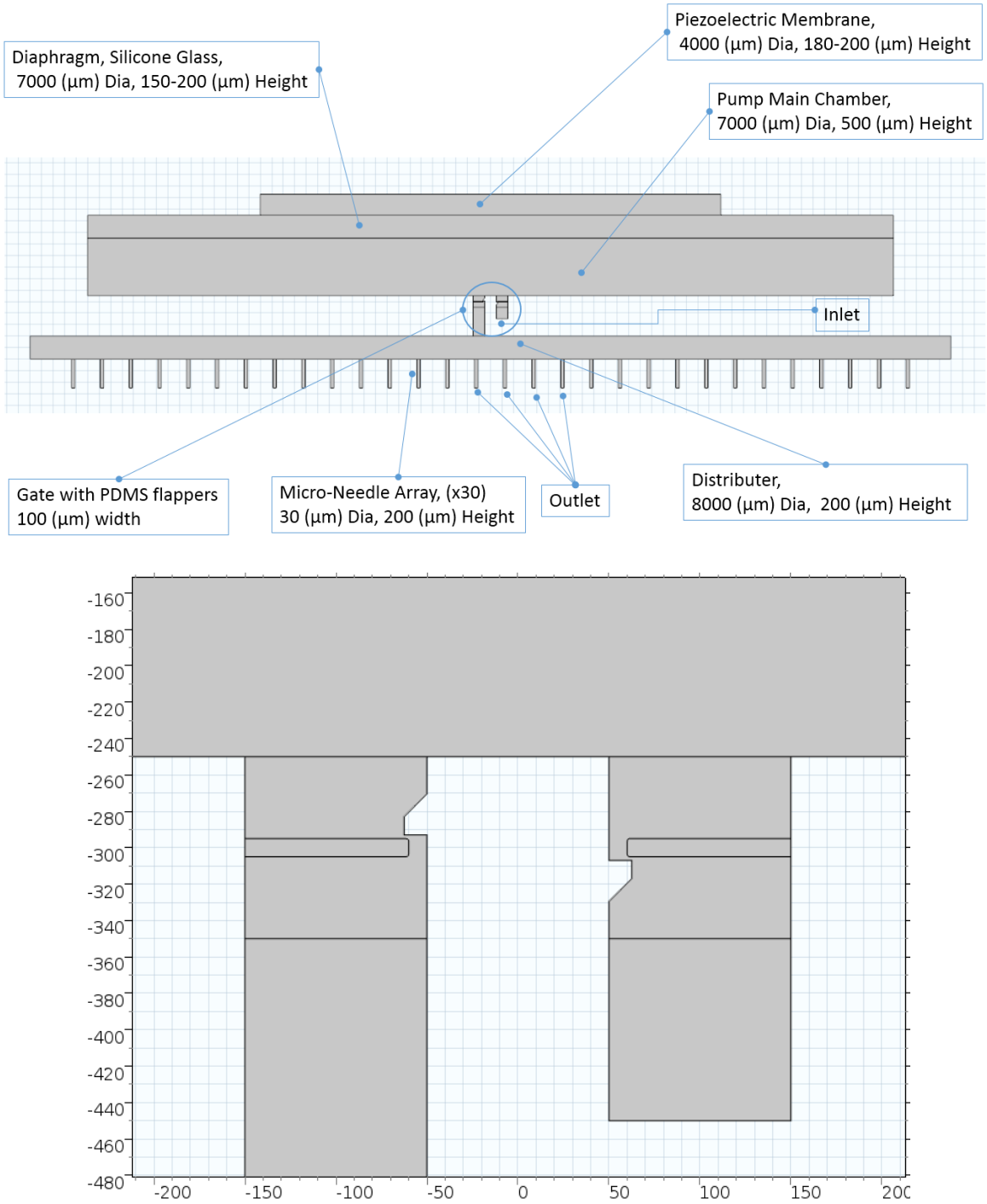

Figure 4.1 Micro-pump 2D simulation model, with a flapper check valves close view

A 3D model is also created to test and verify the accuracy of volume stroke of the 2D set up. Figure 4.2 shows the 3D simulation model of this pump.

Using a 3D model for this simulation with flapper valves and fluid-solid interaction needs many considerations and it is very memory intensive. In order to simplifying the analysis methods and process with same level of accuracy, we combined a 2D model with a 3D verifying model to support output results.

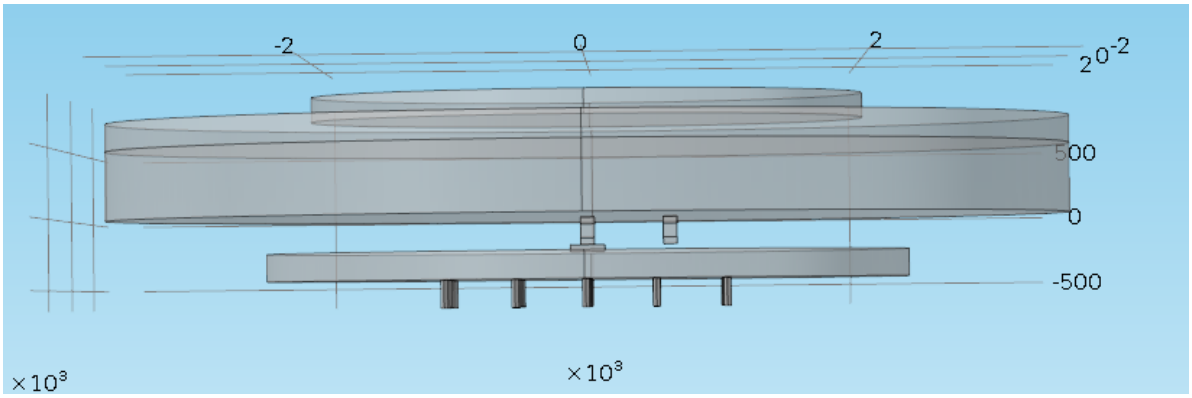

Figure 4.2 Micro-pump 3D simulation model

In this micro-pump simulation model , the fluid flow is described by the single-phase, incompressible Navier-Stokes equations:

$$\boldsymbol{\rho \frac{\partial \mathbf{u}}{\partial t} + \rho \mathbf{u}.\nabla \mathbf{u} = -\nabla p + \nabla.\mu(\nabla \mathbf{u} + (\nabla \mathbf{u})^{T})}$$
$$\boldsymbol{\nabla.\mathbf{u} = 0} \qquad (4\text{-}43)$$

where **ρ** denotes the density (SI unit: kg/m^3), **u** the velocity (SI unit: m/s), **μ** the viscosity (SI unit: Pa·s), and **p** the pressure (SI unit: Pa), **T** the absolute temperature (K) and **t** the time (SI unit: s). The equations are set up and solved inside the pump. The Navier-Stokes equations are solved on a freely moving deformed mesh, which constitutes the fluid domain. The deformation of this

mesh relative to the initial shape of the domain is computed using Hyperelastic smoothing. Inside the solid wall of the pump, the moving mesh follows the structural deformation.

4.2.1 Boundary Conditions at Walls

Boundary Conditions at walls is no-slip (zero velocity):

$$\mathbf{u}_{fluid} = \mathbf{0} \qquad (4\text{-}44)$$

4.2.2 Boundary Conditions at the Inlet and the Outlet

For the fluid simulation, the boundary condition at the inlet and the outlet assumes that the total stress is zero, that is:

$$\mathbf{n}.\left[-p\mathbf{I} + \mu(\nabla\mathbf{u} + (\nabla\mathbf{u})^{T})\right] = \mathbf{0} \qquad (4\text{-}45)\ [22]$$

Boundary conditions at input:

$$\mathbf{n}^{T}\left[-p\mathbf{I} + \mu\left(\nabla\mathbf{u}_{fluid} + \left(\nabla\mathbf{u}_{fluid}\right)^{T}\right)\right]\mathbf{n} = -\hat{p}_{o}$$
$$\hat{p}_{o} \geq p_{o},\ \mathbf{u}_{fluid}.\mathbf{t} = \mathbf{0} \qquad (4\text{-}46)\ [22]$$

And boundary conditions at output:

$$\mathbf{n}^{T}\left[-p\mathbf{I} + \mu\left(\nabla\mathbf{u}_{fluid} + \left(\nabla\mathbf{u}_{fluid}\right)^{T}\right)\right]\mathbf{n} = -\hat{p}_{o}$$
$$\hat{p}_{o} \leq p_{o},\ \mathbf{u}_{fluid}.\mathbf{t} = \mathbf{0} \qquad (4\text{-}47)\ [22]$$

4.2.3 Fluid-Solid Interface boundary

At the fluid-solid boundary, the structural velocity is transmitted to the fluid. As a feedback, the stresses in the fluid flow act as a loading on the inner boundary of the solid wall of the diaphragm. So for Fluid-Solid Interface boundary:

$$\mathbf{u}_{fluid} = \mathbf{u}_w$$

$$\mathbf{u}_w = \frac{\partial u}{\partial t}, \qquad \mathbf{u}_w = \mathbf{fsi.v}\text{Wall}$$

$$\boldsymbol{\sigma}.\boldsymbol{n} = \boldsymbol{\Gamma}.\boldsymbol{n} \ , \ \boldsymbol{\Gamma} = \left[-p\mathbf{I} + \boldsymbol{\mu}\left(\nabla\mathbf{u}_{fluid} + \left(\nabla\mathbf{u}_{fluid}\right)^{T}\right)\right]$$

(4-48) [22]

where $\mathbf{u}_{fluid}$ and $\mathbf{u}_w$ are the velocity vector of fluid and the diaphragm wall, $\boldsymbol{u}$ is the displacement vector, $\boldsymbol{\sigma}$ ($\boldsymbol{\Gamma}$) is the stress tensor, and $\mathbf{n}$ is the normal vector to the FSI boundary.

The model's dependent variables are the displacements of the diaphragm wall together with the fluid velocity $\boldsymbol{u}_{fluid} = (U_{fluid}, V_{fluid})$ and pressure **p**.

4.2.4 Volumetric Integrations in fluid domain boundaries

In 2D model, to get the volumetric flow rate of the fluid $\dot{V}$ in m^3/s and the total volume of pumped fluid on line boundaries, we needed to perform some additional calculations. To obtain the volumetric flow rate at any instant t, we computed a boundary integral over the pump's inlet and outlet boundary. For round sections:

$$\dot{V}_{in} = -\int_{S_{in}} 2\pi x(n.u)ds$$

$$\dot{V}_{out} = \int_{S_{out}} 2\pi x(n.u)ds$$

(4-49)

And for pump's square section inlet and outlet boundary:

$$\dot{V}_{in} = -\int_{S_{in}} 2x(n.u)ds$$

$$\dot{V}_{out} = \int_{S_{out}} 2x(n.u)ds$$

(4-50)

where n is the outward-pointing unit normal of the boundary, u is the velocity vector, and *s* is the boundary length parameter, along which we integrate. In this particular model, the inlet and outlet boundaries are horizontal so $\mathbf{n}\cdot\mathbf{u} = n_x u + n_y v$ simplifies to v or $-v$ depending on the direction of the flow.

4.2.5 Accumulated/Conveyed flow (Vpump)

It is of interest to track how much fluid is conveyed through the outlet during a pumping cycle, this can be calculated as the following time integral:

$$V_{pump}(t) = \int_0^t \dot{V}_{out} dt' \qquad (4\text{-}51)$$

To compute this integral, we specified the corresponding ODE in COMSOL Multiphysics:

$$\frac{dV_{pump}}{dt} = \dot{V}_{out} \qquad (4\text{-}52)$$

with proper initial conditions; the software then will integrate this equation.

4.3 Gating Method and Assumptions

With all benefits from FSI module, the main issue with solid-fluid interaction problems, is the solid to solid contact through fluid domain. Solid to solid contact in structure mechanic module is perfectly achievable but in fluid solid problem due to change in meshing topology is not achievable. And consequently, one of the biggest issues with flapper check valves, is the simulation of moving mesh during "solid contact" in the gate closing process in FSI module. Although there is no mathematical solution available for this concept (due to topology change problem), however, we used a "No-Contact" but minimum gap to emulate the flapper function. It adds a very small leakage rate to the system but enable us to get results and evaluate the micro-pump's function and performance. Obviously, by applying finer mesh, the leakage level will decrease and the results will be more accurate but at the same time, it will be more memory intensive.

Figures 4.3 through 4.5 show the flapper valve in open and close positions. The instantaneous minimum gap in one flapper gate and maximum opening in the other one, provides a satisfactory gating process and fluid direction control during micro-pump operation.

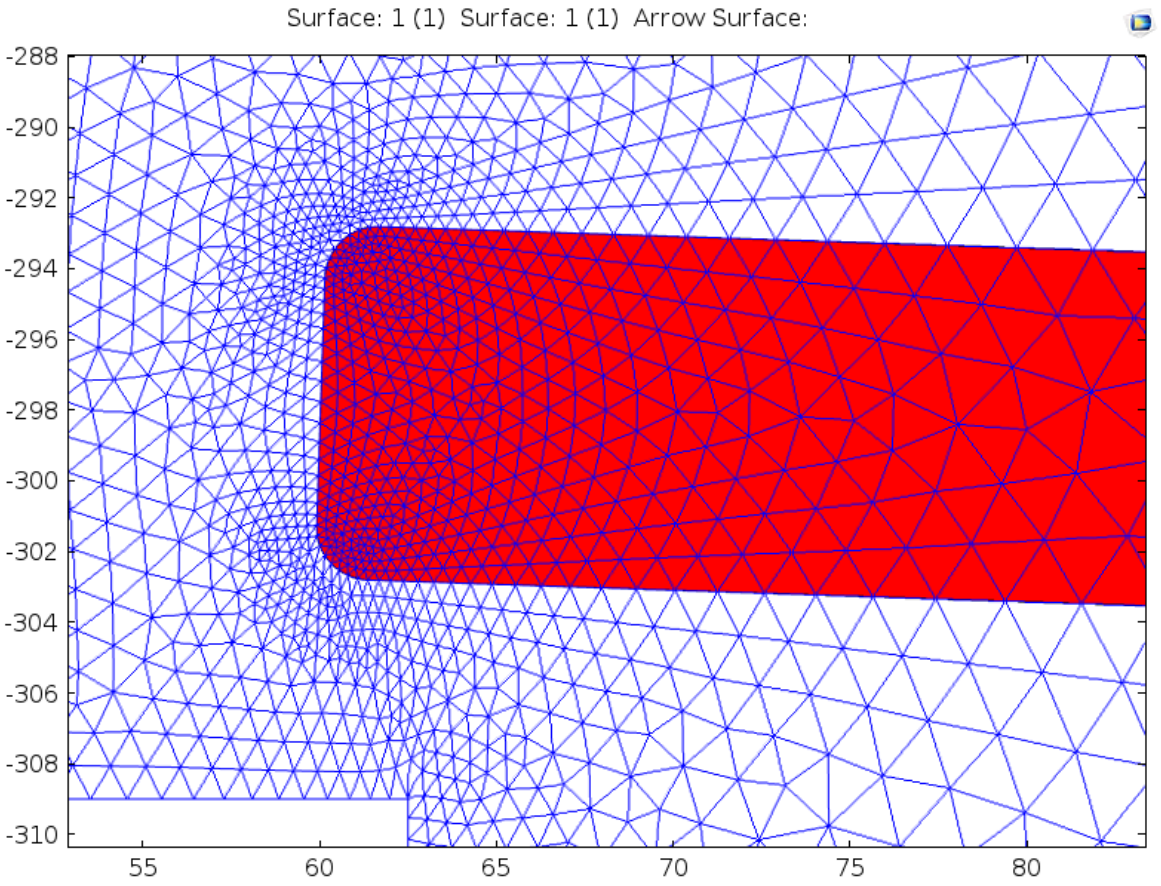

Figure 4.3 Flapper valve Mesh in open position

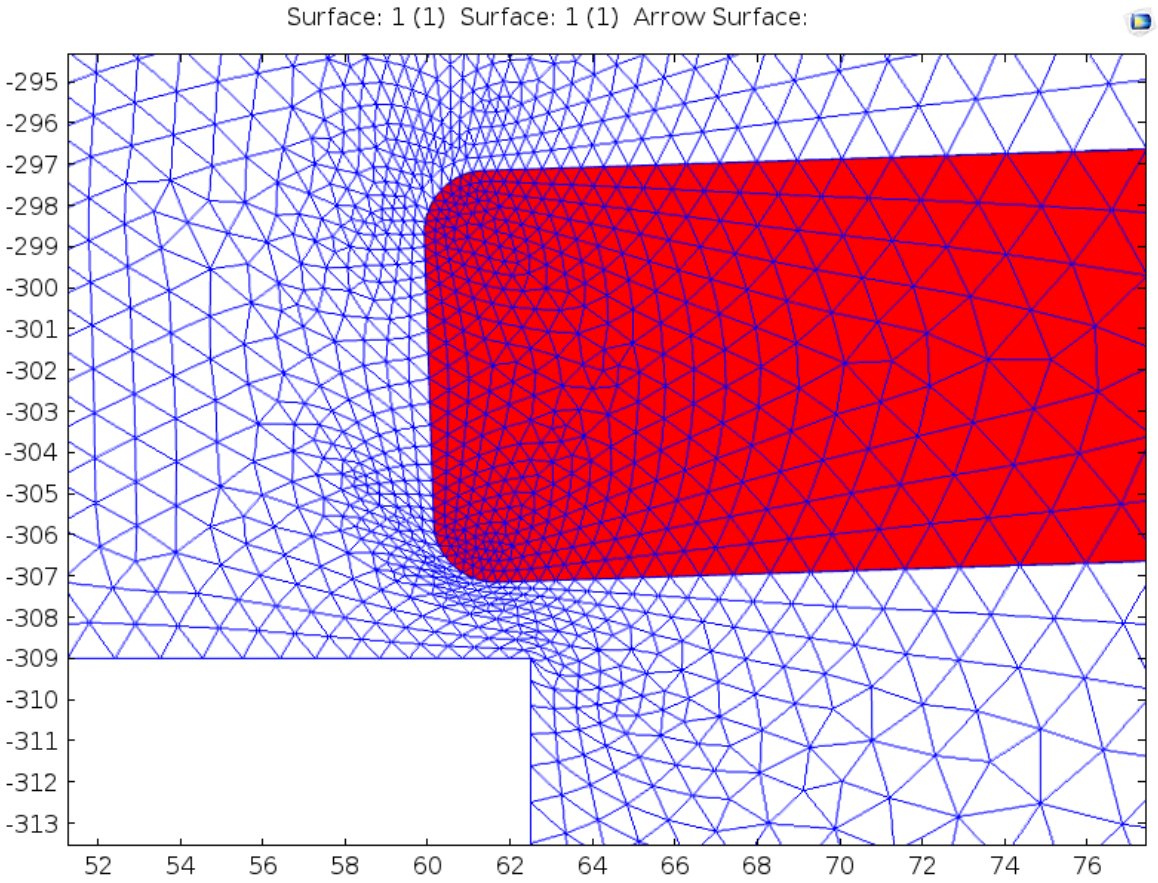

Figure 4.4 Flapper valve Mesh in closed position

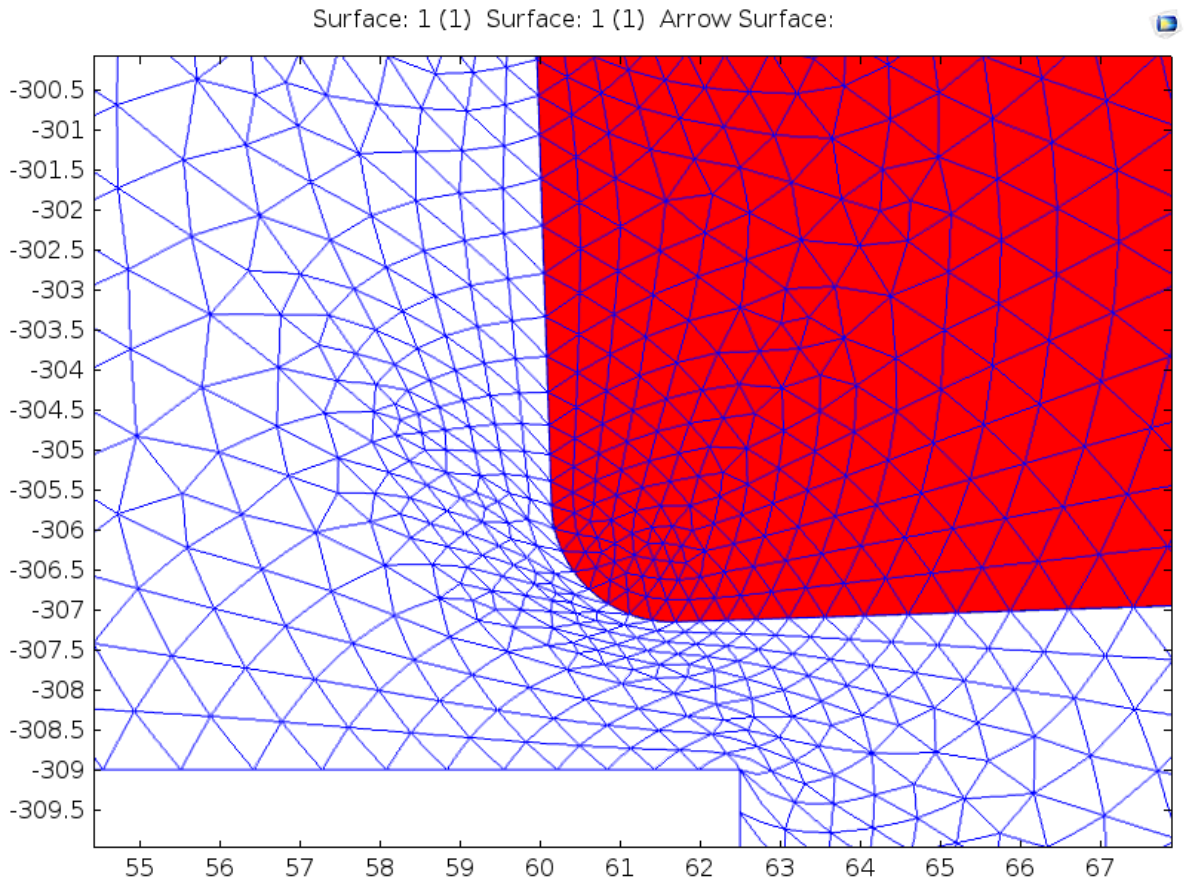

Figure 4.5 Flapper valve Mesh in closed position (Zoomed in)

Figures 4.3 through 4.5 show the velocity field magnitude during gating process. It is obvious from the image that velocity is close to zero at area around in closed position flapper valve. Velocity magnitudes are shown in figures 4.6 through 4.8 in supply and discharge modes at inlet and outlet flapper gates.

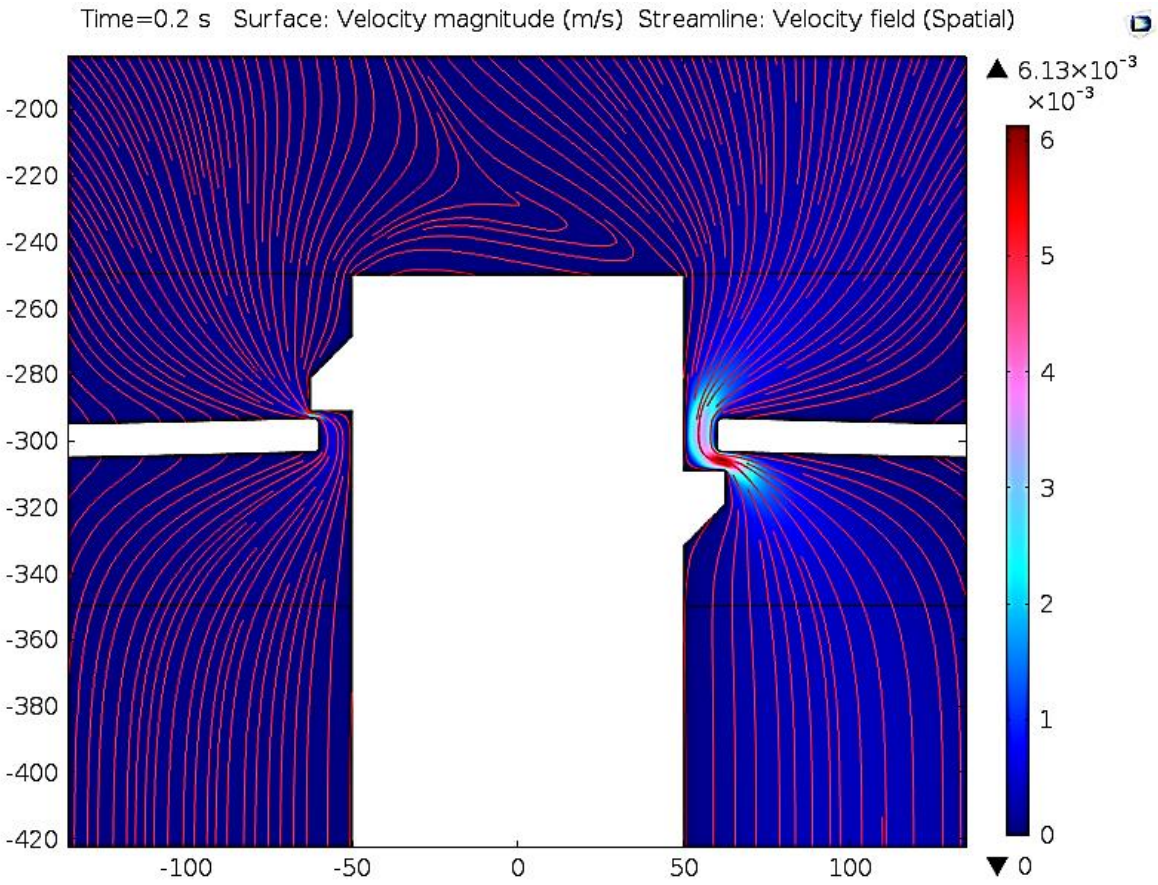

Figure 4.6 Double Flapper gating system – Velocity magnitude in Supply mode.

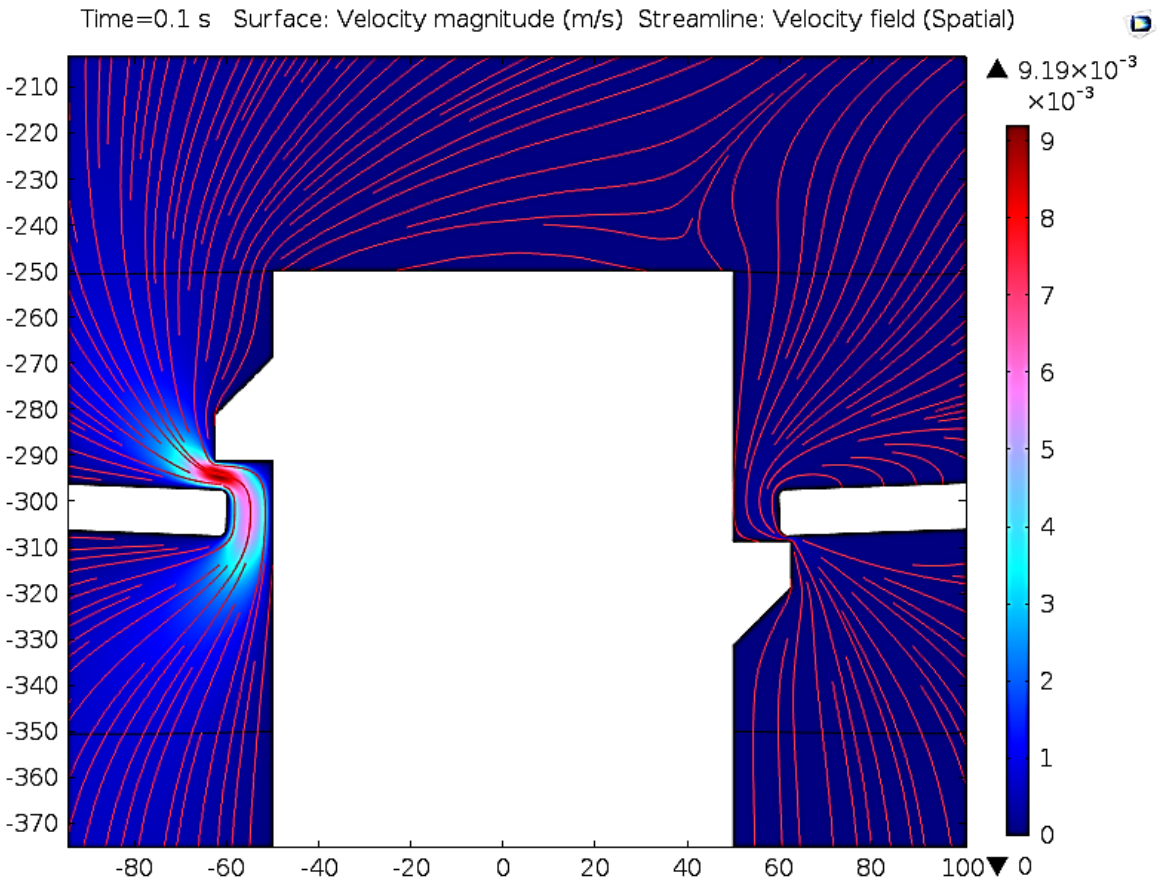

Figure 4.7 Double Flapper gating system - Velocity magnitude in Discharge mode.

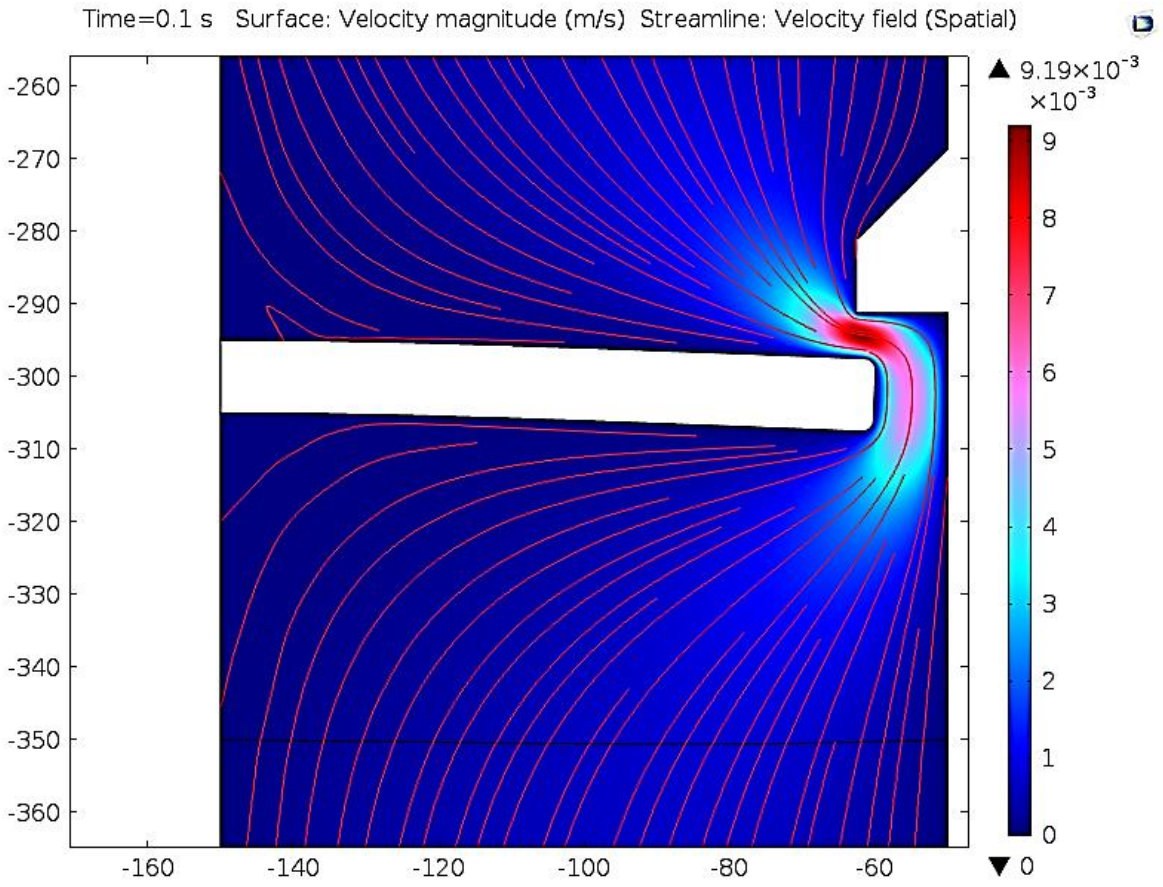

Figure 4.8 Flapper function in open position – Velocity magnitude – close view

4.4 Piezoelectric Actuator Eigenvalues

In order to study frequency response of the piezoelectric unit, we ran an eigenvalue analysis and as shown in figures 4.9 through 4.12, the first modal frequency starts from 21 kHz. That means for the purpose of our study for frequencies below 100, our study will be valid to the results.

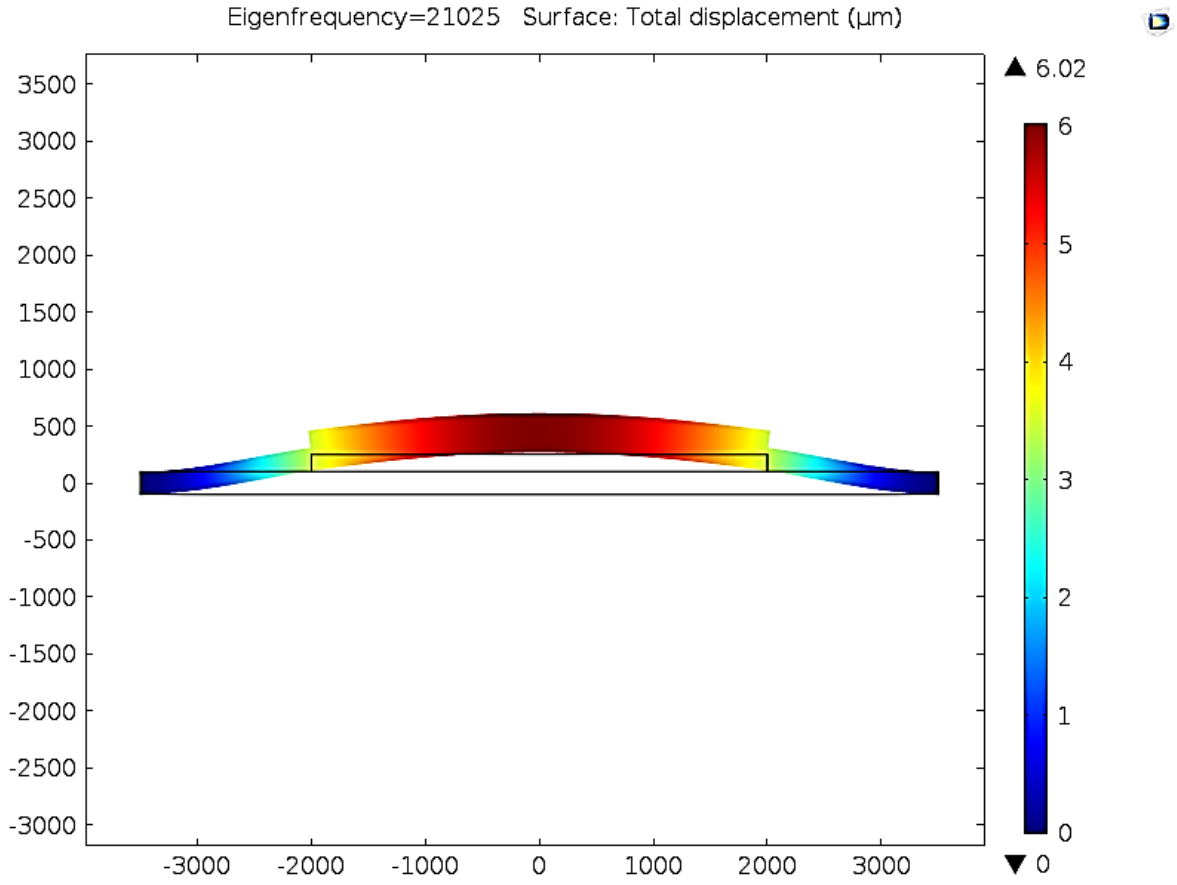

Figure 4.9 First Modal frequency of PZT-5H actuator with Diaphragm

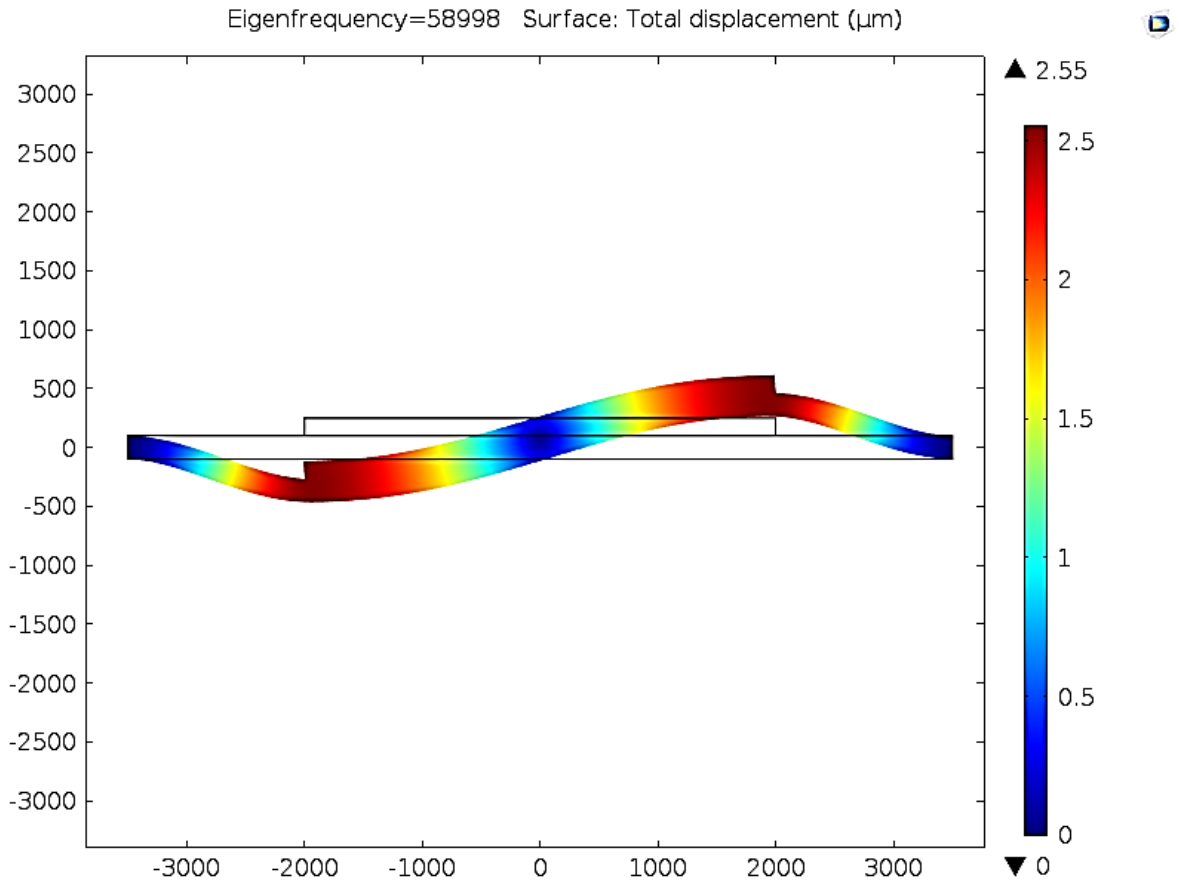

Figure 4.10 2nd Modal frequency of PZT-5H actuator with Diaphragm

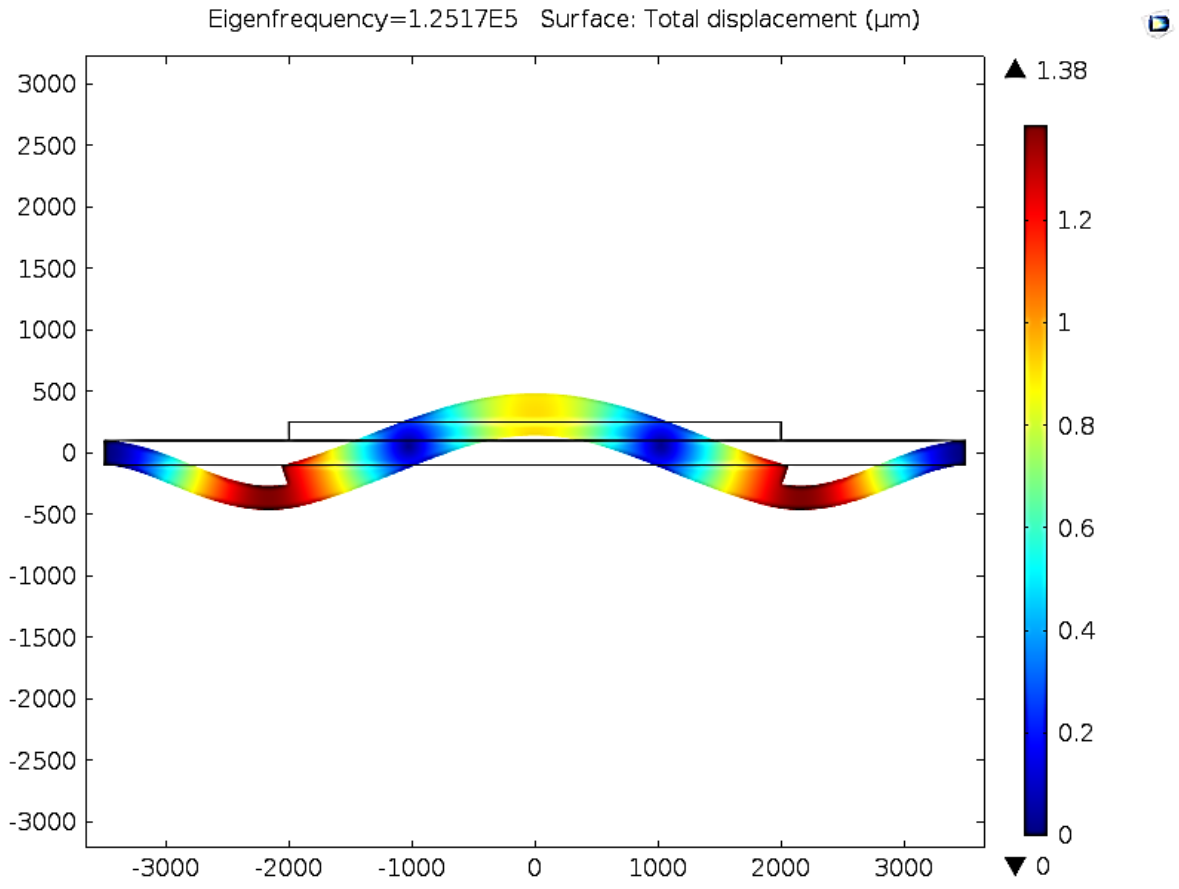

Figure 4.11 3rd Modal frequency of PZT-5H actuator with Diaphragm

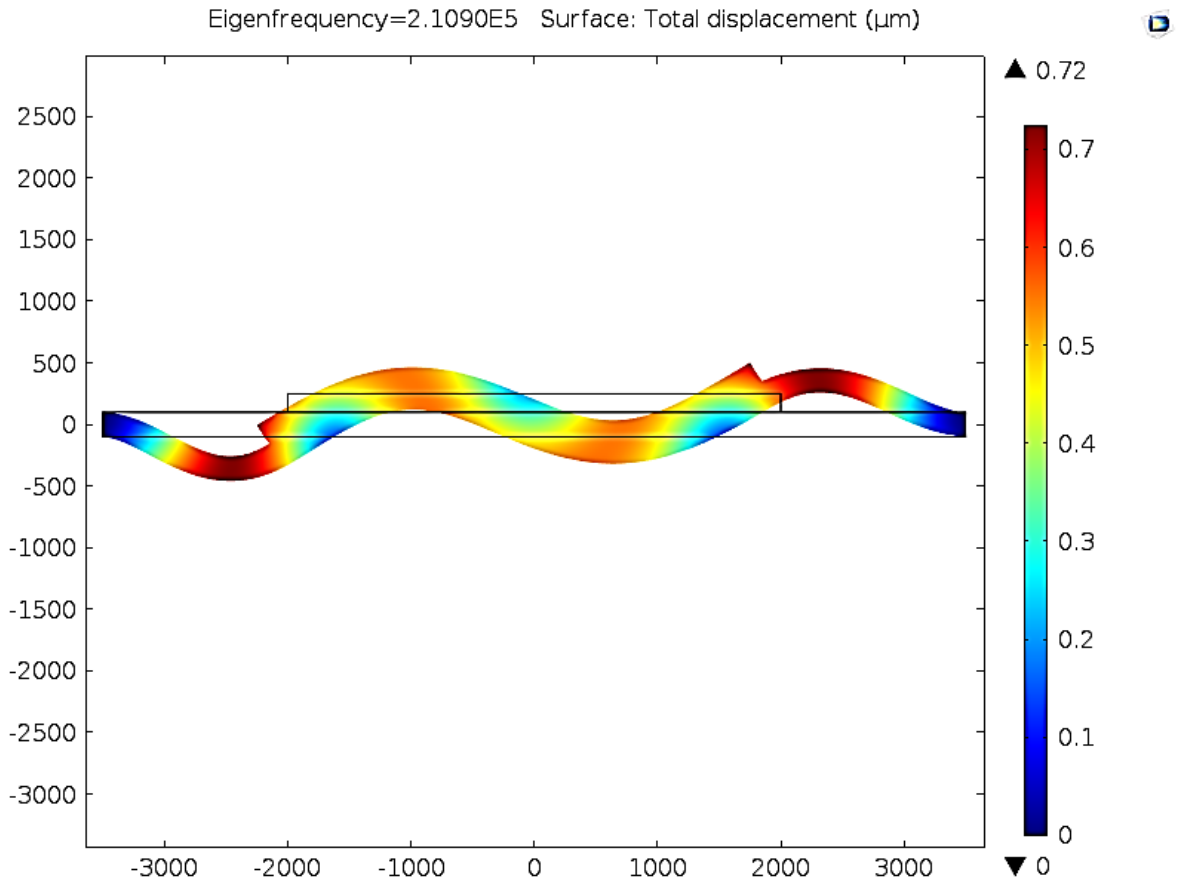

Figure 4.12 4th Modal frequency of PZT-5H actuator with Diaphragm

4.5 Coupling methods

Because of the non-linearity of the system, we used a fully coupled solver.

There are many applications where we can use fluid-solid interaction module in COMSOL multiphysics analysis. Figure 4.13 shows some the applications including, Peristaltic Pump, Energy Harvesting, Cardiovascular simulation, Fluid Mixer and Wind Loading. Generally, there are 4 types of FSI problems:

1. Deformation in solids coupled with internal or external fluid flow.
2. Acoustic-structure interaction
3. Poroelasticity
4. Particulate flow

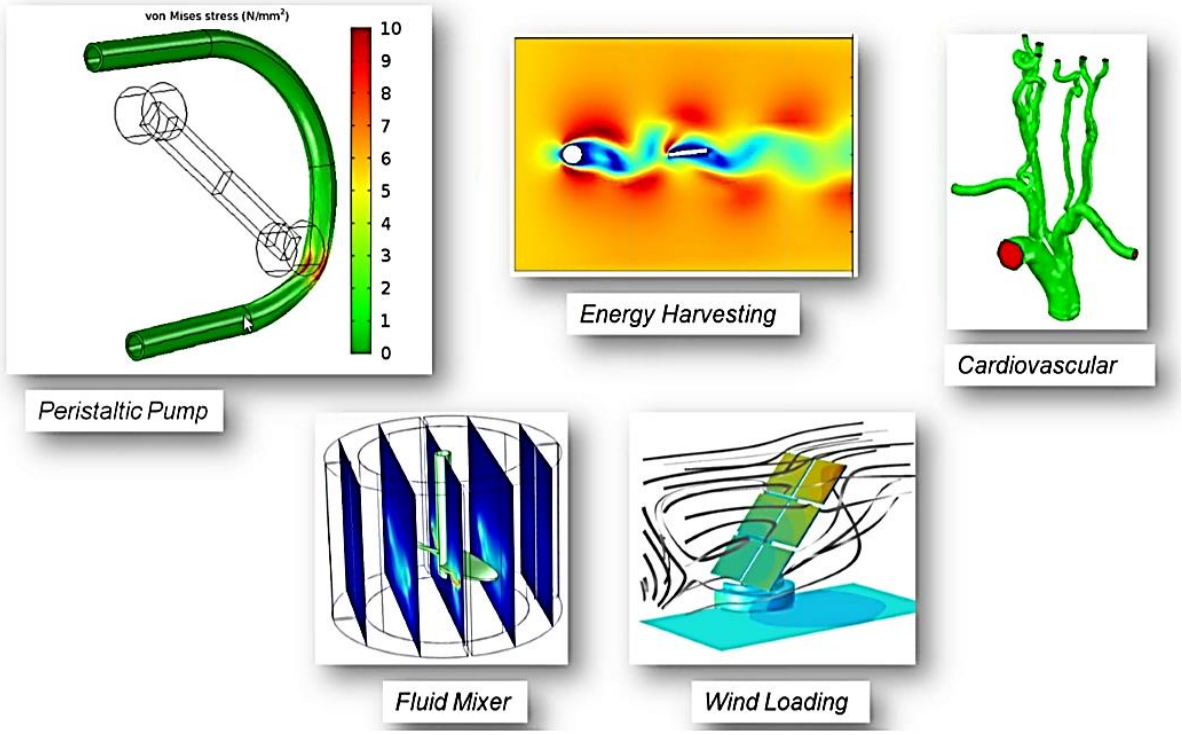

Figure 4.13 Fluid-Structure Interaction (FSI) applications [23]

Figure 4.14 shows some samples of typical FSI problems.

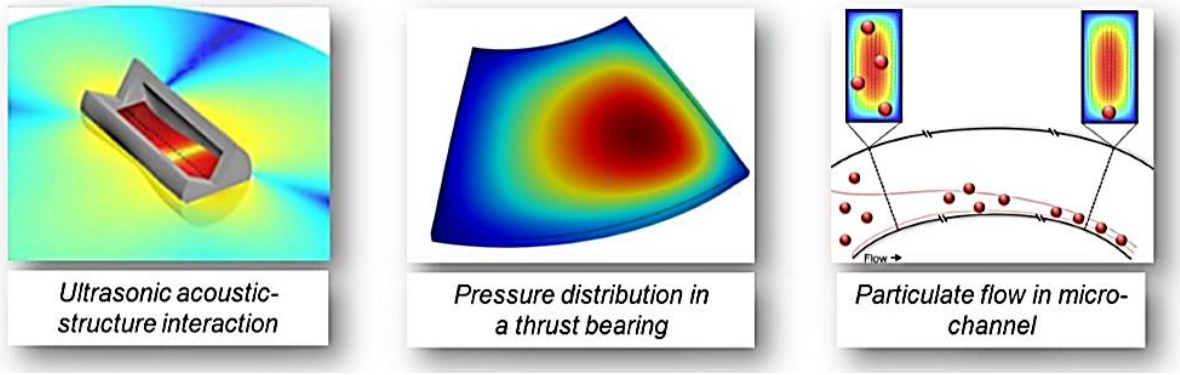

Figure 4.14 Types of FSI problems. [23]

4.6 Types of FSI Coupling

4.6.1 Boundary Coupling – One way

1. When fluid Flow drives structural deformation in one way direction. This method can be used for solids experiencing small elastic deformation like Wind Loading problems (Figure 4.15-a).

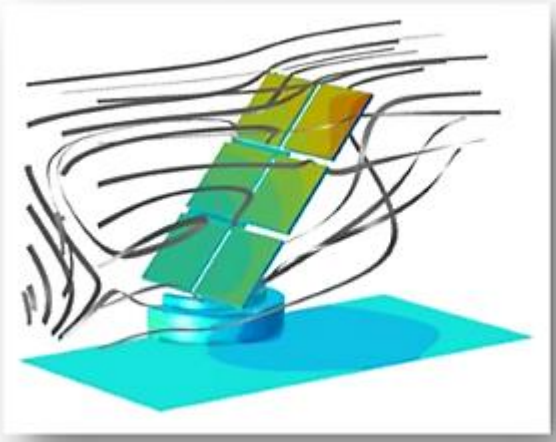

Figure 4.15-a Wind Loading - One way fluid-solid coupling [23]

In Figure 4.15-b, the algorithm of this method is shown. After solving for fluid flow and calculating total fluid stress, it will be applied on solid boundaries and at the end; the displacement for solid is calculated.

1. Solve for fluid flow
2. Calculate total fluid stresses
3. Apply fluid stresses on solid boundaries
4. Solve for the displacements in solids

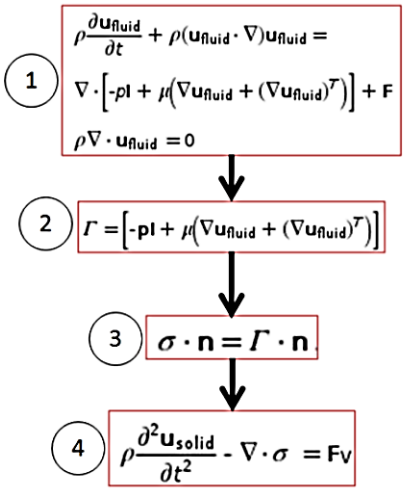

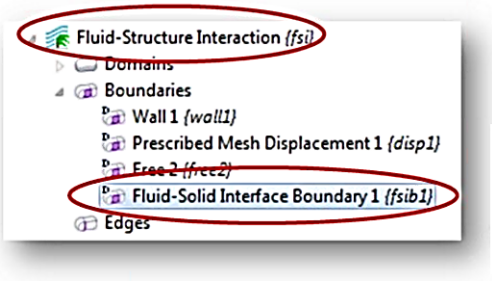

Figure 4.15-b Fluid to Solid Coupling: Small Solid Displacements calculation method.

2. When structure deformation drives fluid flow. This can be used for solids experiencing large rigid displacements like Fluid Mixer problems (Figure 4.16-a). [23]

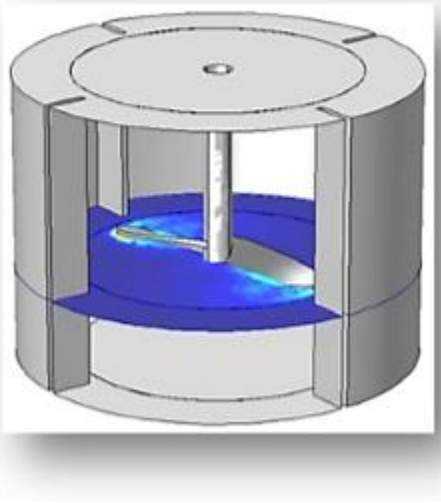

Figure 4.16-a Fluid Mixer - One way solid>fluid coupling [23]

In Figure 4.16-b, the calculation algorithm of this method. In a reverse way COMSOL first solves for displacements of the rigid solid structure through a fluid flow mesh. Then applies the resulted velocity of the solid boundaries to the fluid walls and eventually solves for fluid flow.

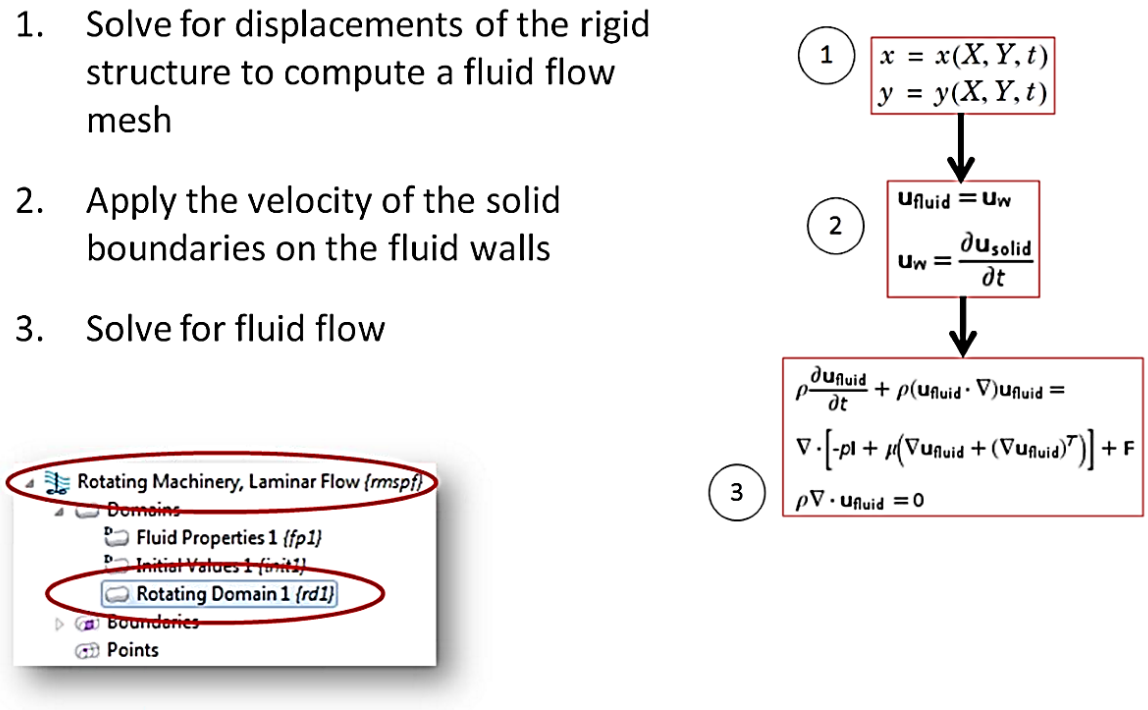

Figure 4.16-b Solid to Fluid Coupling: Large Rigid Displacements. [23]

4.6.2 Boundary Coupling – Two way

1. When fluid Flow and structural deformation interact in two way with each other. This method can be used for solids experiencing small elastic deformation like Energy Harvesting or Piezoelectric Micro-pump problems (Figure 4.17-a).

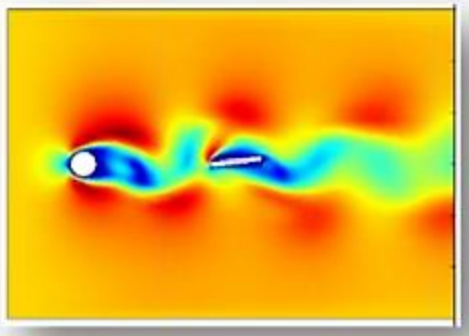

Figure 4.17-a An Energy Harvesting - Two way coupling [23]

Figure 4.10-b shows the calculation algorithm of this method. COMSOL combines the fluid flow and solid deformation domain through a moving mesh. With applying a proper FSI boundary conditions, the program applies fluid forces on solid-fluid boundaries and in next step imposes fluid velocities based on velocity of solid boundaries.

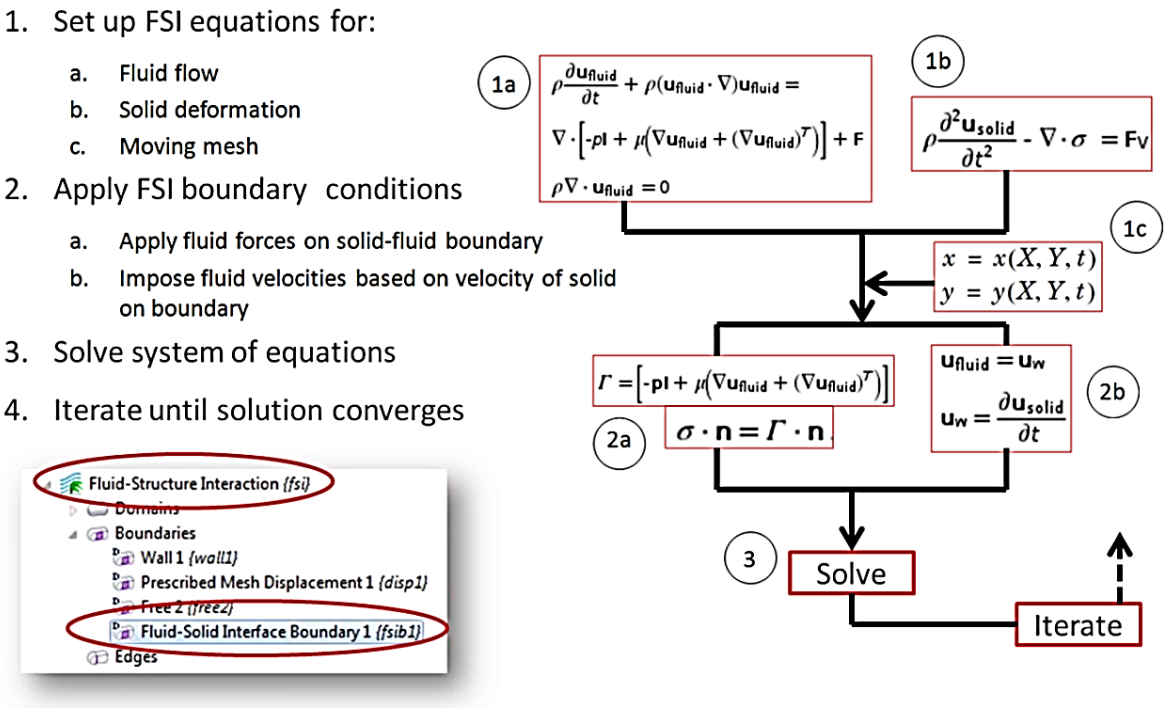

Figure 4.17-b Two-Way Boundary Coupling [23]

4.6.3 Domain Level Coupling

This special type of coupling mostly are used for modeling Flow through a Porous Media or Consolidation analysis (Figure 4.18).

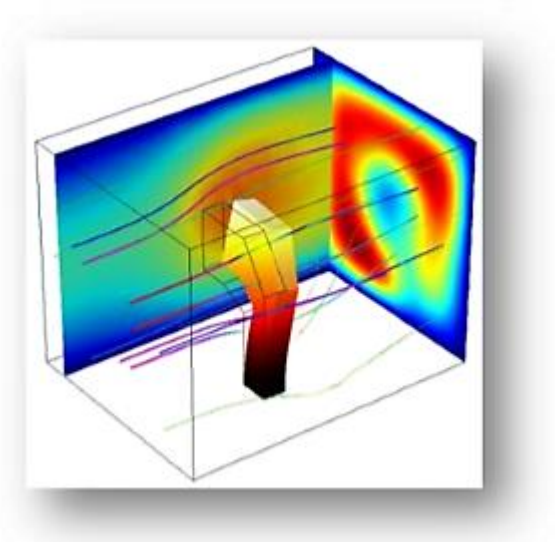

Figure 4.18 Porous Media - Domain Coupling [23]

4.7 Solvers for FSI

Figure 4.19 shows a brief explanation about different solvers available in COMSOL. Segregated Solvers solve for different physics in time order and can be defined in an optimal way for specific physics. For that reason, they are less memory intensive.

Fully Coupled Solvers solve for all variables simultaneously and therefore they are more memory intensive but at the same time they provide a higher level of robustness to the system.

- Segregated Solver
  - Sequentially solves for fluid flow, solid displacement and moving mesh
  - Less memory intensive
  - Each solver can be optimal for the specific physics
- Fully Coupled Solver
  - Solves for all variables simultaneously
  - Memory intensive
  - More robust
- Each type of solver can also be direct or iterative

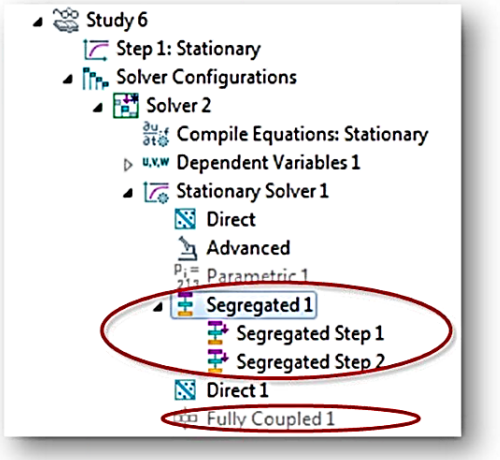

Figure 4.19 FSI Solvers [23]

4.8 Coupling and Solvers targets for this study

FSI problems are nonlinear. They need an accurate and robust calculation method to define a flawless relationship between fluid/solid domains and their boundaries. In this study, we use a Two-Way Boundary coupling with Fully-Coupled Solvers, therefore, the created model is very memory intensive. To avoid that, the simulation model for this study is established based on a 2D model but a 3D model (without flapper valves) was also used to verify the accuracy of volume stroke.

4.9 Meshing system

For entire domain mesh we used Triangular mesh type. We have used 3 different mesh sizes for this study as below:

4.9.1 General Mesh

A general mesh as predefined normal size with minimum element size of 3.36 µm was used as the basic mesh size. We used this mesh size for most part of the model/domains including main cavity and both solid and fluid domains.

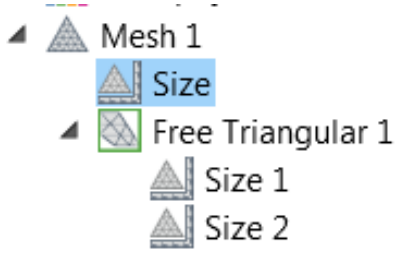

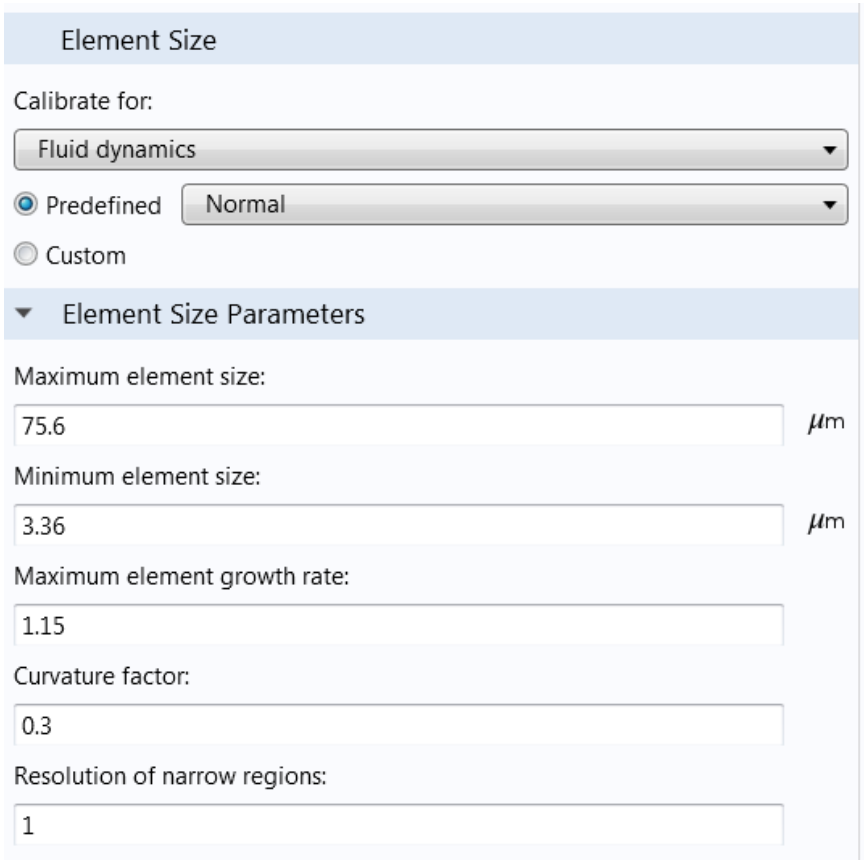

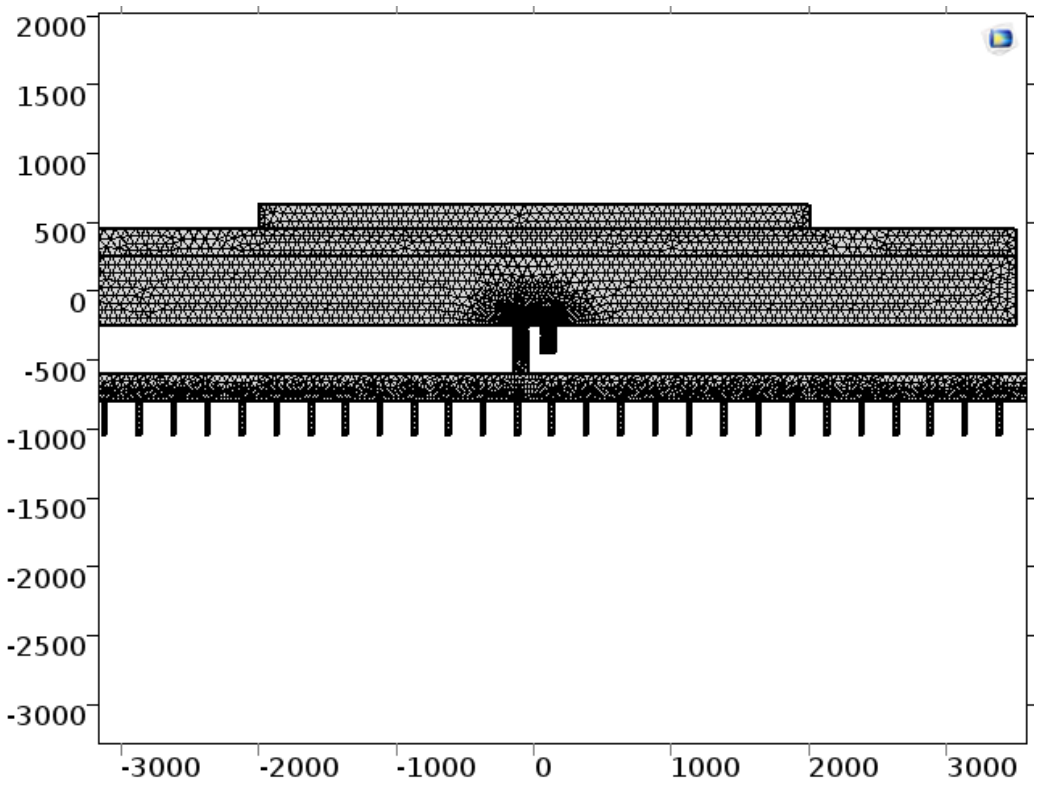

Figure 4.20 General mesh size applied to the model as basic mesh size

4.9.2 Micro-Needls Mesh

A finer mesh was used for micro-needles as predefined extra fine size with minimum element size of 0.6 µm. We used this mesh size for all micro-needle tubes.

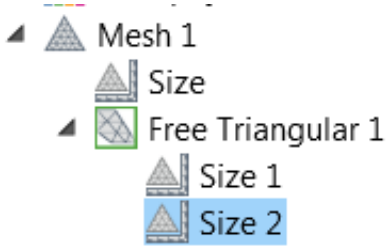

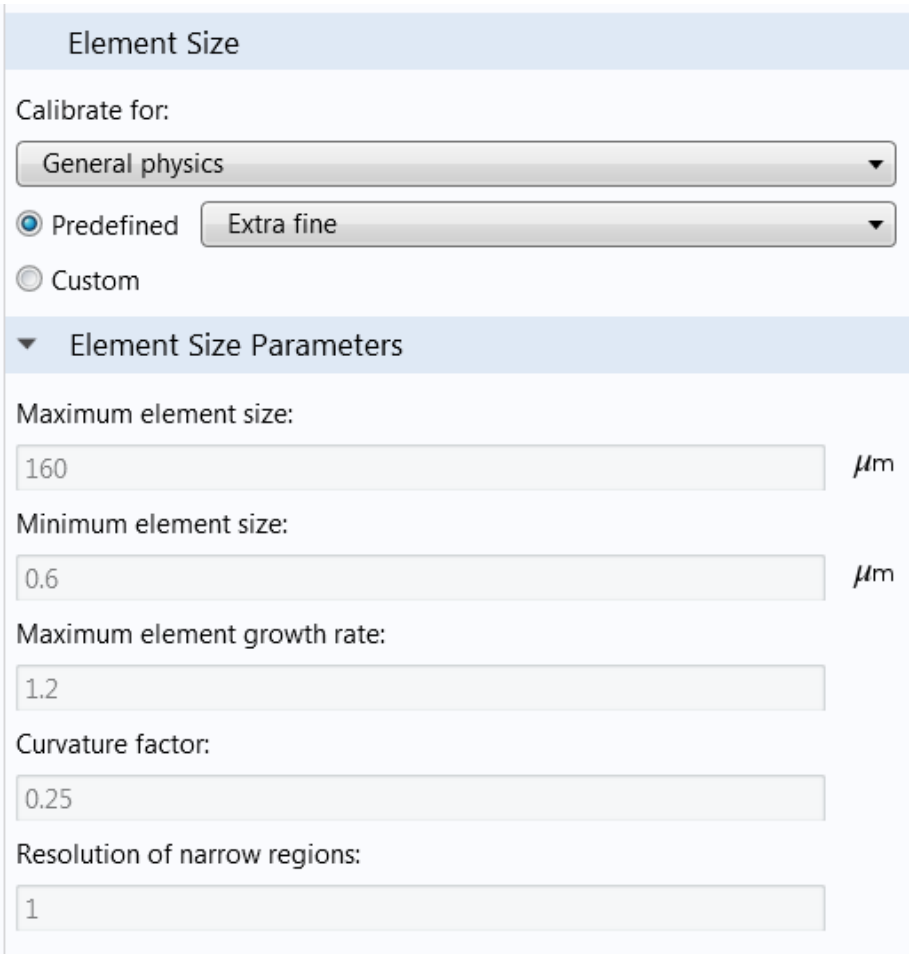
Element Size
Calibrate for:
General physics
Predefined
Extra fine
Custom
Element Size Parameters
Maximum element size:
160
μm
Minimum element size:
0.6
μm
Maximum element growth rate:
1.2
Curvature factor:
0.25
Resolution of narrow regions:
1

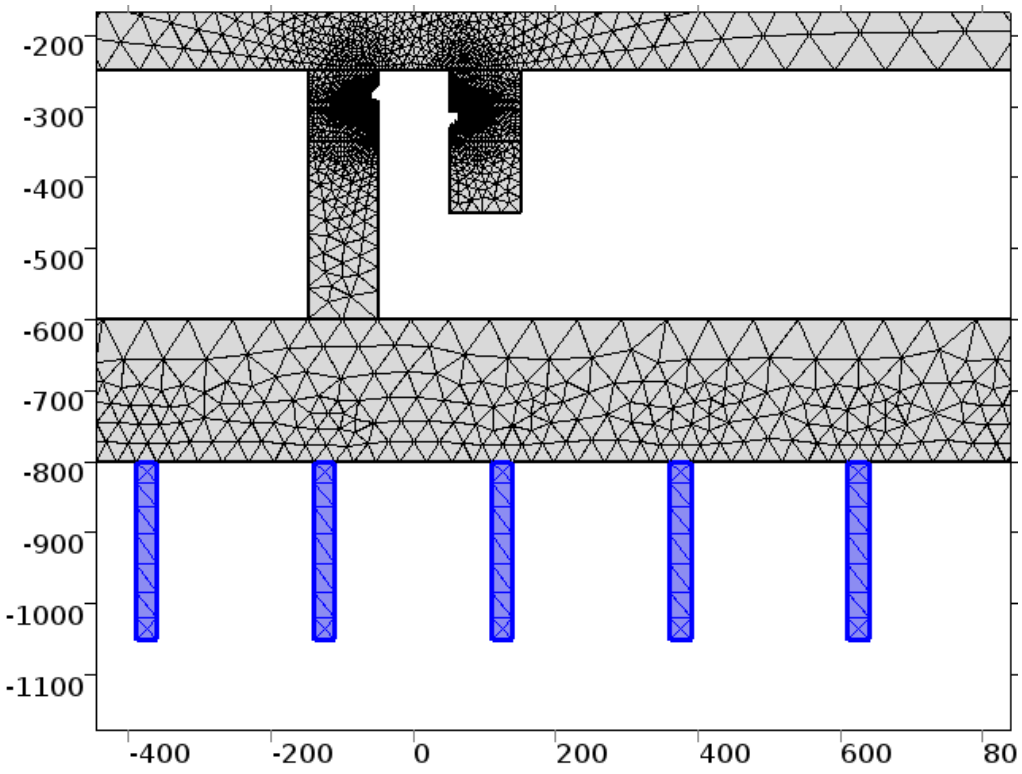

Figure 4.21 Micro-needle mesh system

4.9.3 Flapper/Diaphragm Mesh

And finally an extremely fine mesh was used for both check-valve flappers and pump diaphragm with predefined minimum element size of 0.16 μm. Flapper valves are the most delicate part of this pump and any finer mesh, provides a more precise output results. As we covered before, a finer mesh around the flapper, prevents excessive leakage through the flapper gap during closing part of gating process and therefore it will minimized the error effect of leakage into the system.

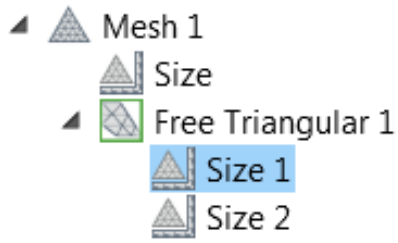

Element Size

Calibrate for:

General physics

Predefined Extremely fine

Custom

Element Size Parameters

Maximum element size:

80 μm

Minimum element size:

0.16 μm

Maximum element growth rate:

1.1

Curvature factor:

0.2

Resolution of narrow regions:

1

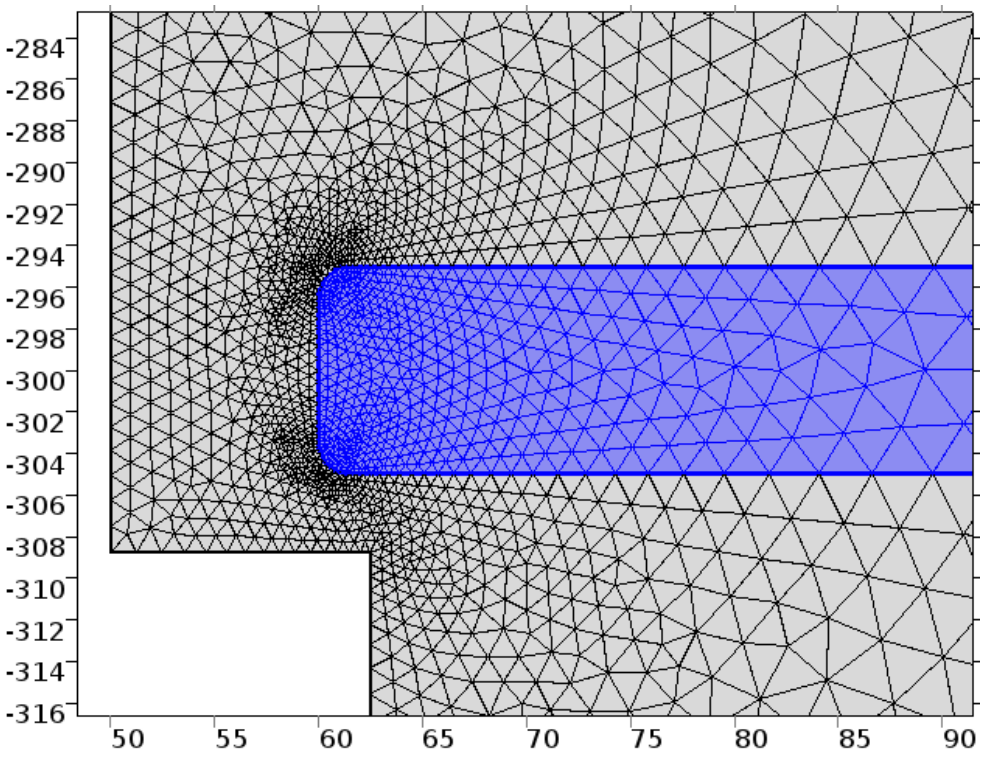

Figure 4.22 Flapper valve mesh system

4.10 Results

The micro-pump simulation model used to study the behavior of this pump for different input voltages (10, 40, 80 and 110 volts) with different input excitation frequencies (1 to 3 Hz). The achievable discharging pressure for each case, with skin interstitial pressure as the back-pressure, was investigated. For each case outflow rates including accumulated flow (total discharge volume) and the netflow (fluctuation volume) were measured. We bring here a detail performance data for each of the cases and then provide a series of micro-pump behavioral graphs as a design guide to use this concept for different output/delivery of fluid/pressure for insulin administration.

We are going to categorize our study here in 4 groups, based on activation voltage, and investigate each group of data through different excitation frequencies.

4.10.1 Analysis data for load case: Voltage=10 volts, Frequency=1 Hz

Figure 4.23 shows the instantaneous inflow/outflow rates of the micro-pump. Theoretically, the inflow rate stays at the minimum constant level during pumping mode and in the same way the outflow stays at minimum level during supply mode. Practically, flapper check valves are leakage free system in fluid gating. However, in our study because of the "Minimum but No-Contact gating concept" which was mentioned before, we see some level of leakage in the system. Essentially, any inflow below zero line during pumping mode and any outflow above zero line during supply mode will be considered as system leakage and affect the calculated volumetric efficiency.

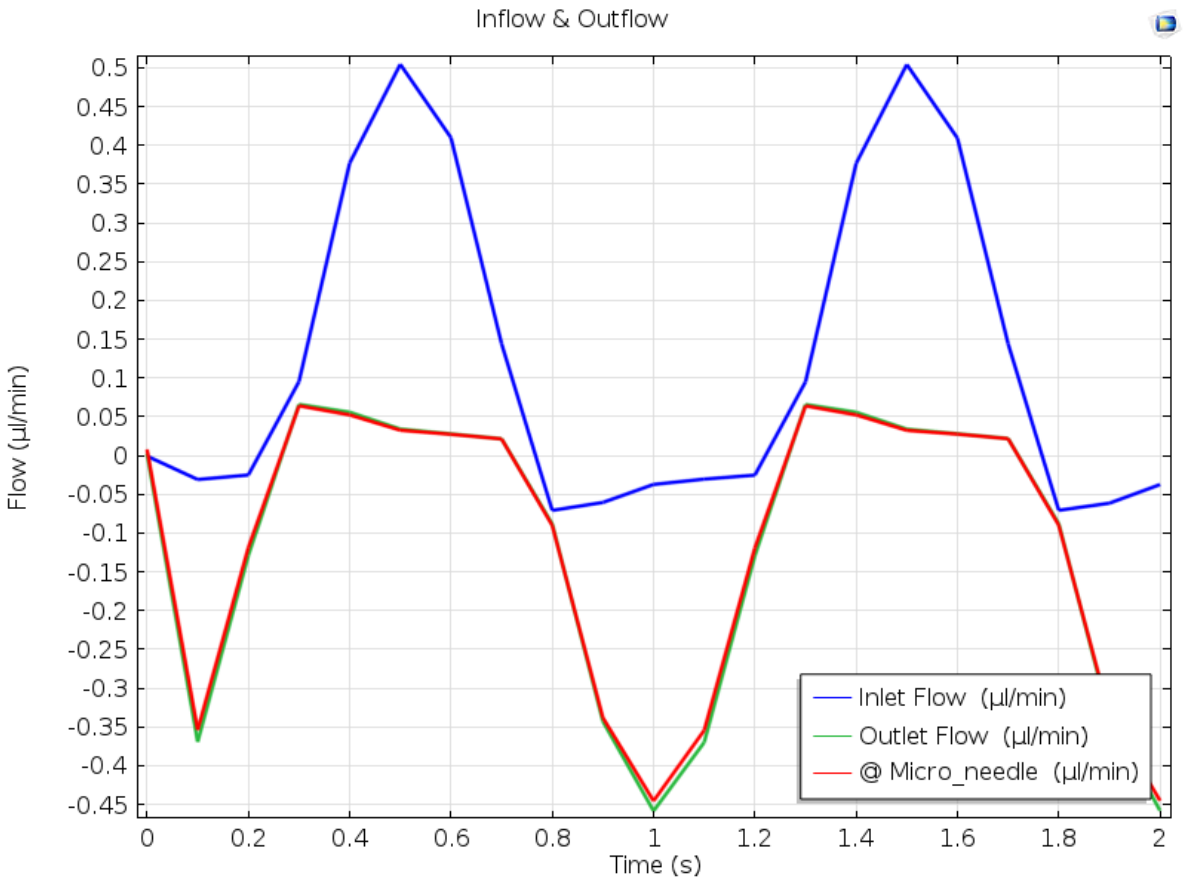

Figure 4.23 Flow rate vs time @ V=10 volts, f =1 Hz

Figure 4.24 shows the average inflow/outflow rates of the micro-pump. The negative values for outflow rates are only showing the reverse direction of outflows. Again, from this graph, the effect of existing leakage in the system can be observed.

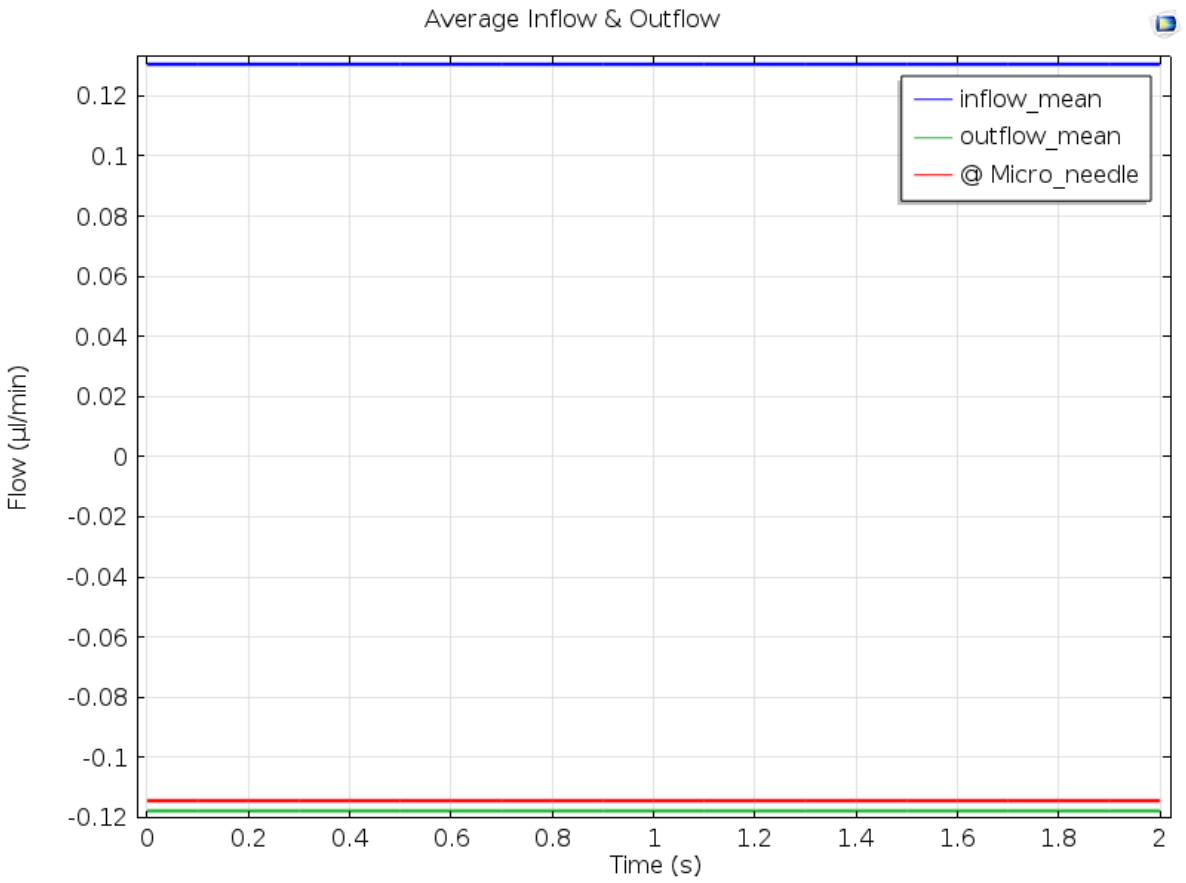

Figure 4.24 Average flow rates @ V=10 volts, f =1 Hz

The most important part of result information in this simulation are shown in Figure 4.25. They are called netflow and Vpump. Netflow or pump fluctuation volume is the internal flow volume (stroke volume). This volume includes internal pump leakage. Vpump or pump accumulated volume is the total conveyed flow during specific period of time. Vpump indicates the real total discharge of the pump during time, therefore, it represents the total amount of injected insulin per hour or per day. Vpump diagram adds up quickly during pumping mode and it is expected to stay constant during supply mode; but as can be seen, it declines representing a leakage in system. For example during first second of operation in figure 4.25, the amount of leakage is about 0.003 µl. Practically this amount for a real flapper check valve is about zero.

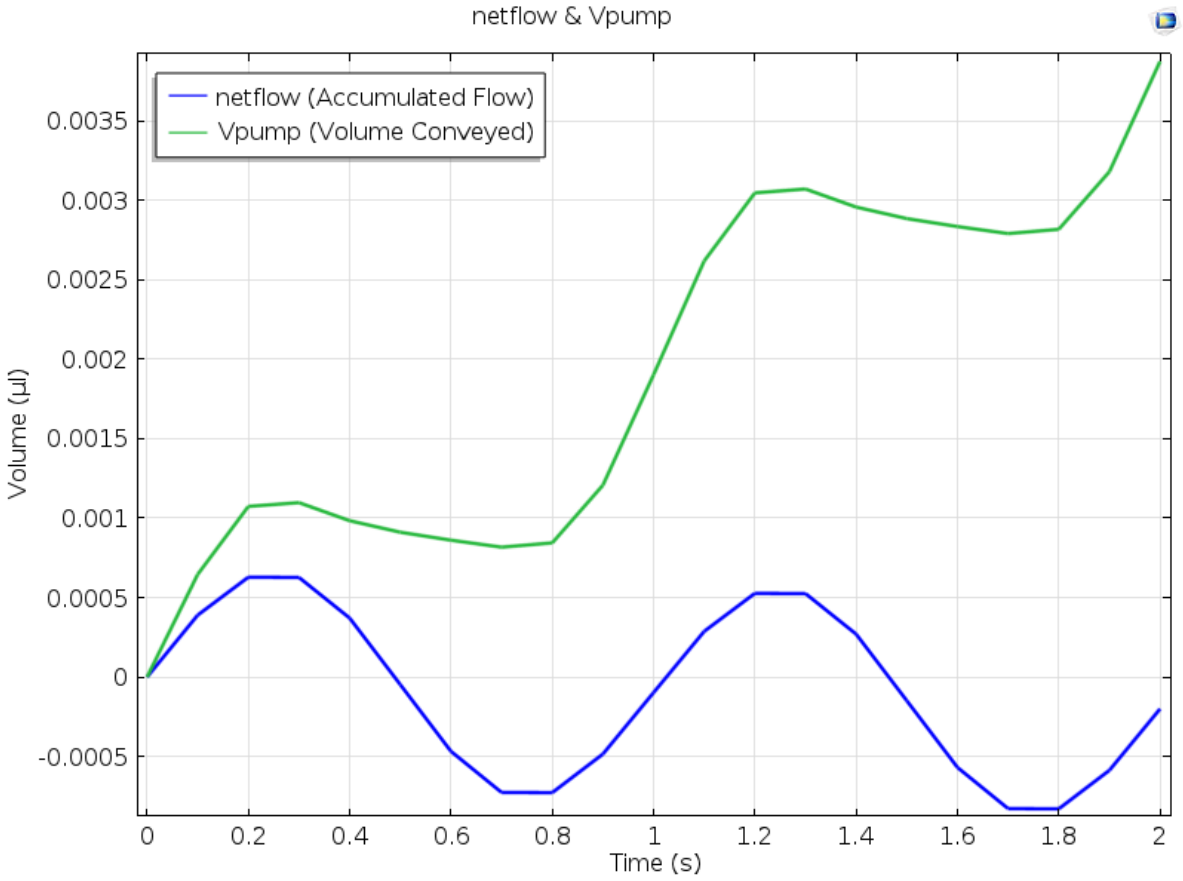

Figure 4.25 netflow and Vpump @ V=10 volts, f =1 Hz

In Figure 4.26, Nominal Pump Delivery versus time is shown. This is calculated internal volume stroke based on internal volume of pump chamber versus time. Comparing this value with Vpump during a time bracket will generate volumetric efficiency of the micro-pump. We will see these results in conclusion chapter.

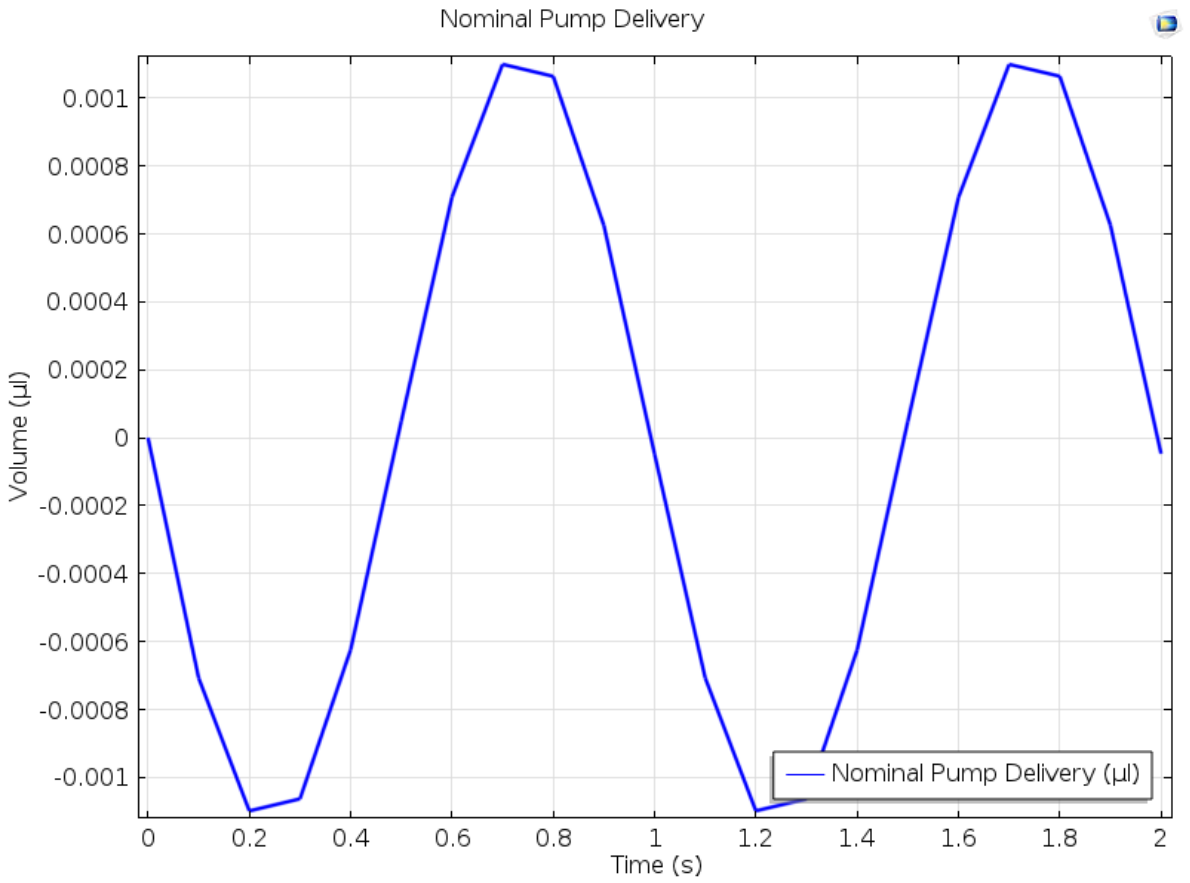

Figure 4.26 Nominal Pump Delivery @ V=10 volts, f =1 Hz

Figure 4.27 shows pressure fluctuation versus time. As it shown, the supply pressure is negative during supply mode and stays almost constant at zero level during pumping mode. In the same way, discharge pressure is positive and maximum during pumping mode and stays at almost constant level during supply mode.

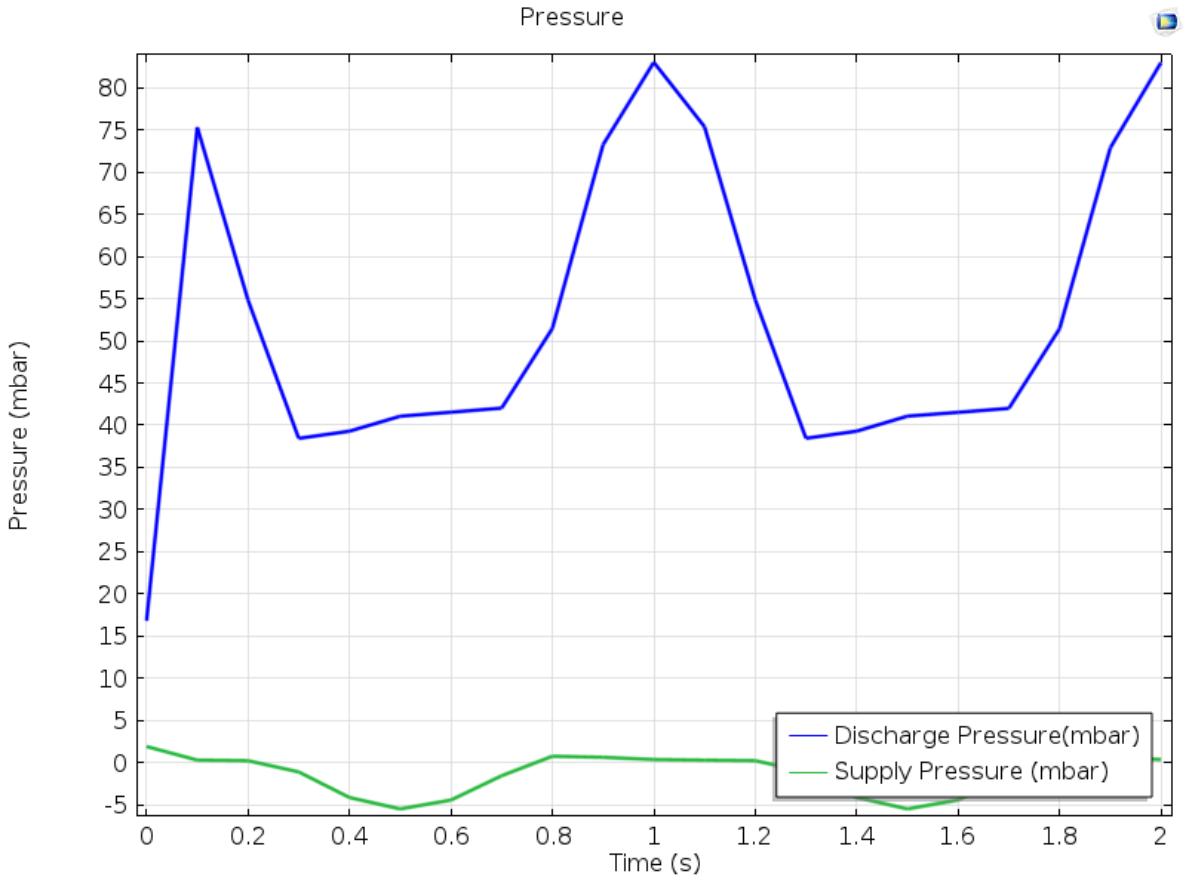

Figure 4.27 Pressure vs Time @ V=10 volts, f =1 Hz

Diaphragm deflection versus Arc length is shown in figure 4.28.

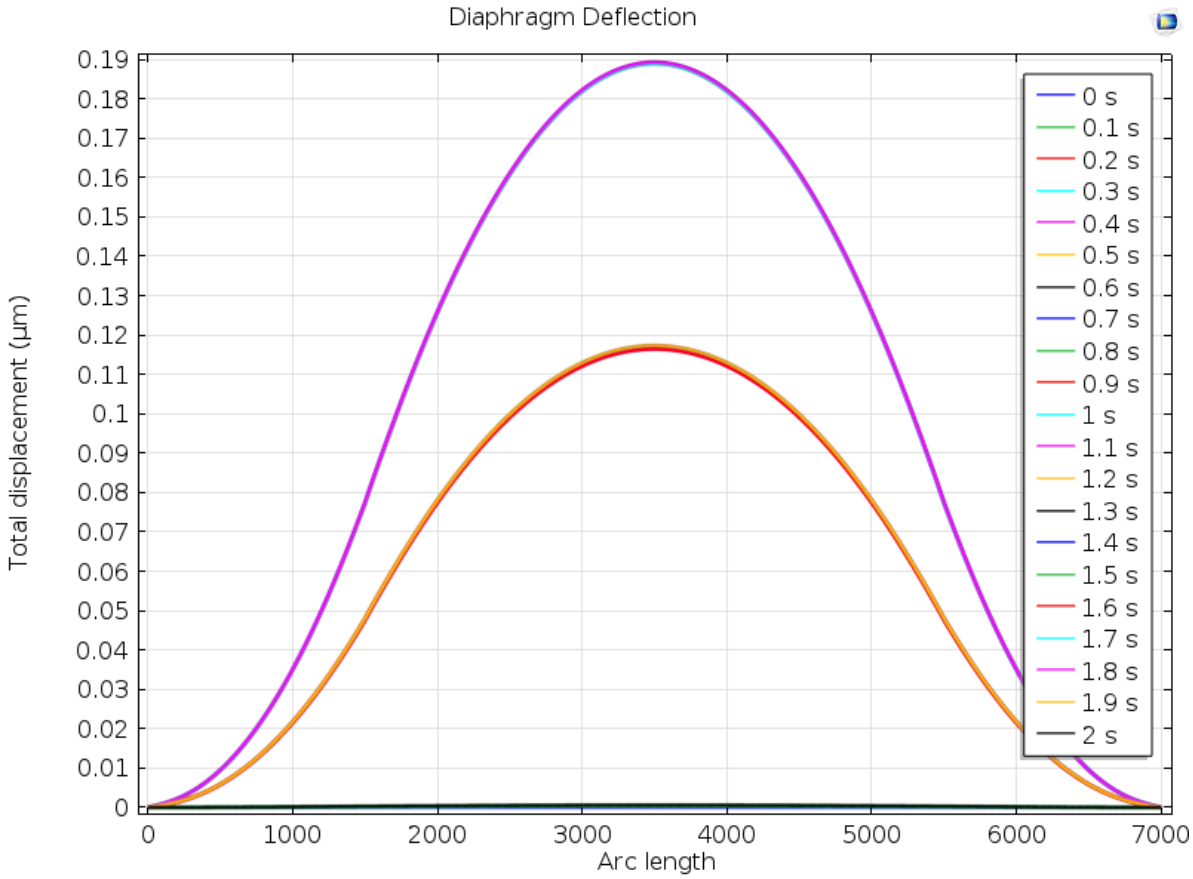

Figure 4.28 Diaphragm Deflection versus Arc length @ V=10 volts, f =1 Hz

Figures 4.29 through 4.30 show “Mesh Deflection” and “Mesh Velocity” for pump’s main diaphragm and flapper check valves.

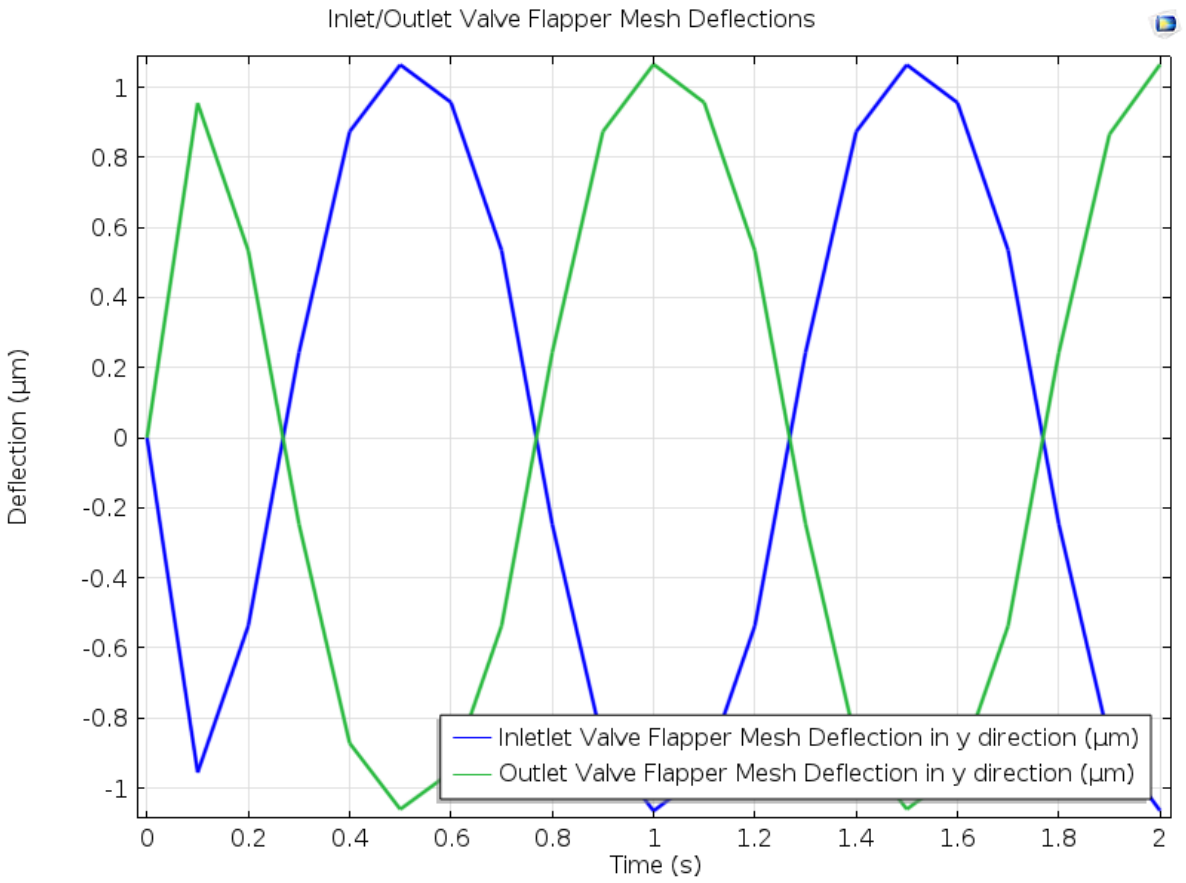

Figure 4.29 Inlet/Outlet Valve Flapper Mesh Deflections versus Time @ V=10 volts, f =1 Hz

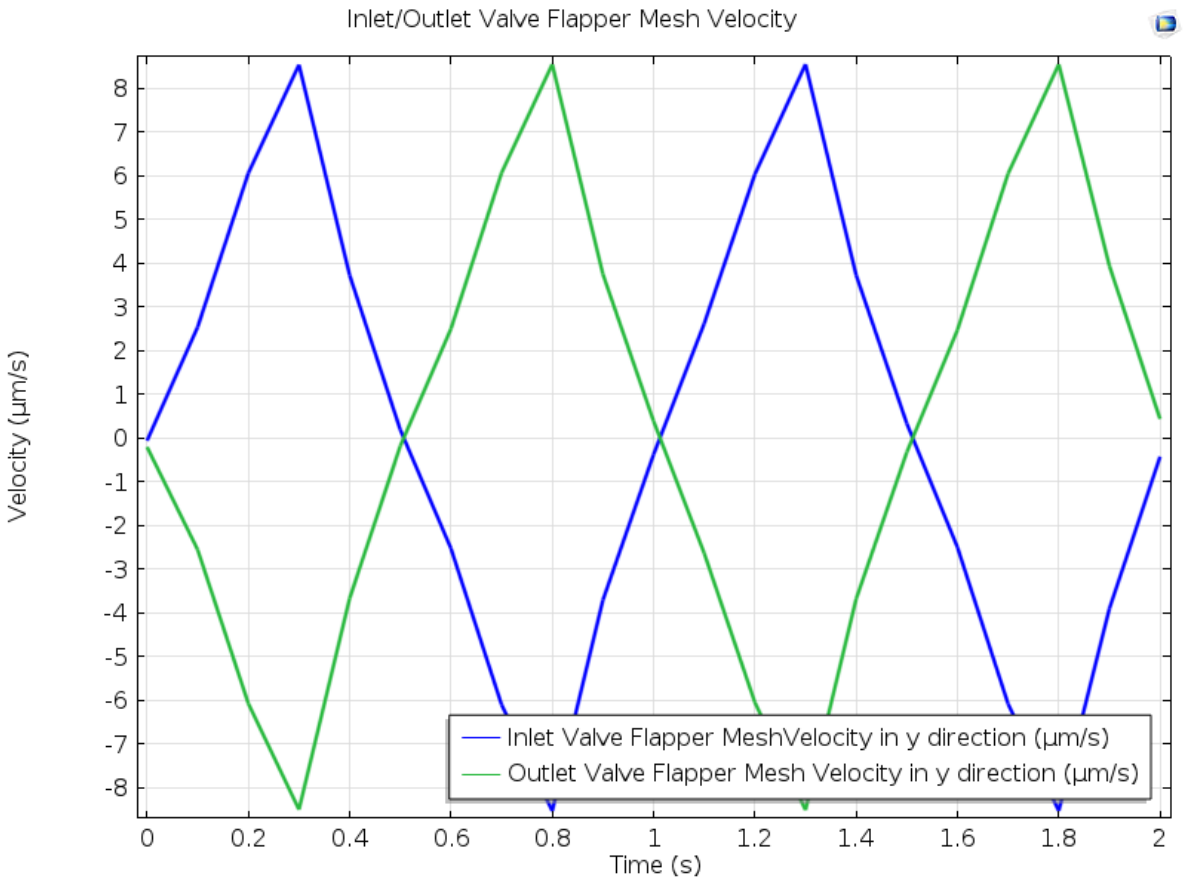

Figure 4.30 Inlet/Outlet Valve Flapper Mesh Velocity versus Time @ V=10 volts, f =1 Hz

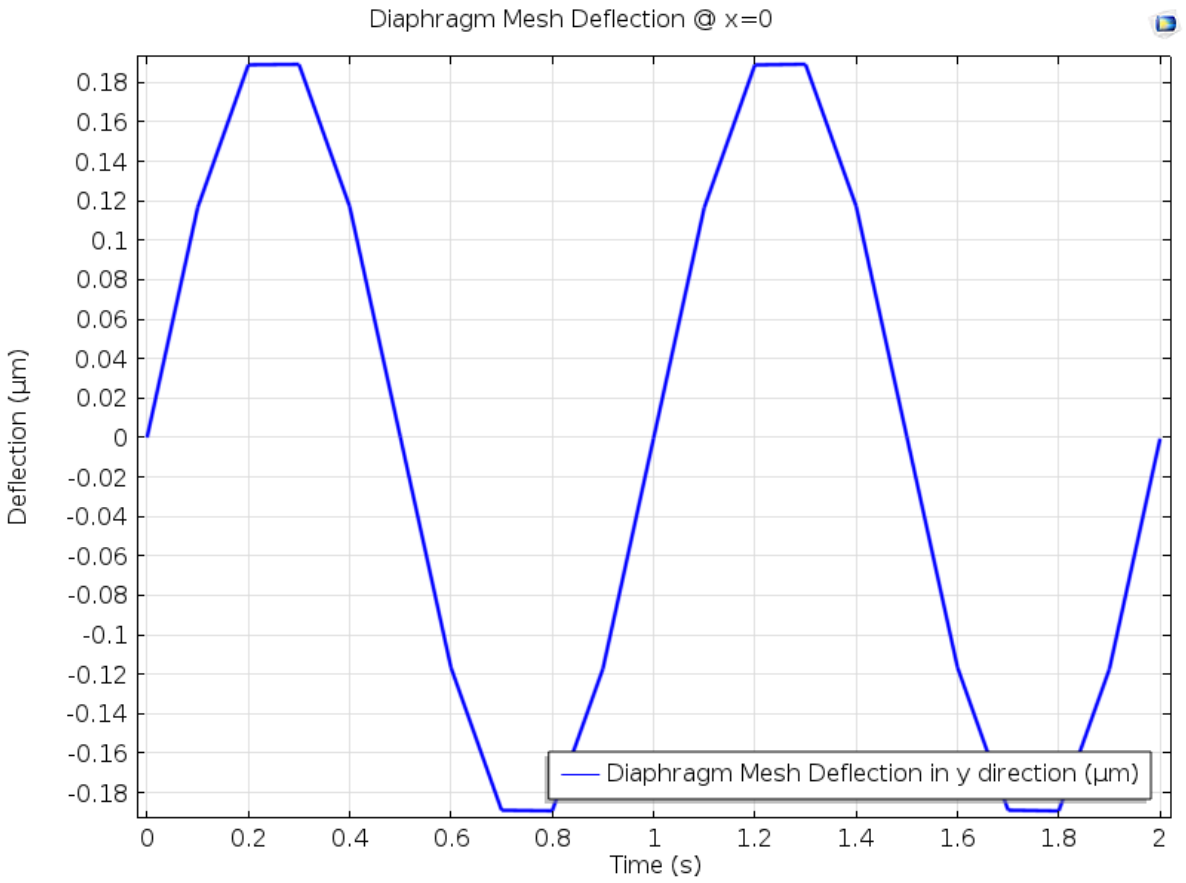

Figure 4.31 Diaphragm Mesh Deflection versus Time @ V=10 volts, f =1 Hz

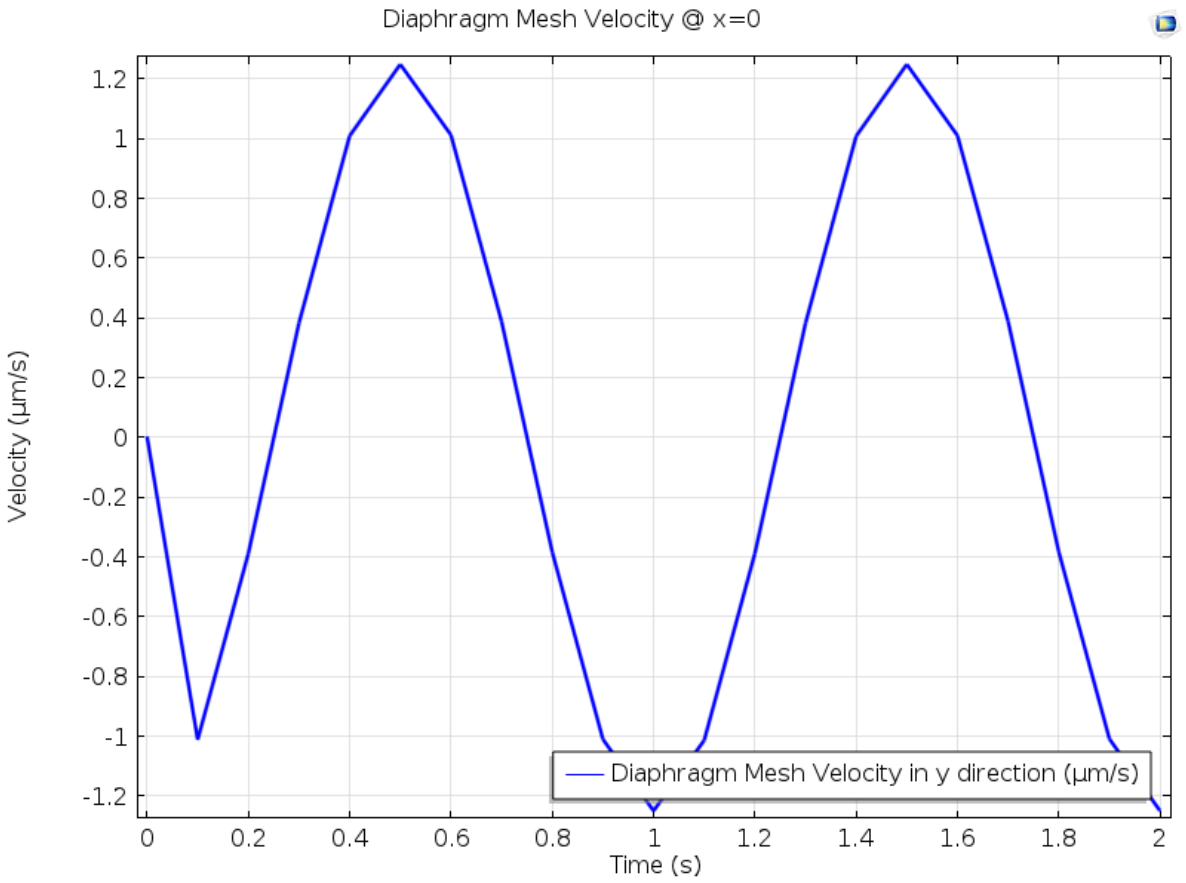

Figure 4.32 Diaphragm Mesh Velocity versus Time @ V=10 volts, f =1 Hz

In Figures 4.33 through 4.35 Velocity Magnitude and Von-Mises Stress in fluid are shown. In Figure 4.35 the difference of velocity magnitudes between inlet and outlet gates are shown with white arrows. It gives a visual understanding how the fluid divides between two gates.

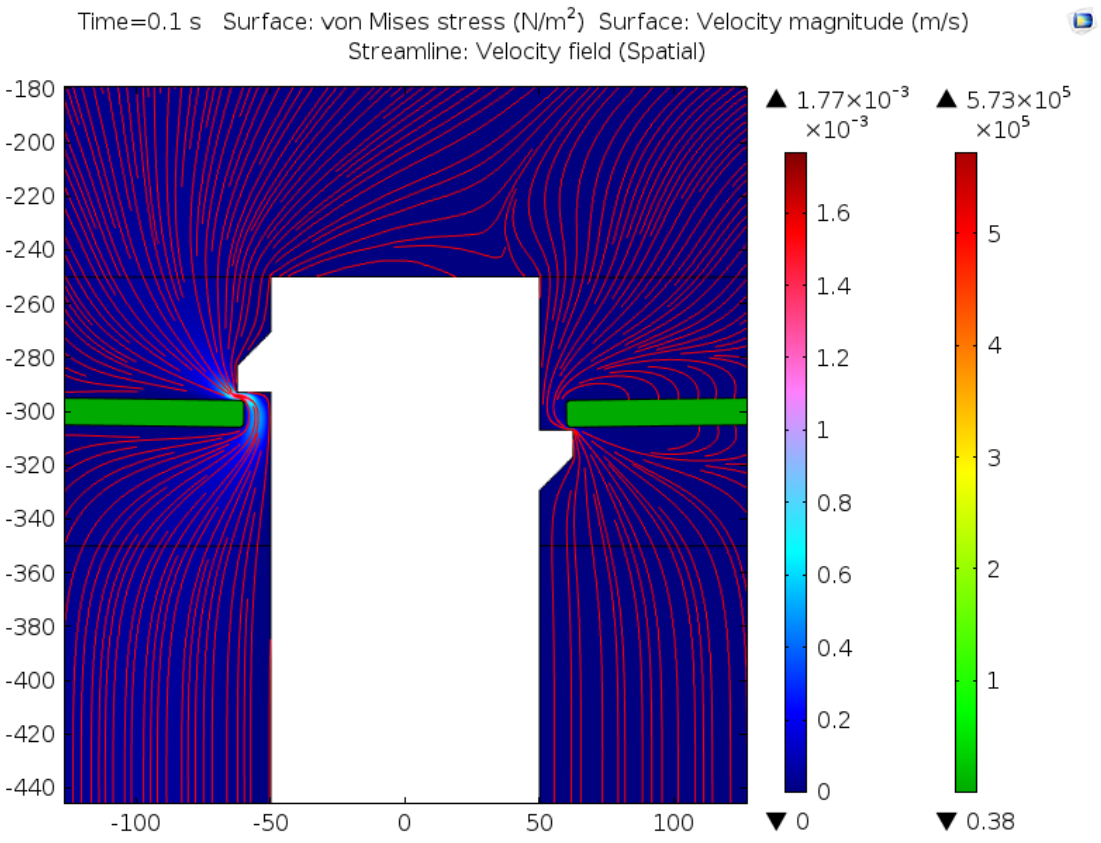

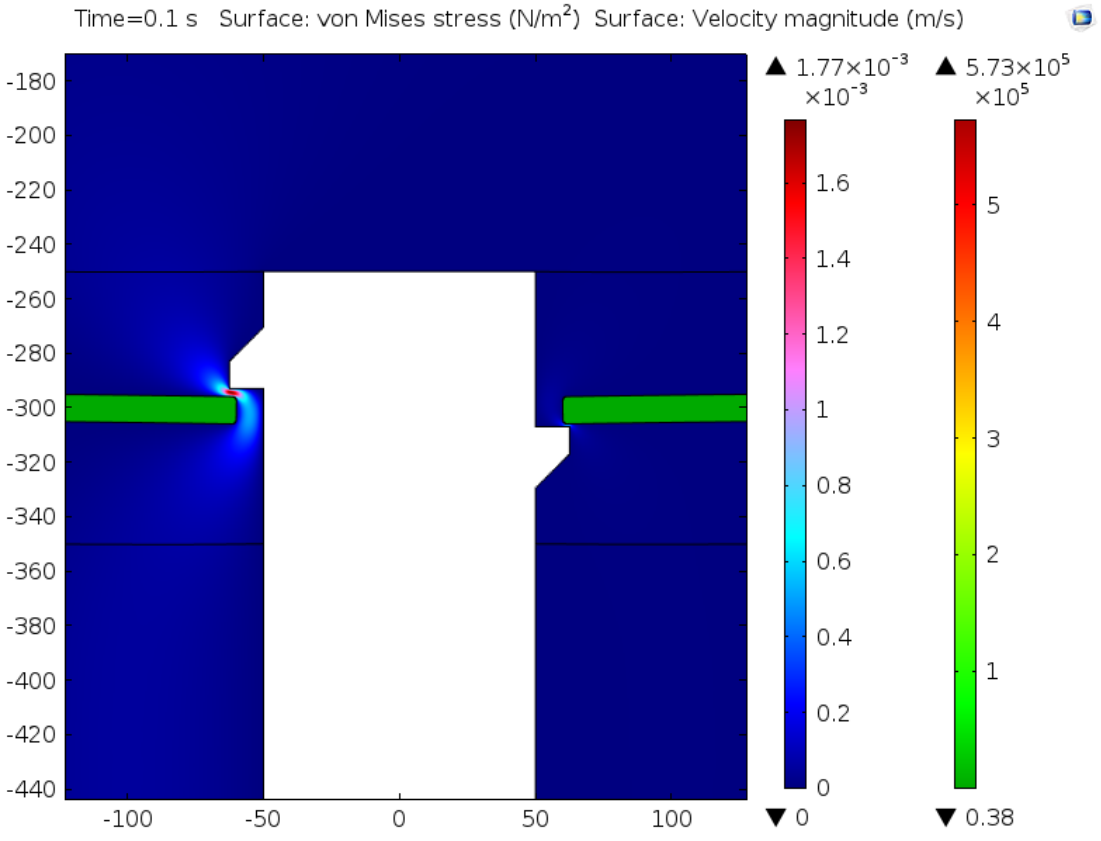

Figure 4.33 von Mises stress and Velocity magnitude @ V=10 volts, f =1 Hz

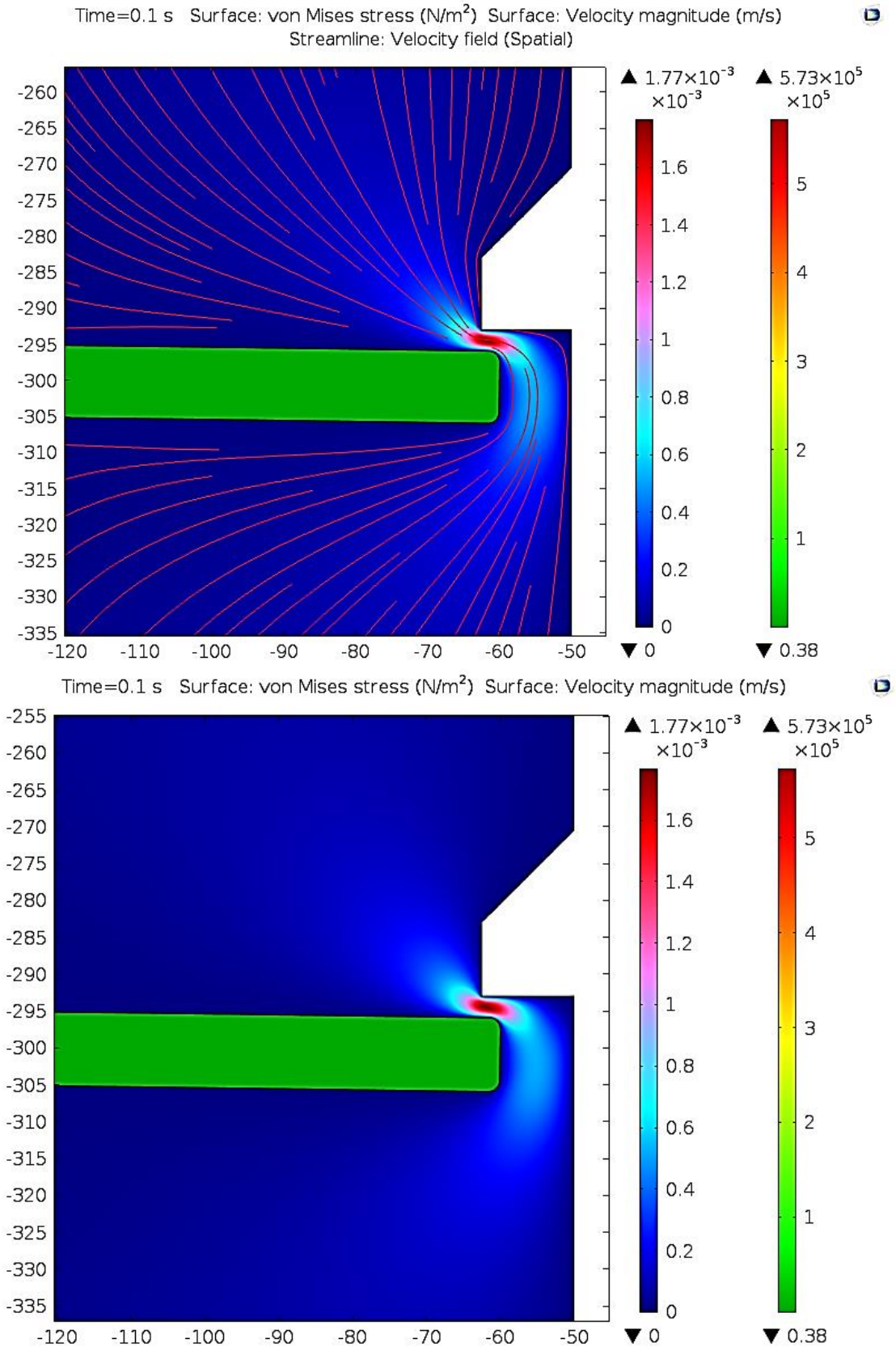

Figure 4.34 von Mises stress and Velocity magnitude @ V=10 volts, f =1 Hz in closer view

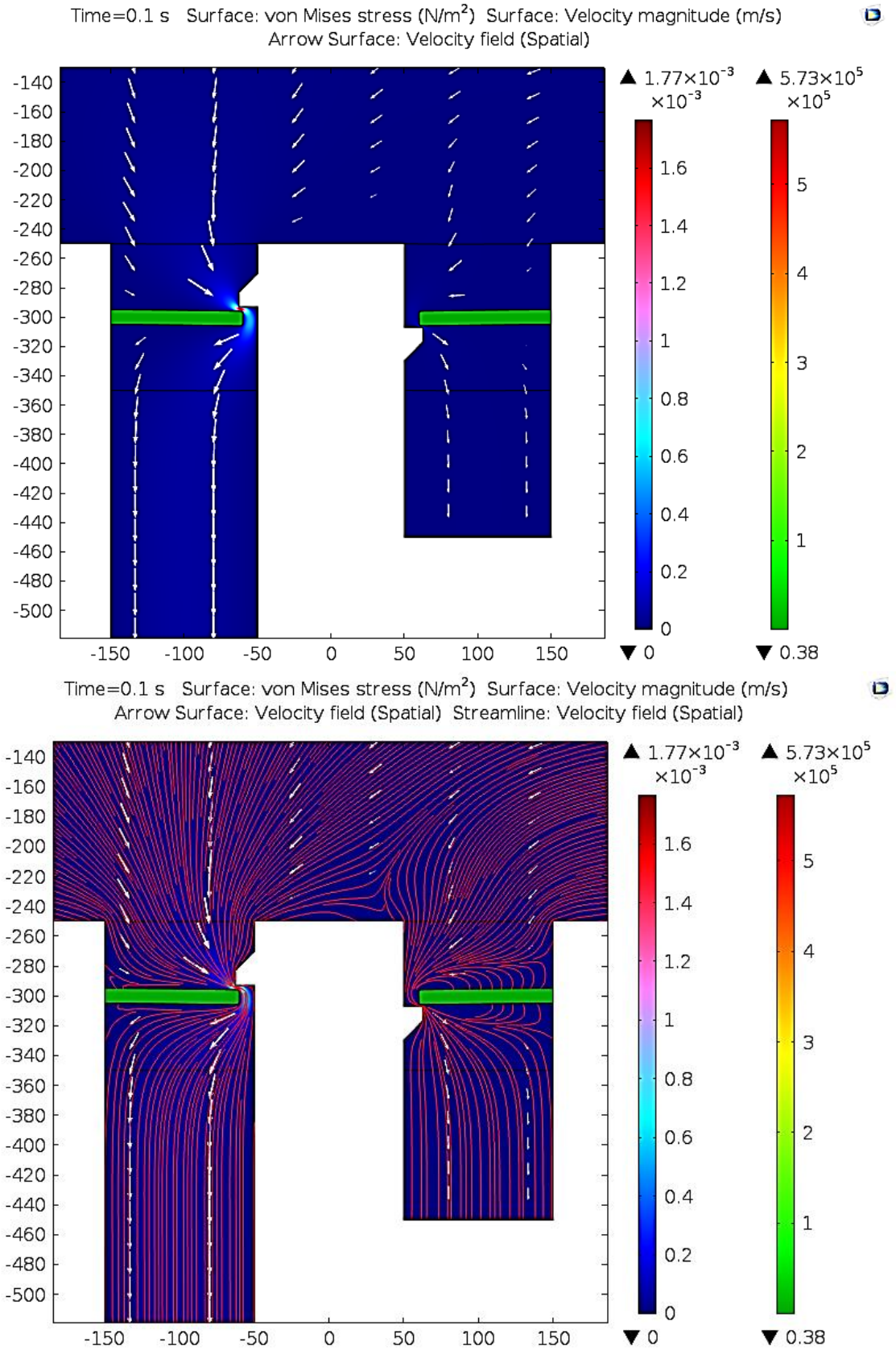

Figure 4.35 von Mises stress and Velocity with arrow magnitude @ V=10 volts, f =1 Hz

In Figure 4.36, Total Displacement and von Mises stresses are shown for flapper valves in the same load cases. Low level stress in flappers provides longer life cycle for the pump performance. The stress level for higher voltages and frequencies are obviously grater but there are still moderately considered as low for studying life cycle expectancies. For PDMS yield stress of 700 KPa [73], the maximum stress in flapper is about 8 KPa at 110 Volt and 3 Hz frequency, which is far below yield stress (Figure 4.37).

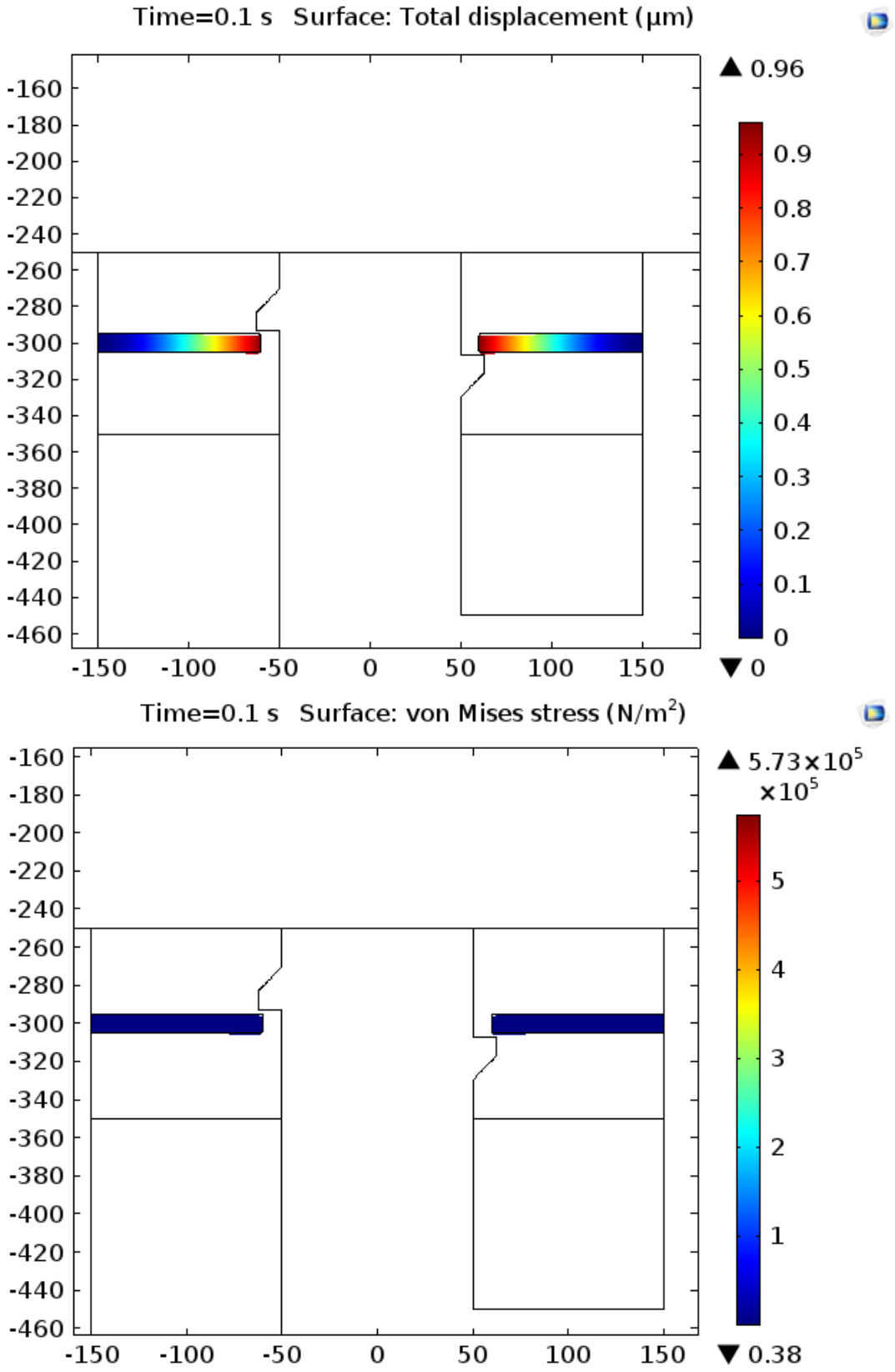

Figure 4.36 Valve Flapper Total Displacement and von Mises stress @ V=10 volts, f =1 Hz

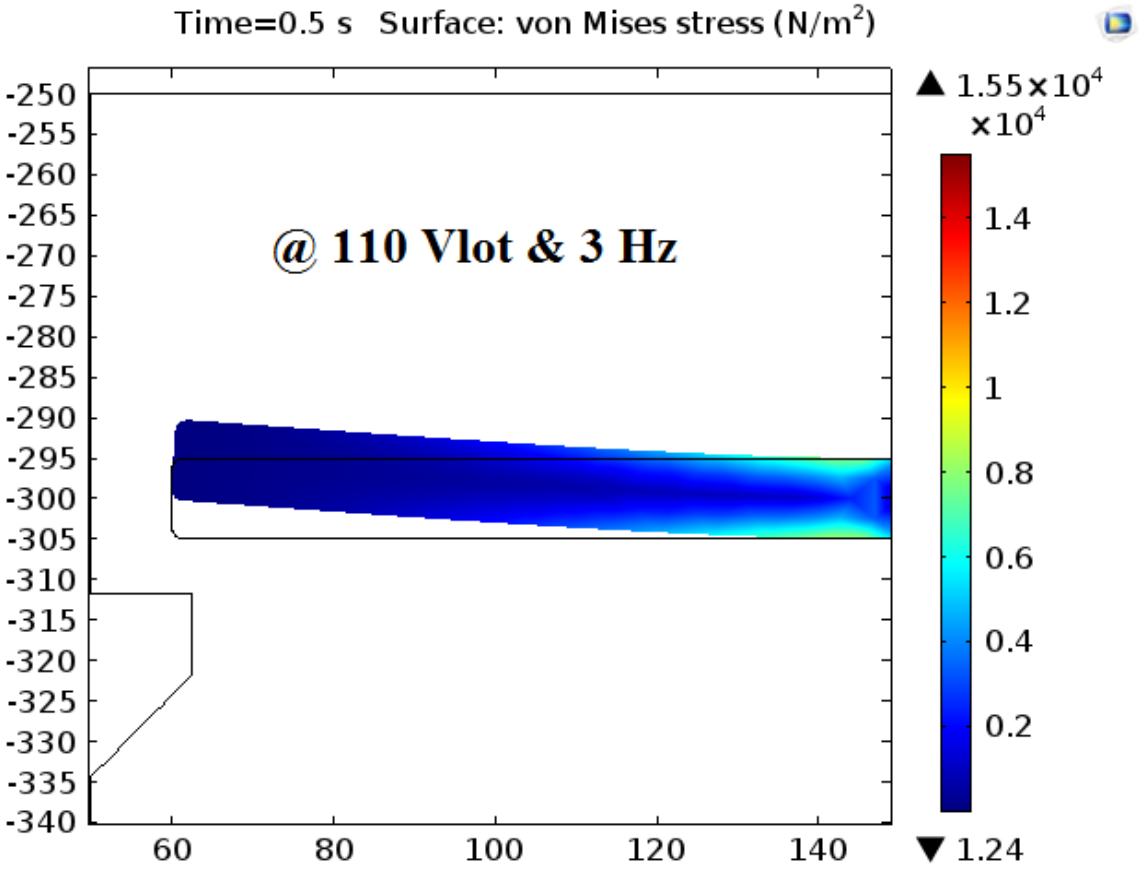

Figure 4.37 Valve Flapper von Mises stress @ V=110 volts, f =3 Hz

We have repeated the same analysis for other load cases and these results are tabulated Table 4.1 below. After collecting all data, we have compiled the results showing the final performance and comparison graphs in the conclusions chapter. For the reference, rest if load cases result graphs can be found in Appendix A.

Electrical Potential (V)	Frequency	Max Inflow (µl/s)	Max Outflow (µl/s)	Max Inflow (µl/min)	Max Outflow (µl/min)	Average Inflow (µl/min)	Average Outflow (µl/min)	Vpump @ 1 Sec (µl)	Vpump @ 2 Sec (µl)	Vpump @ 1 min (µl)	Vpump @ 1 Hour (µl)	NPD (Nominal Pump Delivery) (µl/Stroke)@1	NPD (Nominal Pump Delivery) (µl/Stroke) @2	Max Inlet suction Pressure (Pa)	Max Inlet suction Pressure (mbar)	Max Outlet Discharge Pressure @ Back Ppreassure Zero (Pa)	Max Outlet Discharge Pressure @ Back Preassure Zero (mbar)	Max Diphragm Deflection	Max Outlet Discharge Pressure @ Back Pressure = 3mmHg (400 Pa) (mbar)	Volumetric Efficeincy %
110	1	0.09756	0.08826	5.85353	5.2957	1.67097	1.50755	0.02845	0.04989	1.4967	102.42	0.02377	0.04754	6259	62.59	45350	453.5	2.084	500	99.8
110	2	0.14631	0.16913	8.7783	10.1475	2.81825	2.5411	0.04214	0.08455	2.5365	151.704	0.04732	0.09464	9174	91.74	87184	871.84	2.085	910	88.54
110	3	0.28784	0.25866	17.27	15.52	4.4558	3.9861	0.0663	0.13297	3.9891	238.68	0.06228	0.1278	18295	182.95	133930	1339.3	2.0855	1330	81.94
80	1	0.066	0.0598	3.965	3.5884	0.9705	0.8771	0.01453	0.02916	0.8748	52.308	0.01726	0.03452	4230	42.3	30665	306.65	1.5151	350	82.39
80	2	0.10076	0.11741	6.0493	7.0447	1.81263	1.6305	0.02701	0.05423	1.6269	97.236	0.03452	0.06904	6321.3	63.213	60342	603.42	1.5151	645	76.7
80	3	0.18478	0.16673	11.0873	10.0039	2.31348	2.088474	0.03448	0.06923	2.0769	124.128	0.045175	0.08175	11681	116.81	85897.5	858.975	1.5162	940	71.97
40	1	0.0352	0.0319	2.1135	1.915	0.59363	0.53688	0.00883	0.017775	0.53325	31.788	0.00867	0.01734	2270	22.7	16350	163.5	0.7571	208	98.89
40	2	0.05235	0.05968	3.14	3.58	0.96955	0.877	0.01448	0.0291	0.873	52.128	0.01722	0.03444	3300	33	30600	306	0.7576	350	80.56
40	3	0.0966	0.0857	5.8	5.25	1.36	1.227	0.02026	0.0407	1.221	72.936	0.022725	0.04545	6170	61.7	44960	449.6	0.7578	490	75.92
10	1	0.0084	0.0074	0.505	0.445	0.13	0.1182	0.0019	0.003875	0.11625	6.84	0.0022	0.0044	550	5.5	3900	39	0.1892	83	90.9
10	2	0.0136	0.01515	0.817	0.909	0.254	0.2305	0.00375	0.00758	0.2274	13.5	0.00434	0.00868	869.35	8.6935	7750	77.5	0.1893	120	86.36
10	3	0.0254	0.02225	1.525	1.3767	0.39365	0.35791	0.00584	0.01177	0.3531	21.024	0.005821	0.01164	1640	16.4	11750	117.5	0.1895	160	85.2

Table 4.1 Micro-pump's all analysis data collected for input Voltages; 10, 40, 80 and 110 Volts and Frequencies; 1, 2 and 3 Hz.

4.10.2 Flow-Voltage-Frequency relationship

As seen in Figure 4.38, all collected data has been consolidated to show the relationship between flow rate and voltage for different excitation frequencies. Flow rate increases with voltage and input frequency. The flow rate easily covers a range from just above zero up to 4 µl/min. This graph can be used as a design guide because it provides required voltage/frequency for a specific target outflow rate.

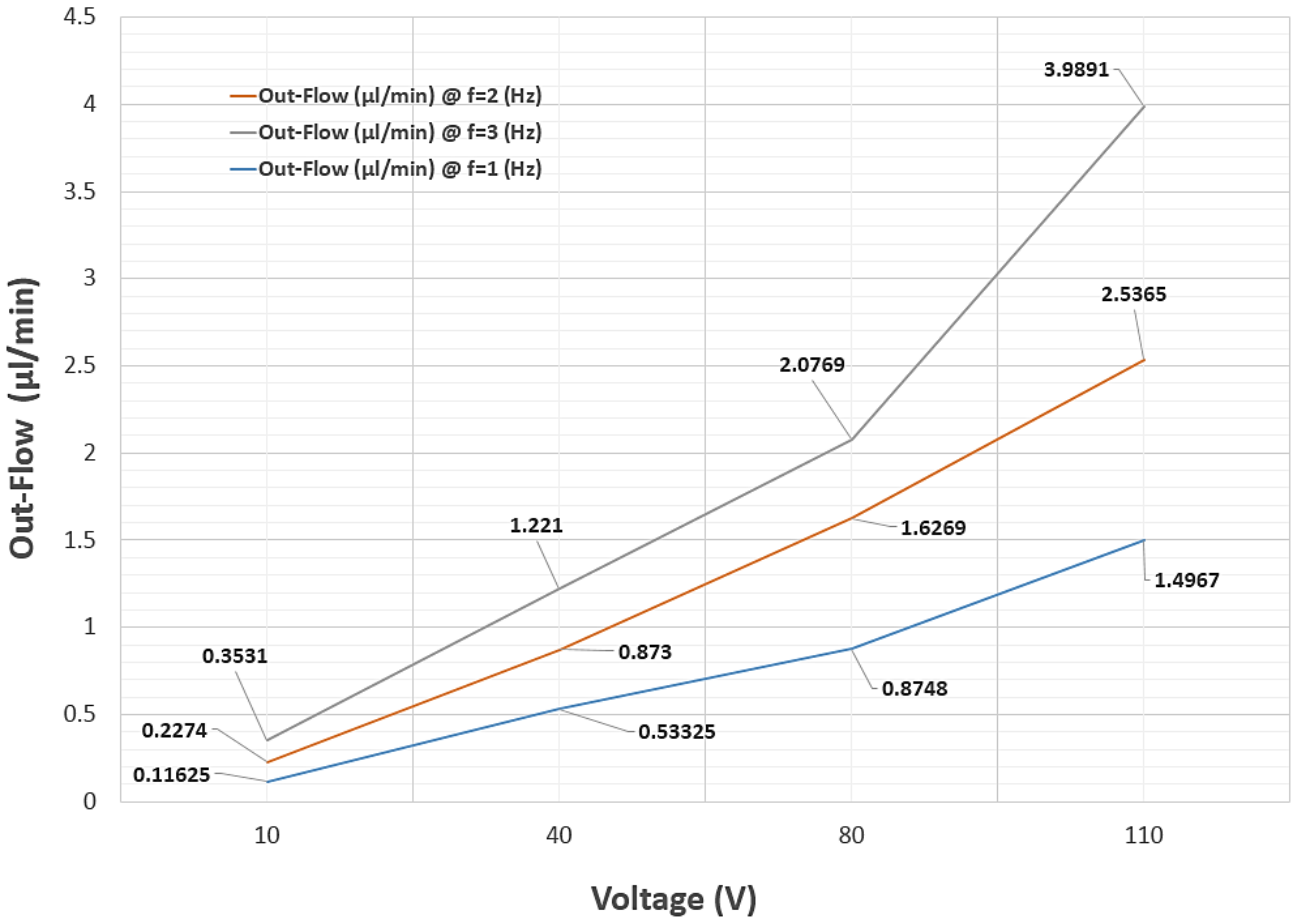

Figure 4.38 Out-Flow versus Voltage in different exciting Frequencies

In the same way Figure 4.39 shows the relationship between flow rate and frequency for different excitation voltages.

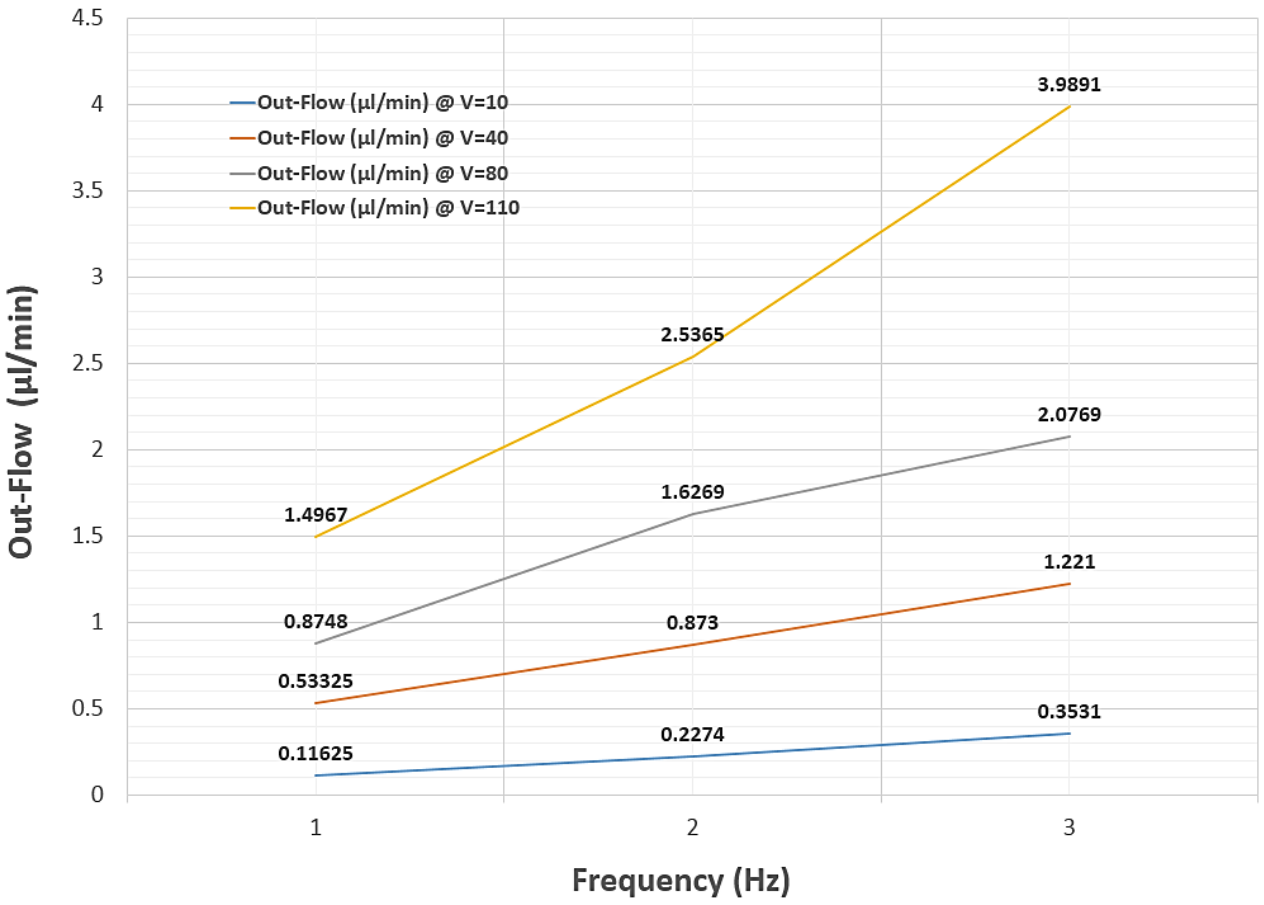

Figure 4.39 Out-Flow versus Frequency in different exciting Voltages

4.10.3 Discharge Pressure and Out-Flow/Frequency relationship

Figures 4.40 and 4.41, explain how this micro-pump performs for different discharge pressures relative to outflow rates, voltages and input frequencies. Clearly, with increasing voltage and frequency, both discharge pressure and outflow will increase and the discharge pressure is high enough for many applications of drug delivery systems. Again, this graphs is an excellent design guide to find the best flow/voltage/frequency and pressure for particular targeted application. Figure 4.40 shows the data for zero back pressure at output and Figure 4.41 provides the same for

backpressure at Interstitial fluid pressure (The interstitial fluid is found in the interstices; the spaces between cells, also known as the tissue spaces) in human skin as a targeted pressure in this insulin administering application. As can be seen, the effect of change in back pressure has minimum effect on outflow rates.

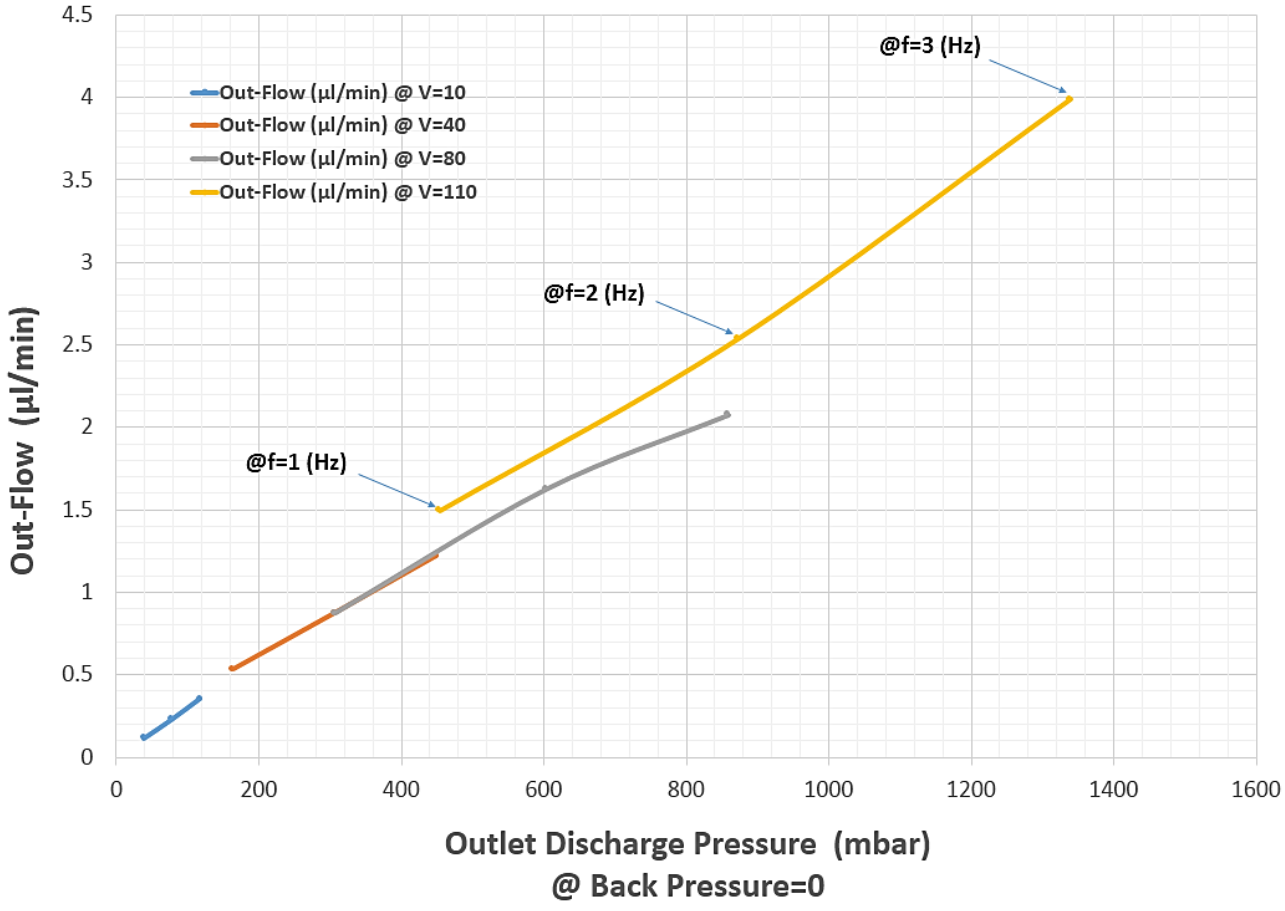

Figure 4.40 Out-Flow versus Discharge Pressure in different exciting Voltages/Frequencies

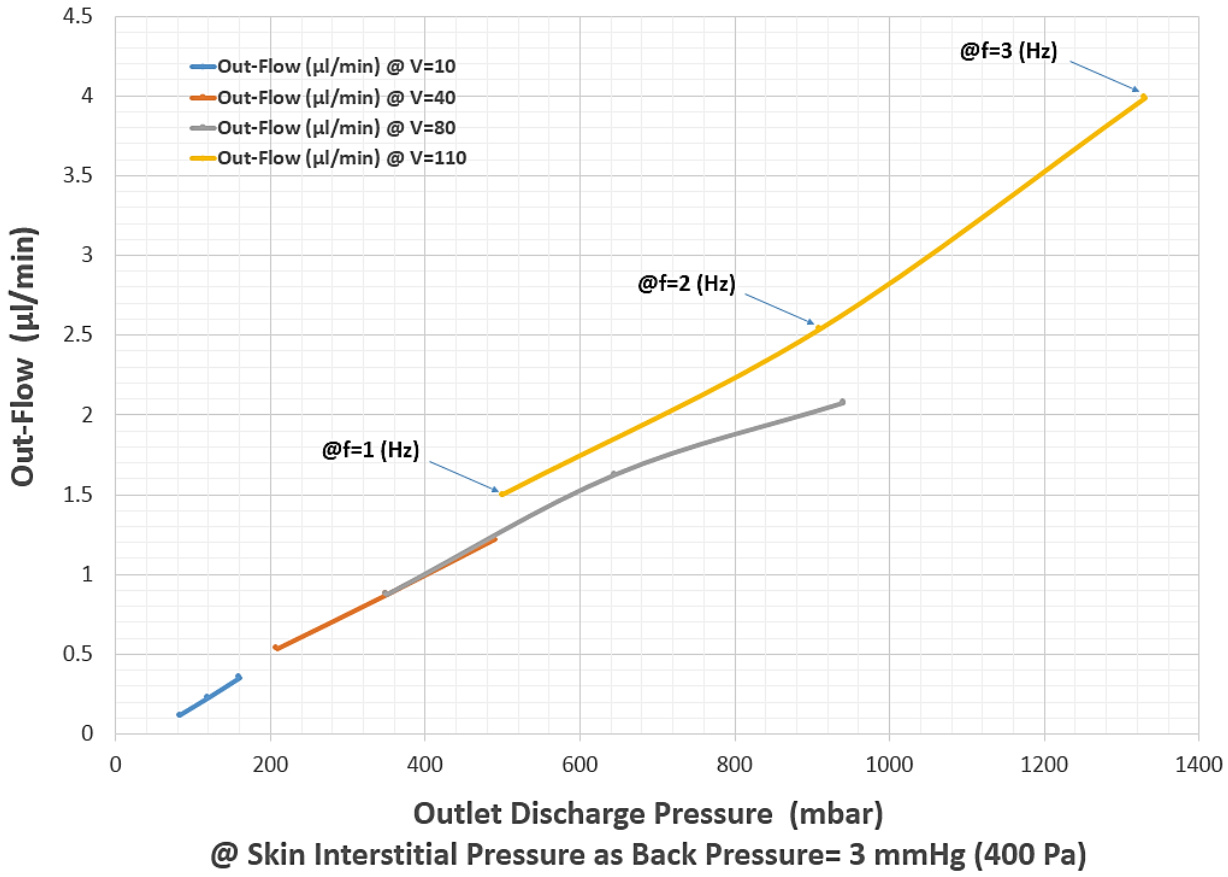

Figure 4.41 Out-Flow versus Discharge Pressure in different exciting Voltages/Frequencies

4.10.4 Leakage and Volumetric Efficiency

Typical positive displacement micro-pumps with flapper check vales provide minimum to zero leakage. Due to this study assumption of "Minimum gap but No-Contact gating" concept, we added some acceptable level of leakage to the system. To be able to understand the realistic behavior of this system we need to calculate the total effect of the leakage on pump performance. As seen in Figures 4.39 and 4.42, with increasing input frequency, both final outflow and amount of leakage will increase but in order to calculate the volumetric efficiency of this micro-pump, as

mentioned earlier, the nominal pump delivery volume should be compared to accumulated Vpump volume. Figure 4.43 provides the micro-pump volumetric efficiency versus frequency for different input voltages. In all cases, the volumetric efficiency drops with increasing frequency. This means more leakage in the system. Although in most applications and in practical cases it is negligible but it needs to be considered in our design.

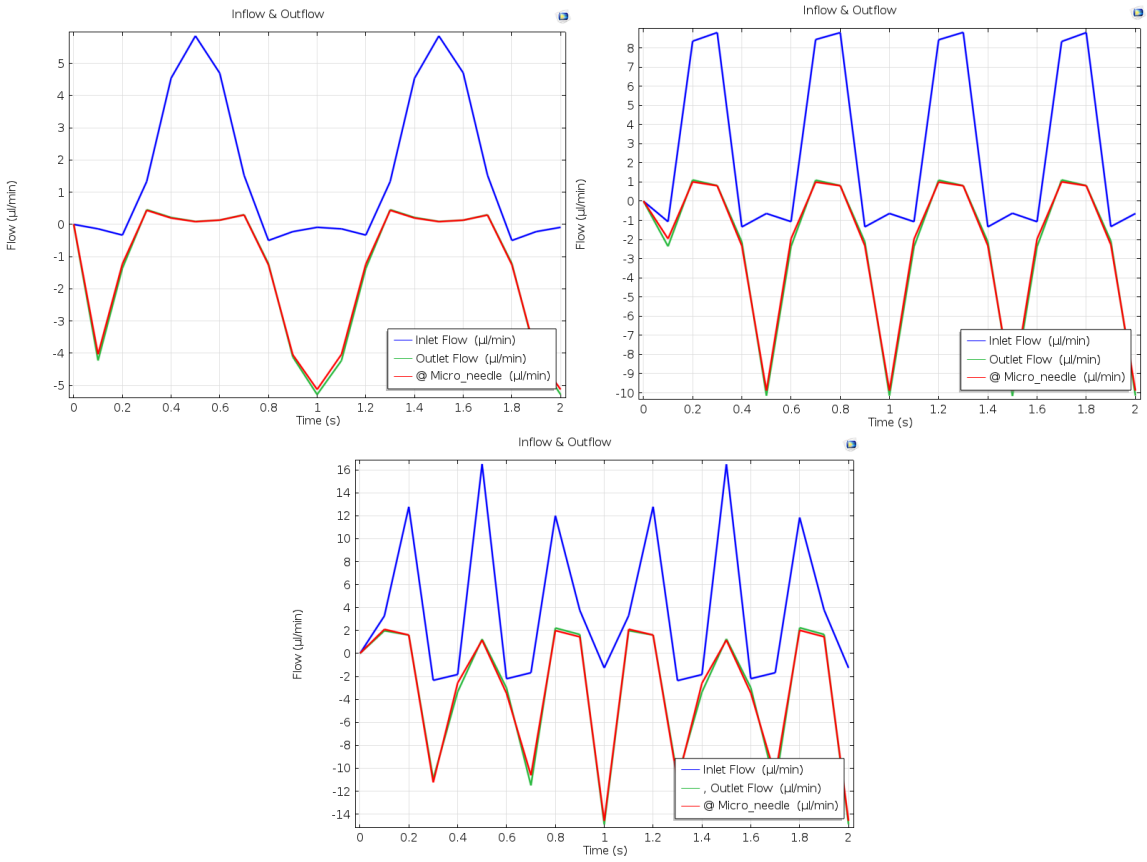

Figure 4.42 Increasing Leakage flow with increasing frequency @ V=110 volts, f =1, 2 and 3 Hz - respectively.

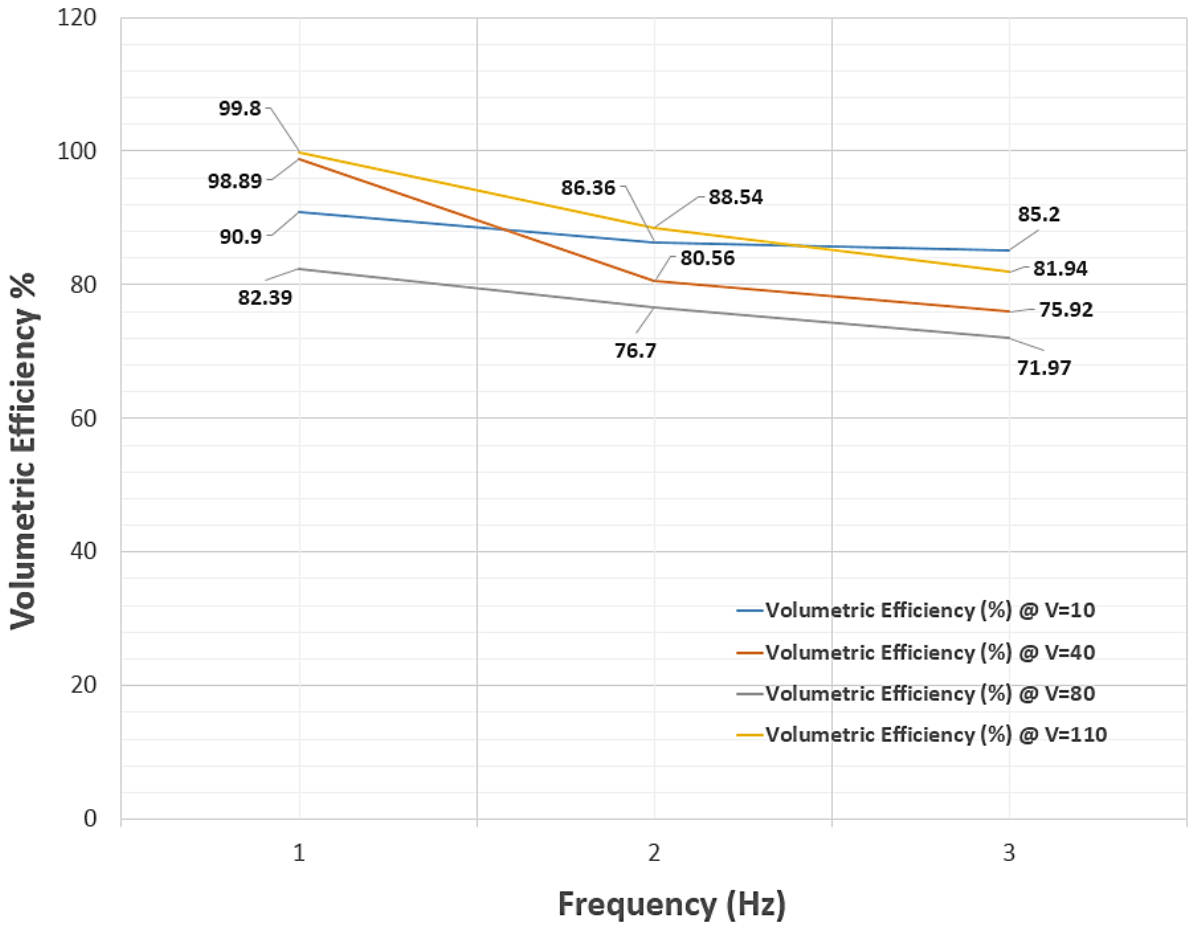

Figure 4.43 Volumetric Efficiency versus input Frequency and Voltage

4.11 Results Comparison with literature target (base pump)

A DEBIOTECH (Van-Lintel) pump as we reviewed in chapter 2, is one of the best nano-pumps clinically available in market. Here, we would like to compare our results with this pump as base target, to get to a better understanding of our design and performance results.

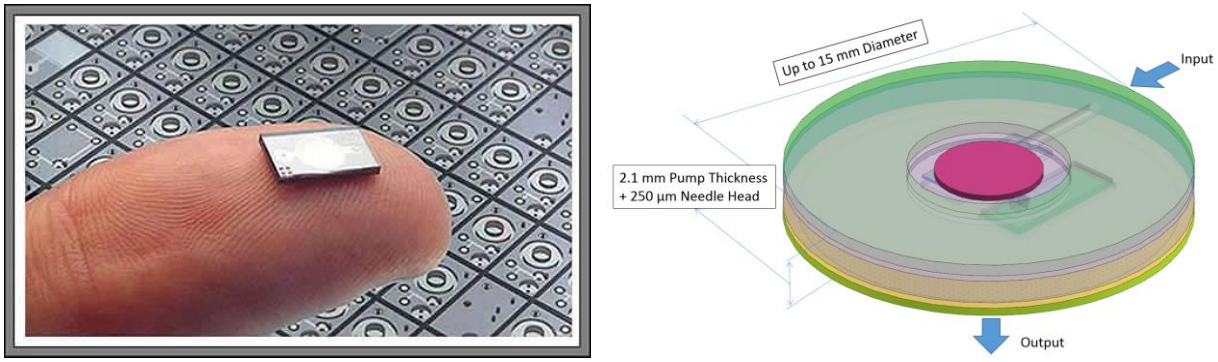

Figure 4.44 DEBOTECH Nano-pump as base target pump comparing with our study micro-pump

4.11.1 Flow rate (Volume Stroke):

The base design has a constant volume stroke (0.15 µl). This is achieved based on specific concept/structure in designing the pump. The flow rate is from Zero to 1.66 µl/min, for 0.2 Hz, and maximum 4.16 µl/min for @ Hz.

Our design intention in this study is not a constant volume stroke. Actually due to the real time administering nature of this application we need a flexible delivery regime to be able to respond to system requirement instantaneously. Therefore we have variable volume stroke based on different Voltage/Frequency inputs, varying from 0.002 to 0.06 µl/Stroke for 40 to 110 Volts and 1 to 3 Hz.

4.11.2 Leakage and Accuracy

The actual measured leakage for base pump is reported less than 0.05 ml/h (0.83 µl/min). The accuracy is shown as +/- 5% which is the overall accuracy of the stroke volume within nominal conditions. Both data are experimental driven and are not available from our simulation study but based on our simulation data, the volumetric efficiency of the pump in worst case scenario is about 70% up to 98% in best condition. Considering the effect of added leakage to our simulation, the actual accuracy of the pump is above 70% which is still within considerably acceptable range.

Since the output volume and the accuracy of outflow rate is the most important factor in insulin administering applications, the pump volumetric efficacy is playing the main role here as accuracy factor.

4.11.3 Inlet-Outlet Pressure:

For the base pump, the inlet pressure is reported from -350 to 350 mbar. The same range for outlet pressure is -400 to +200 mbar.

Our simulation data for outlet pressure shows a minimum of 83 mbar for 10 volts and 1 Hz up to maximum 1330 mbar for 110 volts and 3 Hz.

To reach the base pump maximum outlet pressure (350 mbar) we can use 40 volts with a frequency between 203 Hz or 80 volts with a frequency a little above 1 Hz (from figures 4.40 and 4.41). The outflow for this input voltage and frequency will be around 1 µl/min.

Viscosity:

The base pump has been tested for different viscosities (0-10 mPa.s). In our study we only consider insulin (water: 1 mPa.s) as main target.

4.11.4 Reliability:

The base pump has shown some results for tested reliability. This result is not available for our simulation study.

4.11.5 Compression Ratio:

The base pump provides a compression ratio of 1.15. This value is not available for our simulation study.

4.11.6 Dimensions:

The base pump dimension is: 16 x 12 x 1.86 mm comparing with our design dimension as: 15 mm (Dia.) x 2.35 mm (Thickness) which look very close in size.

Main performance specification		
Flow rate	0 to 100 µl/h **1.66 µl/min**	This is the linear range, stroke volume is constant and the flow rate is proportional to the frequency (Frequency range 0-0.2Hz).
Priming rate	250 µl/h **4.16 µl/min**	This is the maximum flow rate in the uncontrolled range. (Frequency 2Hz).
Stroke volume	150 nl **0.150 µl**	Minimum dosage unit.
Leakage	Non measurable < 0.05 ml/h	Forward and backward leak with 150 mbar overpressure applied on inlet respectively on outlet.
Accuracy	± 5%	Overall accuracy of the stroke volume within nominal conditions.
Inlet pressure Outlet pressure	-350 to +350 mbar -400 to +200 mbar	
Viscosity	0-10 mPa.s	
Actuation voltage	-40V/ +110V	Voltage applied to the piezo disc.
Compression ratio	e=deltaV/V_0=1.15	The pump is self priming and tolerant to small air bubbles.
Reliability	1.8 10^8 stroke 67 days	(equivalent to 25yr of use). Accelerated dry test at 10Hz : no measurable degradation. Real time liquid flow test 0.05Hz (see plot below).
Chip dimensions	16x12x1.86mm	

Table 4.2 Performance specification of DEBIOTECH nano-pump as base target [3] (http://www.debiotech.com)

Study Pump		
Flow Rate	0 to 4 µl/min	This is the output accumulated flow for a range of 10 to 110 Volts and frequencies up to 3 Hz
Max Vpump/ OutFlow	Max 4 µl/min	For Voltage and Frequency range: 110 Volts and 3 Hz
Stroke Volume	0.0022 to 0.06228 µl/Stoke	Minimum Dosage unit for 10-110 Volts and 1-3 Hz
Leakage	N/A	Not achievable, needs experimental-test data
Accuracy	N/A	Not achievable for simulation study, needs experimental-test data
Inlet/Outlet Pressure	Outlet : 83 mbar to 1330 mbar Inlet: -5 mbar to -150 mbar	For Voltage and Frequency range: 110 Volts and 3 Hz
Viscosity	µ = 1.0020 mPa·s @20 °C	Water based
Actuation Voltage	10 V to 110 V	
Compression ratio	N/A	Incompressible Simulation Study
Reliability	N/A	Needs Experimental / Test data
Chip Dimensions	15 mm (Dia) x 2.35 mm Height	

Table 4.3 Performance specification of study micro-pump

CHAPTER 5: Conclusion and Future Works

5.1 Conclusions

A parametric computational model of a MEMS based insulin Micro-Pump was developed using COMSOL Multiphysics. The model captures the pumping action based on the interactions between the piezoelectric, structure solids and the fluid. It was used to study the pump performance under different inputs. The design meets the targets and is acceptable for application of basal insulin administration. The micro-needle device can provide a safe and painless service to diabetes patients and will perform well in this configuration. The Micro-pump performs correctly from the Minimum to Maximum spectrum of pressure and flow rates. Data was collected for different load cases and has been processed and analyzed for different performance scenarios of micro-pump. In following sections, we will describe the final results of the pump performance.

5.2 Recommendation for future works

These are the recommendations for future studies:

- The simulation can be run for wider range of frequencies and backpressure, especially for high frequency responses/studies. Although the system is designed for a low frequency application but high frequency response can define a clearer image of the system behavior.
- The concept needs some support studies on durability and dynamic behavior and stability.

- The study needs experimental results out of testing a prototype sample.
- It can be a good idea to do some study on minimizing manufacturing cost in order to making more affordable insulin administering devices for poor people with diabetes. One of the ways can be using of 3D painting techniques for making the main pump body and using some lees expensive method of micro-machining to fabricate micro-needle arrays.
- The micro-pump concept was designed for administration of basal insulins. However, a robust concept design is achievable to meet both basal (Long-acting) and Rapid-acting insulins requirements. With adding a separate reservoir to the unit with accommodation of a fluid micro-switch, the proposed micro-pump can be used for both Long-acting and Rapid-acting insulin administration.

REFERENCES

[1] D. Maillefer, H. van Lintel, "*A HIGH*-PERFORMANCE SILICON MICRO-PUMP FOR AN IMPLANTABLE DRUG DELIVERY SYSTEM", 0-7803-5194-0/9 @1999 IEEE, (1999)

[2] H.T.V. Van Lintel, HTV, F.C.M. van de Pol and Bouwstra A., "*A PIEZOELECTRIC MICRO PUMP BASED ON MICROMACHINING OF SILICON*", Sensors & Actuators A, 1988(15):153-168 , (1998)

[3] Didier Maillefer, Stephan Gamper, Béatrice Frehner, Patrick Balmer , "*A HIGH-PERFORMANCE SILICON MICRO-PUMP FOR DISPOSABLE DRUG DELIVERY SYSTEMS*". Department of Microsystems, DEBIOTECH SA. Lausanne, Switzerland. 0-7803-5998-4/01 @2001 IEEE, (2001)

[4] Bin Ma, Sheng Liu, Zhiyin Gan1, Guojun Liu, Xinxia Cai, Honghai Zhang, Zhigang Yang., "*A PZT Insulin Pump Integrated with a Silicon Micro Needle Array for Transdermal Drug Delivery*, Microfluid Nanofluid (2006) 2: 417–423, Springer-Verlag (2006)

[5] Canadian Diabetes Association, American Diabetes Association,

[6] Public Health Agency of Canada, www.publichealth.gc.ca, Diabetes in Canada: Facts a nd figures from a public health perspective

[7] UpToDate: Evidence-Based Clinica Decision Support , www.uptodate.com/ UpToDate® is the premier evidence-based clinical decision support resource, trusted worldwide by healthcare practitioners to help them make the right decisions at the point of care. (2015).

[8] Helge Wiiga & Harald Noddelanda, "*Interstitial fluid pressure in human skin measured by micropuncture and wick-in-needle",* Scandinavian Journal of Clinical and Laboratory Investigation, Volume 43, Issue 3, pages 255-260, 1983/2010

[9] Amay J.Bandodkar & Joseph Wang, "Non-invasive wearable electrochemical sensors", Department of NanoEngineering, University of California, San Diego La Jolla, CA 92093, USA.Trends in Biotechnology, Science Direct, Volume 32, Issue 7, July 2014, Pages 363–371, (2014)

[10] G. Piechotta, J. Albers, R. Hintsche, "Novel micromachined silicon sensor for continuous glucose monitoring". Fraunhofer Institute for Silicon Technology, Fraunhoferstr. Itzehoe, Germany Biosensors and Bioelectronics 21 (2005) 802–808.

[11] Yi-Feng Lin,Jinhui Song, Yong Ding, Shih-Yuan Lub and Zhong Lin Wang, School of Materials Science and Engineering, Georgia Institute of Technology, Atlanta, Georgia 30332-0245, USA, Department of Chemical Engineering, Tsing Hua University, Hsinchu, Taiwan 30013, Republic of China *"Piezoelectric nanogenerator using CdS nanowires"* APPLIED PHYSICS LETTERS 92, 022105 ,(2008)

[12] Zhong Lin Wang, *"Top emerging technologies for self-powered nanosystems: nanogenerators and nanopiezotronics"*, School of Materials Science and Engineering, Georgia Institute of Technology, Atlanta GA 30332-0245 USA, 978-1-4244-3544-9 ©2010 IEEE, (2010)

[13] Zhong Lin Wang, "NANOGENERATORS FOR SELF-POWERING NANOSYSTEMS AND PIEZOTRONICS FOR SMART MEMS/NEMS", School of Material Science and Engineering, Georgia Institute of Technology, Atlanta, Georgia 30332-0245 USA, 978-1-4244-9634-1/11 ©2011 IEEE, (2011)

[14] Corey A. Hewitt, Alan B. Kaiser, Siegmar Roth, Matt Craps, Richard Czerw and David L. Carroll, *"Multilayered Carbon Nanotube/Polymer Composite Based Thermoelectric Fabrics"*, Center for Nanotechnology, Wake Forest University, Winston Salem, North Carolina 27105, United States - MacDiarmid Institute for Advanced Materials and Nanotechnology, SCPS, Victoria University of Wellington, Wellington 6140, New Zealand - School of Electrical Engineering WCU Flexible Nanosystems, Korea University, Seoul, Korea - NanoTechLabs, Yadkinville, North Carolina 27055, United States. © 2012 American Chemical Society, pubs.acs.org/NanoLett. dx.doi.org/10.1021/nl203806q | Nano Lett. 2012, 12, pages 1307−1310. (2012)

[15] L. Saggere, N. W. Hagood, D. C. Roberts, H -Q. Li, J. L. Steyn, K. Turner, J. A. Carretero, Yaglioglu, Y -H. Su, R. Mlcak, S . M. Spearing,K. S. Breuer, M. A. Schmidt.*"Design, Fabrication, and Testing of a Piezoelectrically Driven High Flow Rate Micro-Pump"*, Massachusetts Institute of Technology, Cambridge, MA 02 139 USA - Boston Microsystems, Inc., Woburn, MA 01801 USA -Brown University, Providence, RI 02912 USA. 0-7803-5940-2/01/ 2001 IEEE. (2001).

[16] Anders Olsson, GoranStemme, Erik Stemme. *"A Valve-less Planar Fluid Pump with two Pump chambers"*, Instrumentation Laboratory, Royal Institute of Thechnology, S-100 44 Stochholm, Sweeden - Depatment of Computer Engineering, Chalmers university of thechnology, S-412 96 Goteberg, Sweden. Sensors and Actuators A 46-47 (1995) 549-556.

[17] P. K. Podder, D. P. Samajdar, D. Mallick and A. Bhattacharyya. *"Design, Simulation and Study of Micro-pump, Micro-valve and Micro-needle for Biomedical Applications"*,

Institute of Radio Physics & Electronics, University of Calcutta, Comsol Conference 2012, Bangalore.

[18] H. Yangl, T.-H.Tsai, C.-C.Hu. "Portable Valve-less Peristaltic Micro-pump Design and Fabrication" , Institute of Precision Engineering, National Chung Hsing University, Taiwan - Department of Mechanical Engineering, WuFeng Institute ofTechnology, Taiwan. ©EDA Publishing/DTIP 2008, ISBN: 978-2-35500-006-5, (2008).

[19] Shawn P. Davis, Wijaya Martanto, Mark G. Allen and Mark R. Prausnitz. *"Hollow Metal Micro-needles for Insulin Delivery to Diabetic Rats"*, IEEE TRANSACTIONS ON BIOMEDICAL ENGINEERING, VOL. 52, NO. 5, MAY 2005.

[20] P. Zhang, and G.A. Jullien. *"Micro-needle Arrays for Drug Delivery and Fluid Extraction"* . ATIPS Laboratory, ECE, University of Calgary, Proceedings of the 2005 International Conference on MEMS, NANO and Smart Systems (ICMENS'05) 0-7695-2398-6/05 © 2005 IEEE.

[21] Liu Chang, Fundations of MEMS, 2006 Pearson Education, Inc. ISBN 0.13-147286-0.

[22] COMSOL Multiphysics, www.comsol.com,

[23] COMSOL on-line documentions and training webinars, www.comsol.com,

[24] J Ruhhammer, M Zens, F Goldschmidtboeing, A Seifert and P Woias, "*Highly elastic conductive polymeric MEMS"*, Laboratory for Design of Microsystems, Department of Microsystems Engineering—IMTEK, University of Freiburg, Georges-Koehler-Allee 102, 79110 Freiburg, Germany - Gisela and Erwin Sick Chair of Micro-optics, Department of Microsystems Engineering—IMTEK, University of Freiburg, Georges-Koehler-Allee 102, 79110 Freiburg, Germany. Published 28 January 2015 • © 2015 National Institute for Materials Science • Science and Technology of Advanced Materials, Volume 16, Number 1. doi:10.1088/1468-6996/16/1/015003, (2015)

[25] Nava Setter, "*Electroceramic-based MEMS: fabrication-technology and applications*", © 2005 Springer Science-Business Media, Inc, ISBN 0.387-23310-5, 2005

[26] Yifan Gao and Zhong Lin Wang, *"Electrostatic Potential in a Bent Piezoelectric Nanowire. The Fundamental Theory of Nanogenerator and Nanopiezotronics"*, NANO LETTERS (2007) Vol. 7, No. 8, 2499-2505

[27] Gianni Ciofani · Arianna Menciassi (Eds.), *"Piezoelectric Nanomaterials for Biomedical Applications"*, ISBN 978-3-642-28043-6 e-ISBN 978-3-642-28044-3, DOI 10.1007/978-3-642-28044-3, Springer Heidelberg New York Dordrecht London, Library of Congress Control Number: 2012931316 _c Springer-Verlag Berlin Heidelberg 2012.

[28] Chengliang Sun, Jian Shi, and Xudong Wang, *"Fundamental study of mechanical energy harvesting using piezoelectric nanostructures"*, JOURNAL OF APPLIED PHYSICS 108, 034309, 2010.

[29] Jin Woo Cho, Churl Seung Lee, Kyoung Il Lee, Seon Min Kim,1 Sung Hyun Kim and Young Keun Kim, *"Morphology and electrical properties of high aspect ratio ZnO nanowires grown by hydrothermal method without repeated batch process"*, APPLIED PHYSICS LETTERS 101, 083905 (2012).

[30] D.V. McAllister, S . Kaushk, P.N. Patel, J.L. Mayberry, M.G. Allen, and M.R. Prausnitz, *"MICRONEEDLES FOR TRANSDERMAL DELIVTERY OF MACROMOLECULES"*, 0-7803-5674-8/991, IEEE 1999.

[31] Ayumi Kabata and Hiroaki Suzuki, Yasuhiro Kishigami and Makoto Haga, *"Micro System for Injection of Insulin and Monitoring of Glucose Concentration*", 0-7803-9056-3/05 © 2005 IEEE.

[32] Zhi Xu', Sheng Liu 1, Zhiyin Gan', Bin Ma', Guojun Liu2, Xinxia Cai3, Honghai Zhang', Zhigang Yang2, *"An Integrated Intelligent Insulin Pump"*, 7th International Conference on Electronics Packaging Technology, 1-4244-0620-X/06 © 2006 IEEE.

[33] Niclas Roxhed, Björn Samel, Lina Nordquist, Patrick Griss, and Göran Stemme, *"Painless Drug Delivery Through Microneedle-Based Transdermal Patches Featuring Active Infusion"*, IEEE TRANSACTIONS ON BIOMEDICAL ENGINEERING, VOL. 55, NO. 3, MARCH 2008.

[34] Zhenqing Hou, Chenghong Lin and Qiqing Zhang, *"Design of a smart transdermal insulin drug delivery system"*, 978-1-4244-4713-8/10, ©2010 IEEE.

[35] Jian Chen, Claudia R. Gordijo, Michael Chu, Xiao Yu Wu and Yu Sun. *"A GLUCOSE-RESPONSIVE INSULIN DELIVERY MICRO DEVICE EMBEDDED WITH NANOHYDROGEL PARTICLES AS SMART VALVES"*, 978-1-4577-0156-6/11, ©2011 IEEE.

[36] Yongjun Zhao, Siqi Li, Arthur Davidson, Bozhi Yang, QianWang and Qiao Lin, *"A MEMS viscometric sensor for continuous glucose monitoring"*, IOP PUBLISHING, JOURNAL OF MICROMECHANICS AND MICROENGINEERING, doi:10.1088/0960-1317/17/12/020, J. Micromech. Microeng. 17 (2007) 2528–2537.

[37] Xian Huang, Siqi Li, Jerome Schultz, Qian Wang, and Qiao Lin, *"A Capacitive MEMS Viscometric Sensor for Affinity Detection of Glucose"*, JOURNAL OF MICROELECTROMECHANICAL SYSTEMS, VOL. 18, NO. 6, DECEMBER 2009.

[38] G. Piechotta , J. Albers and R. Hintsche, *"Novel micromachined silicon sensor for continuous glucose monitoring"*, Biosensors and Bioelectronics 21 (2005) 802–808.

[39] R. Zengerle, W. Geiger, M. Richter, J. Ulrich, S. Kluge, A. Richter, *"Transient measurements on miniaturized diaphragm pumps in microfluid systems"*, Sensors and Actuators A 46-47 (1995) 557-561.

[40] R. Zengerle, J. Ulrich, W S. Kluge, M. Richter, A. Richter, *"A bidirectional silicon micropump"*, Sensors and Actuators A 50 (1995) 81-86.

[41] Sebastian Bo¨hm , Wouter Olthuis and Piet Bergveld, "*A plastic micropump constructed with conventional techniques and materials*", Sensors and Actuators, 77 _1999. 223–228

[42] Ansgar Wego*, Lienhard Pagel, "*A self-filling micropump based on PCB technology"*, Sensors and Actuators, A 88 (2001) 220-226.

[43] F C M VAN DE POL, H T G VAN LINTEL, M ELWENSPOEK and J H J FLUITMAN, *"A Tbermopneumatic Mcropump Based on Micro-enineering Techniques"*, Sensors and Actuators, A21 -A23 (1990) 198-202.

[44] F. C. M. VAN DE POL, D. G. J. WONNINK, M. ELWENSPOEK and J. H. J. FLUITMAN, *"A THERMO-PNEUMATIC ACTUATION PRINCIPLE FOR A MICROMINIATURE PUMP AND OTHER MICROMECHANICAL DEVICES"*, Sensors and Actuators, 17 (1989) 139 – 143.

[45] Asuncion V. Lemoff, Abraham P. Lee, *"An AC magnetohydrodynamic micropump"*, Sensors and Actuators B 63 (2000) 178–185.

[46] Mir Majid Teymoori , Ebrahim Abbaspour-Sani, *"Design and simulation of a novel electrostatic peristaltic micromachined pump for drug delivery applications"*, Sensors and Actuators A 117 (2005) 222–229.

[47] Kan Junwu, Yang Zhigang, Peng Taijiang, Cheng Guangming and Wu Boda, *"Design and test of a high-performance piezoelectric micropump for drug delivery"*, Sensors and Actuators A 121 (2005) 156–161.

[48] Liguo Chen, Yongyang Zhu, Yaxin Liu, Weibin Rong and Lining Sun, "Liguo Chen, Yongyang Zhu, Yaxin Liu, Weibin Rong, Lining Sun", 978-1-4244-2693-5/09, ©2009 IEEE.

[49] Tay Eng Hock and Francis and Mr Holden Li, *"Designing a Fluid Pump for Microfluidic Cooling Systems in Electronic Components"*, 0-7803-4157-0/97, ©1997 IEEE.

[50] Ok Chan Jeong, Sang Sik Yang, *"Fabrication and test of a thermopneumatic micropump with a corrugated pq diaphragm"*, Sensors and Actuators 83 (2000) 249–255.

[51] Peter Woias, *"Micropumps: past, progress and future prospects"*, Sensors and Actuators B 105 (2005) 28–38

[52] M Koch, N Harris, R Maas, A G R Evans, N M White and A Brunnschweiler, *"A novel micropump design with thick-film piezoelectric actuation"*, PII: S0957-0233(97)76957-1, Meas. Sci. Technol. 8 (1997) 49–57.

[53] Tao Zhang, Qing-Ming Wang, *"Valveless piezoelectric micropump for fuel delivery in direct methanol fuel cell (DMFC) devices"*, Journal of Power Sources 140 (2005) 72–80.

[54] M C Carrozza, N Croce, B Magnani and P Dario, *"A piezoelect ric-d riven stereolit hography-fabricated micropump"* , J. Micromech. Microeng. 5 (1995) 177-179.

[55] Francis E. H. Tay, W. 0. Choong, H. Liu and G. L. Xu, *"AN INTELLIGENT MICRO-FLUIDIC SYSTEM FOR DRUG DELIVERY"*, 0-7803-58 12-0/00, ©2000 EEE

[56] Nayana.L, Premila Manohar and Supriya Babu, *"Design and Simulation of Valveless Piezoelectric Micropump"* , Excerpt from the Proceedings of the 2012 COMSOL Conference in Bangalore.

[57] H. K. Ma, B. R. Hou, H. Y. Wu, C. Y. Lin, J. J. Gao and M. C. Kou, *"Development and application of a diaphragm micro-pump with piezoelectric device"* , DOI 10.1007/s00542-007-0462-6, Microsyst Technol (2008) 14:1001–1007.

[58] H. K. Ma1, B. R. Hou, H. Y. Wu, C.Y. Lin, J. J. Gao, *"Development of a Micro-diaphragm Pump with Piezoelectric Device"* , 1-4244-0959-4/07, ©2007 IEEE.

[59] Chou-Lin Wu, Jinn-Cherng Yang, Ying-Chi Chen, *"Low Power Consumption PZT Actuated Micro-Pump"*, 1-4244-0735-4/06, ©2006 IEEE.

[60] Zunqiang Fan, Jingshi Dong and Zhigang Yang, Wei Zheng, *"New Type of Piezoelectric Pump with Built-in Self Test"*, 978-1-4244-6712-9/10, ©2010 IEEE

[61] KONG Xiang-bing, CHEN Li-guo, SHAO Chao, LIU De-li, QU Dong-sheng, *"Piezoelectric-Stack Pump for Micro-Reagents Dispense"*, 978-1-4577-0399-7111, ©2011lEEE

[62] A. Nisar, Nitin Afzulpurkar, Banchong Mahaisavariya and Adisorn Tuantranont, *"MEMS-based micropumps in drug delivery and biomedical applications"*, Sensors and Actuators B 130 (2008) 917–942.

[63] Junwu Kan, Kehong Tang, Guojun Liu, Guoren Zhu and Chenghui Shao, *"Development of serial-connection piezoelectric pumps"*, Sensors and Actuators A 144 (2008) 321–327.

[64] Swadeshmukul Santra, Paul Holloway and Christopher D. Batich, *"Fabrication and testing of a magnetically actuated micropump"*, Sensors and Actuators B 87 (2002) 358–364.

[65] Nam-Trung Nguyen and Thai-Quang Truong, *"A fully polymeric micropump with piezoelectric actuator"*, Sensors and Actuators B 97 (2004) 137–143.

[66] Helene Andersson, Wouter van der Wijngaart, Peter Nilsson, Peter Enoksson, Goran Stemme, "A valve-less diffuser micropump for micro¯uidic analytical systems", Sensors and Actuators B 72 (2001) 259-265.

[67] C. Yamahata, C. Lotto, E. Al-Assaf, M. A. M. Gijs, *"A PMMA valveless micropump using electromagnetic actuation"*, DOI 10.1007/s10404-004-0007-6, Microfluid Nanofluid (2005) 1: 197–207

[68] Anders Olsson, Goran Stemme and Erik Stemme, *"Numerical and experimental studies of flat-walled diffuser elements for valve-less micropumps"*, Sensors and Actuators 84 _2000. 165–175.

[69] Enk Stemme, *"A valveless diffuser/nozzle-based fluid pump"*, Sensors and Actuators A, 39 (1993) 159-167.

[70] Anders Olsson, Goran Stemme and Erik Stemme, *"Diffuser-element design investigation for valve-less pumps"*, Sensors and Actuators A 57 (1996) 137-143.

[71] Ivano Izzo, Dino Accoto, Arianna Menciassi, Lothar Schmitt, Paolo Dario, *"Modeling and experimental validation of a piezoelectric micropump with novel no-moving-part valves"*, Sensors and Actuators A 133 (2007) 128–140.

[72] V. T. Dau, T. X. Dinh, K. Tanaka and S. Sugiyama, *"Study on Geometry of Valveless-Micropump"*, 978-1-4244-2853-3/09, ©2009 IEEE

[73] Angel S. Cruz Félix, A. Santiago-Alvarado, " *Physical-chemical properties of PDMS samples used in tunable lenses*", International Journal of Engineering Science and Innovative Technology (IJESIT) Volume 3, Issue 2, March 2014.

Appendix A: Detailed Results of the Simulation

For the reference, rest of the load cases and result graphs are shown below based on different voltages and input frequencies.

A.1 Analysis data for load case: Voltage=10 volts, Frequency=2 Hz

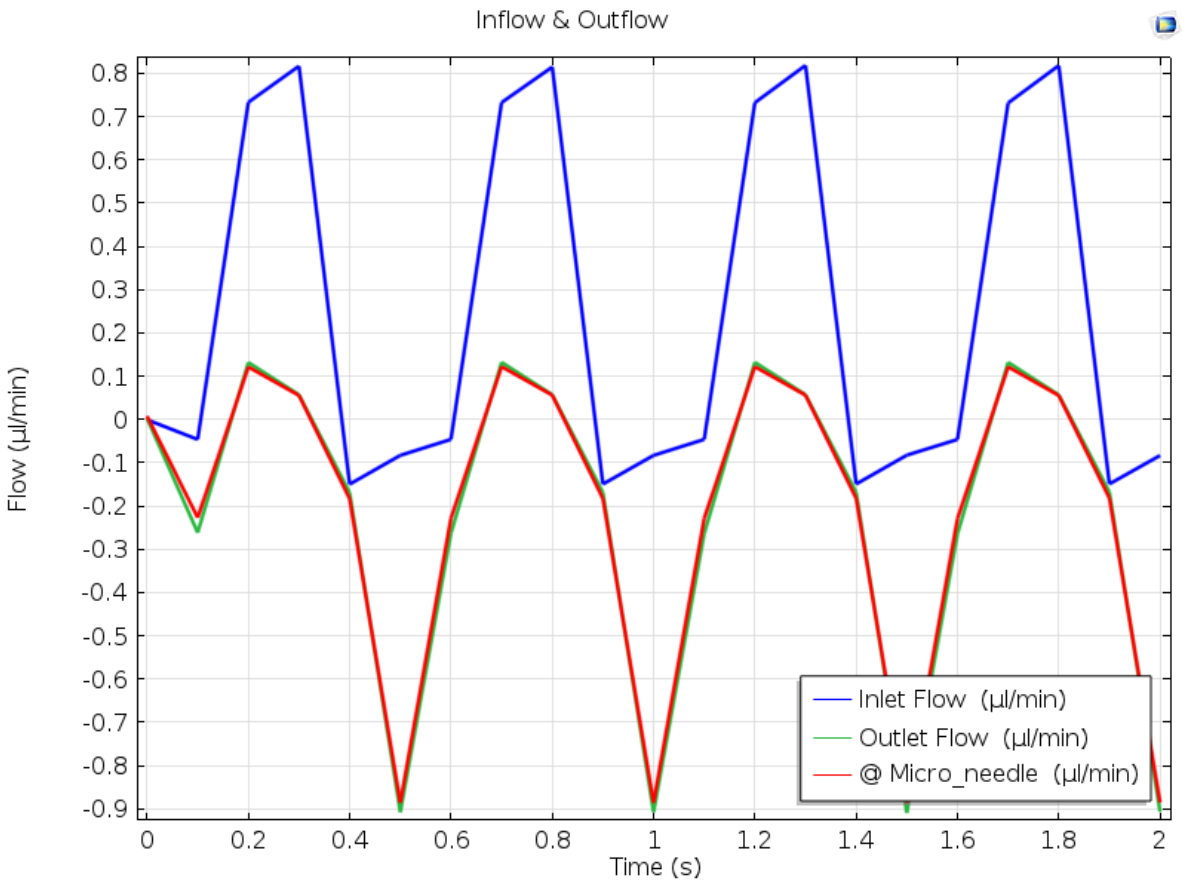

Figure A.1 Flow rate vs time @ V=10 volts, f =2 Hz

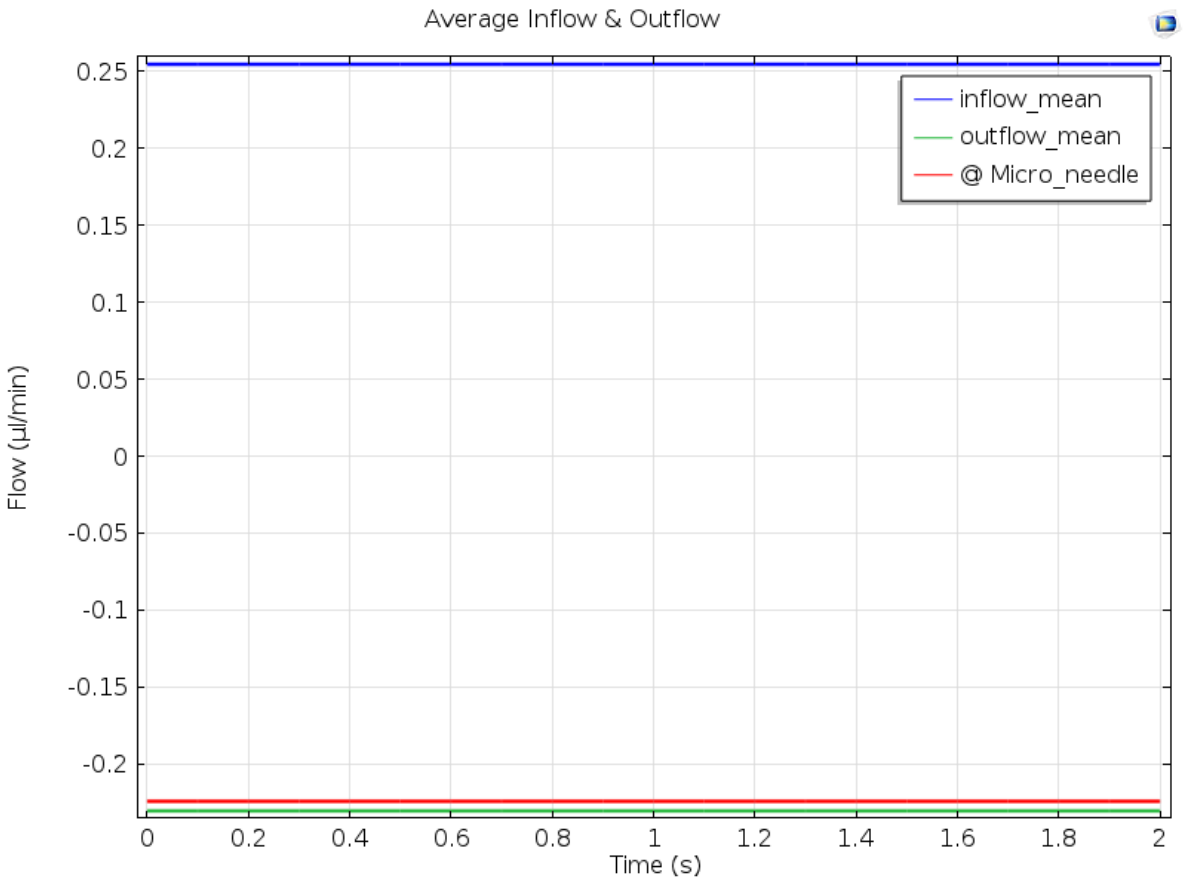

Figure A.2 Average flow rates @ V=10 volts, f =2 Hz

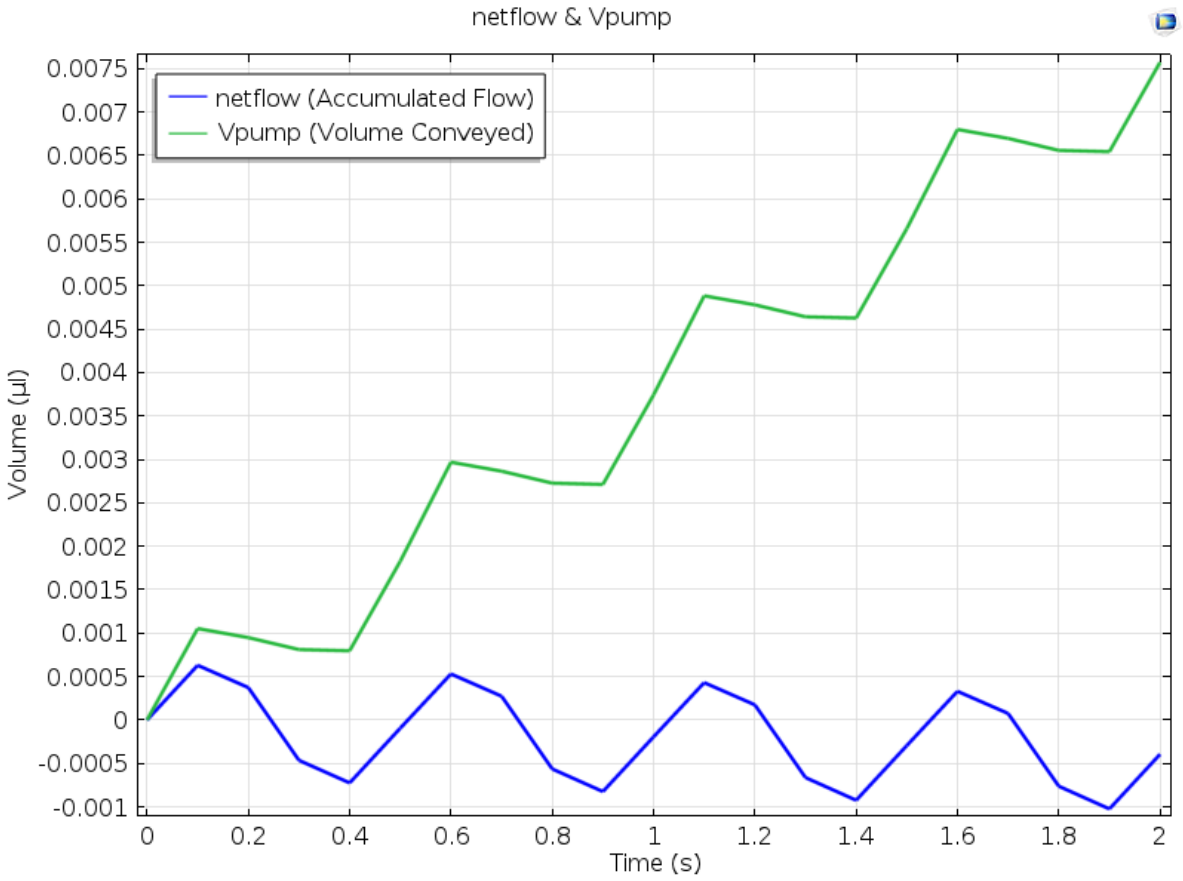

Figure A.3 netflow and Vpump @ V=10 volts, f =2 Hz

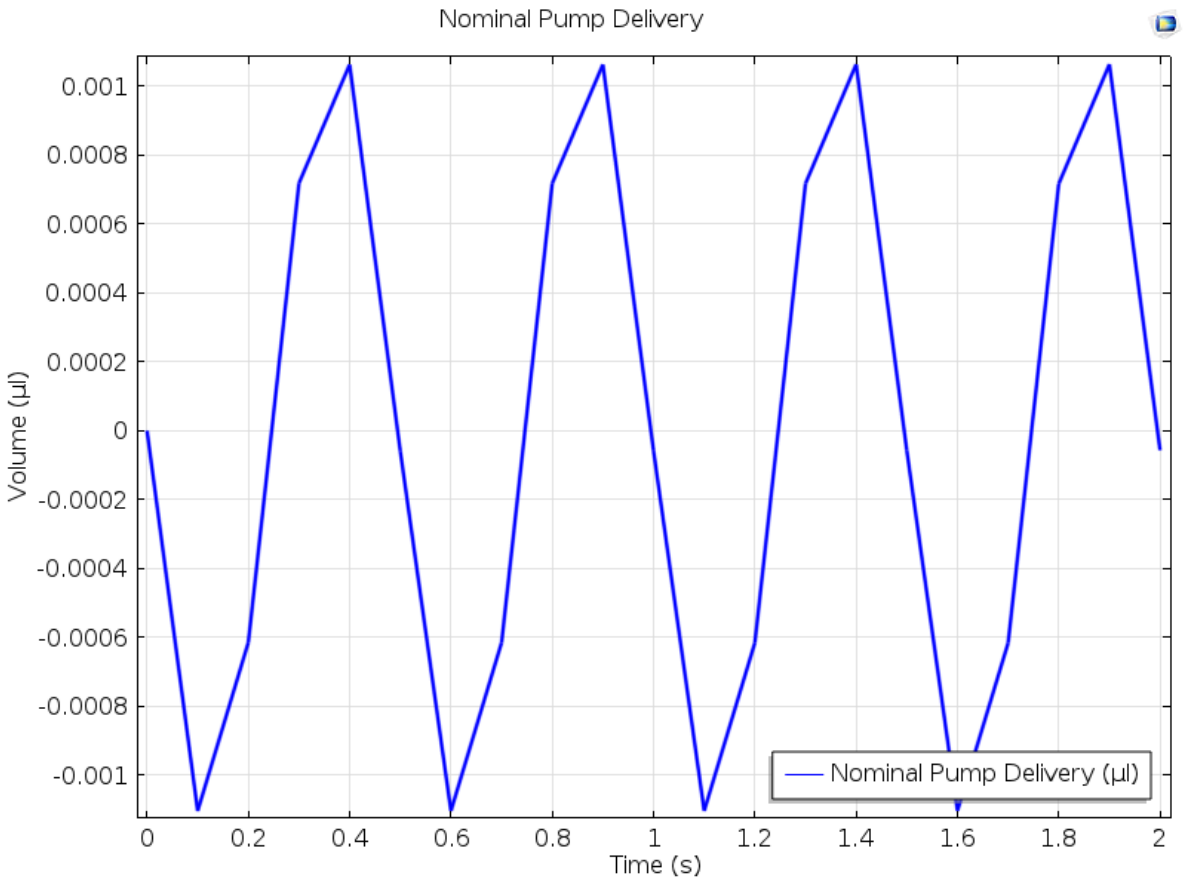

Figure A.4 Nominal Pump Delivery @ V=10 volts, f =2 Hz

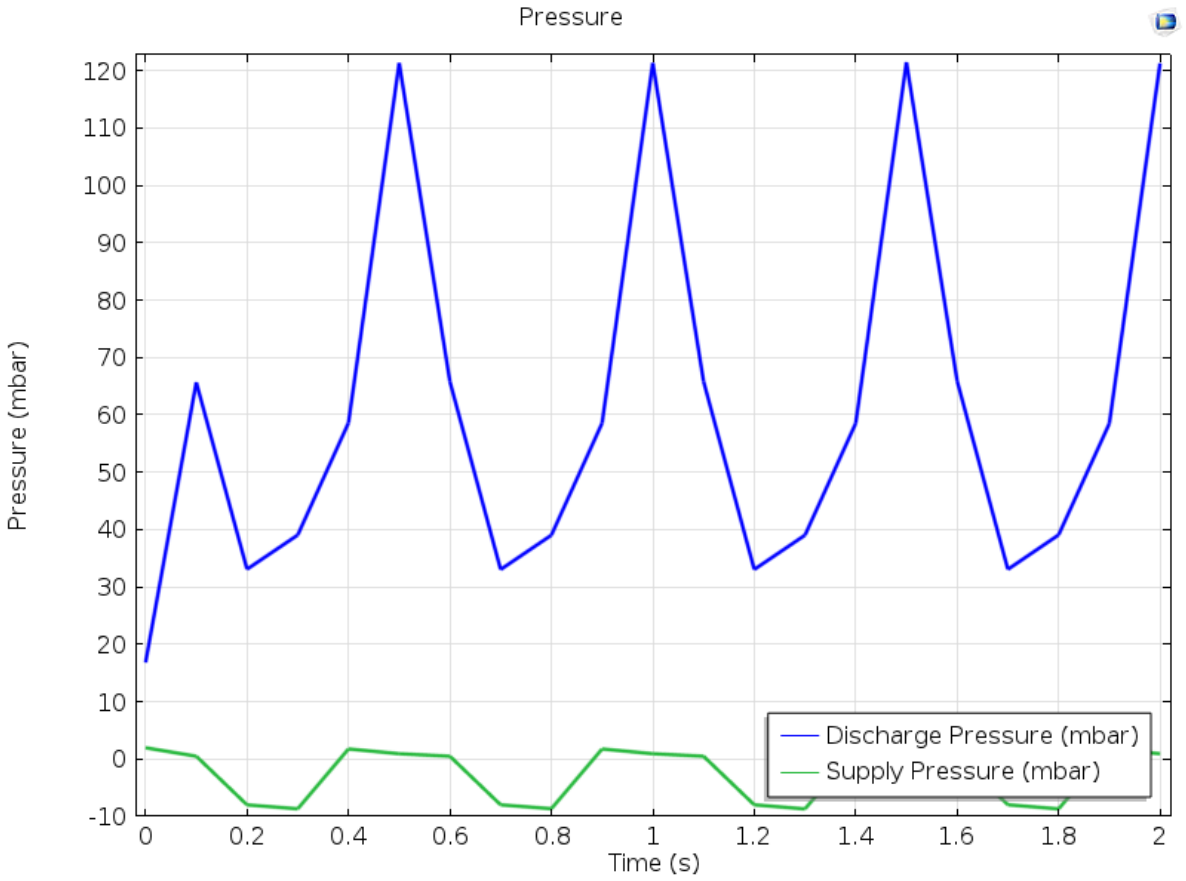

Figure A.5 Pressure vs Time @ V=10 volts, f =2 Hz

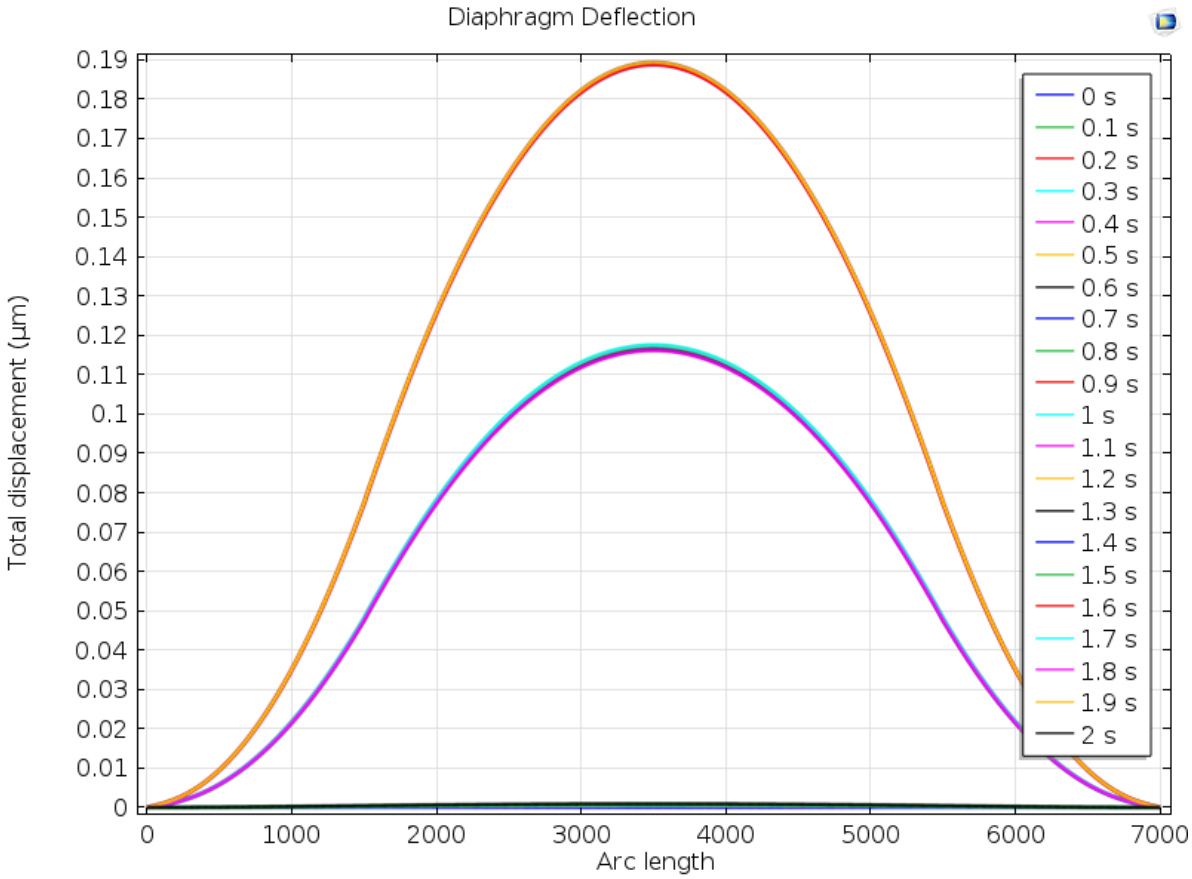

Figure A.6 Diaphragm Deflection versus Arc length @ V=10 volts, f =2 Hz

A.2 Analysis data for load case: Voltage=10 volts, Frequency=3 Hz

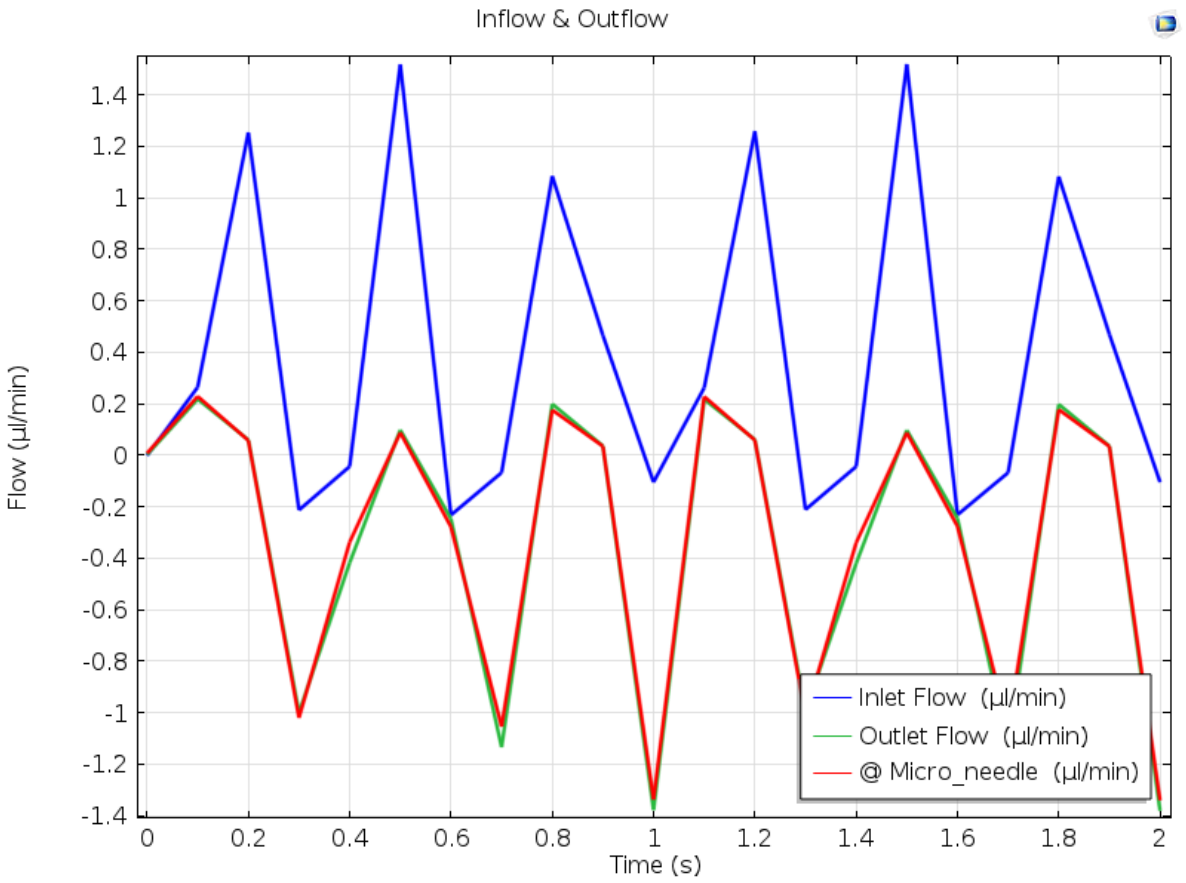

Figure A.7 Flow rate vs time @ V=10 volts, f =3 Hz

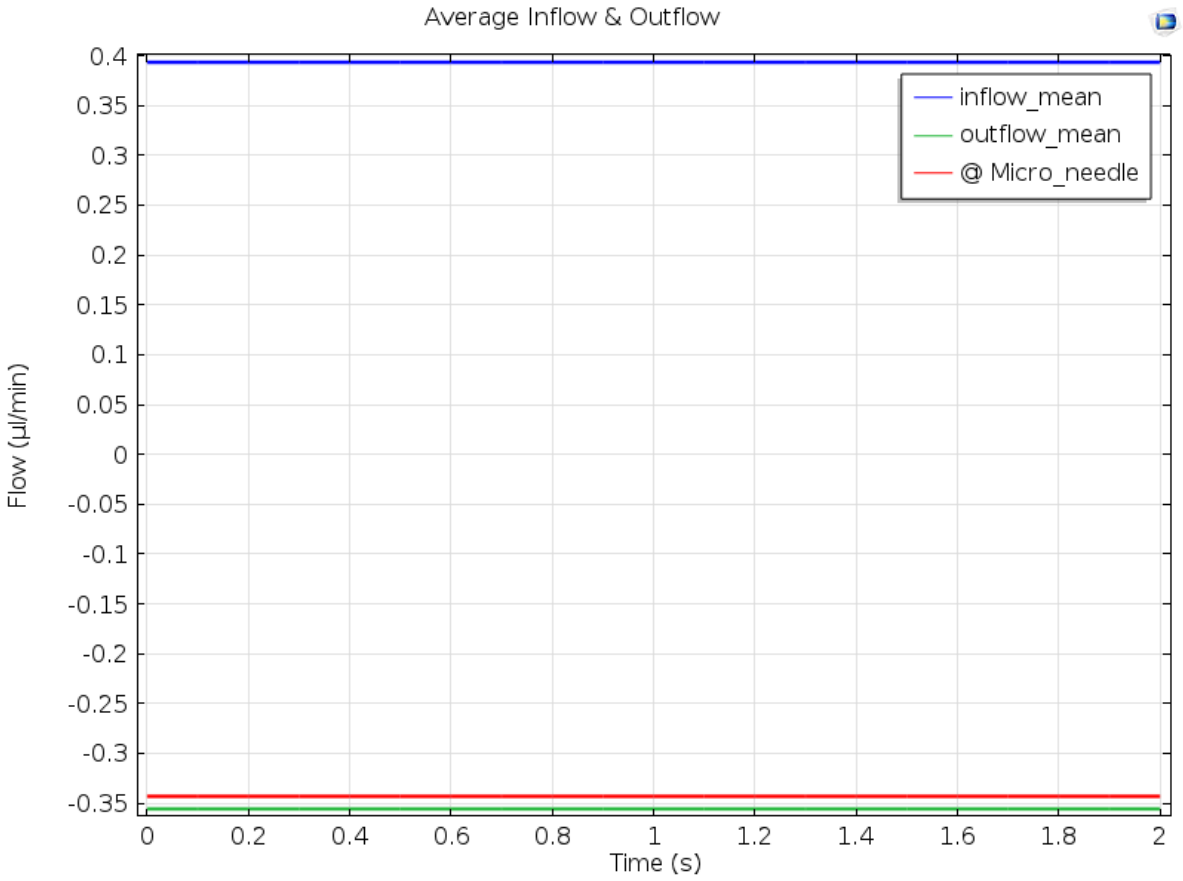

Figure A.8 Average flow rates @ V=10 volts, f =3 Hz

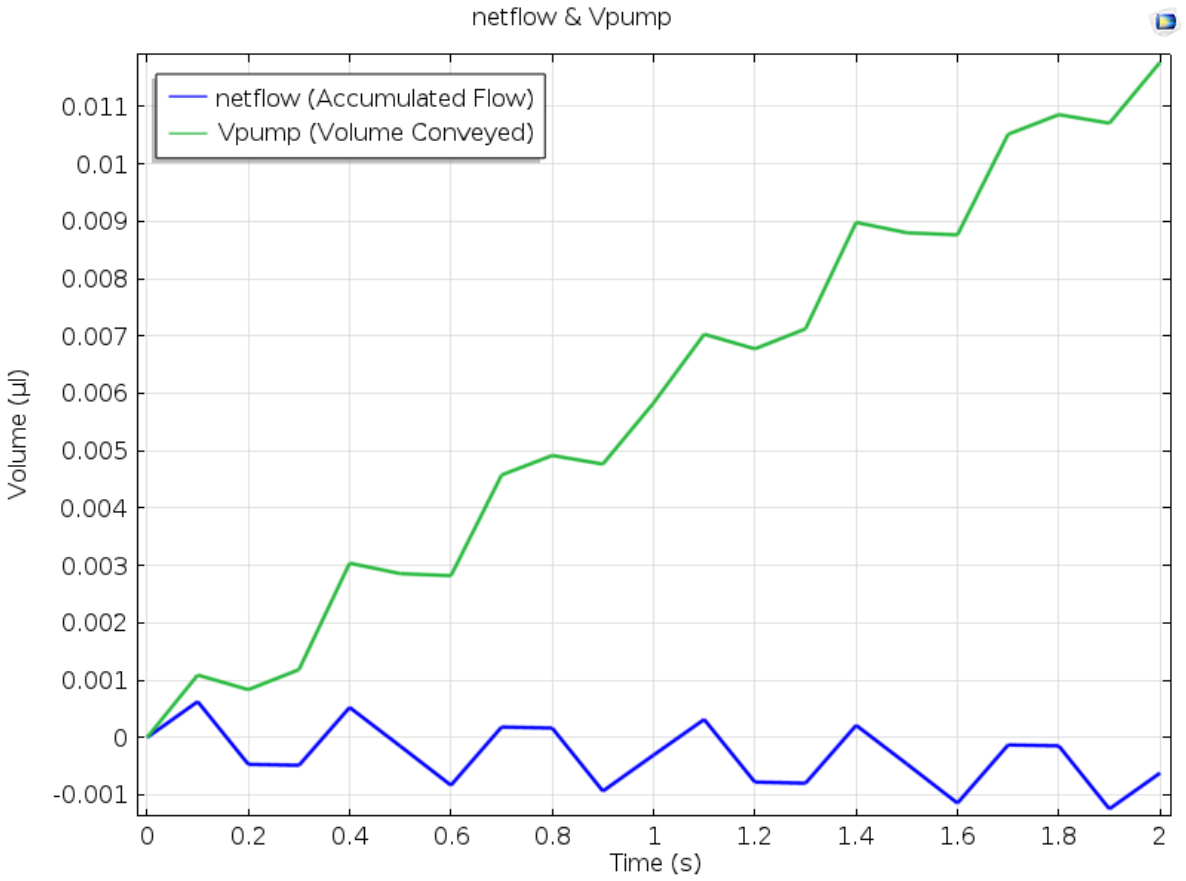

Figure A.9 netflow and Vpump @ V=10 volts, f =3 Hz

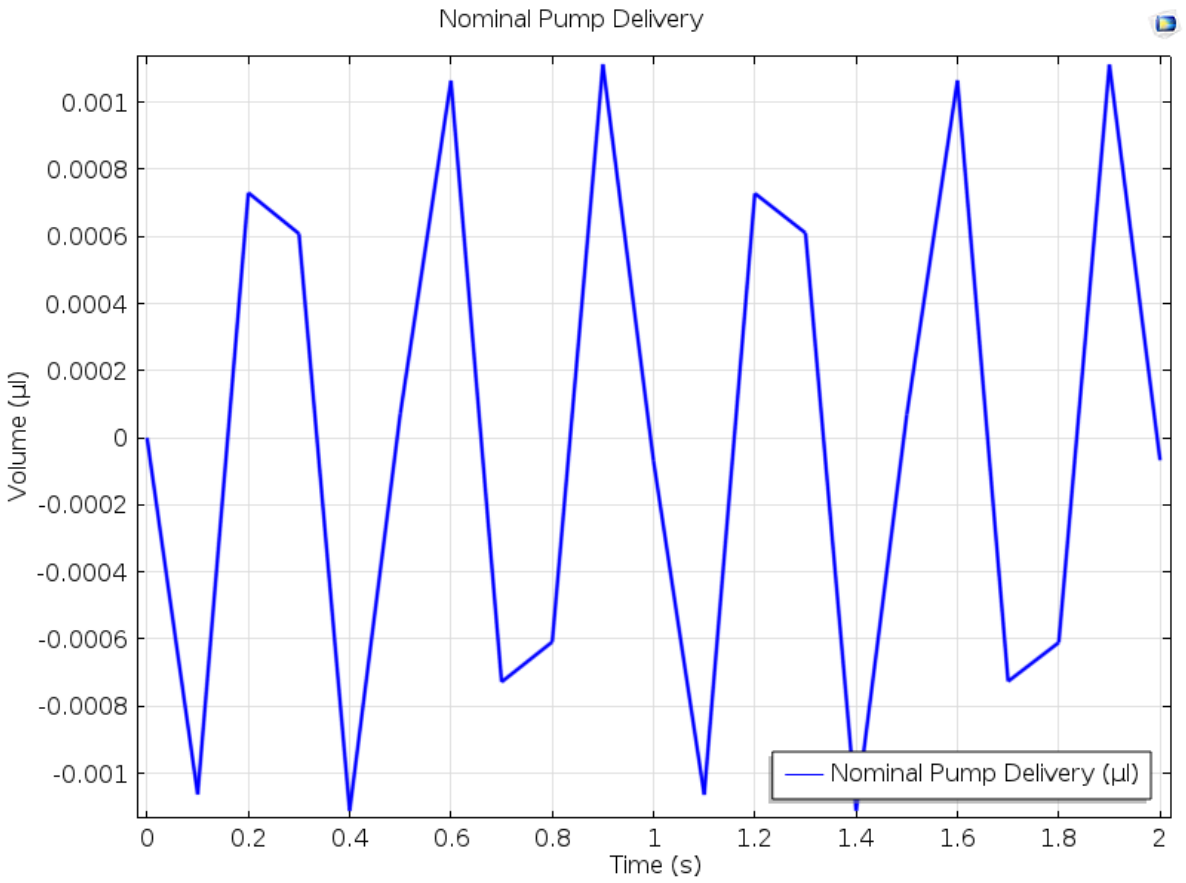

Figure A.10 Nominal Pump Delivery @ V=10 volts, f =3 Hz

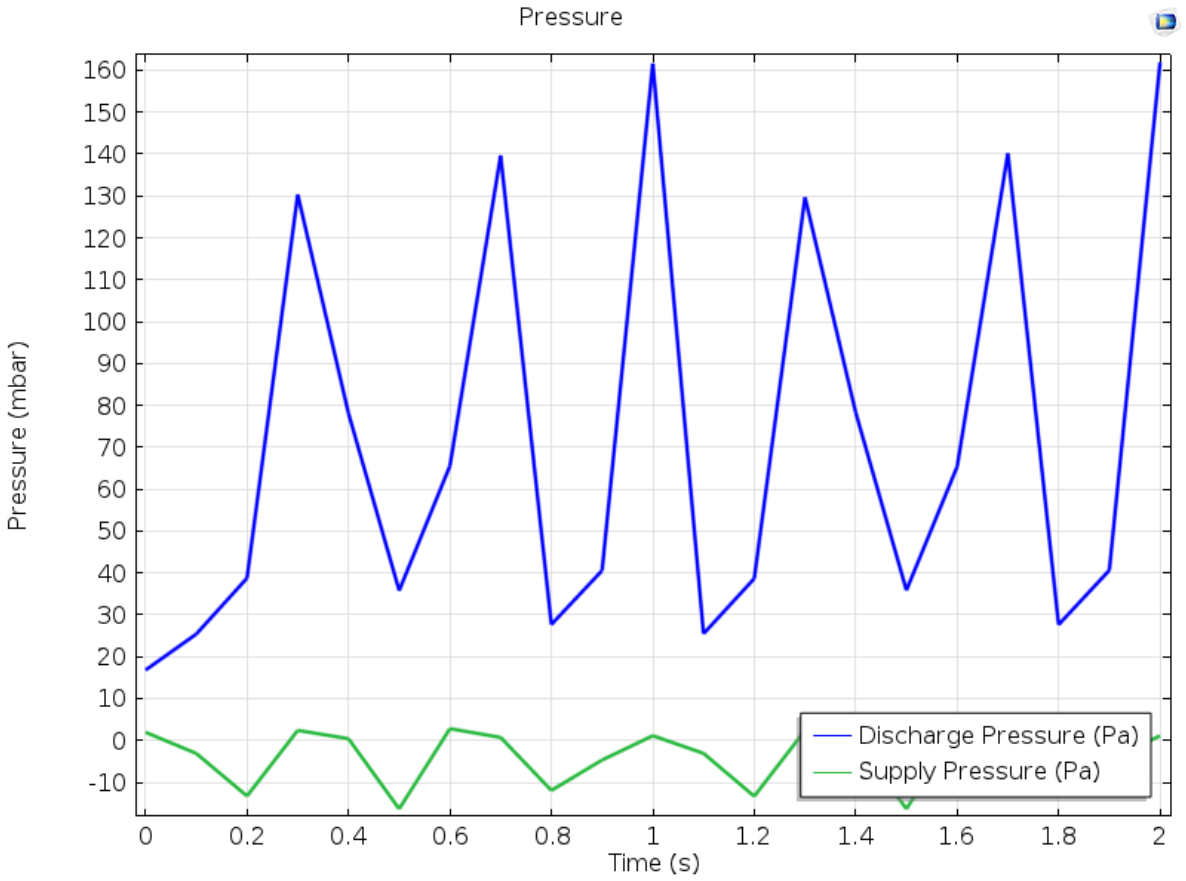

Figure A.11 Pressure vs Time @ V=10 volts, f =3 Hz

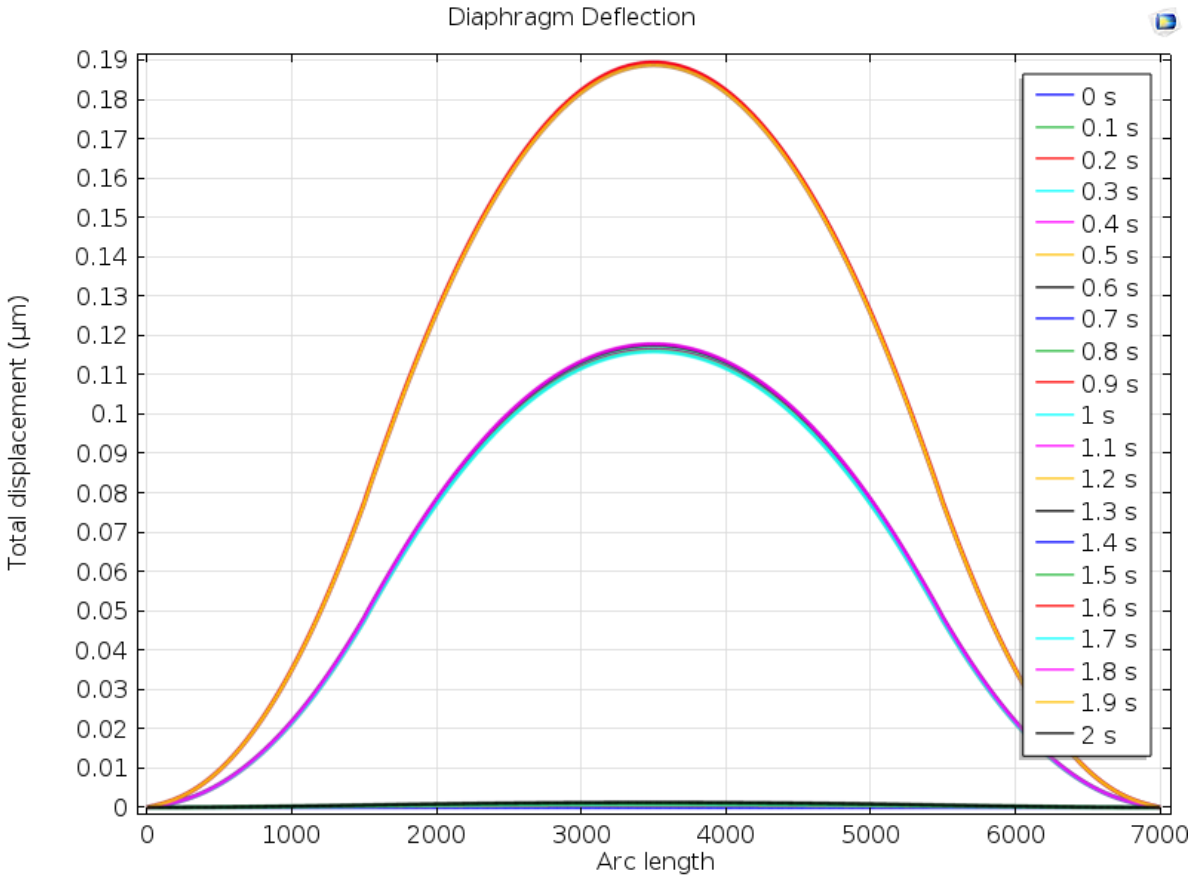

Figure A.12 Diaphragm Deflection versus Arc length @ V=10 volts, f =3 Hz

A.3 Analysis data for load case: Voltage=40 volts, Frequency=1 Hz

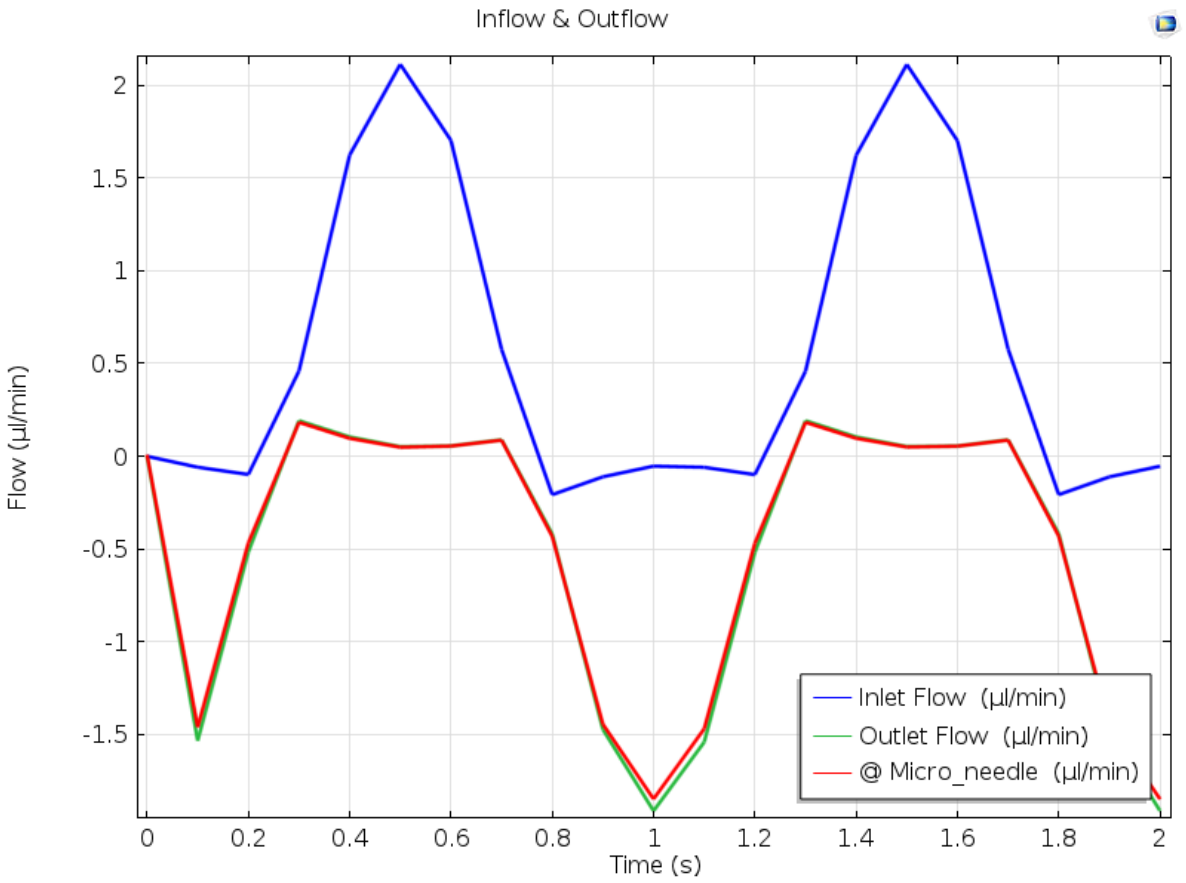

Figure A.13 Flow rate vs time @ V=40 volts, f =1 Hz

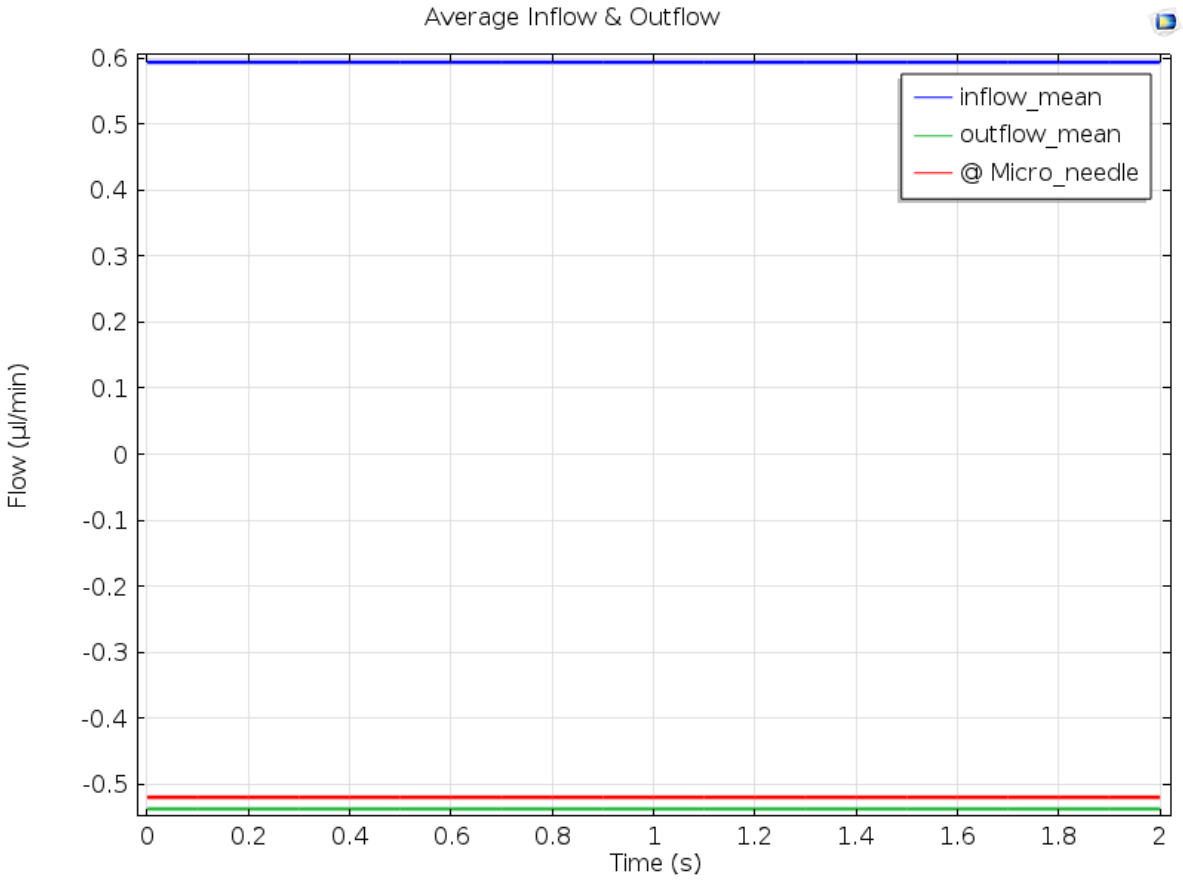

Figure A.14 Average flow rates @ V=40 volts, f =1 Hz

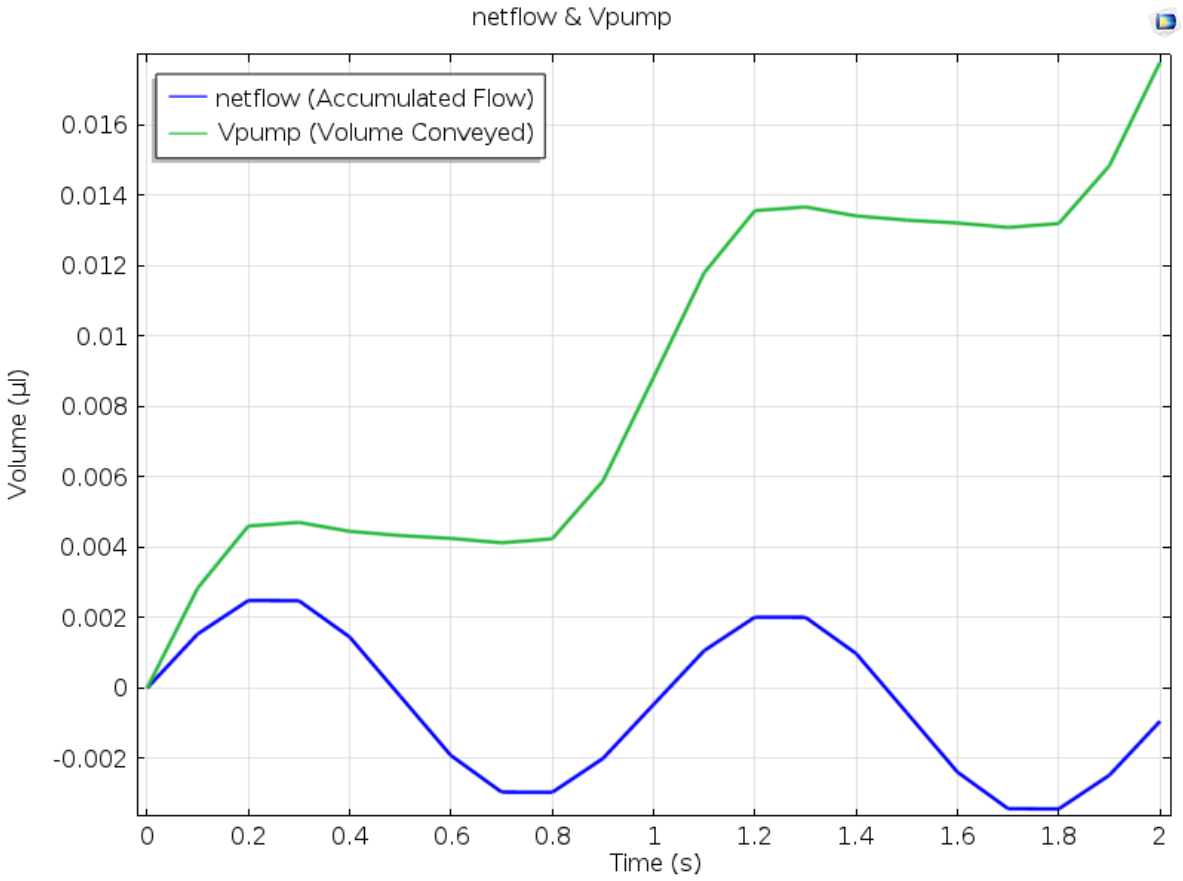

Figure A.15 netflow and Vpump @ V=40 volts, f =1 Hz

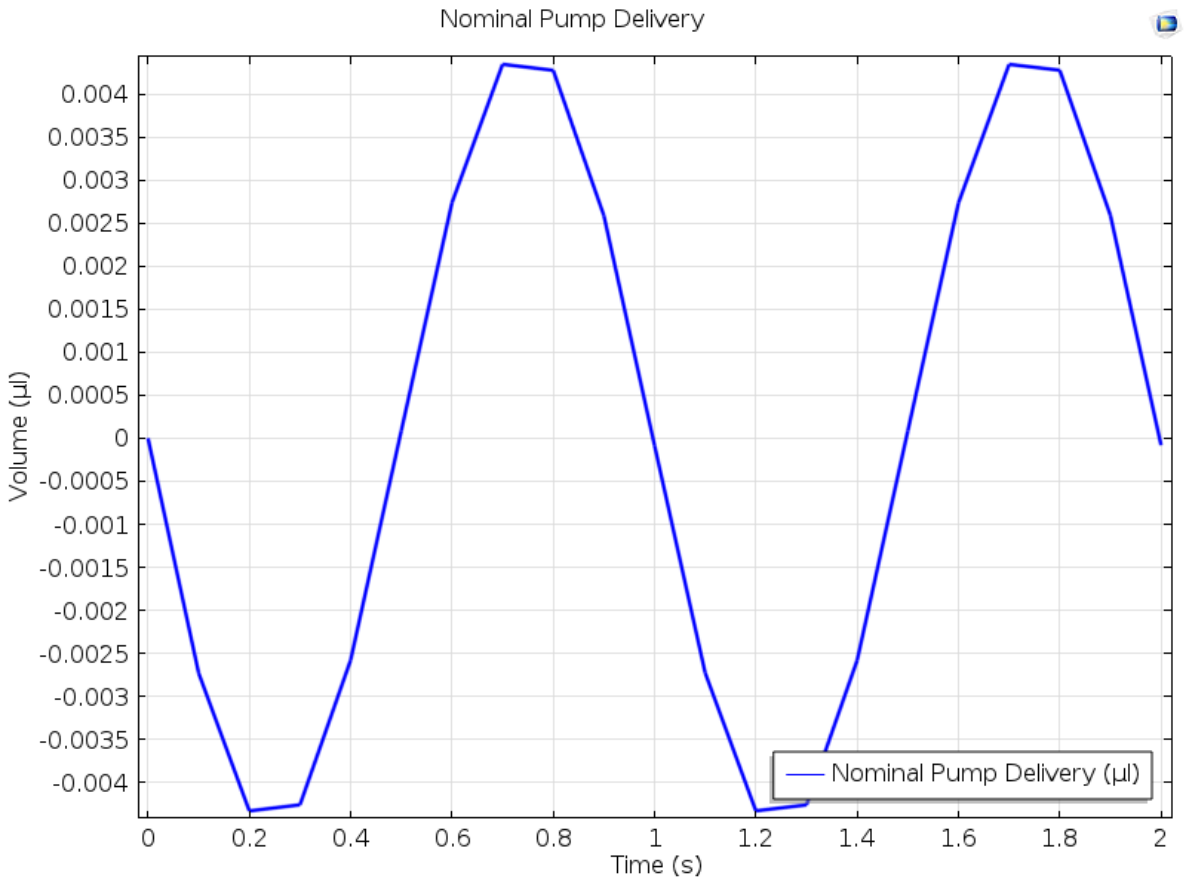

Figure A.16 Nominal Pump Delivery @ V=40 volts, f =1 Hz

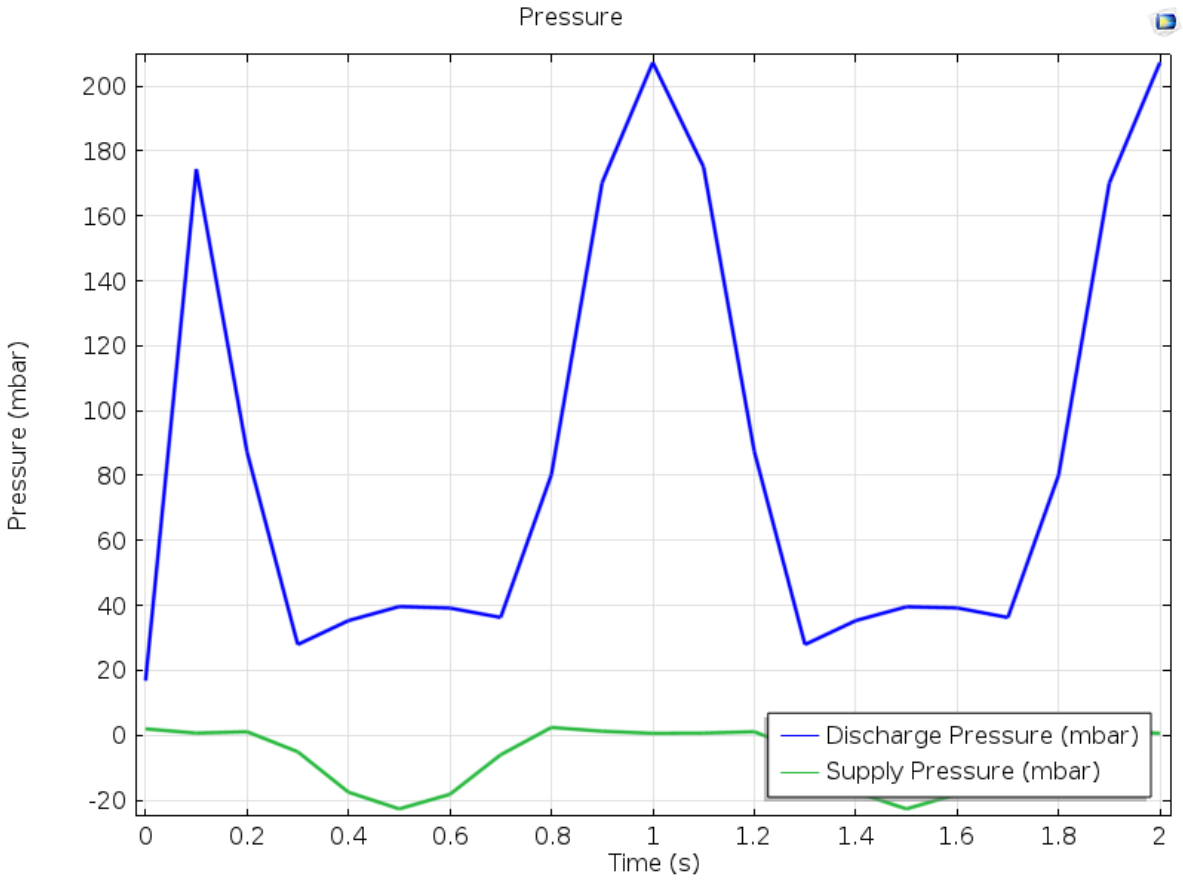

Figure A.17 Pressure vs Time @ V=40 volts, f =1 Hz

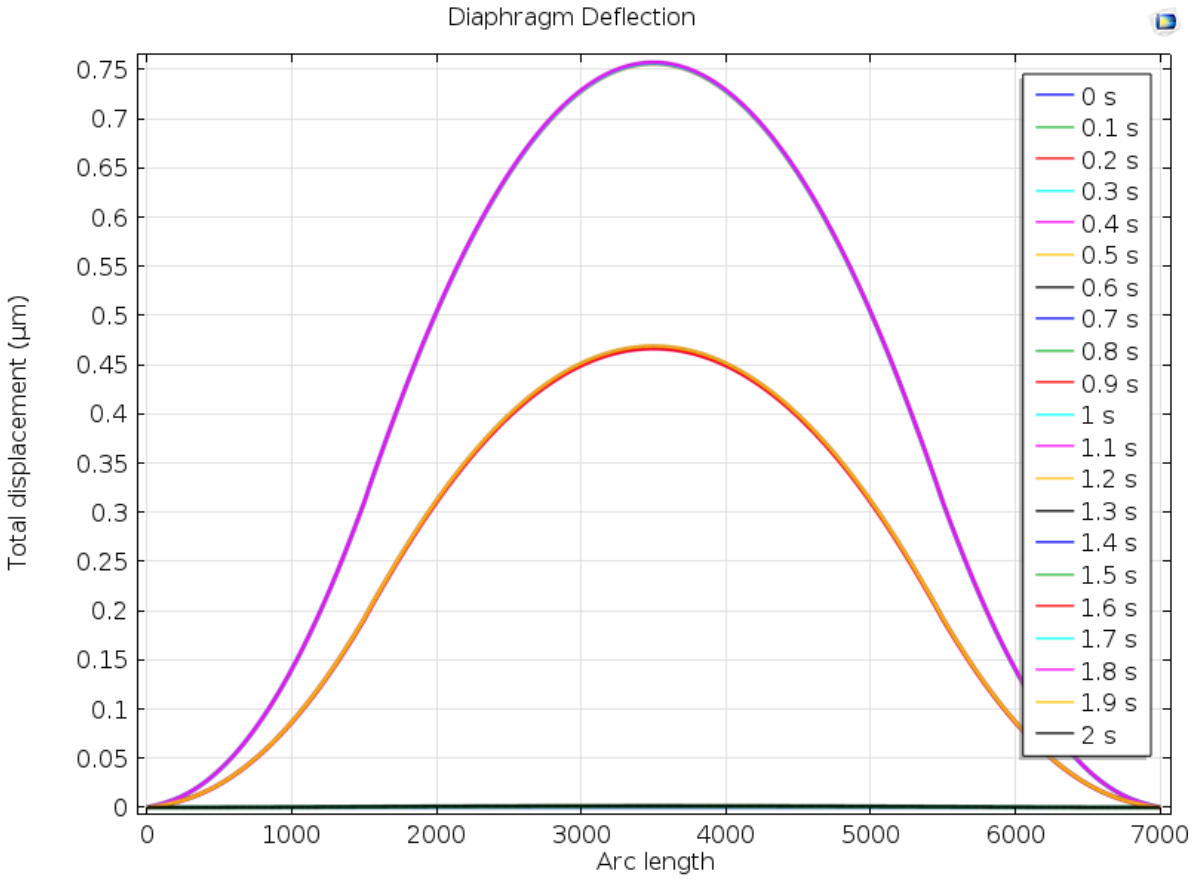

Figure A.18 Diaphragm Deflection versus Arc length @ V=40 volts, f =1 Hz

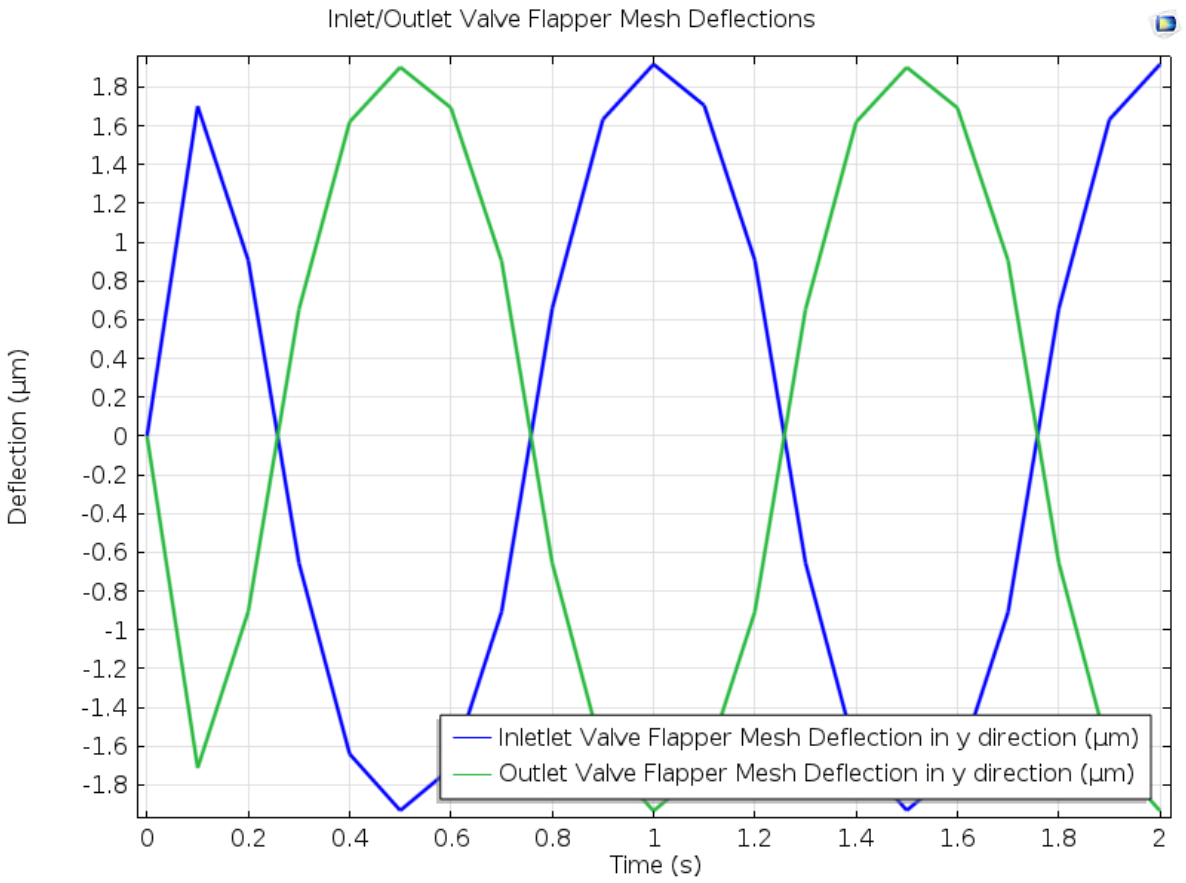

Figure A.19 Inlet/Outlet Valve Flapper Mesh Deflections versus Time @ V=40 volts, f =1 Hz

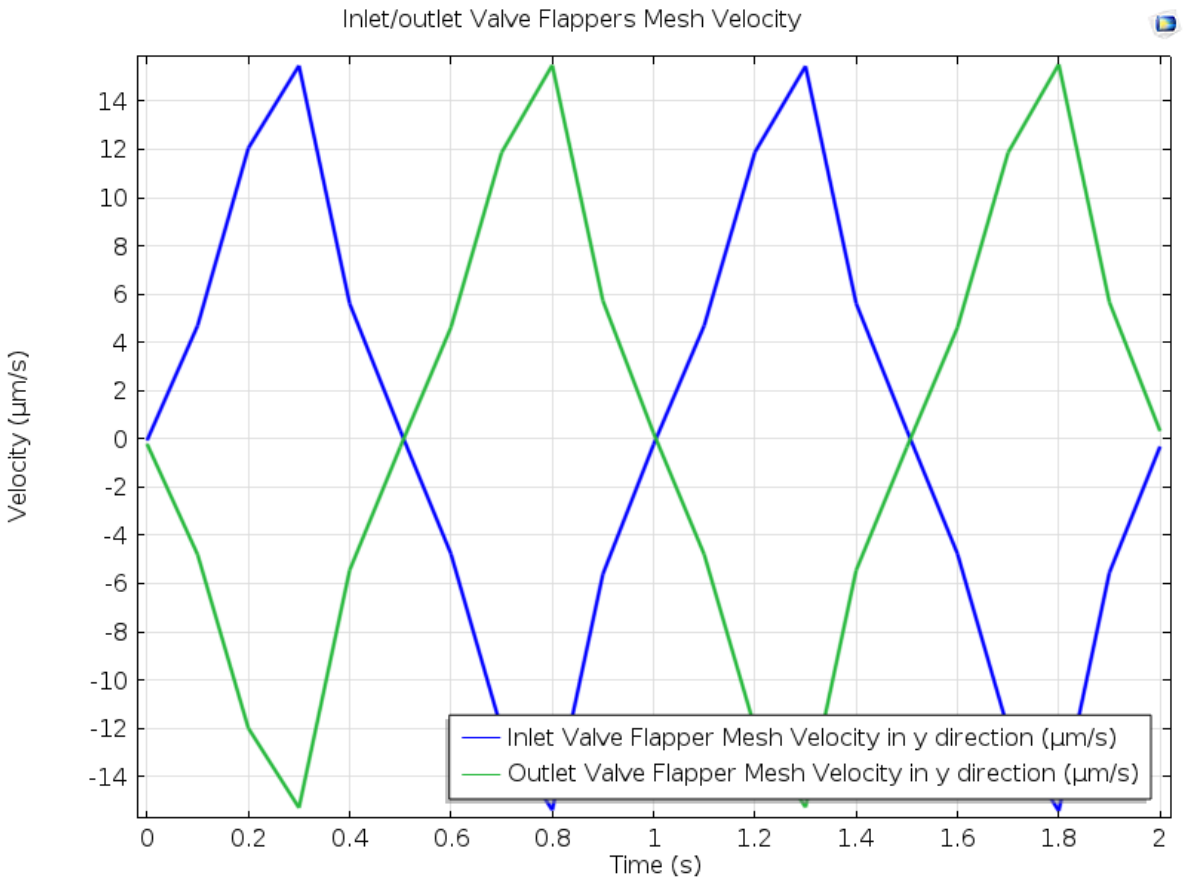

Figure A.20 Inlet/Outlet Valve Flapper Mesh Velocity versus Time @ V=40 volts, f =1 Hz

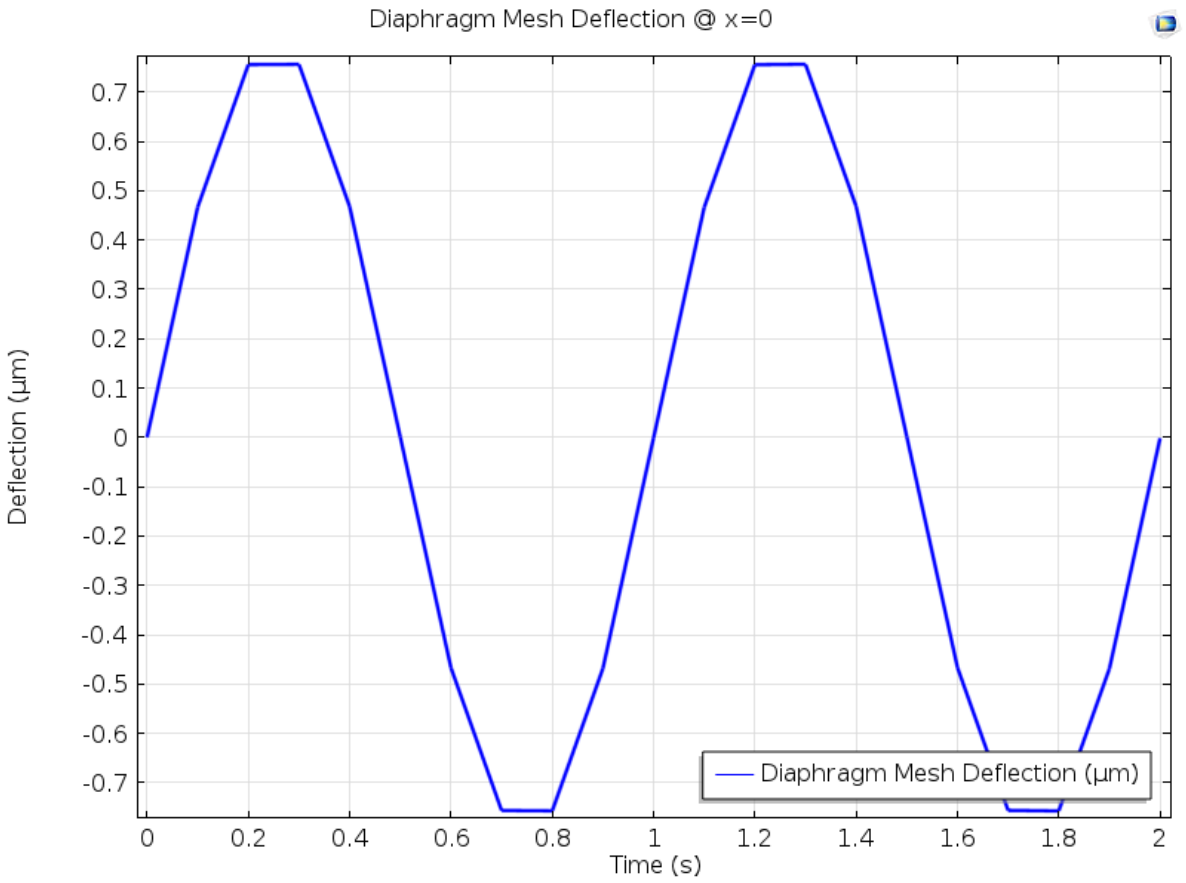

Figure A.21 Diaphragm Mesh Deflection versus Time @ V=40 volts, f =1 Hz

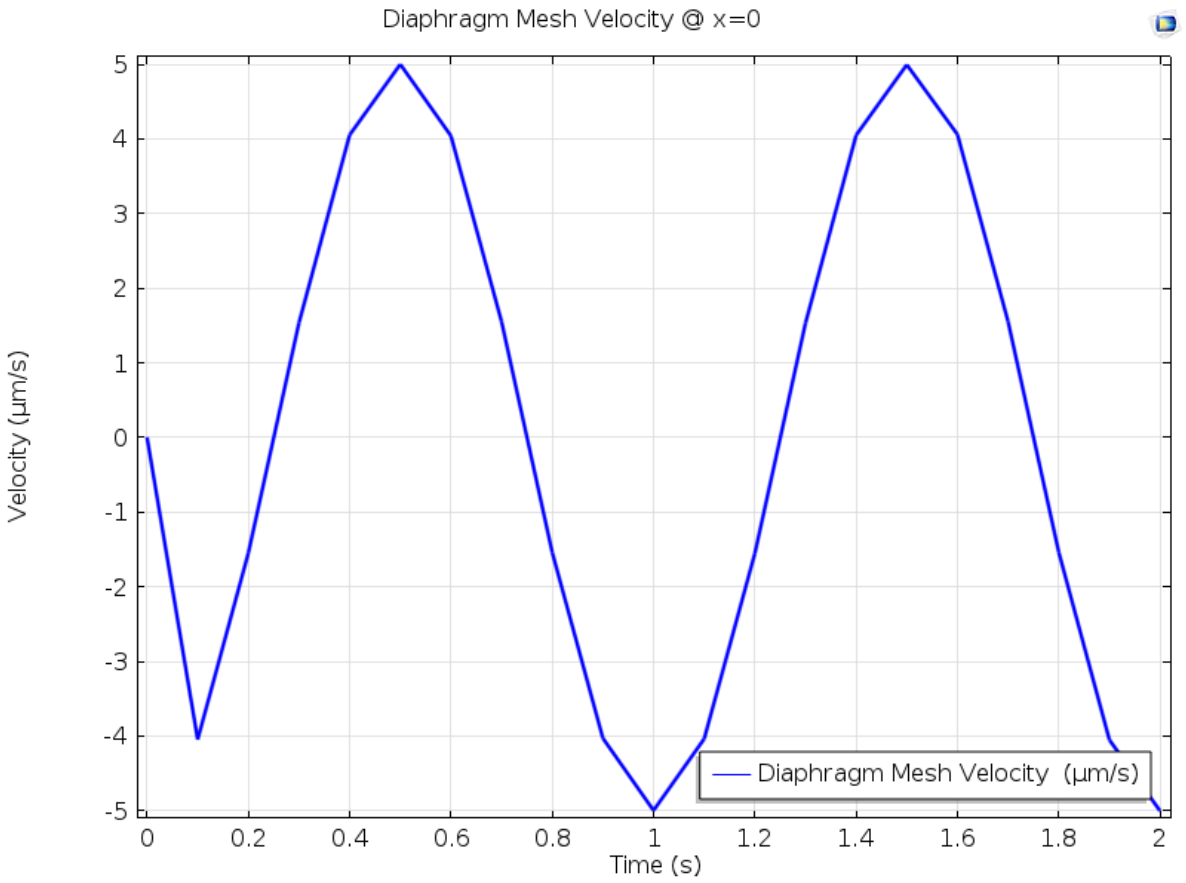

Figure A.22 Diaphragm Mesh Velocity versus Time @ V=40 volts, f =1 Hz

A.4 Analysis data for load case: Voltage=40 volts, Frequency=2 Hz

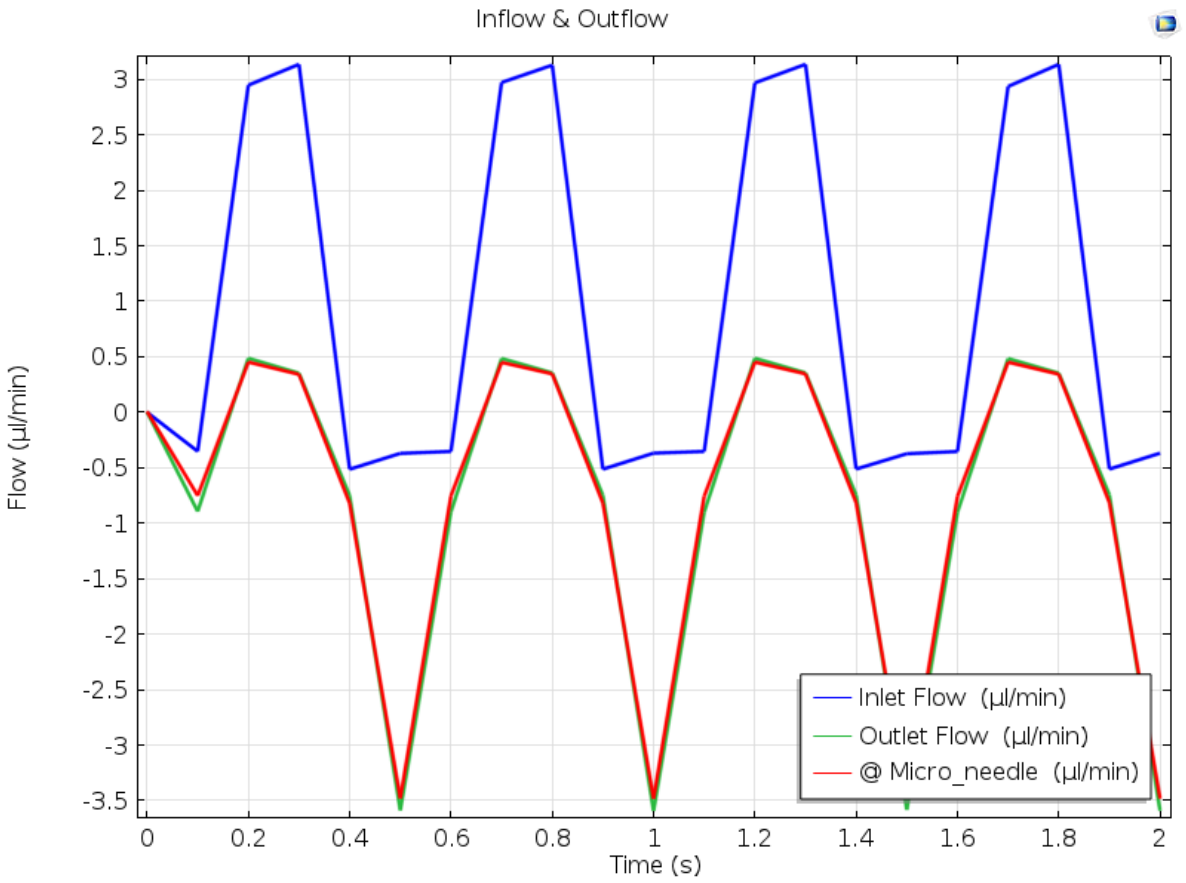

Figure A.23 Flow rate vs time @ V=40 volts, f =2 Hz

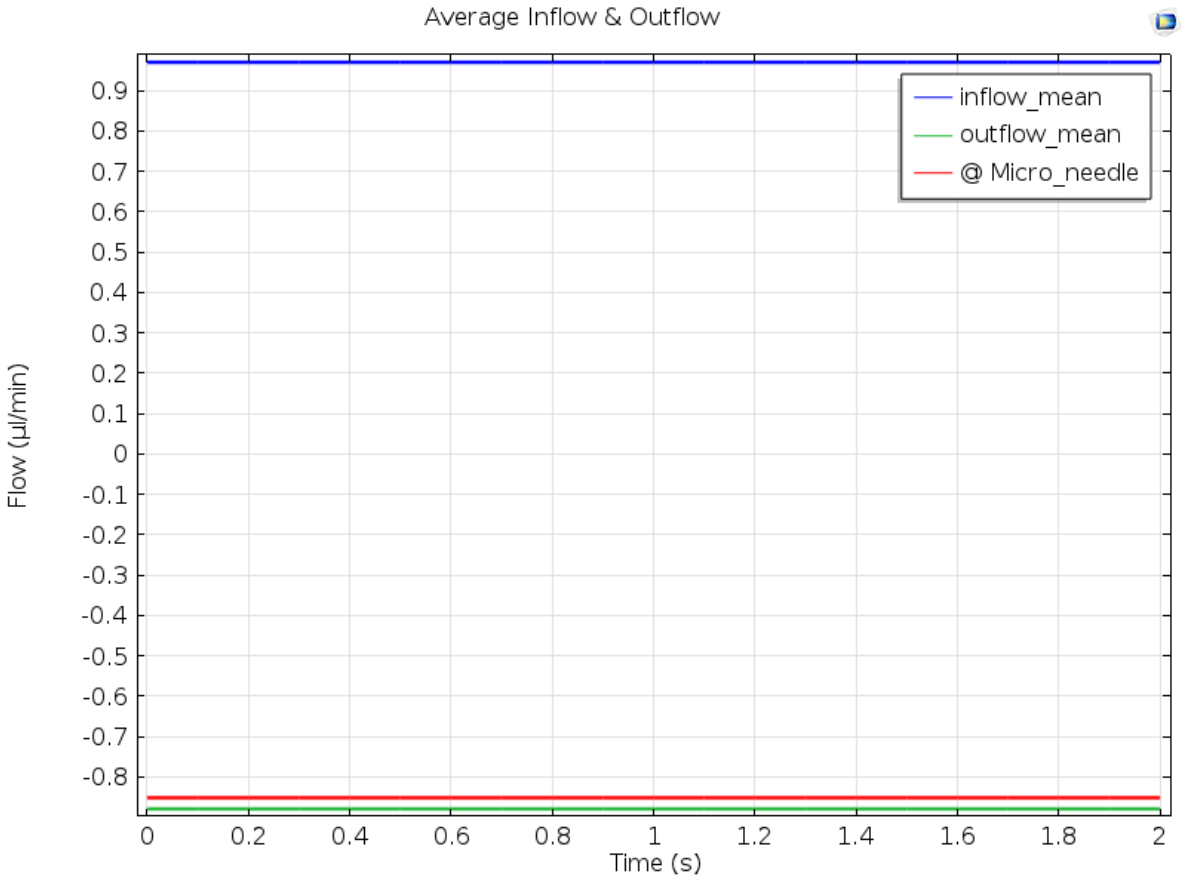

Figure A.24 Average flow rates @ V=40 volts, f =2 Hz

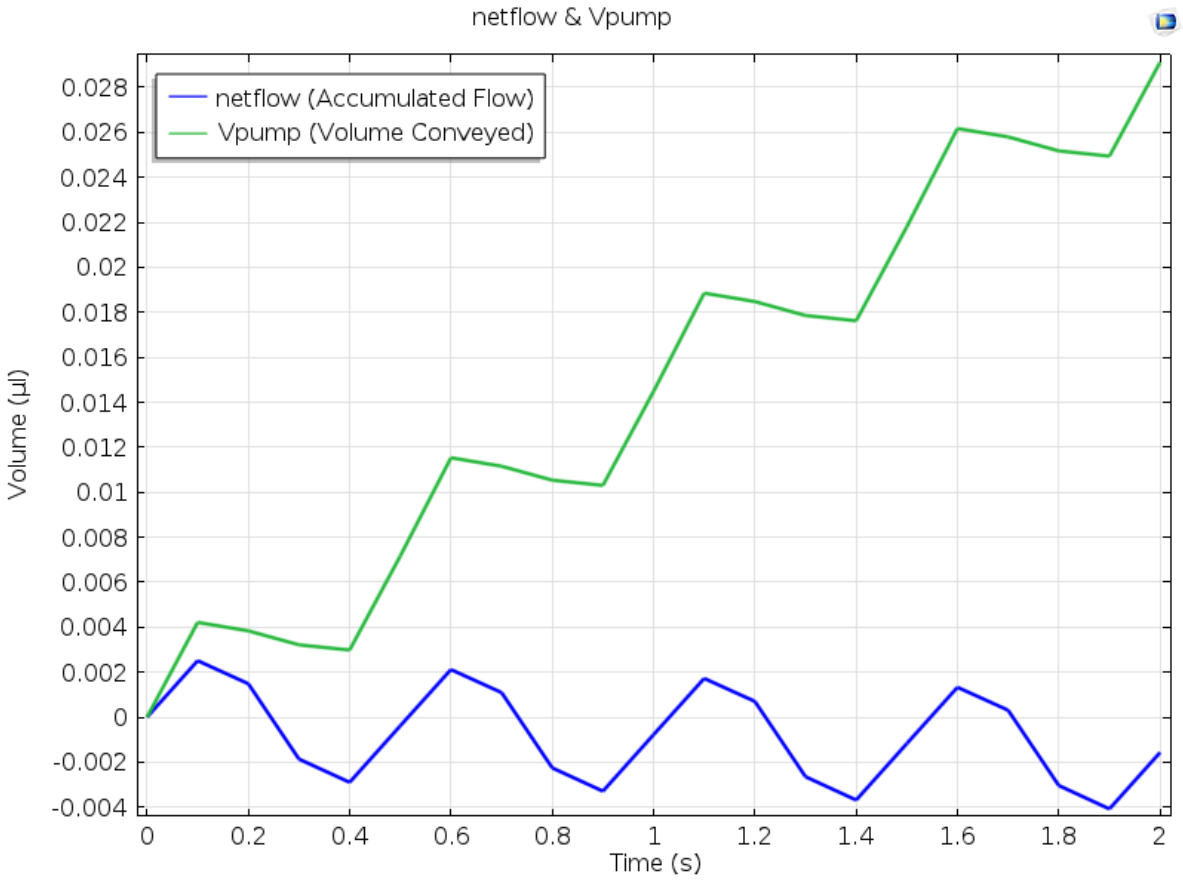

Figure A.25 netflow and Vpump @ V=40 volts, f =2 Hz

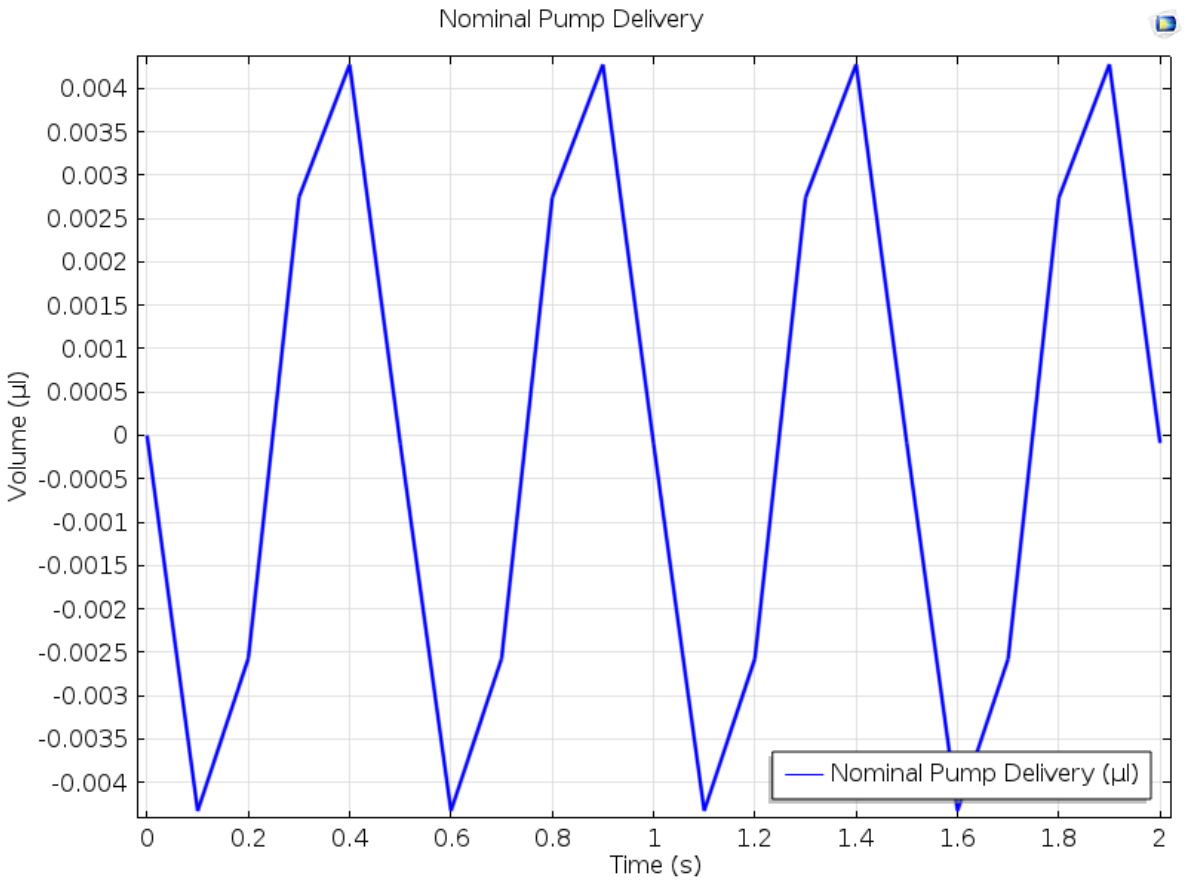

Figure A.26 Nominal Pump Delivery @ V=40 volts, f =2 Hz

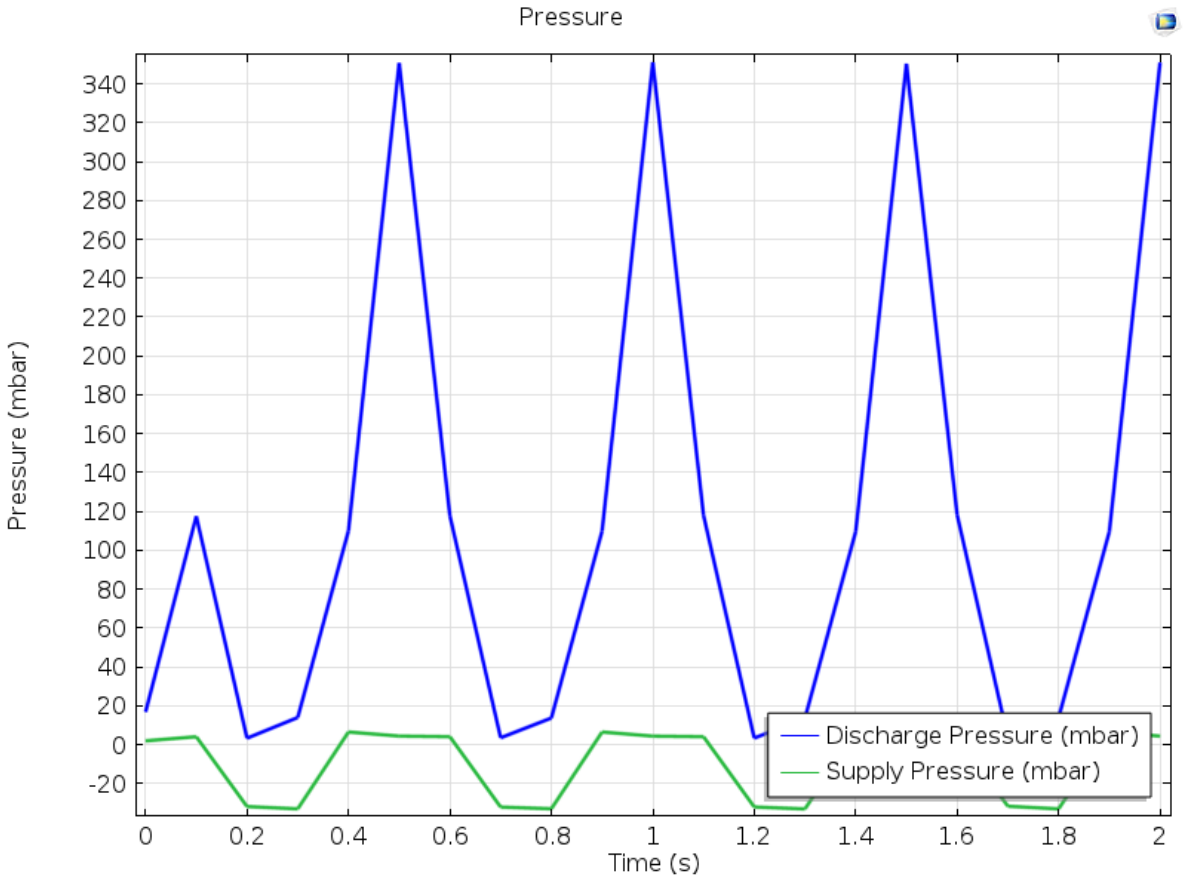

Figure A.27 Pressure vs Time @ V=40 volts, f =2 Hz

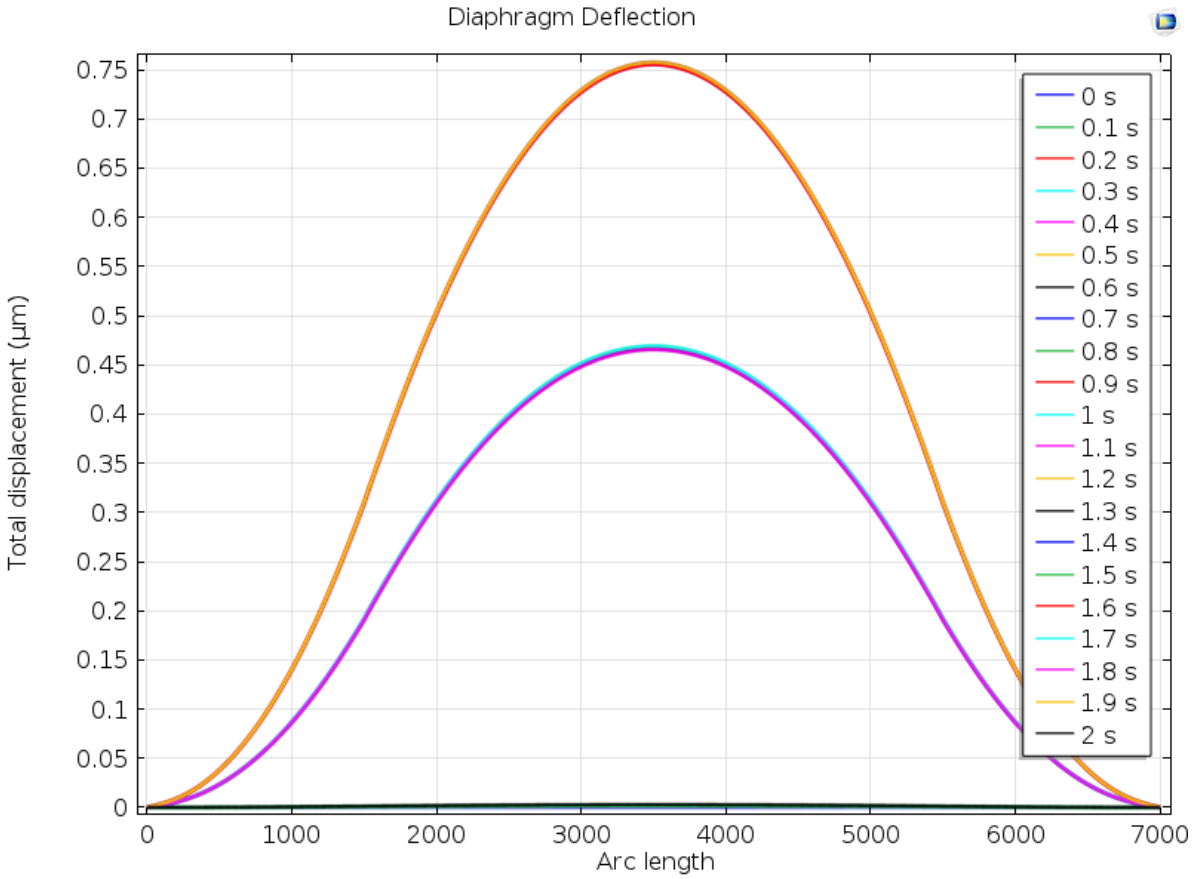

Figure A.28 Diaphragm Deflection versus Arc length @ V=40 volts, f =2 Hz

A.5 Analysis data for load case: Voltage=40 volts, Frequency=3 Hz

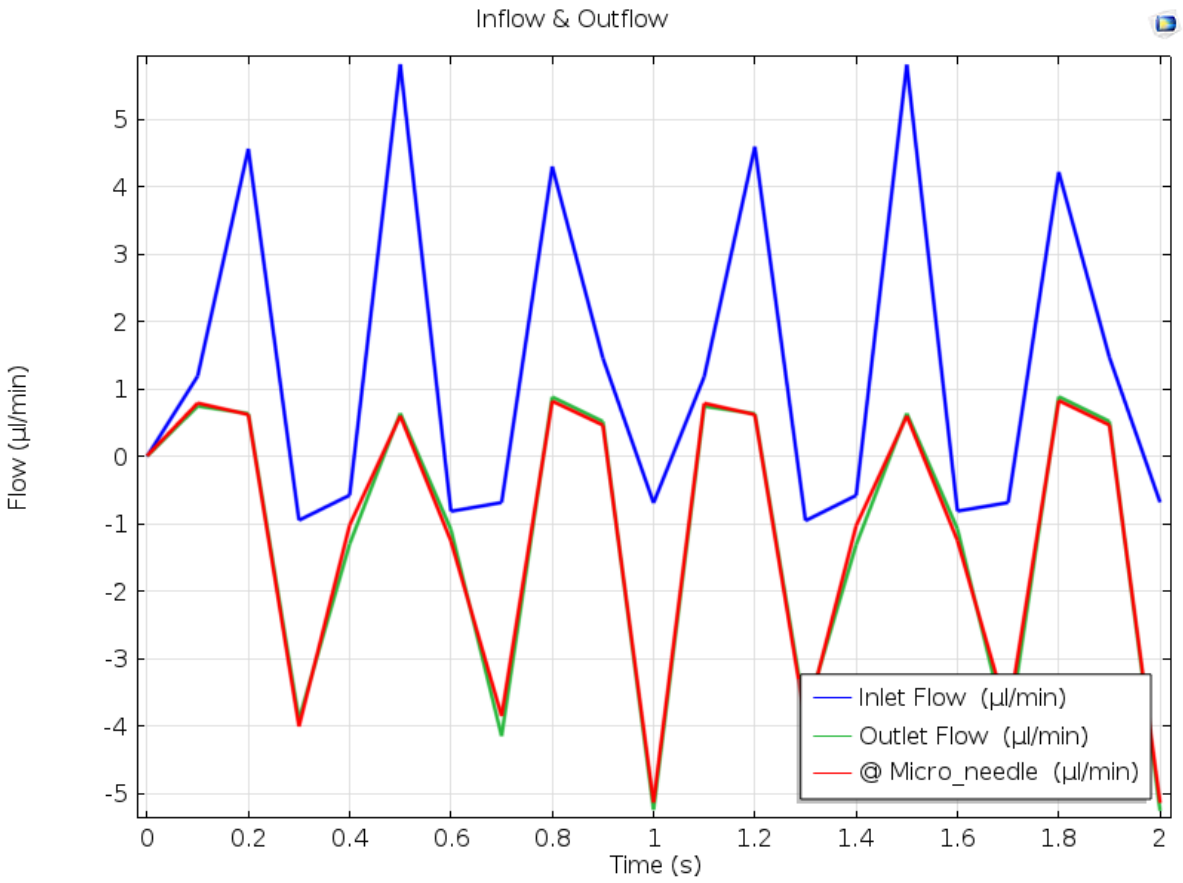

Figure A.29 Flow rate vs time @ V=40 volts, f =3 Hz

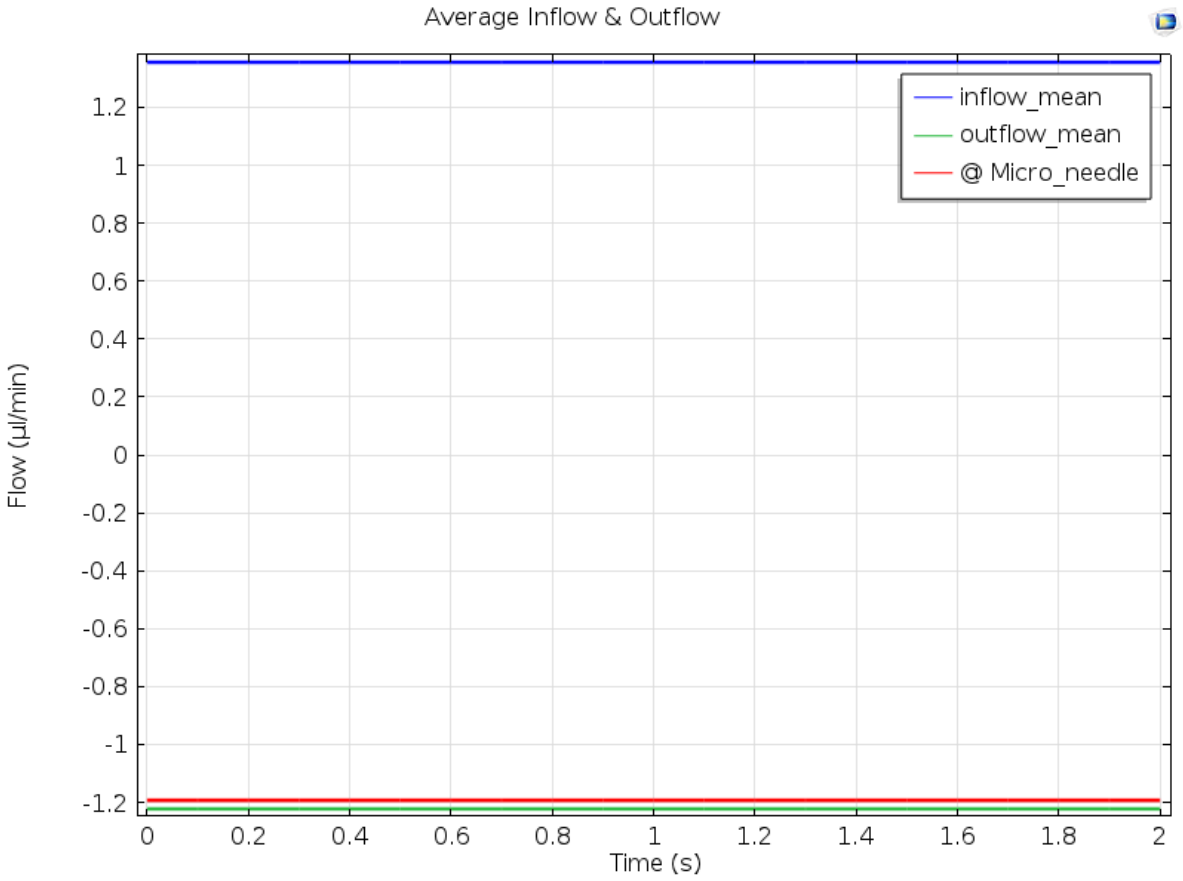

Figure A.30 Average flow rates @ V=40 volts, f =3 Hz

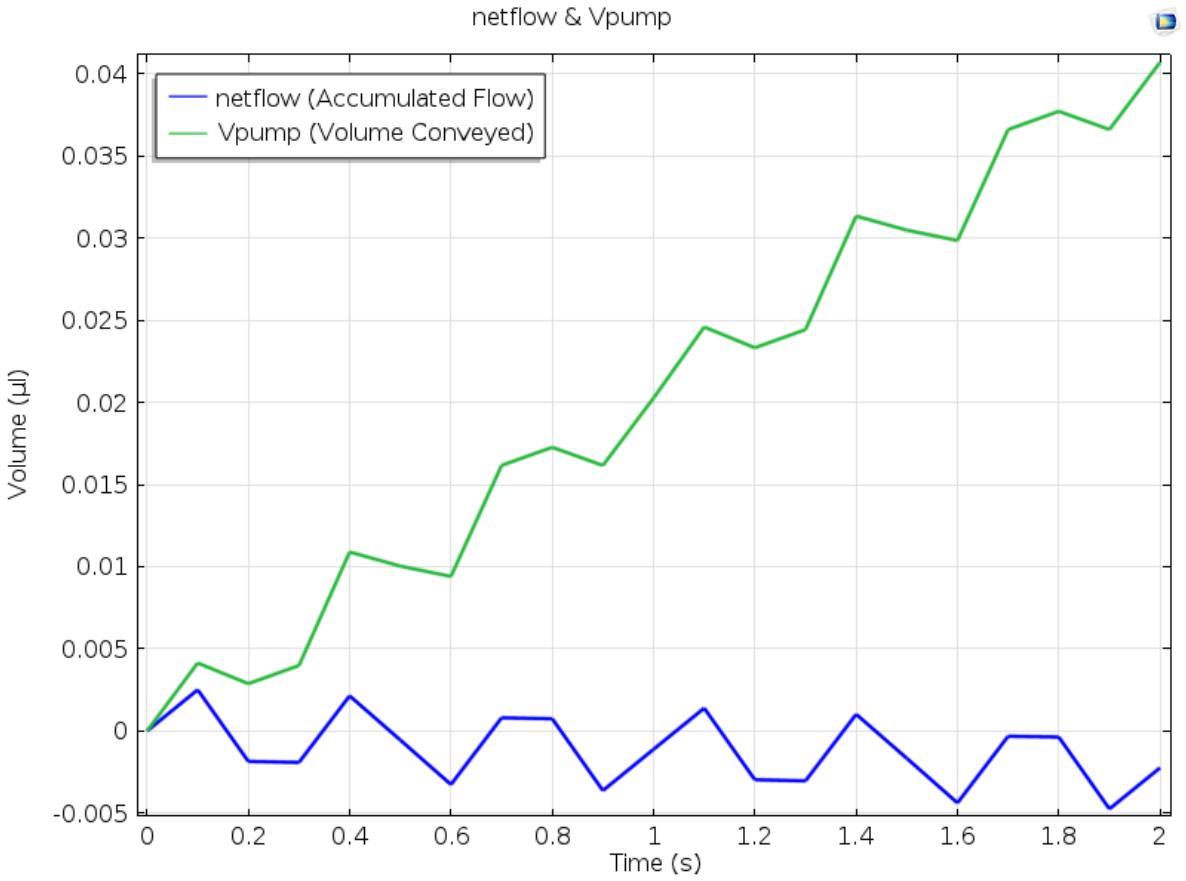

Figure A.31 netflow and Vpump @ V=40 volts, f =3 Hz

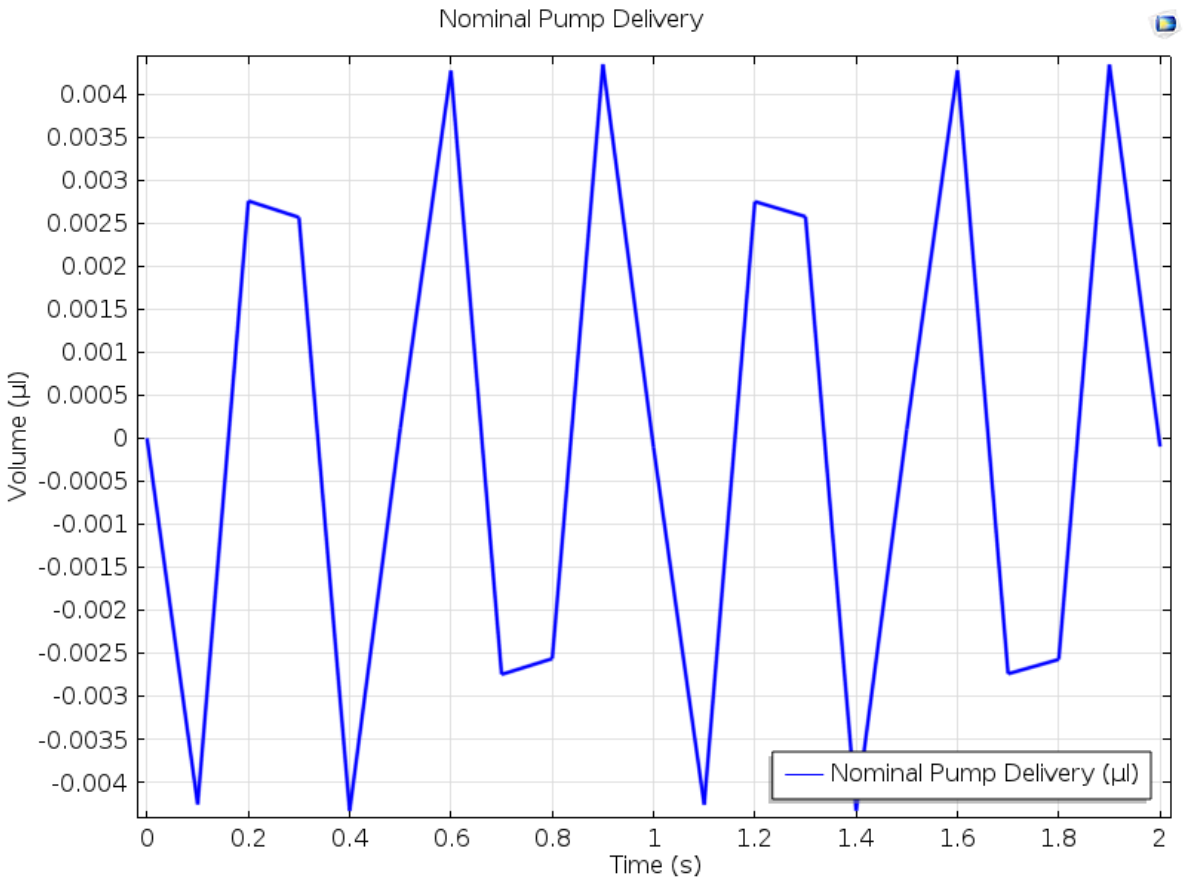

Figure A.32 Nominal Pump Delivery @ V=40 volts, f =3 Hz

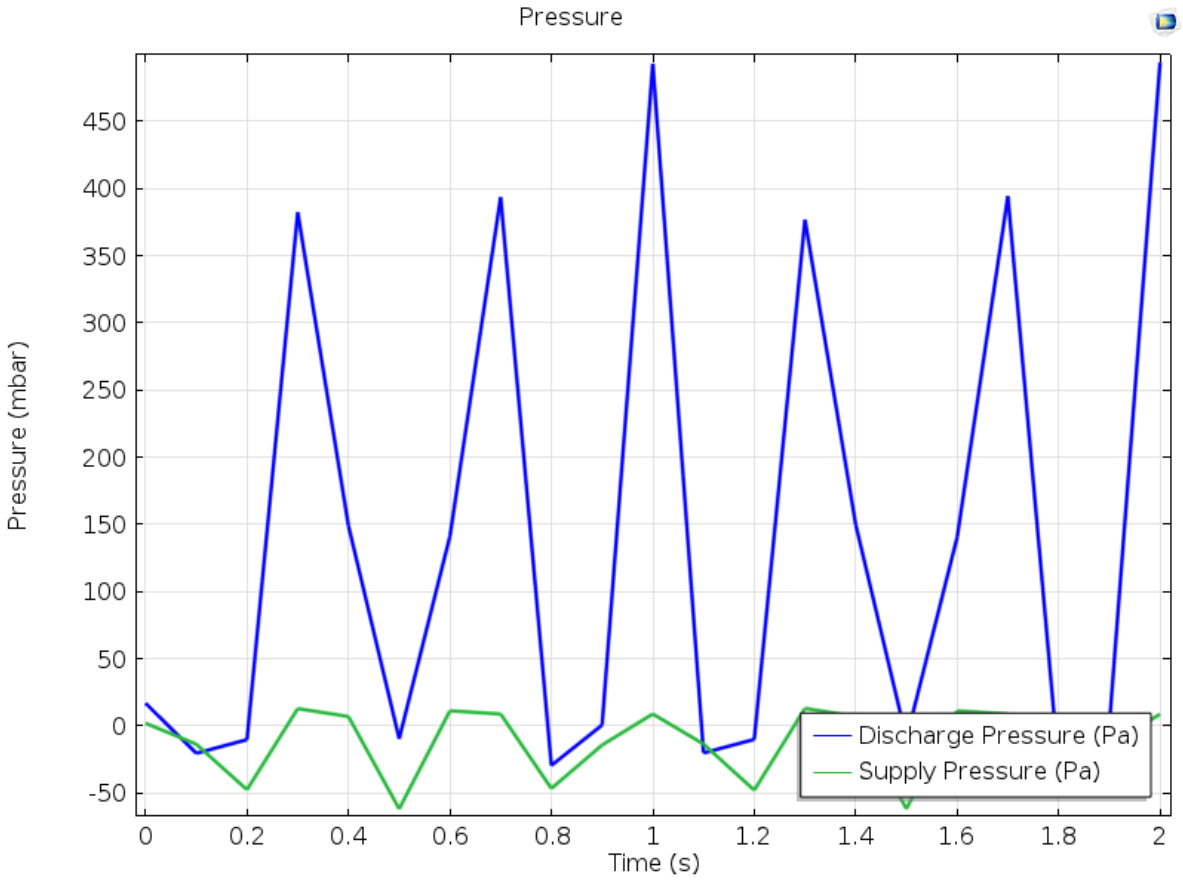

Figure A.33 Pressure vs Time @ V=40 volts, f =3 Hz

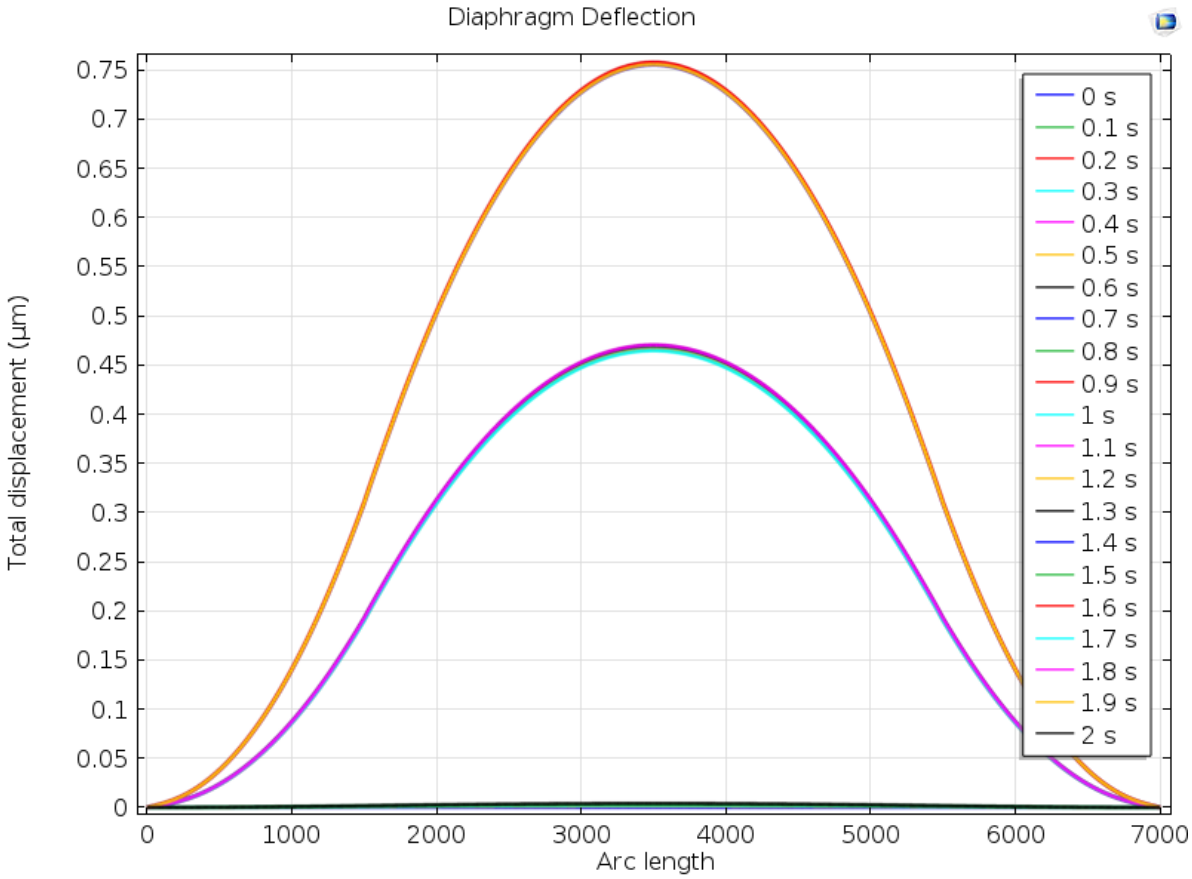

Figure A.34 Diaphragm Deflection versus Arc length @ V=40 volts, f =3 Hz

A.6 Analysis data for load case: Voltage=80 volts, Frequency=1 Hz

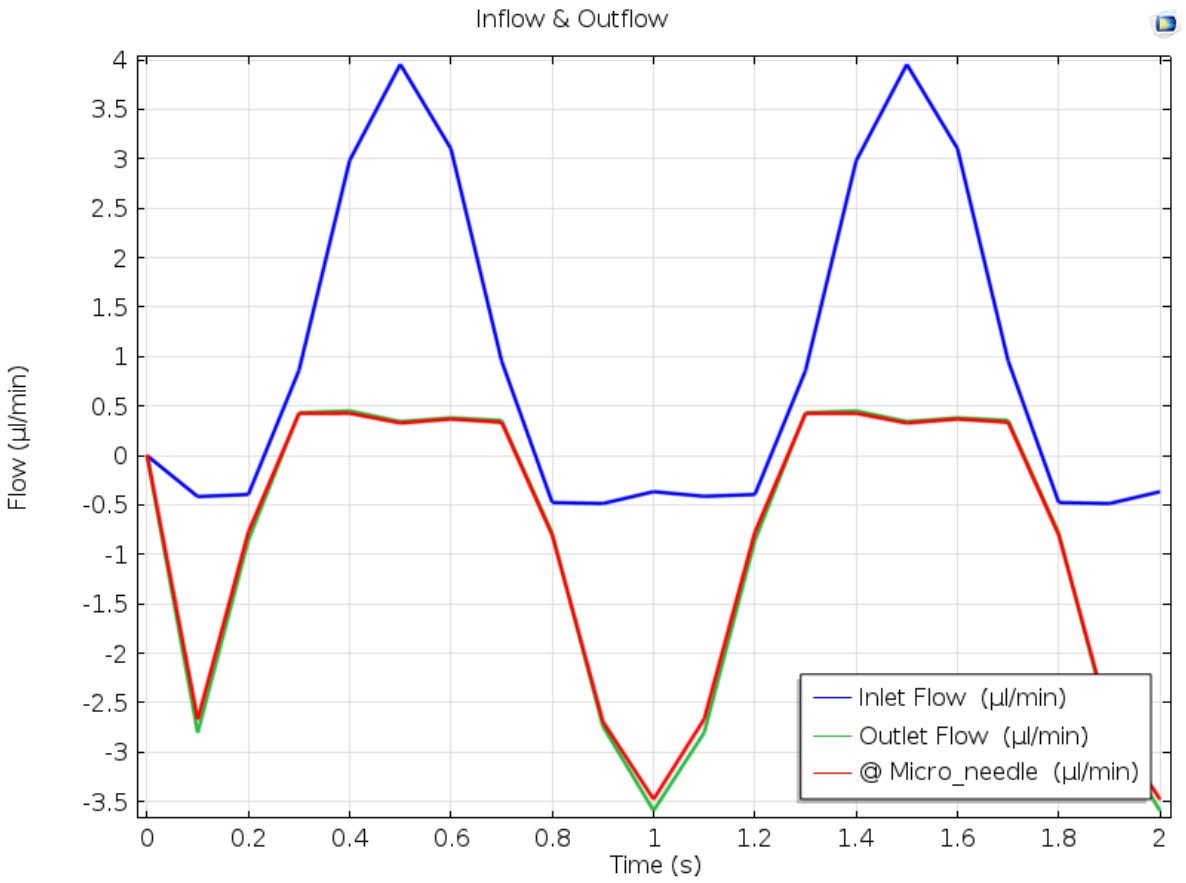

Figure A.35 Flow rate vs time @ V=80 volts, f =1 Hz

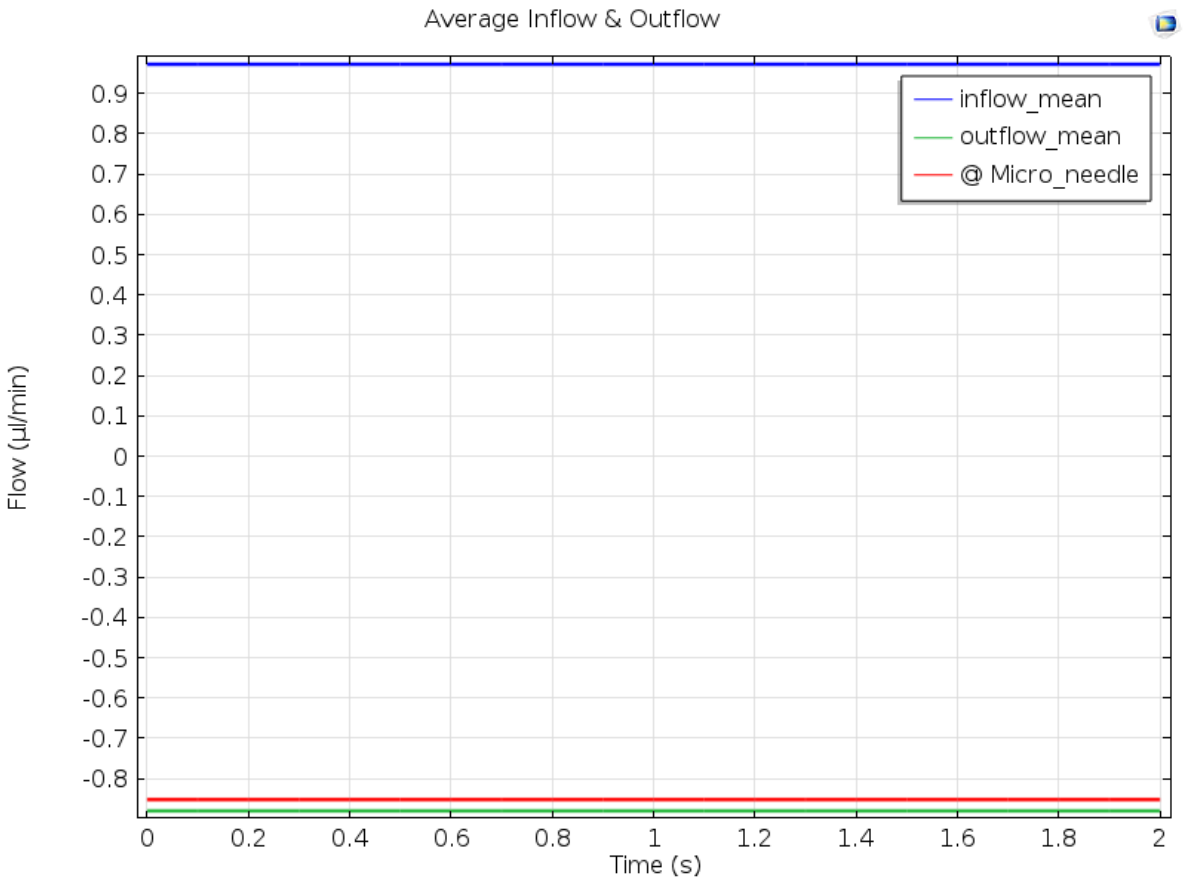

Figure A.36 Average flow rates @ V=80 volts, f =1 Hz

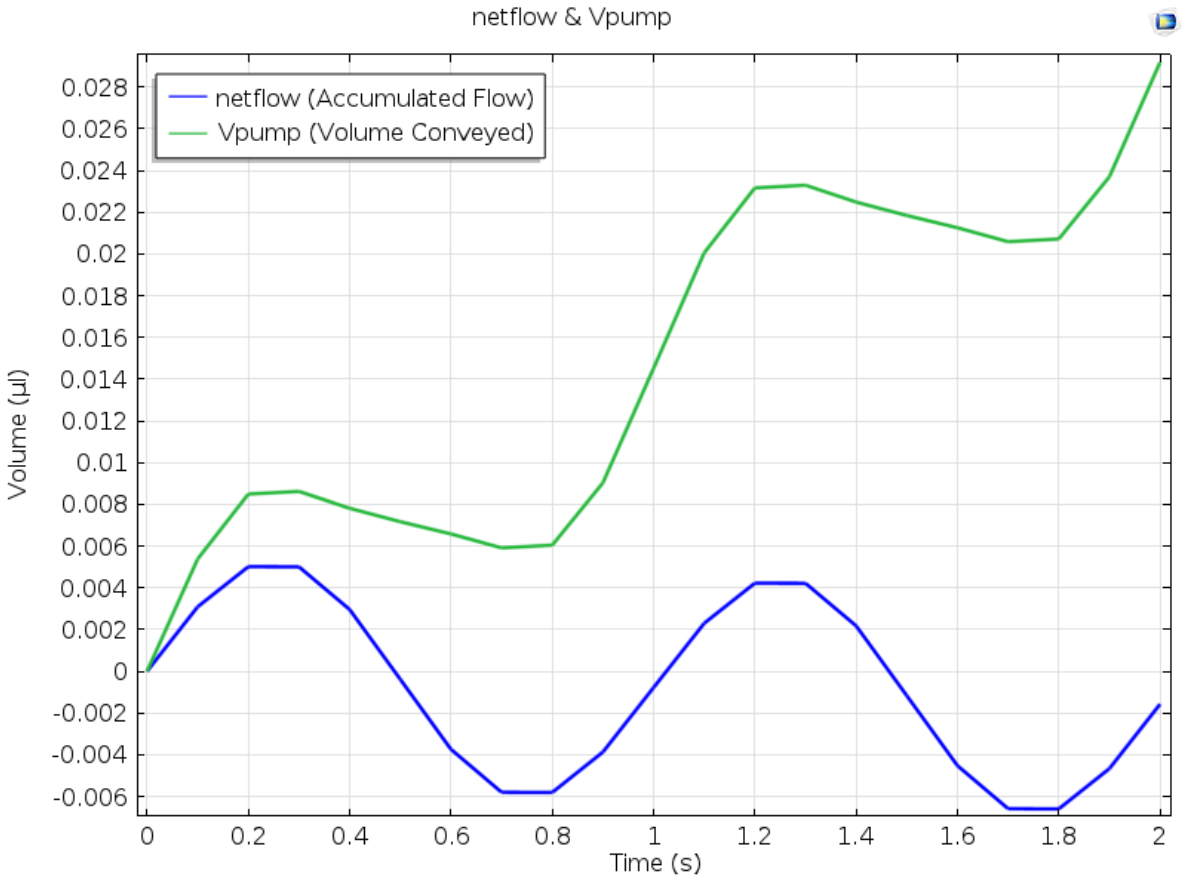

Figure A.37 netflow and Vpump @ V=80 volts, f =1 Hz

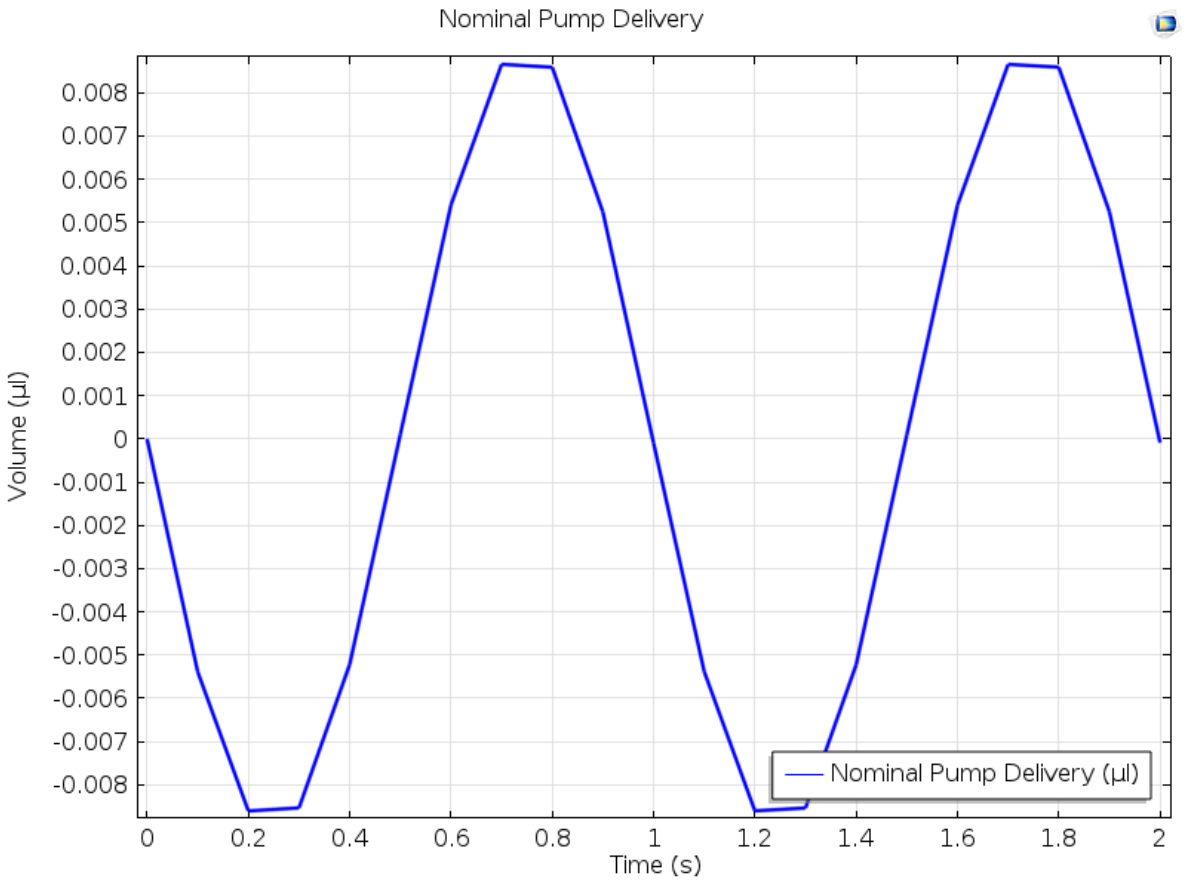

Figure A.38 Nominal Pump Delivery @ V=80 volts, f =1 Hz

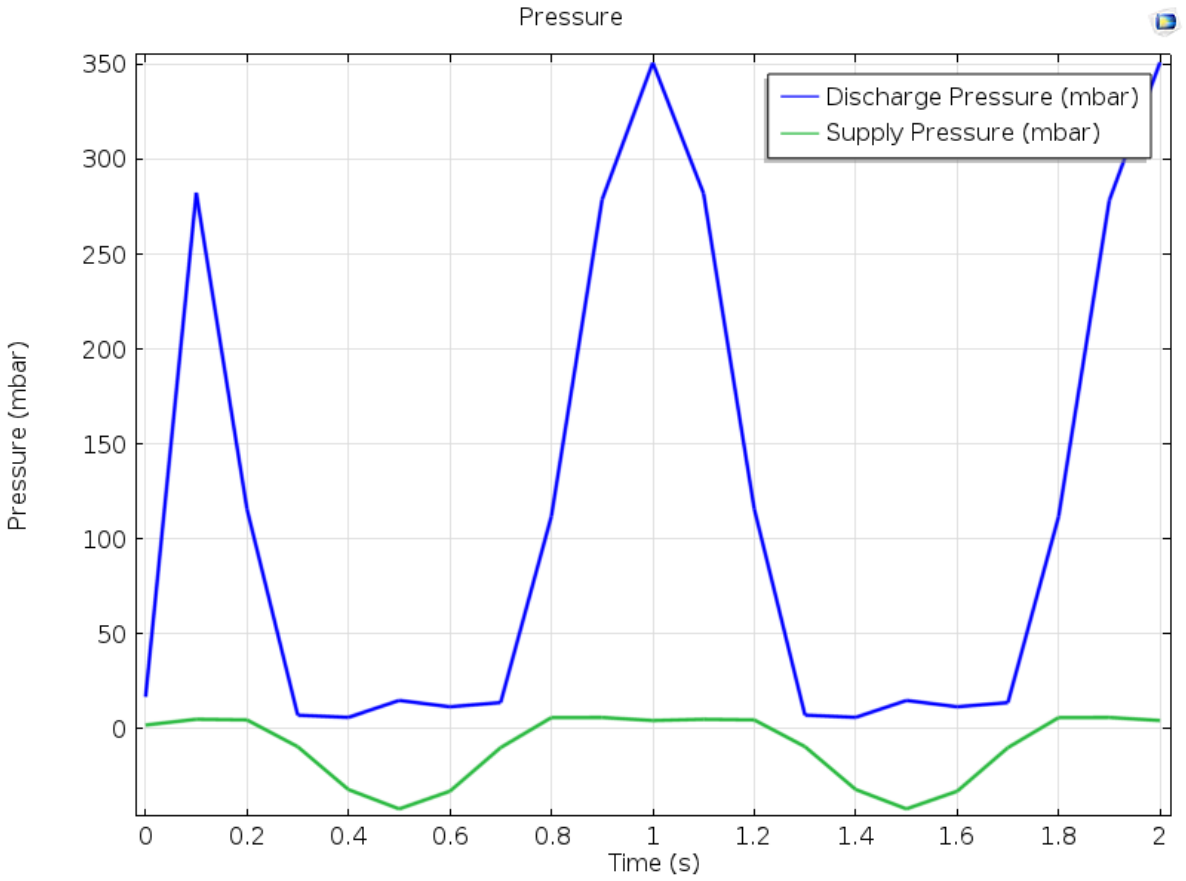

Figure A.39 Pressure vs Time @ V=80 volts, f =1 Hz

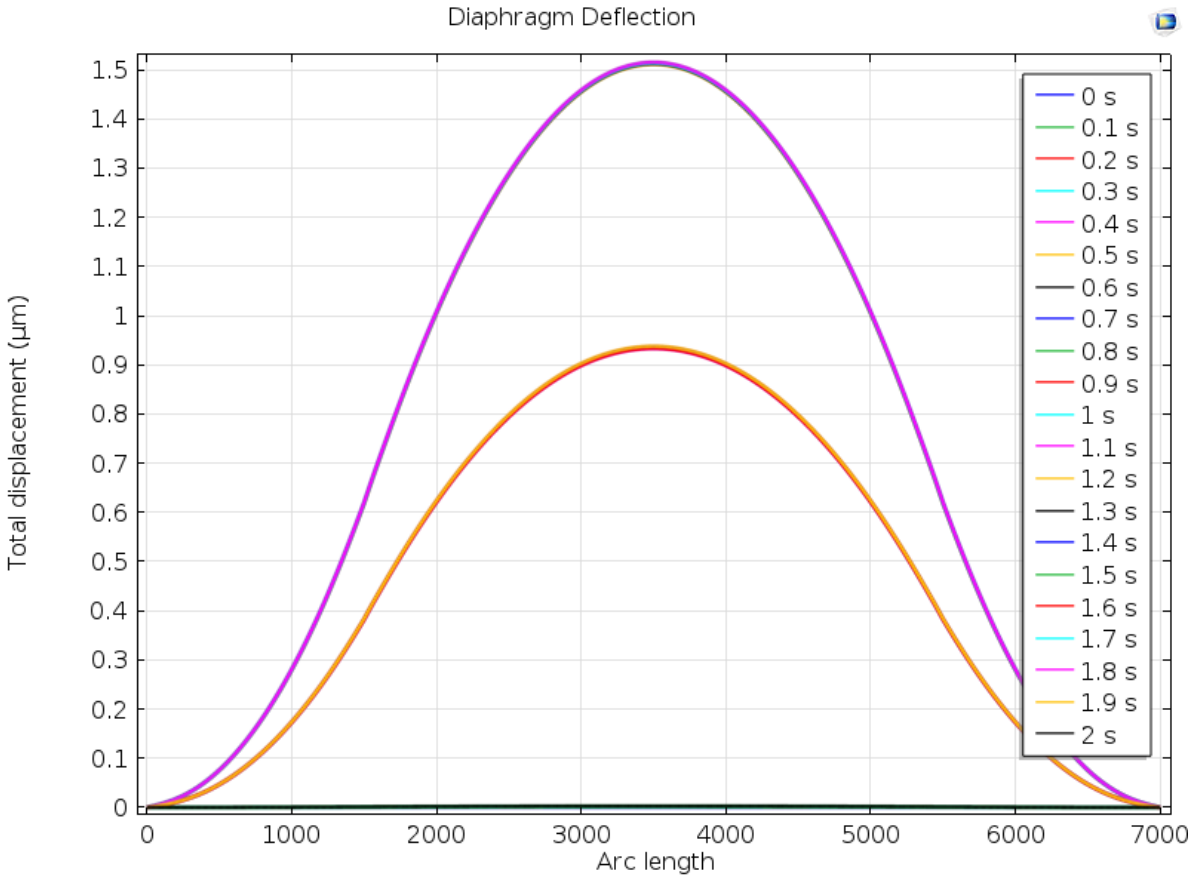

Figure A.40 Diaphragm Deflection versus Arc length @ V=80 volts, f =1 Hz

A.7 Analysis data for load case: Voltage=80 volts, Frequency=2 Hz

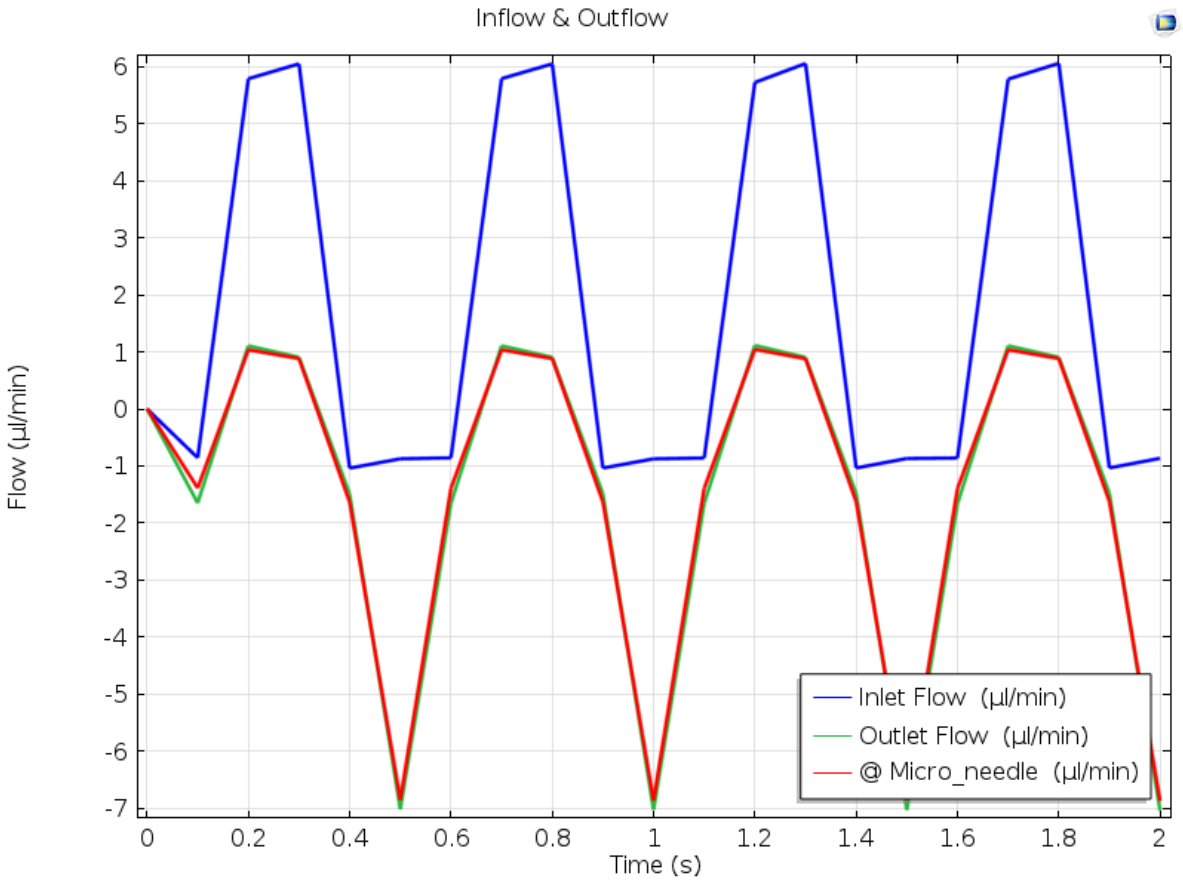

Figure A.41 Flow rate vs time @ V=80 volts, f =2 Hz

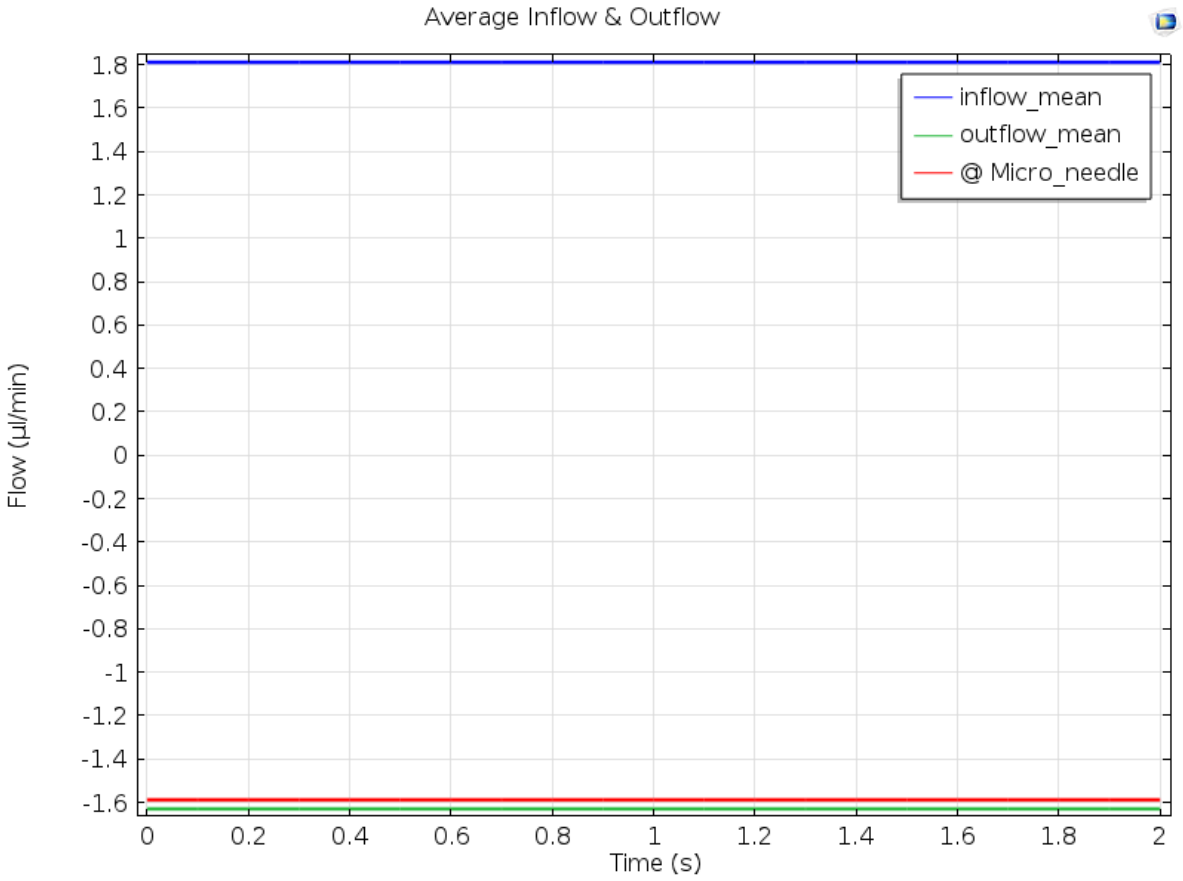

Figure A.42 Average flow rates @ V=80 volts, f =2 Hz

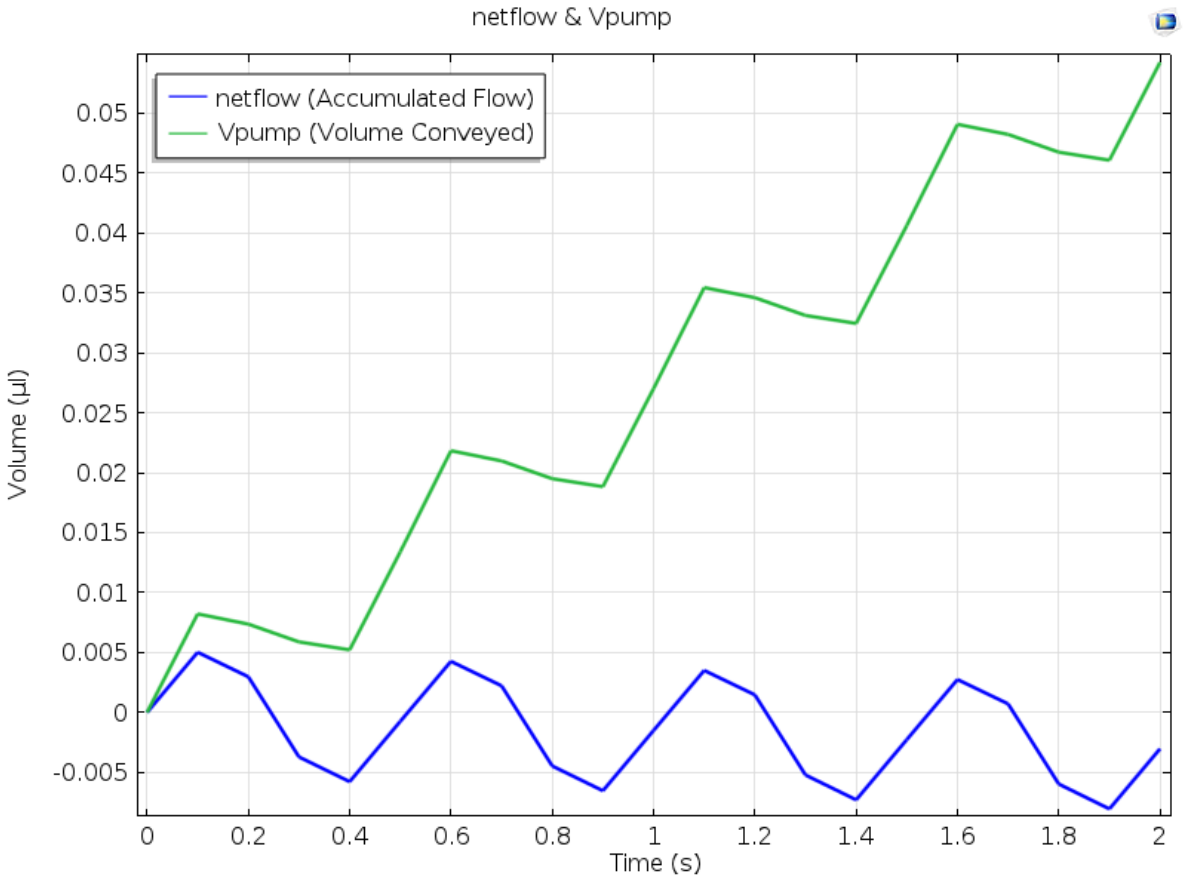

Figure A.43 netflow and Vpump @ V=80 volts, f =2 Hz

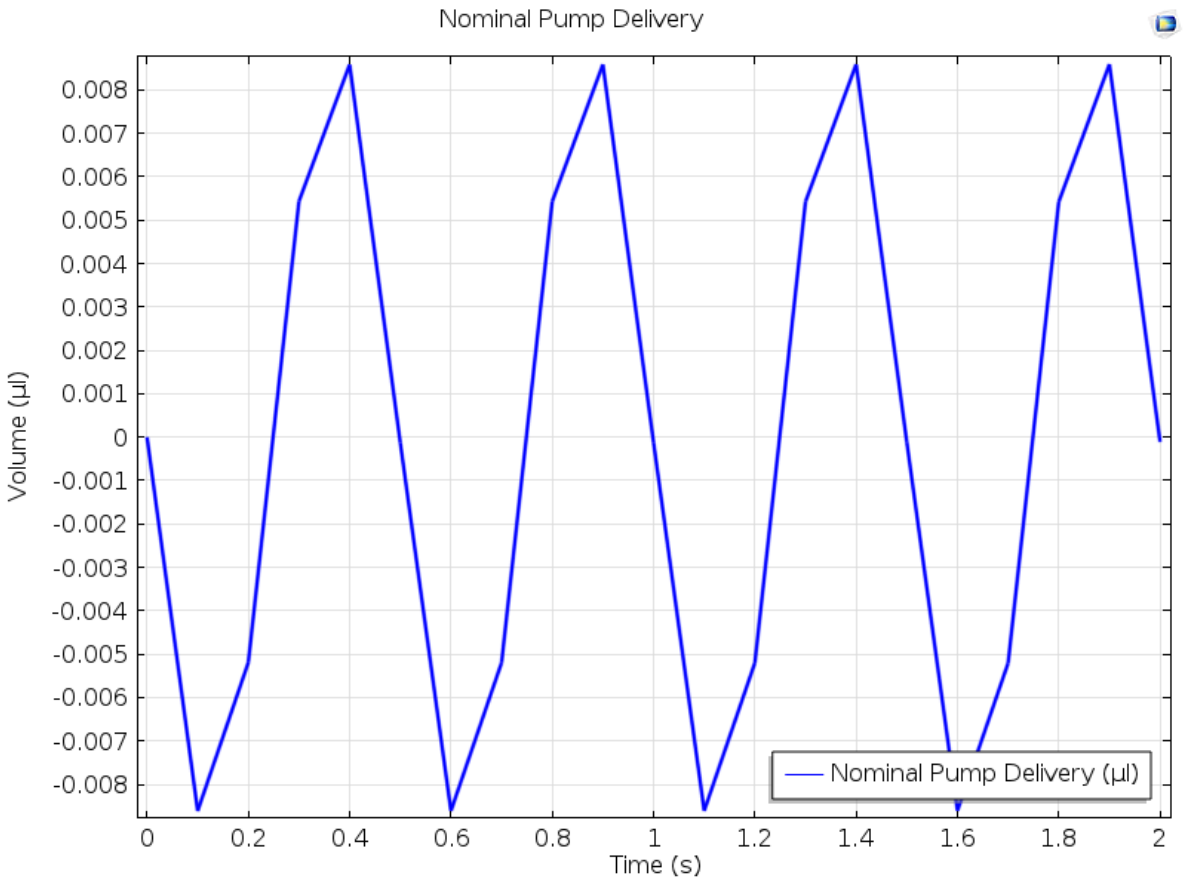

Figure A.44 Nominal Pump Delivery @ V=80 volts, f =2 Hz

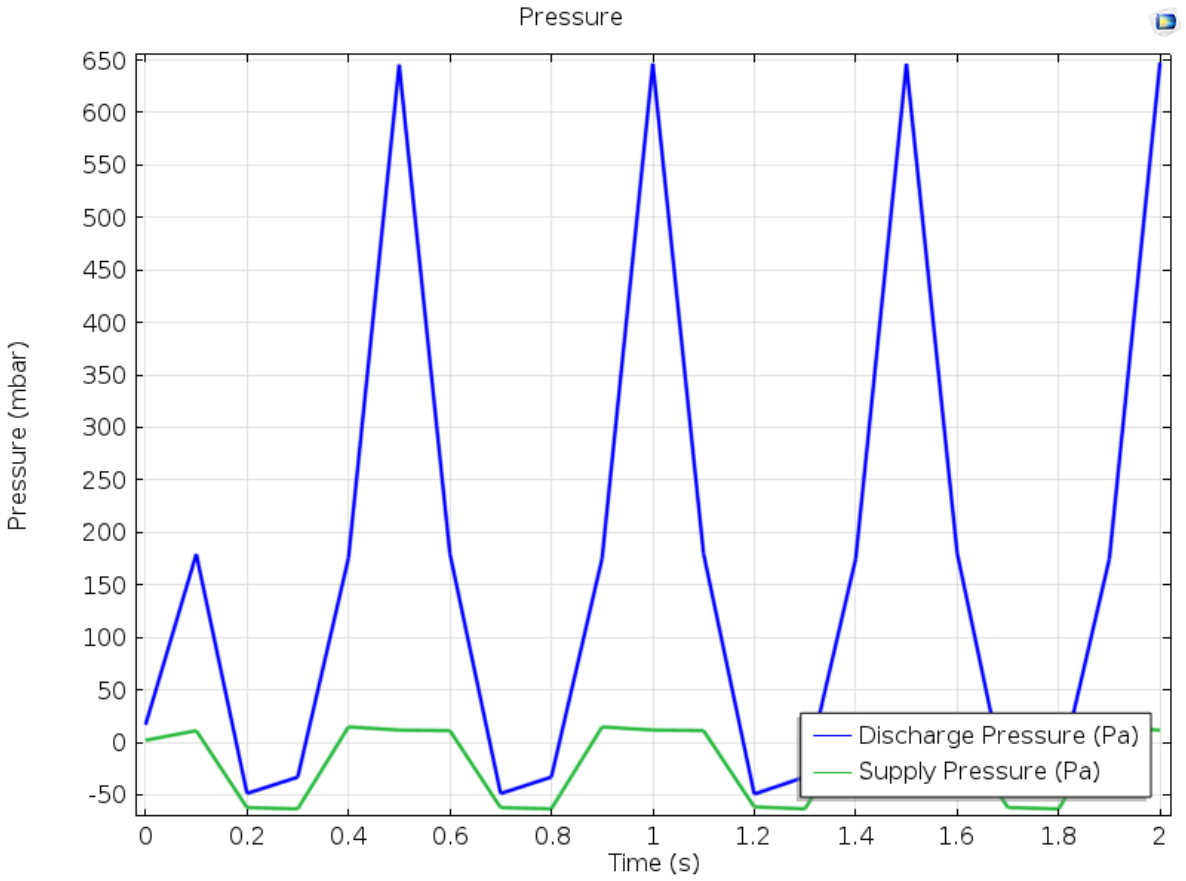

Figure A.45 Pressure vs Time @ V=80 volts, f =2 Hz

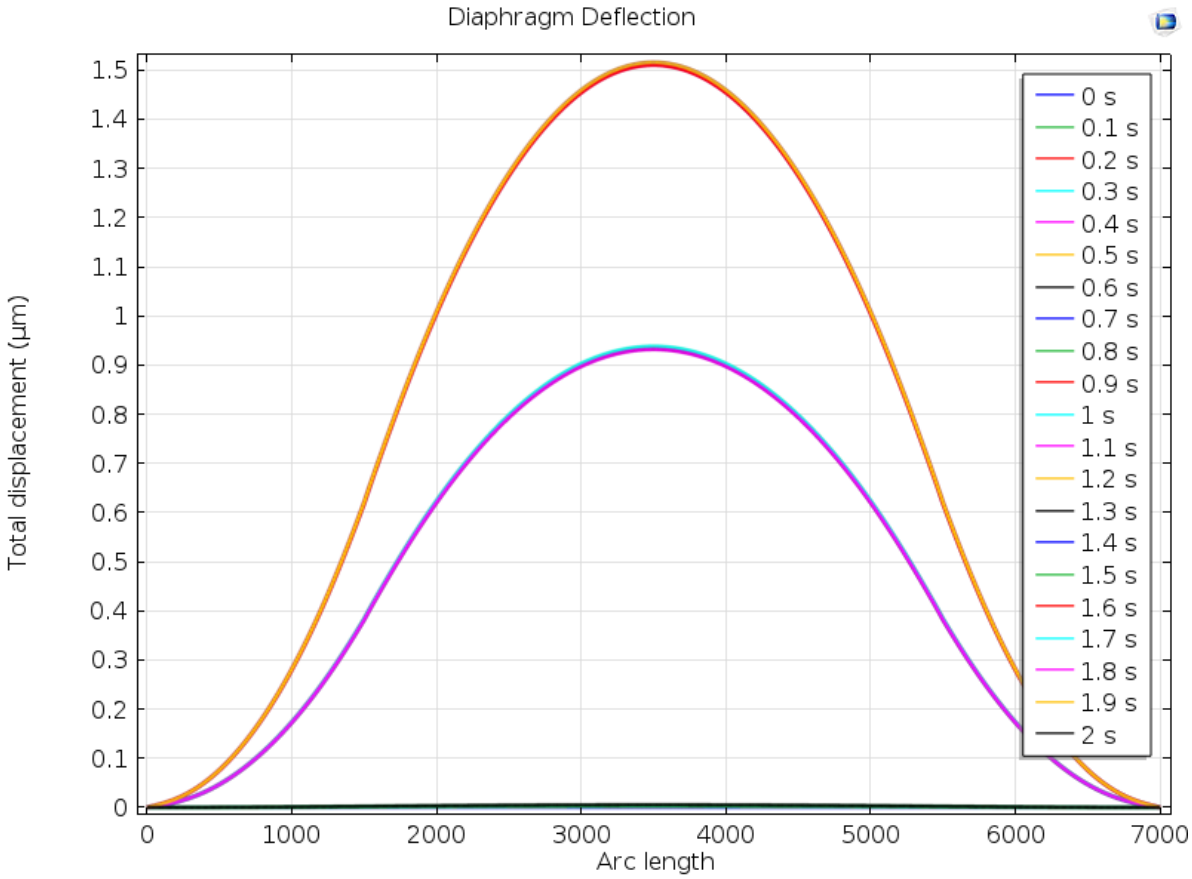

Figure A.46 Diaphragm Deflection versus Arc length @ V=80 volts, f =2 Hz

A.8 Analysis data for load case: Voltage=80 volts, Frequency=3 Hz

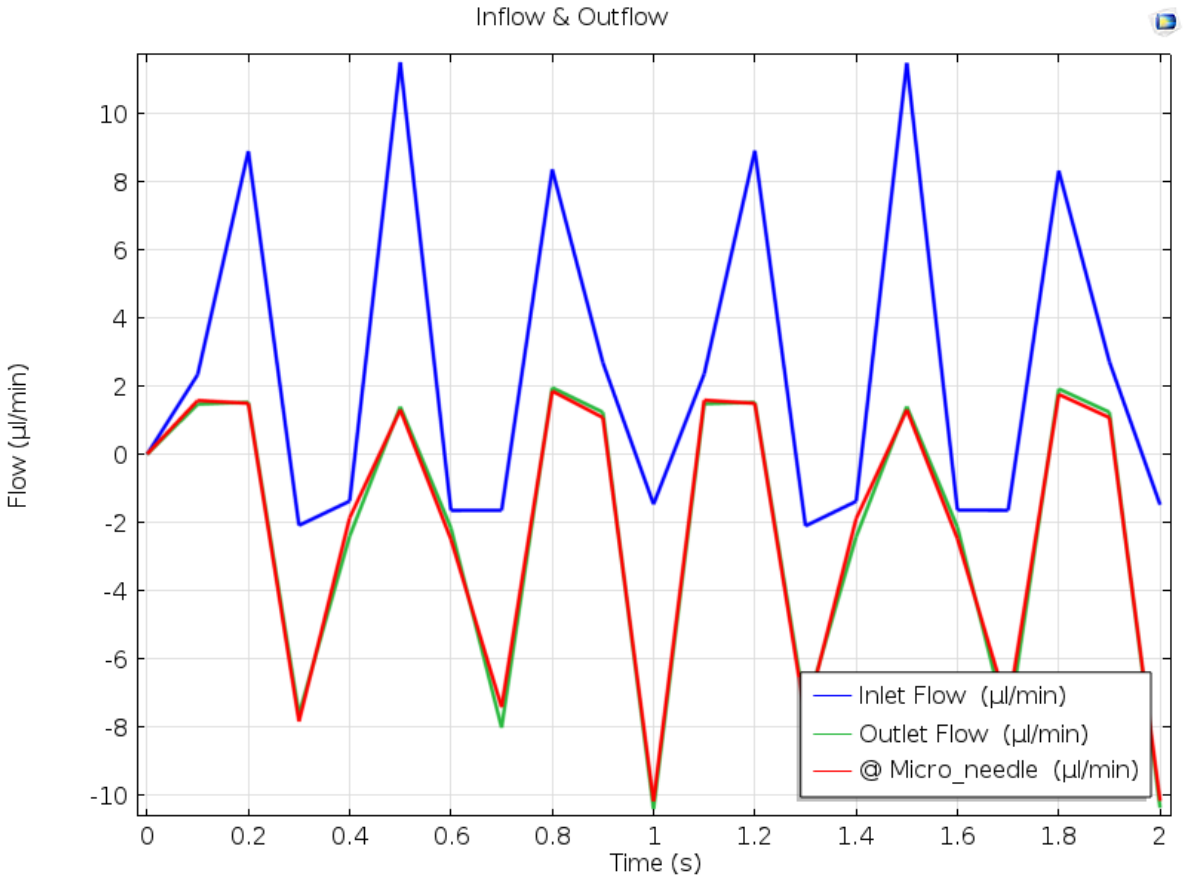

Figure A.47 Flow rate vs time @ V=80 volts, f =3 Hz

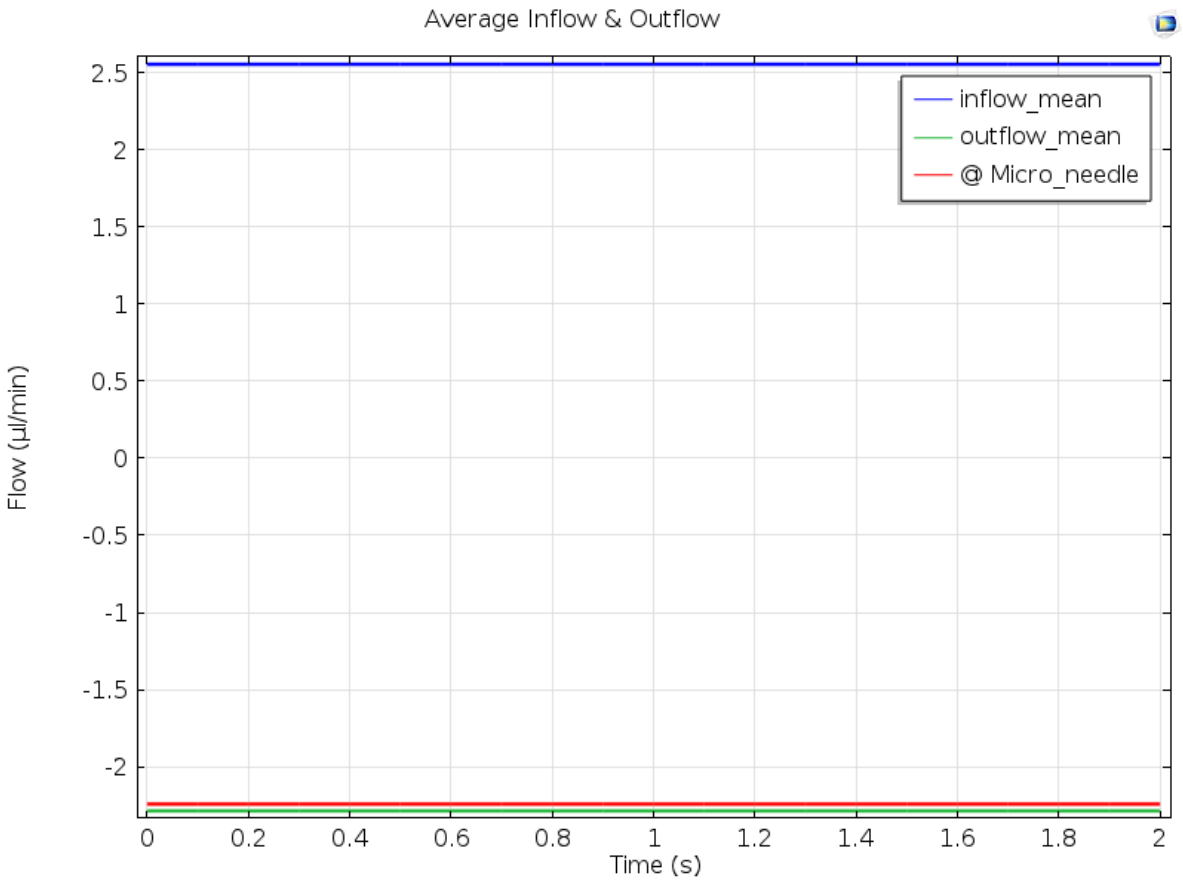

Figure A.48 Average flow rates @ V=80 volts, f =3 Hz

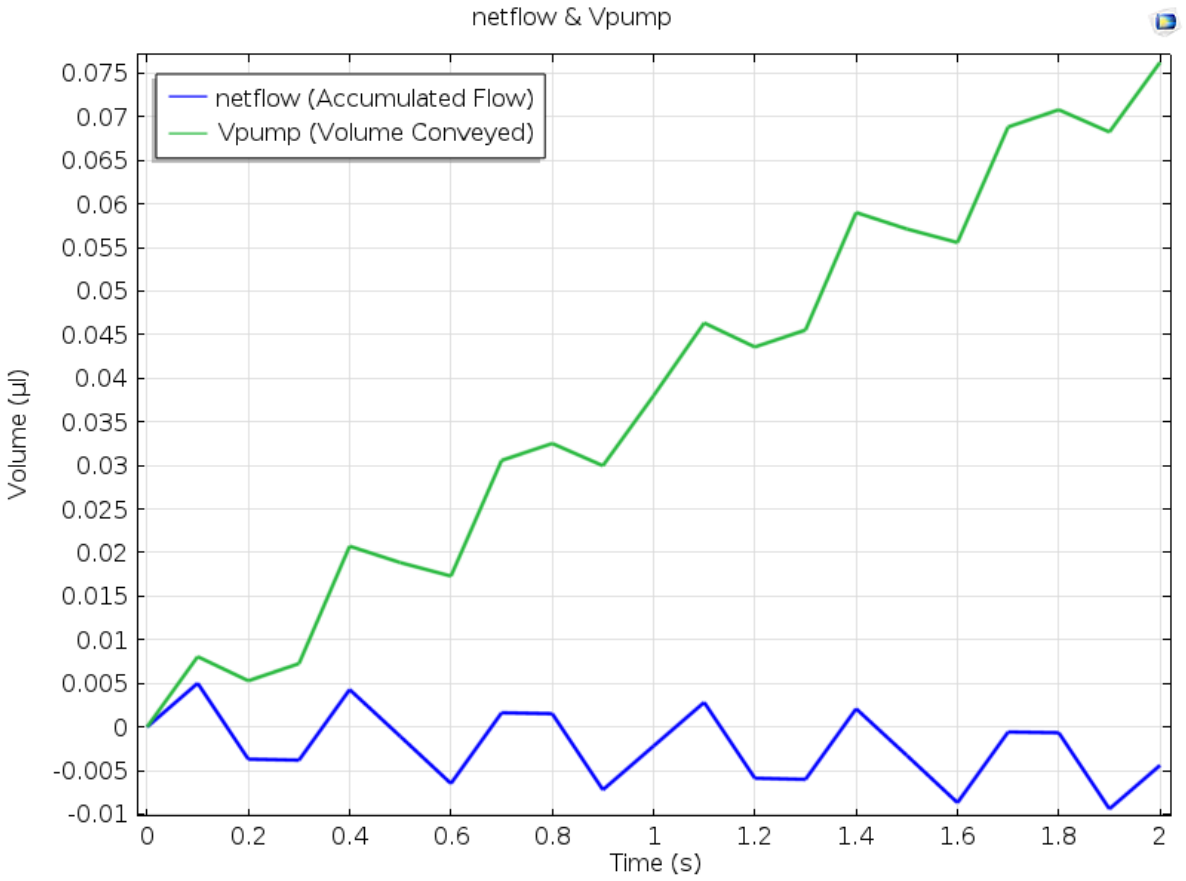

Figure A.49 netflow and Vpump @ V=80 volts, f =3 Hz

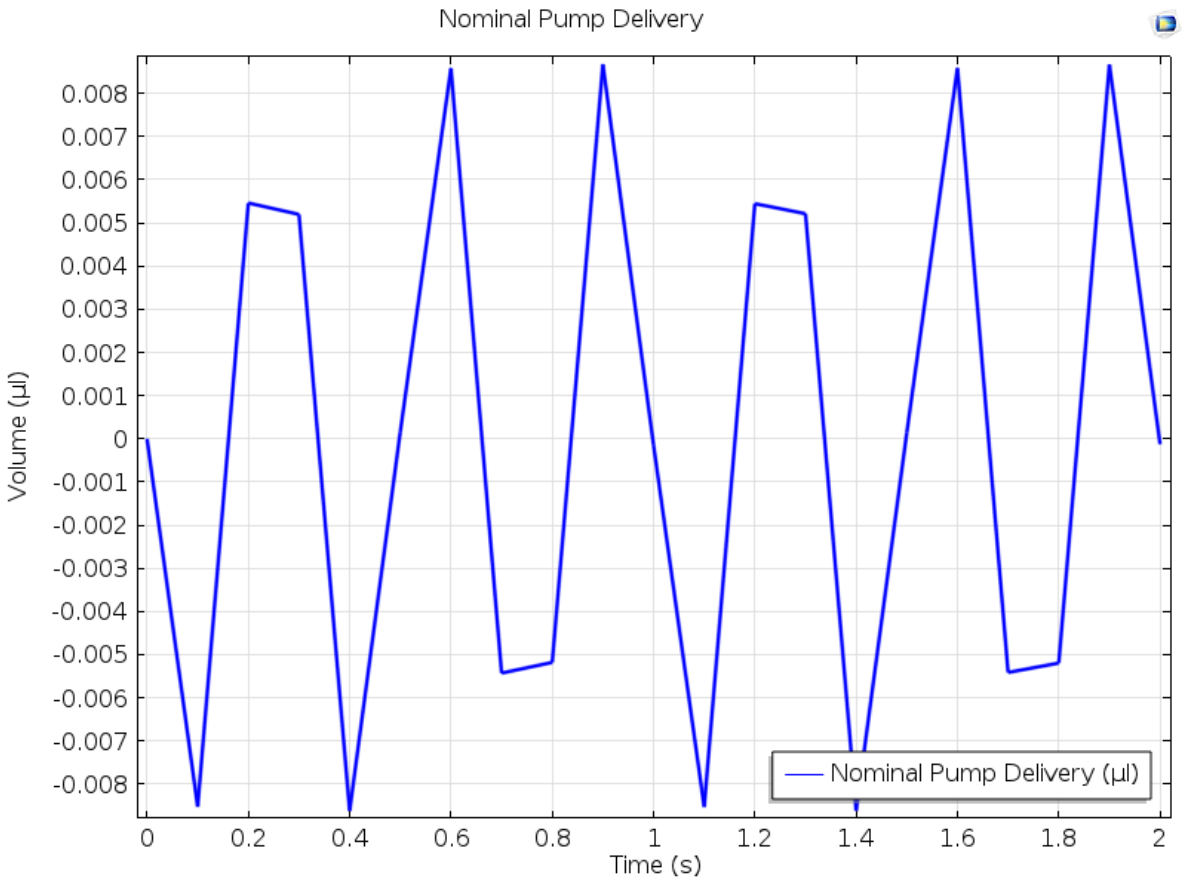

Figure A.50 Nominal Pump Delivery @ V=80 volts, f =3 Hz

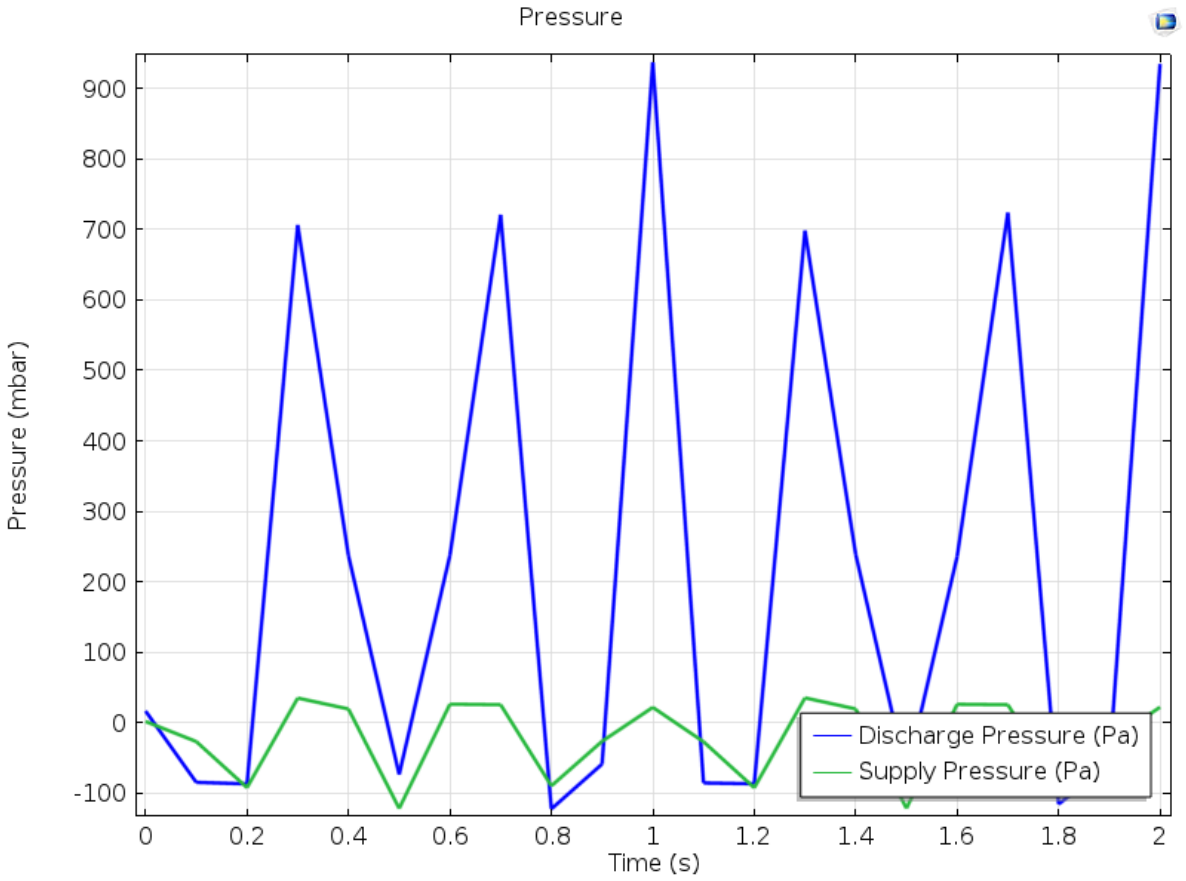

Figure A.51 Pressure vs Time @ V=80 volts, f =3 Hz

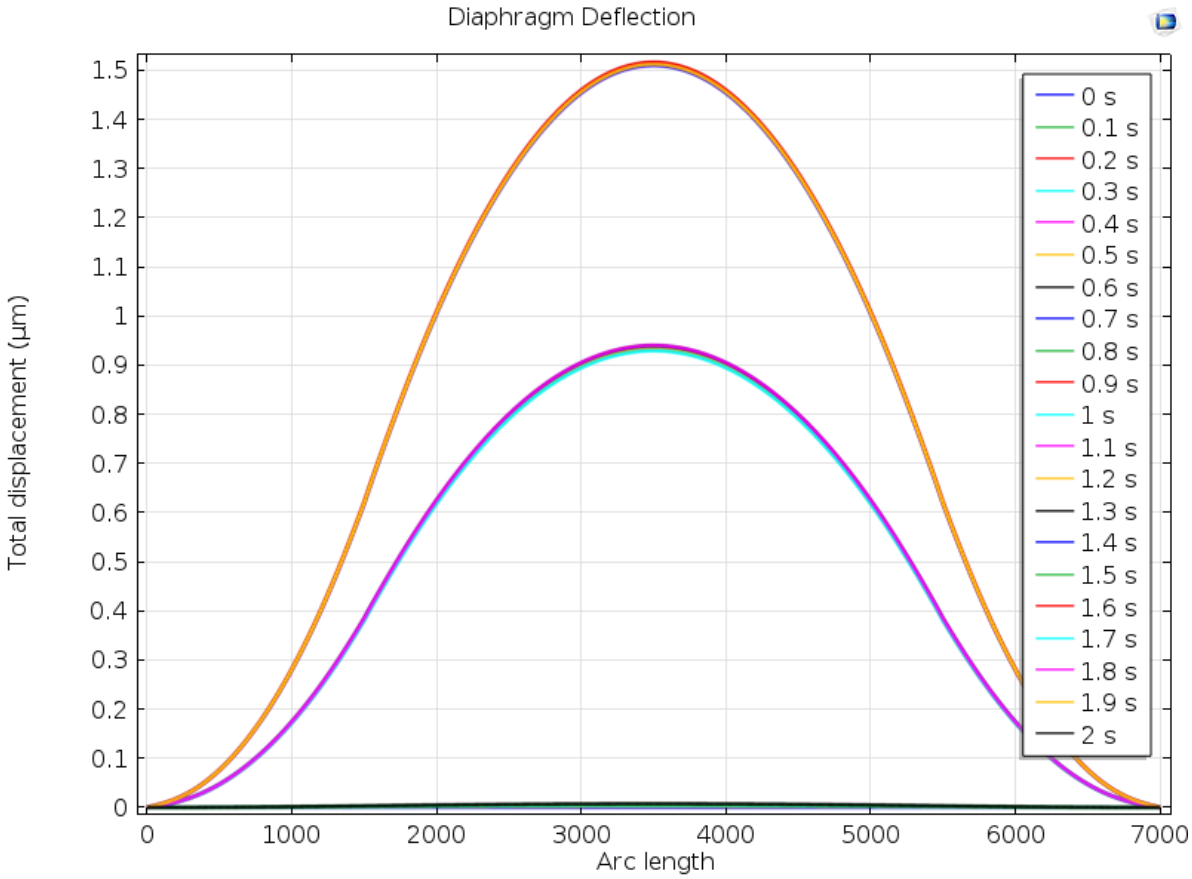

Figure A.52 Diaphragm Deflection versus Arc length @ V=80 volts, f =3 Hz

A.9 V Analysis data for load case: oltage=110 volts, Frequency=1 Hz

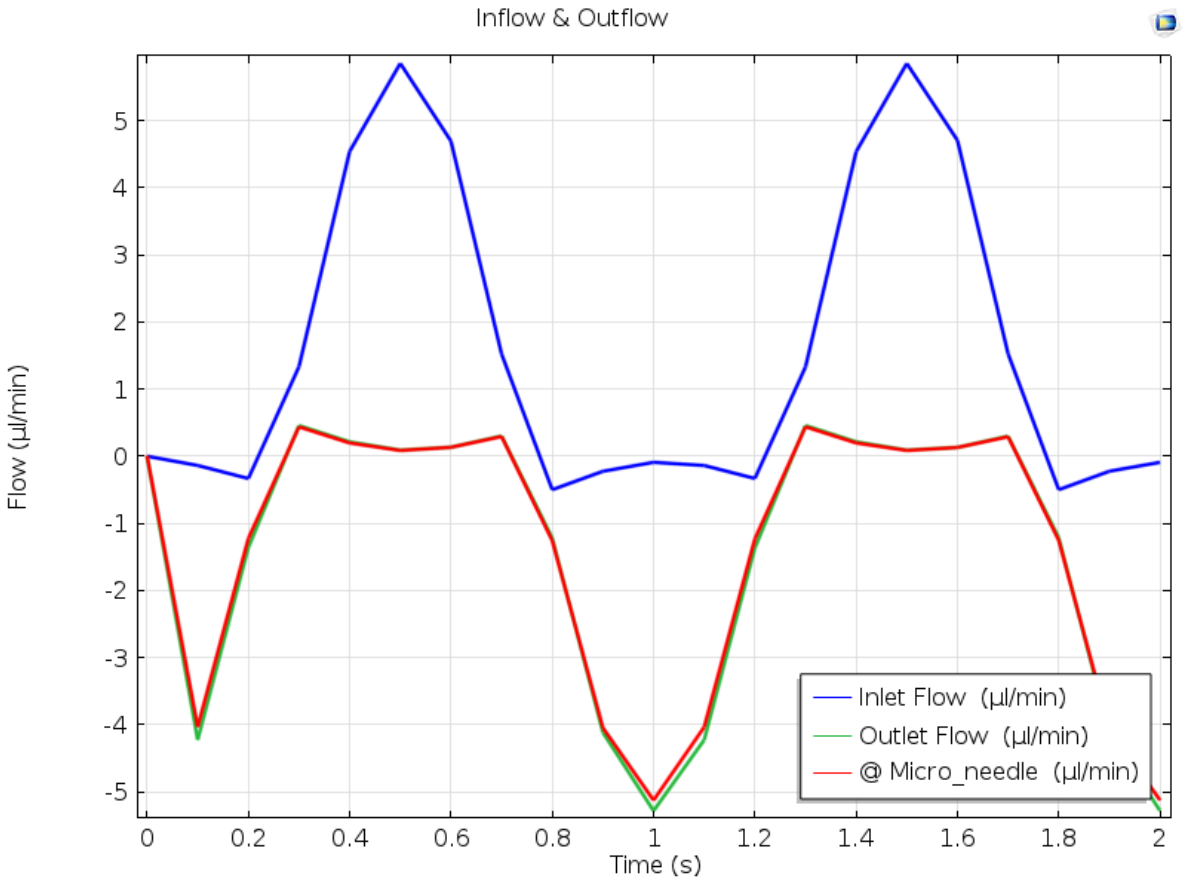

Figure A.53 Flow rate vs time @ V=110 volts, f =1 Hz

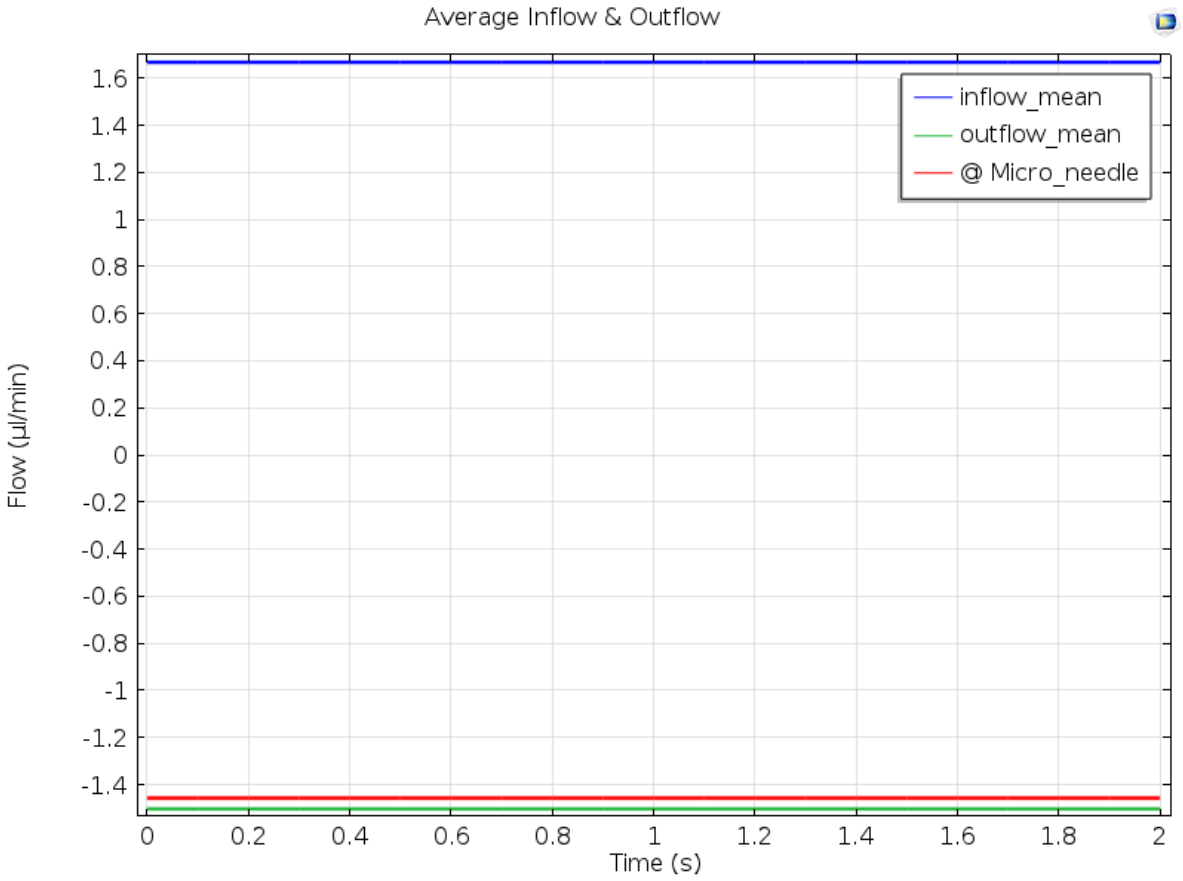

Figure A.54 Average flow rates @ V=110 volts, f =1 Hz

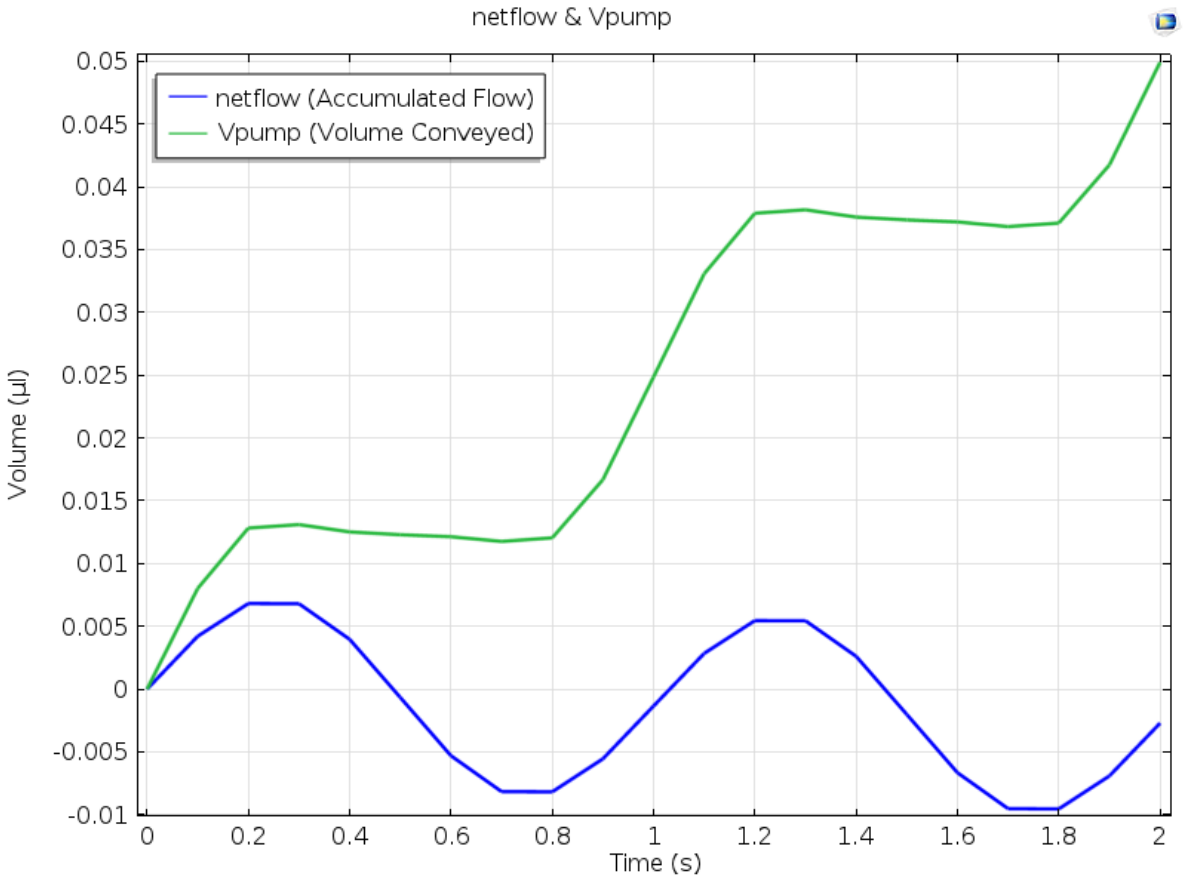

Figure A.55 netflow and Vpump @ V=110 volts, f =1 Hz

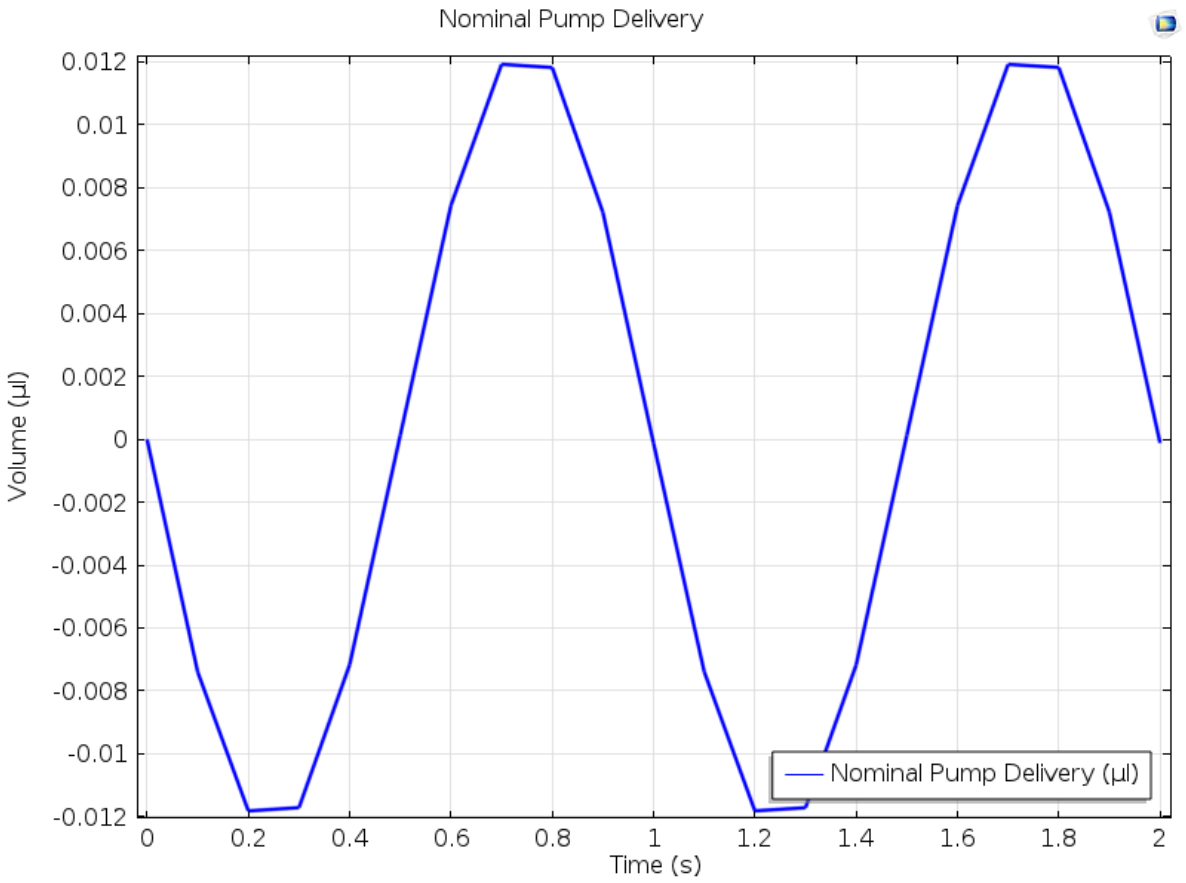

Figure A.56 Nominal Pump Delivery @ V=110 volts, f =1 Hz

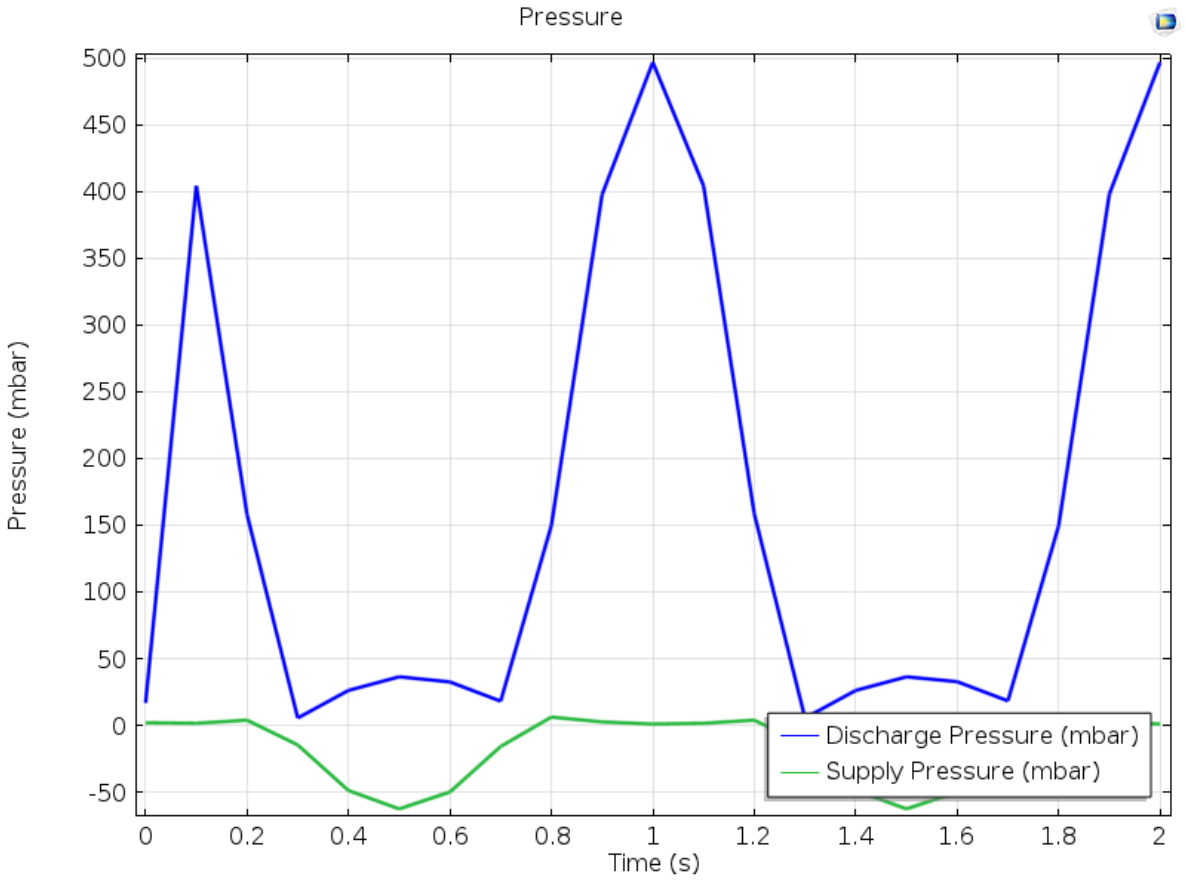

Figure A.57 Pressure vs Time @ V=110 volts, f =1 Hz

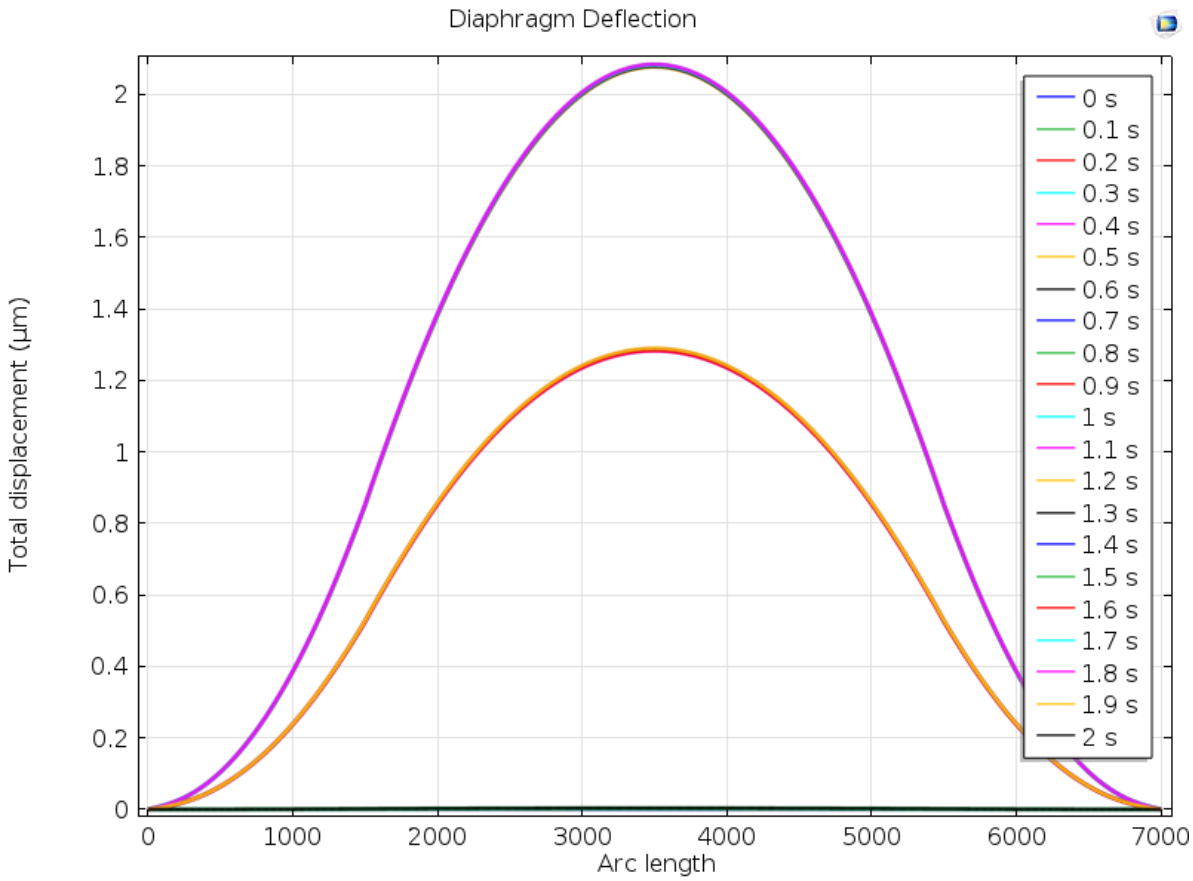

Figure A.58 Diaphragm Deflection versus Arc length @ V=110 volts, f =1 Hz

A.10 Analysis data for load case: Voltage=110 volts, Frequency=2 Hz

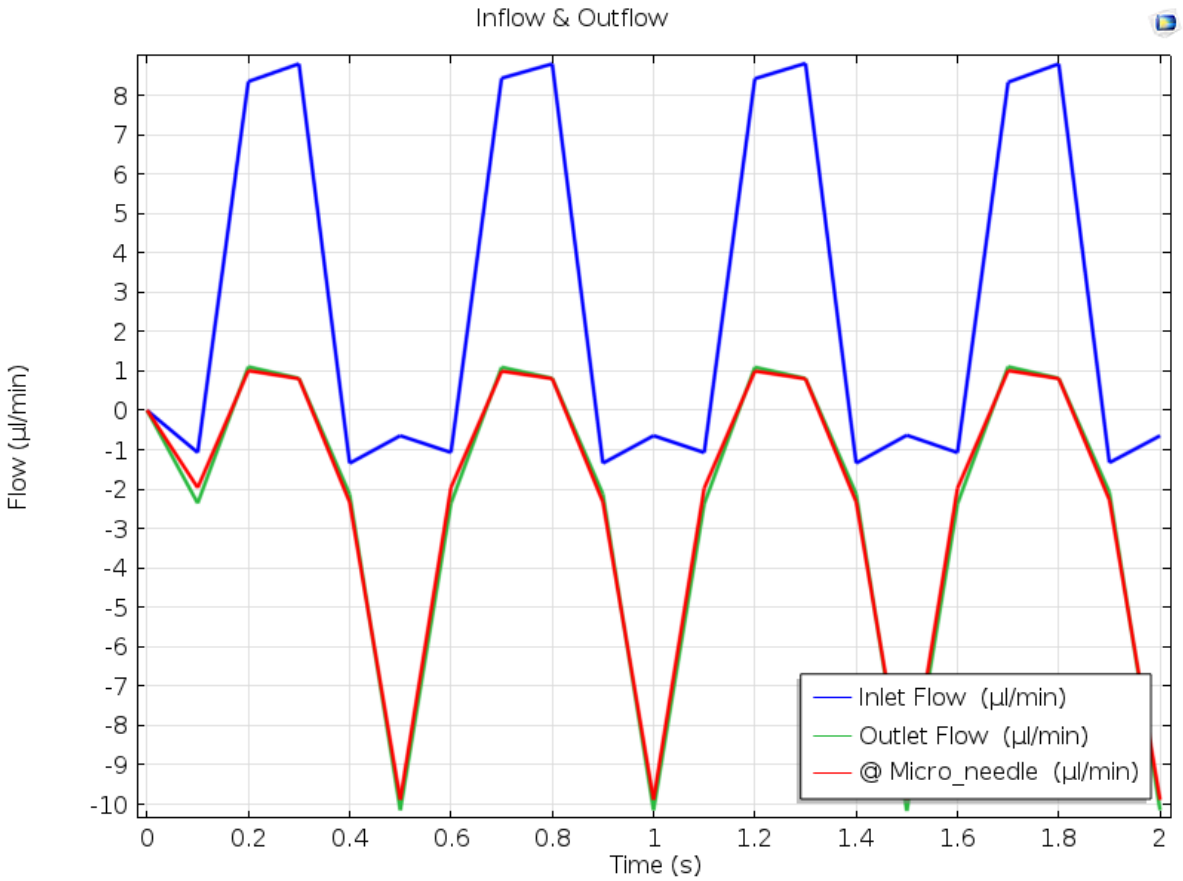

Figure A.59 Flow rate vs time @ V=110 volts, f =2 Hz

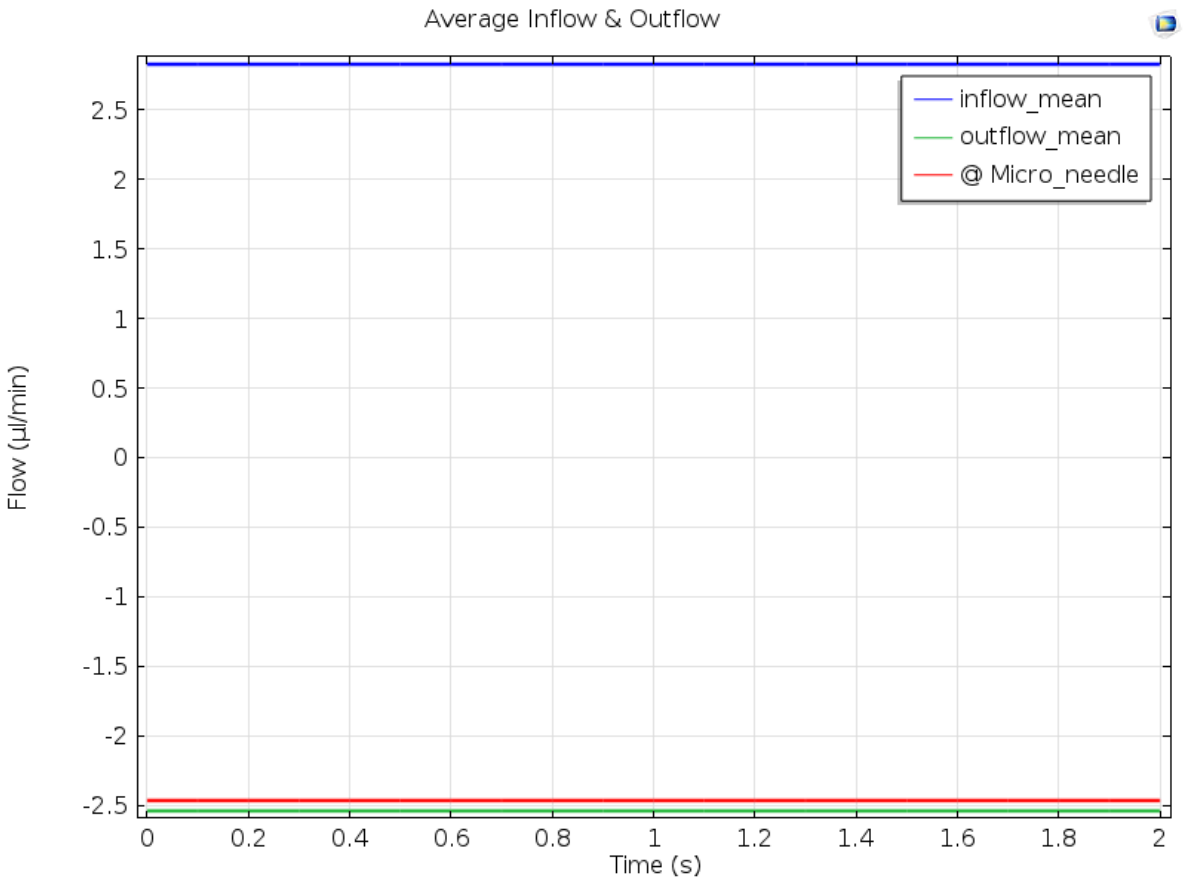

Figure A.60 Average flow rates @ V=110 volts, f =2 Hz

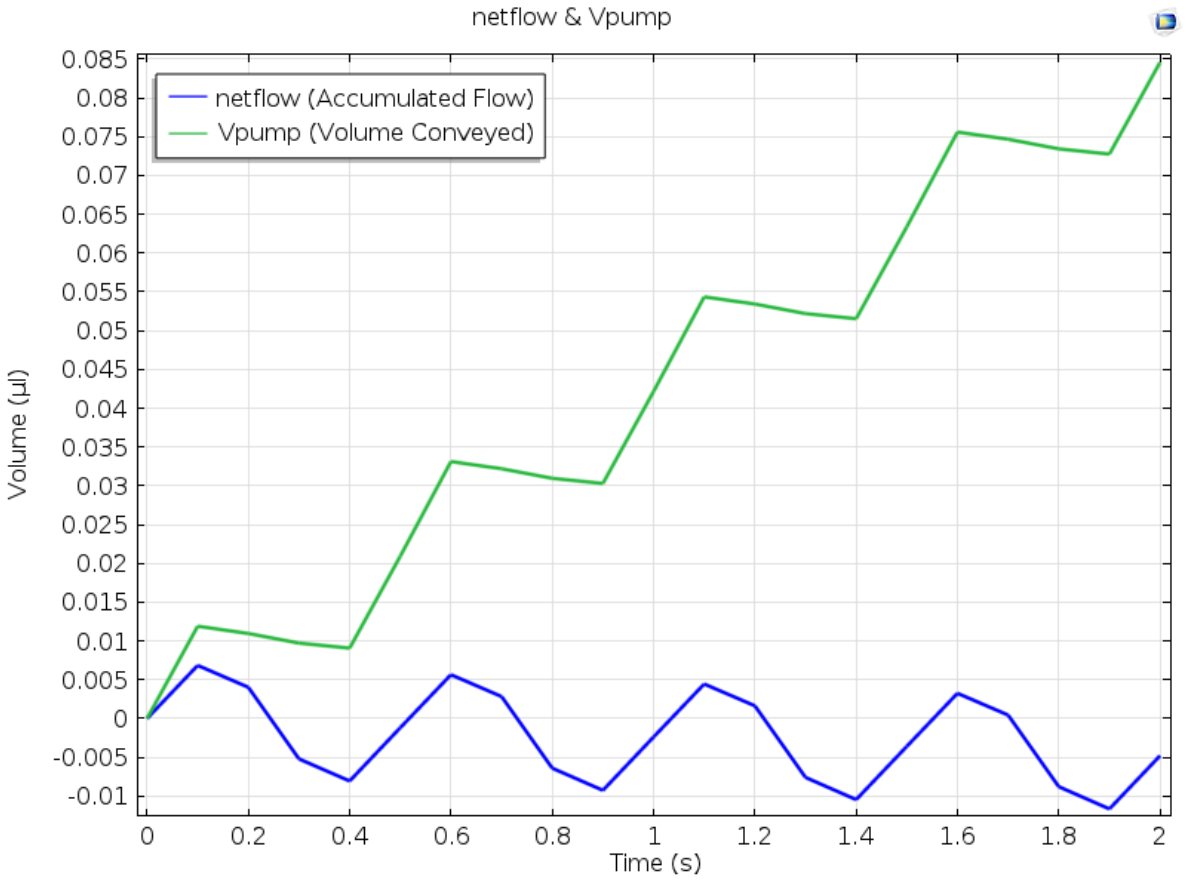

Figure A.61 netflow and Vpump @ V=110 volts, f =2 Hz

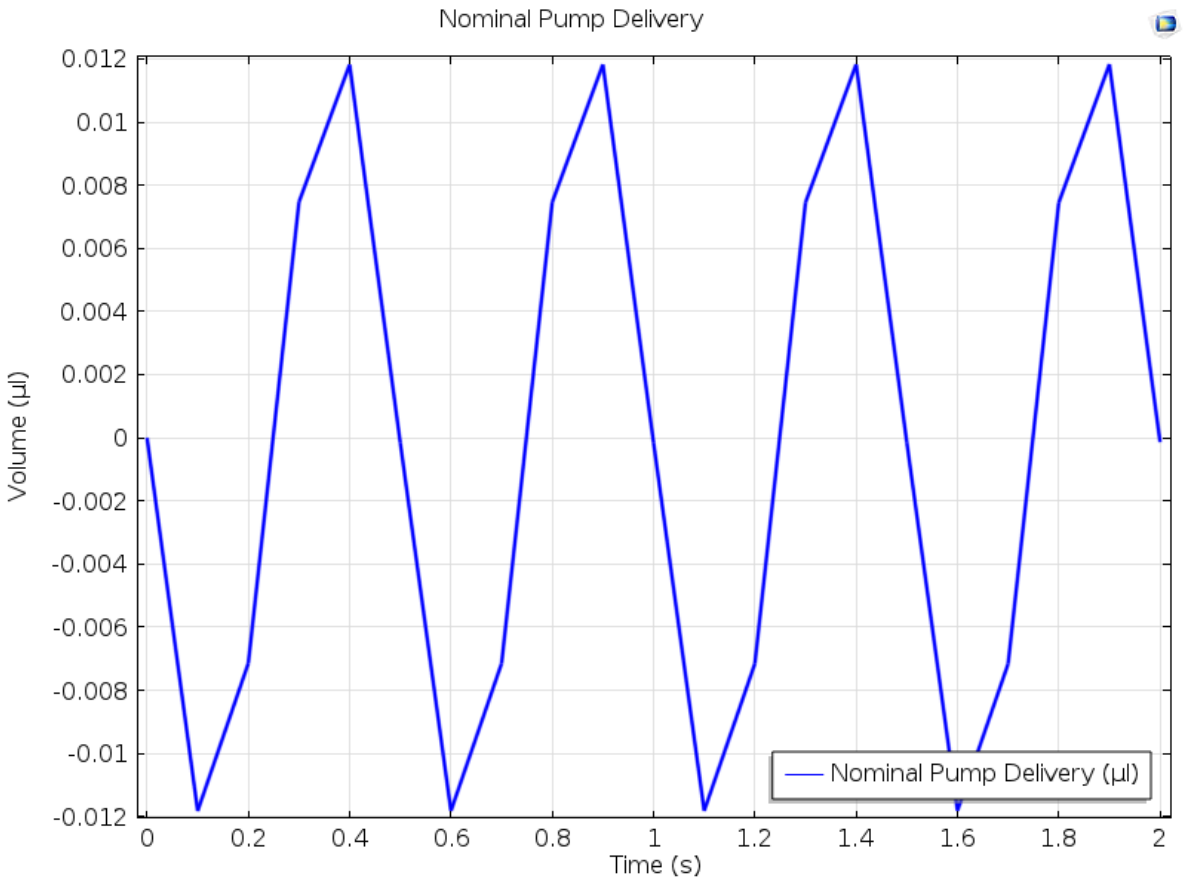

Figure A.62 Nominal Pump Delivery @ V=110 volts, f =2 Hz

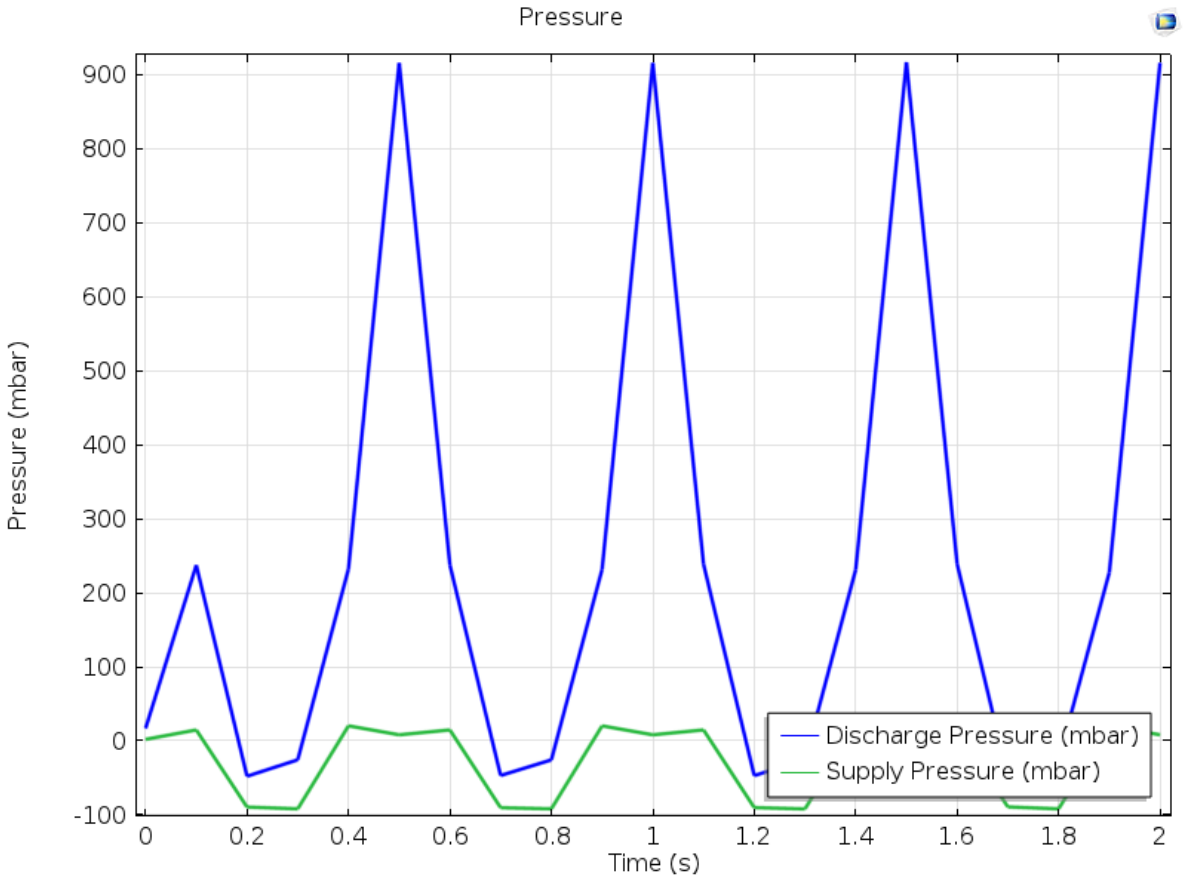

Figure A.63 Pressure vs Time @ V=110 volts, f =2 Hz

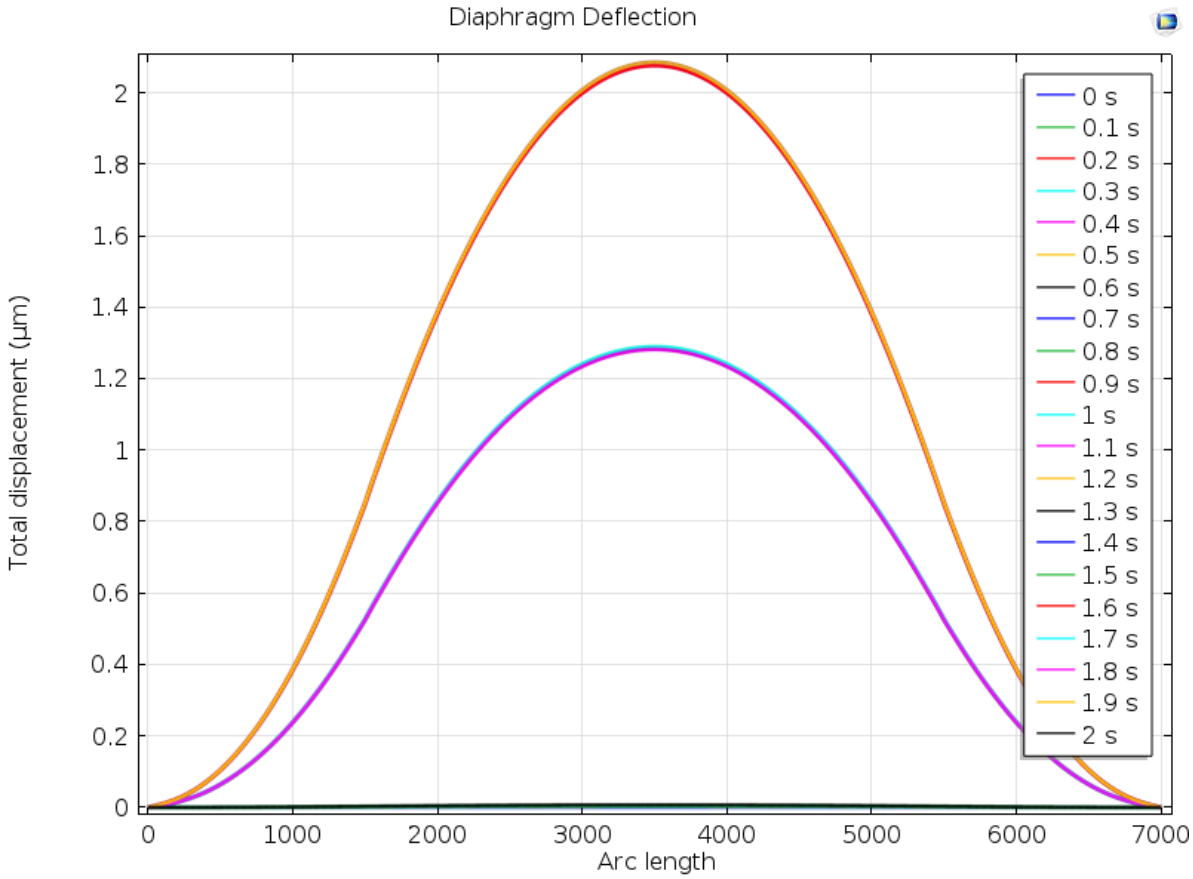

Figure A.64 Diaphragm Deflection versus Arc length @ V=110 volts, f =2 Hz

A.11 Analysis data for load case: Voltage=110 volts, Frequency=3 Hz

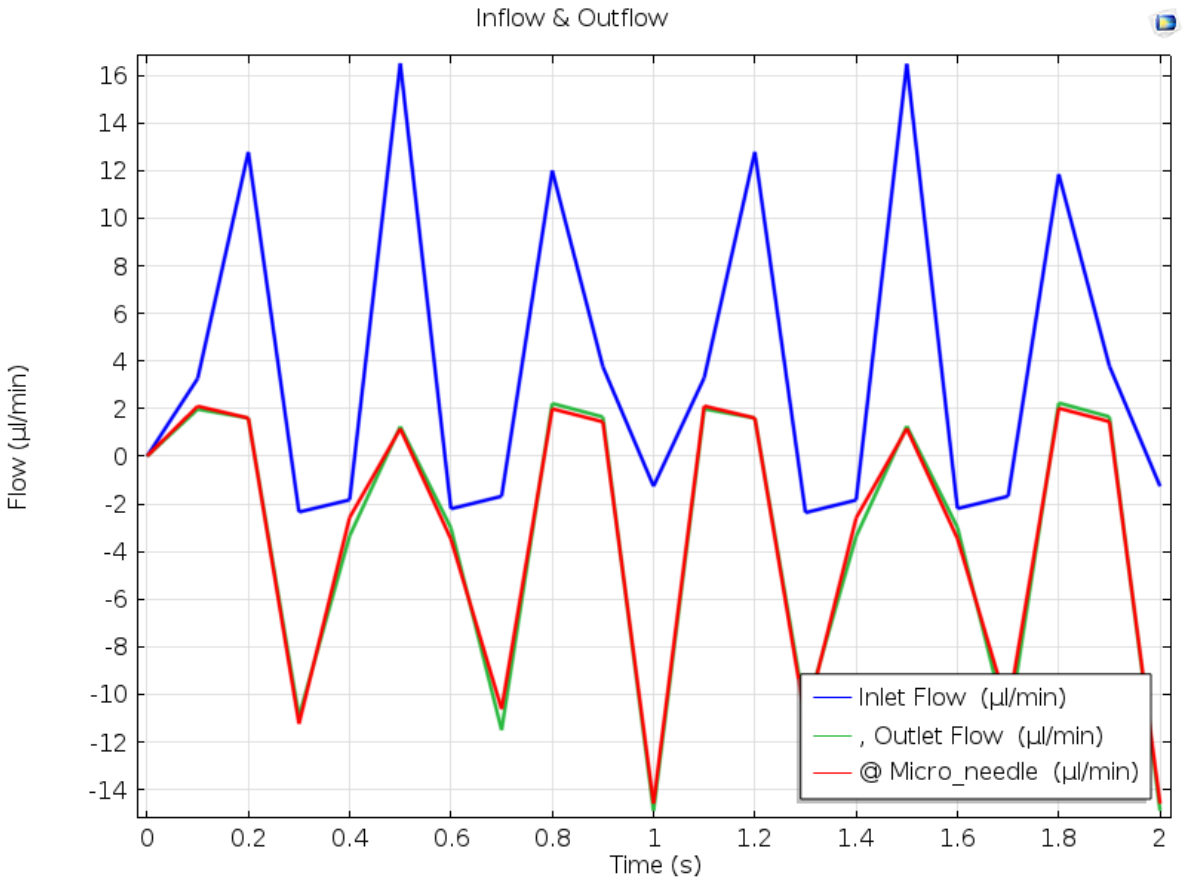

Figure A.65 Flow rate vs time @ V=110 volts, f =3 Hz

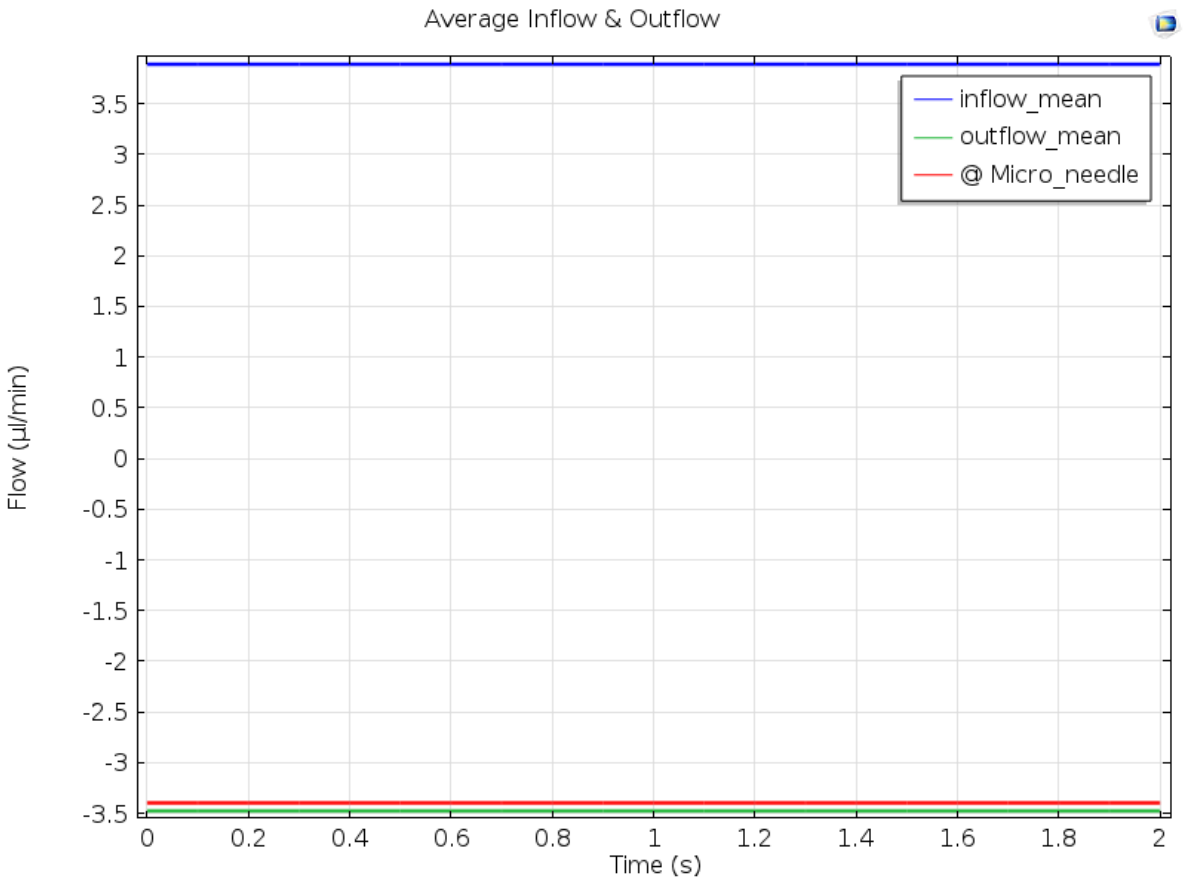

Figure A.66 Average flow rates @ V=110 volts, f =3 Hz

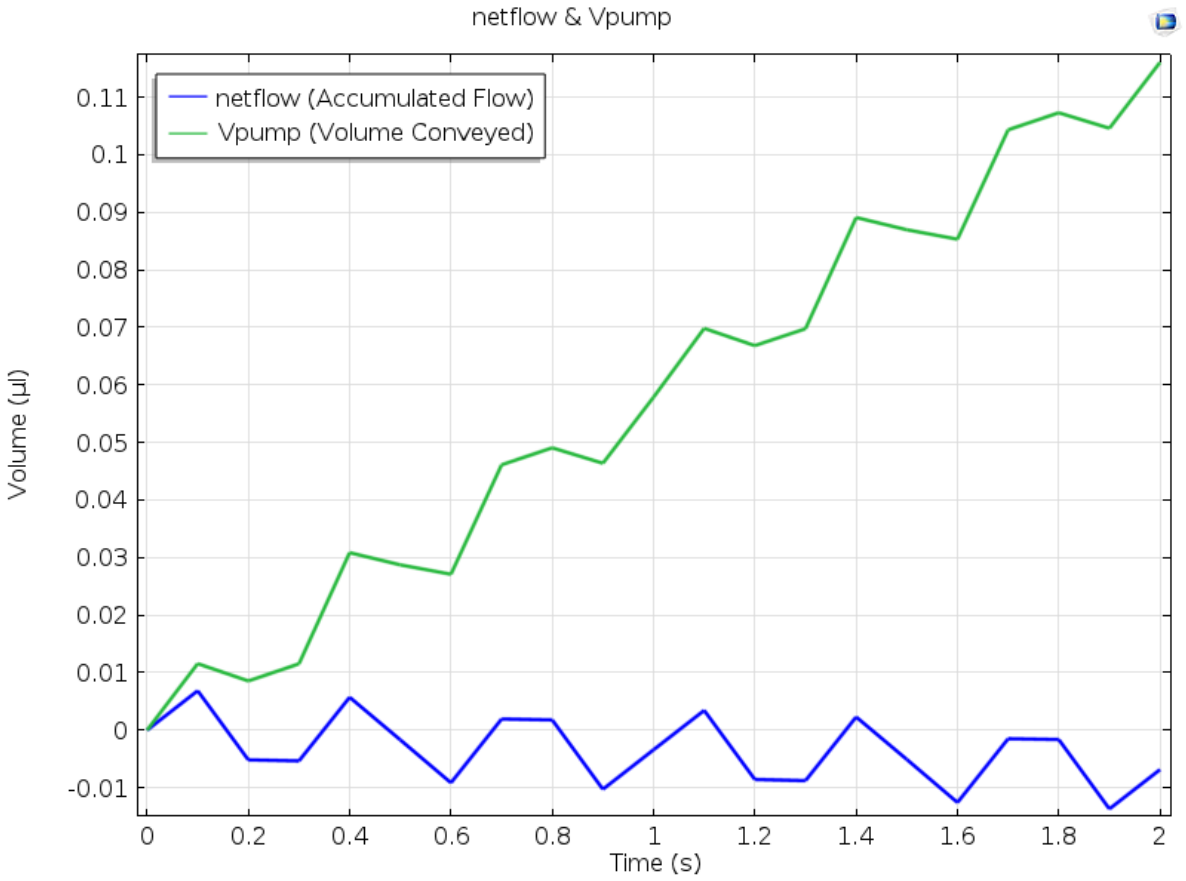

Figure A.67 netflow and Vpump @ V=110 volts, f =3 Hz

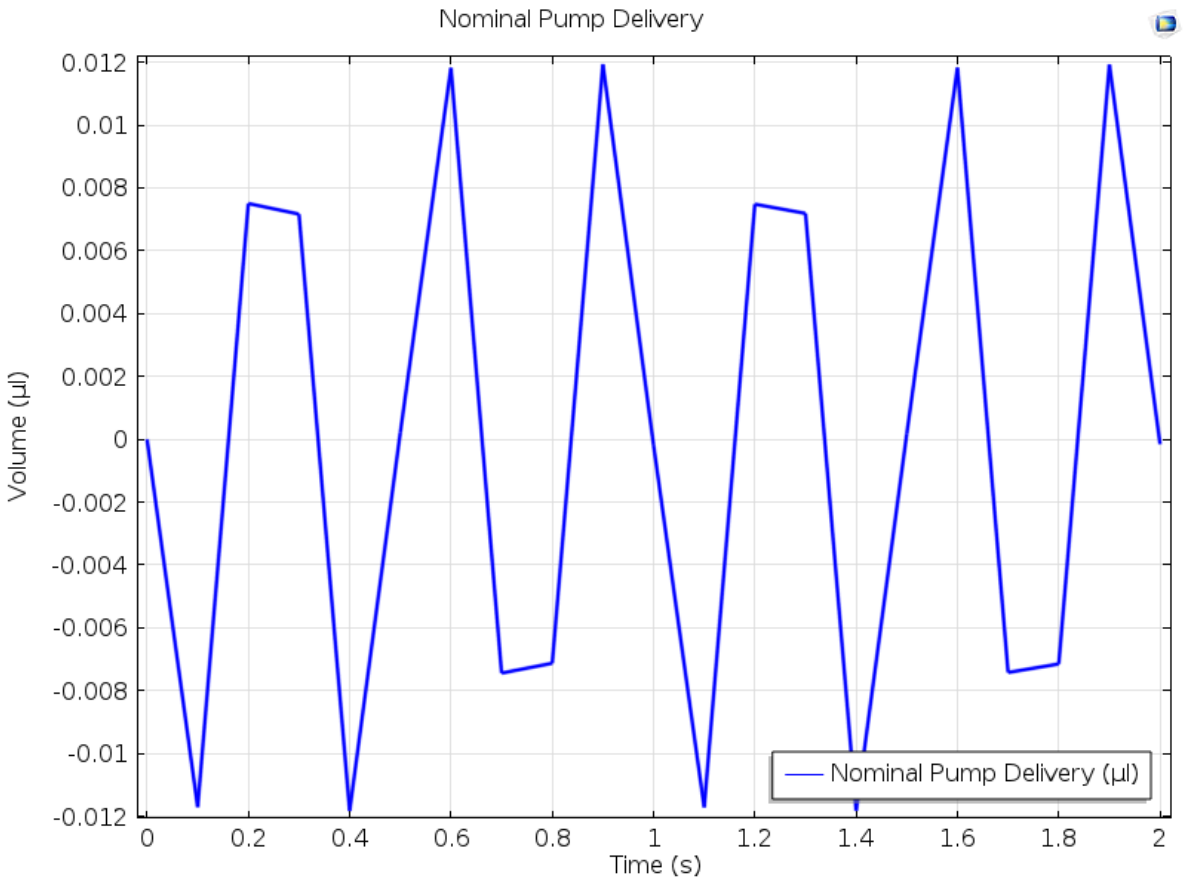

Figure A.68 Nominal Pump Delivery @ V=110 volts, f =3 Hz

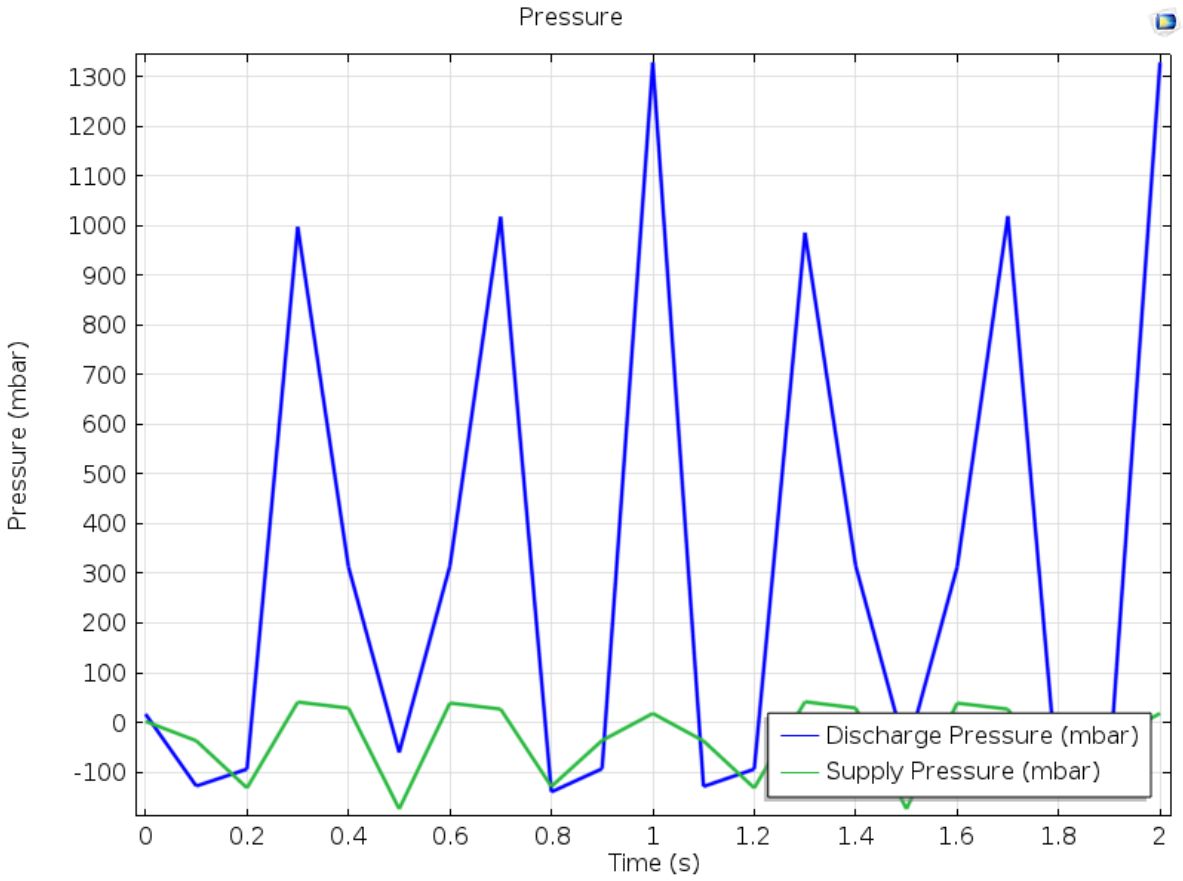

Figure A.69 Pressure vs Time @ V=110 volts, f =3 Hz

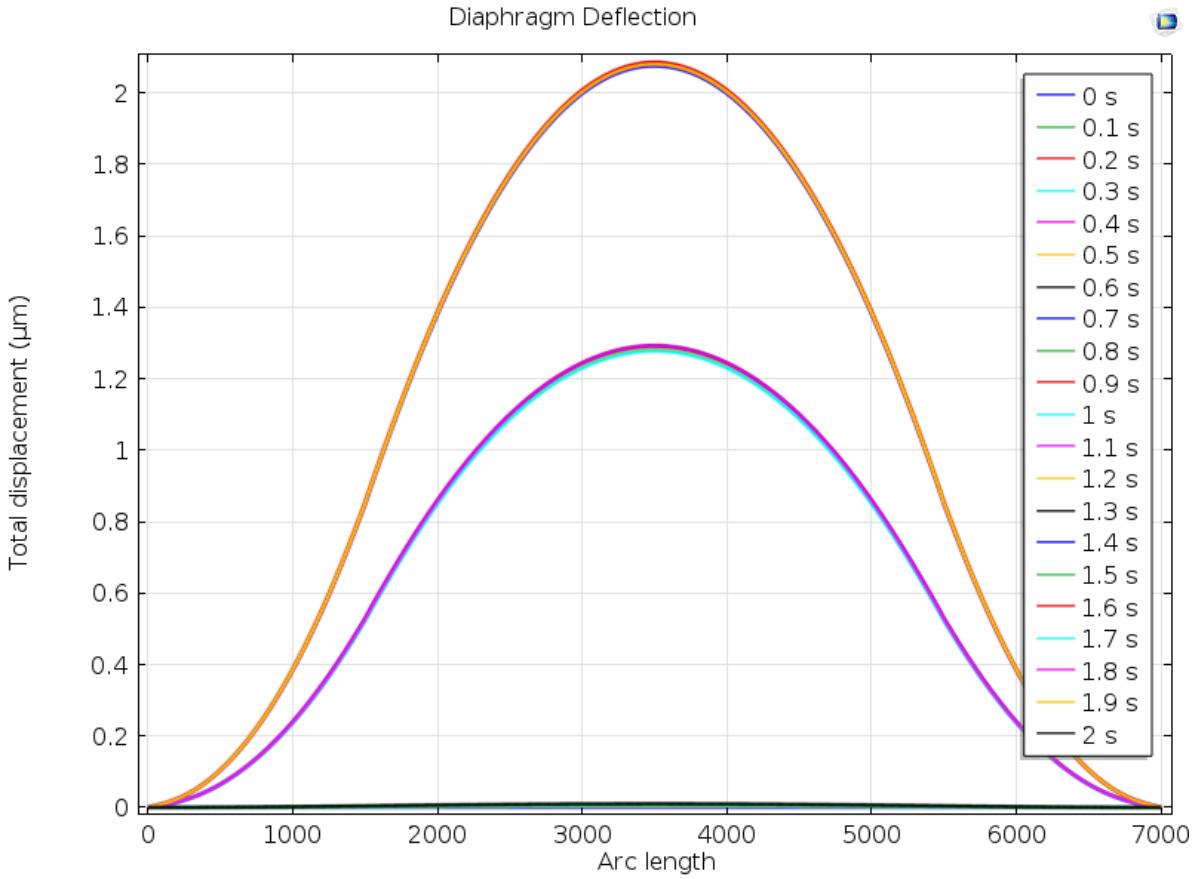

Figure A.70 Diaphragm Deflection versus Arc length @ V=110 volts, f =3 Hz